RELATIVISTIC BEAMING IN ACTIVE GALACTIC NUCLEI

by

Prajval Shastri

Tata Institute of Fundamental Research

Bombay 400 005

A thesis submitted to the

University of Bombay

for the Ph.D. degree in Physics.

1989

SYNOPSIS

Several of the observed properties of radio-powerful active galactic nuclei can be understood if Doppler enhancement of the radio continuum radiation due to bulk relativistic motion in their nuclear regions is invoked. In particular, in the framework of the "unified interpretation" for the radio emission from quasars (Blandford & Königl, 1979; Kapahi & Saikia, 1982; Orr & Browne, 1982), the apparent differences between objects with dominant radio lobes (steep overall spectrum at radio wavelengths) and those with dominant nuclear radio components (flat overall radio spectrum) is a consequence of the differing angles from which the objects are viewed. Because only the radiation from the nuclear region is assumed to be beamed, the ratio of the radio emission from the nuclear component to that from the extended structure is a statistical measure of the angle of orientation of the nuclear jet to the line of sight.

In this thesis, some of the observed properties of radio quasars have been explored in order to ascertain their consistency with the relativistic beaming hypothesis. The data used include observations reported as a part of this thesis work (which are mainly at radio wavelengths) and also those gleaned from the literature. The results are generally consistent with the predictions of the "unified scheme".

Firstly, the question of bulk relativistic velocities in the outer radio components has been investigated. While most radio-powerful active galactic nuclei which show extended radio structure have lobes of radio emission on opposite sides of the nuclear component, a significant number have been known to show extensions on

only one side. That the twin radio lobes are due to radiatively dissipative plasma that is squirted out on opposite sides of the active nucleus is now conventional wisdom. The special feature of "one-sidedness" of radio structure seen in some of them is sought to be explained in the framework of the unified interpretation, by attributing it to Doppler enhancement of the flux density from the approaching outer component relative to that from the receding one at small viewing angles. To examine this hypothesis in detail, a sample of about forty quasars showing "one-sided" structure has been chosen and imaged at radio wavelengths (in both total intensity and linear polarization) with high angular resolution. The Very Large Array synthesis telescope of the National Radio Astronomy Observatory, U.S.A. has been used for the imaging. These observations have been used to confirm the radio structure of the objects and make a systematic study of their properties.

The results, briefly, are as follows. Many of the objects have two-sided structure that is mostly very asymmetric (spatially and/or in surface brightness) with respect to the nuclear component. It appears that the earlier observations, on the basis of which the classification as "one-sided" was made, had missed the second of the twin lobes due to insufficient angular resolution, sensitivity or dynamic range. Radio jets have been detected in many cases, with structural and (inferred) magnetic field properties that are characteristic of quasars. The radio jet points towards the brighter of the two hot spots in almost every case, consistent with the supposition that at least mild bulk relativistic motion is present in the hot spots. A comparison with other quasar samples indicates that relatively large asymmetry in peak surface brightness of the outer hot spots is associated with relatively dominant nuclear

components and smaller projected linear sizes, again consistent with the hypothesis. The unified interpretation is not valid for the class of Compact Steep Spectrum Quasars, where observations suggest that interaction of the radio jets with a possibly gas-rich interstellar medium may play an important role.

Secondly, the question of misalignments of the nuclear jets has been explored using inferences from radio polarimetry. According to the unified scheme, core-dominated quasars are inclined at small angles to the line of sight, and therefore are expected to show relatively large misalignments of the nuclear jet with respect to the overall radio axis. To test this prediction for a large sample of quasars, polarimetry of the nuclear radio component at 5 GHz was used to infer the direction of the nuclear jet. It is assumed that the magnetic field in the nuclear jets orients along the jet (which has been observed to be the case in several quasars). The test shows that while there are large misalignments in evidence in core-dominated quasars, the nuclear jets appear well-aligned with the overall radio axis in lobe-dominated quasars, which is consistent with the prediction. An analogous investigation for the case of radio galaxies also reveals a trend toward alignment.

Thirdly, the possibility that the optical-ultraviolet nuclear emission may be aspect dependent in quasars has been examined. If the unified scheme is valid, it follows that relativistic beaming effects at radio wavelengths are accompanied by an apparent enhancement of the optical-ultraviolet continuum emission from the nucleus in a quasar (Browne & Wright, 1985). Several other observed properties of radio quasars are found here to be consistent with this interpretation.

The prominence of the radio nuclear component is shown to directly correlate with the apparent optical brightness, and also with the ratio of nuclear to host galaxy emission at optical wavelengths. These observations can be understood if the nuclear optical continuum is aspect dependent in the same sense as the nuclear radio emission is. There is a marginal trend for radio jets of kiloparsec scales to occur more frequently among the optically brighter quasars. This is to be expected if the optical continuum is aspect dependent and there is bulk relativistic motion at kiloparsec scales.

The aspect dependence could arise from relativistic beaming of optical synchrotron emission, or, alternatively, from inclination effects of radiation from a hot optically thick but geometrically thin accretion disc. It appears that both these components might be significant contributors to the optical-ultraviolet continuum emission from these objects. The two would, however, show quite different aspect-dependent behaviour, and therefore dominate to different degrees depending on the aspect.

Some of the implications of the aspect dependence of the optical continuum have then been investigated. Optical aspect dependence can introduce a serious orientation bias into existing samples of quasars even when selected at low radio frequencies. (At these frequencies, they get selected by their extended radio emission that is not strongly Doppler beamed). The relativistically beamed component of the optical continuum would contribute to increasing the scatter in the Hubble diagram of flat spectrum (core-dominated) quasars; on the other hand, the aspect dependence of the disc component would increase the scatter for the steep

spectrum (lobe-dominated) quasars.

Lastly, limited evidence has been found that the enhancement of the nuclear radio emission might be accompanied by enhancement of a component of the x-ray emission from these nuclei.

In conclusion, the evidence in favour of the unified scheme is summarized. Some observational results in the literature that do not support the scheme are also discussed. Adopting the point of view that the unified scheme and its implications suggest and promise significant order and progress in the search for a unified phenomenology for active galactic nuclei, some directions in which observational investigations might be profitably pursued are pointed out.

CONTENTS

ACKNOWLEDGEMENTS

It is with great pleasure that I acknowledge Prof. Govind Swarup, who is primarily responsible for my entry into the field of astronomy and who has guided this work. His untiring enthusiasm for the problems in quasar astronomy have always been inspiring. I thank D. J. Saikia for introducing me into the subject of active galactic nuclei, and involving me in a project to study these objects.

It is with the most profound sense of gratitude that I acknowledge the guidance, help and support of Prof. Vijay Kapahi, who has co-guided my work in the most encouraging manner, with much patience, tolerance and understanding, especially through trying periods. He has come up with numerous ideas, suggestions and criticisms with characteristic insight and inspiring enthusiasm, and interactions with him have thus always been a rewarding experince. His examination of the manuscript and helpful comments on it are also gratefully acknowledged.

Alokranjan Patnaik and Lakshmi Saripalli bravely shared the office with me, and provided companionship and invaluable moral support throughout the ups and the downs. My senior colleagues Christopher Salter, C. R. Subrahmanya, Pramesh Rao, N. C. Rana, Ashok Singal, Dilip Banhatti, P. K. Manoharan, S. Krishnamohan, Vasant Kulkarni, and Gopal-Krishna shared their astronomical knowledge and experience in the most encouraging way. My colleagues Tapasi Ghosh, Ravi Subrahmaniam, Latha P., Ranganathan, Viraf Hathiram, Sridhar, Mathew Joseph, Jaydeep Bagchi, Asimendu Bose, Sydney D'Silva and Sunita Nair made the study of astronomy a happy, multi-faceted expereince.

It is with a profound sense of gratitude that I acknowledge all the assistance provided by the staff of the TIFR Centre and RAC, Ooty; and my very special thanks to Meena Srinivasan, Shri Mathews, Shri Unni, Smt. N. Shanthakumari, Shri. T. Sahadevan and Shri. Desayya. Shri. Murugesan inked several of the figures with characteristic skill.

I acknowledge the many serene and inspiring hours spent at the Raman Research Institute, and the use of their facilities; special thanks to Girija Srinivasan, Geeta, Brinda, and Alina for ever willing help with the library. I would particularly like to express my deep appreciation of all the unfailing support provided by Shri Ratnakar, who often drove me to shame with his enthusiasm and meticulousness!

I am very grateful to my friends Michael Maniates and Kathy Greely for their very generous help during the final stages of the thesis work. I also thank R. Muralidharan, Sumathi Krishnamachari, Rafael Friedmann, Sarah Grünstein, Harvey Michaels, Shobha Veeraraghavan and Gary Fuller for their kind help.

Part of the VLA data analysis presented was done by Christopher Salter and Timothy Cornwell. The National Radio Astronomy Observatory is operated by Associated Universities Inc. under contract with the National Science Foundation. Some of the data were processed at the Radio Astronomy Centre, Ooty using the National Image Processing Facility for Astronomy financed by the Department of Science and Technology.

Symbols and Abbreviations

Symbols/ Abbreviations	Description
AGN	active galactic nuclei
b, l	Galactic latitude and longitude
CDQ	core-dominated quasar
CSS	Compact Steep Spectrum
D	Doppler factor *(cf. section 1.3.1)*
H_0	Hubble's constant; assumed to be 50 $km\ s^{-1}\ Mpc^{-1}$
l	projected linear size *(cf. section 4.4.2)*
LAS	the largest angular distance between the outermost peaks of radio emission
LDQ	lobe-dominated quasar
LPQ	low polarization quasar
L_{gxy}	optical luminosity of the host galaxy of the quasar
L_{nucl}	optical luminosity of the quasar nucleus
mas	milliarcsecond
m_v	apparent optical magnitude

M_v	absolute optical magnitude
OVV	optically violently variable
PA	position angle (measured anti-clockwise w.r.t. North)
q_0	the cosmological deceleration parameter; assumed to be 0.5 unless stated otherwise
QSO	Quasi Stellar Object (herein referring to the optical object)
R, $R_{observed}$	Ratio of the observed radio emission from the nucleus to that from the outer components
R_{emit}	Ratio of the radio emission from the nucleus to that from the outer components at an emitted frequency of 8 GHz
RM	(Faraday) Rotation Measure
RPAGN	radio-powerful active galactic nuclei
S	radio flux density
VLBI	Very Long Baseline Interferometry
z	redshift
α	radio spectral index ($\partial \log S / \partial \log \nu$)
β	v/c, where v is the velocity, and c is the velocity of light
γ	Lorentz factor $\frac{1}{\sqrt{1-\beta^2}}$
γ	spectral index of the radiating relativistic particles

θ	angle of inclination of the radio axis to the line of sight
λ	emission wavelength
ν	emission frequency
ϕ	angle between orientation of the nuclear polarization and the radio axis
ψ	intrinsic polarization position angle

Chapter 1

INTRODUCTION

At the hearts of galaxies of stars reside as yet unraveled but fascinating entities that manifest themselves as the most powerful natural phenomena known to humankind. They often occur in extraordinarily remote galaxies (some of them are the farthest objects known), and often assume sizes of mind-boggling scale. While the myriad of stars and related objects that constitute galaxies are themselves seats of intensely energetic events, the physical processes that appear to be occurring at the centres of galaxies far surpass stellar processes in power and extent. These entities have come to be known collectively as *active galactic nuclei* (AGN).

The manifestation of the "activity" is multifarious. It is observable as highly polarized and variable non-stellar optical continuum emission, non-stellar optical line emission that is often highly Doppler-broadened, powerful polarized nonthermal radio emission, and x-ray, ultraviolet and infrared radiation. Many emission mechanisms are in evidence: thermal emission, synchrotron emission, inverse Compton processes, to name some. Several types of AGN have been discussed in the literature, e.g., Seyfert galaxies, Markarian galaxies, radio galaxies, BL Lacertids and Quasi Stellar Objects (QSOs). A benign version of an active galactic nucleus exists at the centre of our own Galaxy. Despite the diversity in some of their properties (and the varied, often historical, nomenclature), evidence has been rapidly growing that all these objects are similar. It appears that the diversity reflects the differing degrees to which various physical processes dominate;

and also that the "central engine" that gives rise to the "activity" is in all cases powered by mass accretion onto a supermassive black hole at the centre of the galaxy of stars.

Many AGN are extremely powerful emitters at radio wavelengths. This thesis deals with some aspects of the nature of this emission. In this chapter, a semi-historical account of the developments in the understanding of *radio-powerful AGN* (RPAGN) that were inspirational to this work is given. An outline of the subsequent chapters follows.

1.1 Radio emission from RPAGN

It is now well established that in those cases where the emitted radio powers exceed ~ 10^{23} W Hz^{-1} at 408 MHz, it is the synchrotron process that is the predominant emission mechanism by far. The consensus is that the observed radiation is incoherent synchrotron emission produced by relativistic electrons in a plasma in which a magnetic field is embedded.

1.1.1 Incoherent synchrotron radiation

The salient features of emission from a uniform synchrotron source (Moffet, 1975) with the energy spectrum of the relativistic particles obeying a decreasing power law ($N(E)dE \sim E^{\gamma}dE$), are the following. In the wavelength interval where the source is transparent, the radiation spectrum would also be a decreasing power law with a spectral index α that is directly related to γ ($\alpha = (1+\gamma)/2$). The radiation is linearly polarized with the E–vector oriented perpendicular to the magnetic field projected onto the plane of the sky. When the

magnetic field is uniform, the fractional linear polarization is ~ 70 percent. If the radiation energy density becomes comparable to the magnetic energy density, inverse Compton scattering produces additional catastrophic loss of electron energy. There is therefore an upper limit to the observable brightness temperature of a source of electron synchrotron radiation, and this value turns out to be ~ 10^{12}K (Kellermann & Pauliny-Toth, 1969).

The proposition that the powerful radio emission from AGN is incoherent synchrotron radiation rests on the following arguments. Firstly, the energy spectrum of the radiating particles, as inferred from the radiation spectrum of optically thin sources, agrees very well with the directly measured energy spectrum of cosmic rays. Secondly, the fractional polarization of the radiation measured from a transparent emitting region never exceeds the predicted maximum value of 70 percent. Finally, the measured brightness temperatures are often very close to but seldom greater than the predicted maximum.

1.1.2 The radio morphology

The capability of observing RPAGN with fine angular resolutions ($\lesssim$ a few arcminutes) revealed several years ago that often a major fraction of the observed radio power was due to radio emitting material that extended from the "parent" (optical galaxy or QSO) out to very large distances (~ several hundred kiloparsecs). Jennnison & Das Gupta (1953) were the first to discover this in the case of the radio source Cygnus A. Subsequent observations (cf. Miley, 1980, and references therein) showed this to be the case for a majority of powerful radio galaxies and quasars.

Earlier, the (optically) "quasi-stellar" sources were regarded as somewhat different from the regular pantheon of extragalactic sources, irrespective of whether or not they were powerful radio sources. At optical wavelengths, these objects appeared point-like on photographic plates, and were known to have emission lines of very large redshifts. That they were regarded as "different" was primarily due to these large redshifts, which, if taken to be cosmological, implied extraordinarily large distances. Consequently, unbelievably high power outputs were inferred, given their observed brightness. It is now, however, beyond reasonable doubt that QSOs and/or quasars are *galactic* nuclei, though with emission that overwhelms the radiation from the rest of the galaxy at optical wavelengths.

The angular resolution and sensitivity of radio telescopes have improved a great deal since Cygnus A first revealed itself. Multi-element instruments using aperture synthesis and related interpolation techniques achieve images of radio sources that far transcend single dish radio telescopes in terms of angular resolution. Many RPAGN have been observed in this manner, and a great variety in morphology has been found. The prototype may be described as follows. Coincident with the "parent" galaxy or QSO is a compact, often variable, "core" component, which has a flat radio spectrum. Straddling this core component, up to several hundred kiloparsecs away from and by and large symmetrical with respect to it, are the outer "lobe" components—diffuse, plume-like, with steep radio spectrum. Compact regions of highly enhanced surface brightness, referred to in the literature as "hot spots", are often found embedded in these lobes. Between the central core component and the outer lobes are narrow elongated regions of radio emission—

highly polarized and of steep radio spectrum—which are commonly referred to as "jets".

All these structures are revealed at angular resolutions of the order of an arcsecond. Even before the jets were discovered, it was proposed that the extended radio lobes were powered by kinetic energy that was continuously supplied by twin beams that went outward from the nuclei (Rees, 1971; Scheuer, 1974; Blandford & Rees, 1974). Thus the "jets" provided the circumstantial evidence needed to vindicate this "beam" model, and are therefore termed as such, although there is no direct evidence for outflow in them. Meanwhile, the technique of Very Long Baseline Interferometry (VLBI; see Thompson *et al.*, 1986), which yields angular resolutions of the order of milliarcseconds, has provided a probe into the heart of the matter. Correlated data from radio receivers separated by nearly the diameter of our planet have indicated that the "core" radio component consists of one "fixed" and one or more "outwardly-moving" subcomponents. If the moving nuclear subcomponents are thought of as precursors of the larger beams/jets, then this motion could be said to constitute further evidence in support of outflow and the beam model.

1.2 Why relativistic speeds—the historical context

One of the unanswered questions with respect to the beam model concerns the typical velocities with which the radio-emitting plasma moves out from the nucleus. It is important for the development of dynamical theories of the phenomenon to know whether or not their velocities are supersonic and whether or not they are relativistic. But since no emission lines have been detected from this material, and

since proper motion has not been observed over the large length scales to which the radiating effluents extend, the velocities cannot, in general, be estimated directly.

Why then are relativistic velocities a possibility at all? Several phenomena observed near the active galactic nucleus warrant such a hypothesis, if they are to be understood in the "synchrotron emission + cosmological redshifts" framework. These phenomena and the arguments made are outlined below.

1.2.1 Variability at low radio frequencies

To begin at the beginning, Sholomitsky (1965) and Dent (1965) found quasars to undergo very rapid variations in their radio flux density. (The former study was at a wavelength of 32 cm while the latter was at 3.75 cm). The rapidity of these variations was a severe embarrassment to the synchrotron model. Briefly, if the time-scale of the variation is taken to be the light crossing time for the source, then causality implies a corresponding maximum linear size for the source. This in turn implies a *maximum* angular size, provided the redshift is taken to be cosmological (and thereby a measure of the distance). On the other hand, the maximum observable brightness temperature derived from synchrotron theory gives a *minimum* angular size for the source, beyond which the radio emission would be rapidly extinguished because the radio photons would be up-scattered to x-ray photons. The embarrassment was that in the case of the rapid flux density changes mentioned above, the inferred maximum size was less than the predicted minimum size by a factor of ~ 100 (e.g., Kellermann & Pauliny-Toth, 1981). While expansion of a synchrotron-emitting cloud would produce variations at high radio frequencies (van der Laan, 1966), this picture predicts that the magnitude of the variations

decreases with frequency. Thus, large variations at low frequencies are a problem.

1.2.2 Solutions to the puzzle?

There appeared four ways out of the difficulty: (a) more exotic coherent emission mechanisms as alternatives to the synchrotron process (e.g., Cocke & Pacholczyk, 1975; Benford, 1977); (b) noncosmolgical redshifts (e.g., Burbidge, 1985); (c) relativistic expansion speeds in the source (Rees, 1966; 1967), and (d) propagation effects as opposed to intrinsic ones as the cause of the variations in flux density.

With regard to the first, it might be said that there is no evidence apart from the phenomenon in point that warrants discarding the synchrotron model. The evidence in favour of this model has only grown, while the suggested alternative mechanisms have not gained ground.

In the case of the second, if the redshifts are not cosmological and the varying objects are actually much closer to us, then this would reduce the inferred photon density and increase the magnetic field, and the embarrassment would be mitigated. However, in recent years, a nebulous "fuzz" has been seen around several QSOs, and it is well established that this fuzz has the photometric properties of a galaxy (Hutchings *et al.*, 1984; Wyckoff *et al.*, 1981; Gehren *et al.*, 1984; Malkan, 1984; Smith *et al.*, 1986). In several cases, slit spectra of the fuzz have revealed stellar absorption features at the redshift of the QSO (Boroson & Oke, 1982; Balick & Heckman, 1983), serving to confirm that the fuzz is starlight from an underlying galaxy. Thus the notion of a quasar as a stellar object is now well buried. It is

beyond doubt that quasars (both radio-loud and -quiet) that are at redshifts ≤ 0.5 are active *galactic* nuclei. Host galaxies have been looked for and not detected at redshifts higher than ~ 0.5 (Malkan, 1984; Fried, 1986). Indeed, they are not expected to be detected by ground-based observations if the redshifts are cosmological; because then, beyond these redshifts, the rapid fading of the surface brightness of the host galaxy would shrink it to within the seeing disc (Weedman, 1986). Thus, abandoning the hypothesis of non-cosmological redshifts for quasars is quite irresistible.

How are relativistic speeds a way out of the quandary? If the radio source expands relativistically, then the time scale of the change in flux density as measured on earth would be lower than that measured by a comoving observer. The inferred comoving size would then be much larger than that estimated in the terrestrial frame of reference, and the observed rapidity of the variations in flux density would no longer be uncomfortable.

What is the evidence in favour of this possibility?

(i) Subsequent to its conjecture by Rees (1967), x-ray observations of several AGN were made during outbursts of radio flux density. In no cases were x-ray photons detected. The upper limits on the x-ray flux density were lower by many orders of magnitude than the inverse Compton x-ray flux density expected (if the source was taken to be as small as the light-crossing-time argument implied).

(ii) Rees (1966) predicted that an object moving relativistically in suitable directions may appear to a distant observer to have a transverse velocity much greater than the velocity of light. (In particular, these "superluminal" velocities

would be observed if the relativistic motion is directed close to the line of sight.) One of the most dramatic events in the story of AGN is the observational confirmation of this prediction, made possible with the technique of VLBI. Moffet *et al.* (1972) reported preliminary data that indicated changes in source structure that were rapid enough to imply superluminal speeds. These findings were subsequently confirmed beyond doubt for several quasars (e.g., Kellermann & Pauliny-Toth, 1981, and references therein). The reality of superluminal motions continues to constitute the strongest evidence in favour of relativistic speeds in AGN. (It should be mentioned, however, that while the effect of light travel time is the widely accepted explanation for the superluminal phenomenon, it is not the only one: e.g., Scheuer, 1984).

(iii) The advent of VLBI enabled estimation of the angular size of the central radio components. Given this and a measurement of the x-ray flux density, lower limits on the relativistic Doppler factor can be inferred, assuming that all the x-ray emission is due to inverse Compton processes (e.g., Cohen, 1985). The results of this exercise once again warrant bulk relativistic motion in some of these objects.

The above is the key evidence in support of relativistic speeds in AGN. Accumulation of data over the years has mostly served to reinforce the results, and the argument in favour of bulk relativistic motions close to the nuclei of these objects is now compelling.

What about the possibility that propagation effects causing may be the cause of fast variations in radio flux density at low radio frequencies (alternative (d) above)? Shapirovskaya (1978) and more recently, Rickett *et al.* (1984) have shown that

rapid variability at low radio frequencies could be due to scattering effects of the interstellar medium of our Galaxy. Indeed, about 35 percent of the known "low frequency variables" show variations at low frequencies that are not accompanied by any change in flux density at high frequencies, and they represent evidence in support of the interstellar scattering phenomenon (Padrielli *et al.*, 1988a). It is also possible that effects due to propagation through the interstellar medium of our Galaxy may be the explanation of other types of variability recently observed (e.g., Heeschen, 1984; Fiedler *et al.*, 1987).

Nevertheless, in 15-20 percent of the known cases of low frequency variability bulk relativistic motion is still the likely explanation for the variations (Padrielli *et al.*, 1988a). (The outbursts in these cases are either quasi-simultaneous at all observed radio frequencies or drift to lower frequencies with time and decreasing amplitude. Accompanying structural changes have been observed for a few among them, and the Lorentz factors thus derived are consistent with those implied by the variability.) It is ironical though that what was initially the stimulus for the postulation of relativistic velocities in AGN has turned out now to be perhaps the most dilute evidence in favour of it !

1.3 Relativistic beaming and unified schemes

Following the work of Rees (1967), there were several models proposed for RPAGN that incorporated bulk relativistic motion of the radio-emitting effluents (e.g., Blandford *et al.*, 1977; Scheuer & Readhead, 1979; Blandford & Königl, 1979). These models are now discussed.

1.3.1 The Doppler enhancement of flux density

The model of Blandford & Königl (1979) formulated the theory of bulk relativistic motion for a two-component "jet version" of the original model, and explored some of the consequences. In this model, the radio emission originates within a collimated supersonic jet that supplies the extended radio lobes with mass, momentum and energy. The required *in situ* acceleration of the emitting particles is achieved by means of mildly relativistic shocks propagating into the plasma and confined to a jet. The "fixed" component observed in the VLBI observations is identified in this model with the base of the jet.

One of the direct consequences of this bulk relativistic motion is that when the motion is in directions close to the line of sight, the observed radio flux density is apparently enhanced due to Doppler effects. The observed flux density S_{obs} of the jet at a frequency ν is related to the flux density S that would be observed in the comoving frame at the same emitted frequency ν as

$$S_{obs}(\nu) = S(\frac{\nu}{D})D^3 ,$$

where D, the Doppler factor, is the ratio of observed to emitted frequency and is given by

$$D = \gamma^{-1}(1 - \frac{v}{c}\cos\theta)^{-1} ,$$

where θ is the angle of inclination of the direction of bulk relativistic motion to the line of sight, v is its velocity, and γ the Lorentz factor. Blandford & Königl (1979) showed that for the base of the jet, S_{obs} is independent of frequency, thus explaining the observed flat radio spectra of core components.

1.3.2 Radio sources with steep and flat radio spectra

Early radio spectral studies of RPAGN had led to the broad classification of these objects into those with steep or flat radio spectrum. Both classes consisted of quasars and radio galaxies, although the latter were mostly of steep radio spectrum. The former often tended to be "compact", (i.e., of relatively small angular size), mostly unresolved by the then prevalent low angular resolutions. The "integrated" spectrum for the latter kind of source as a whole was flat, since these objects were almost wholly the "core" component of the prototype source outlined earlier. In the objects with steep spectrum, diffuse lobes (of steep spectrum) dominated the total flux density, and often no radio core component was detected for them. It was in the case of the former class that superluminal motion was looked for and detected.

1.3.3 Unification

In the relativistic beaming model wherein the radio core component was constituted of relativistically moving sub-components, the observed flux density would be enhanced by Doppler effects. In view of this, Blandford & Königl (1979) suggested a "unified interpretation" for the above two categories of radio sources. They postulated that the steep spectrum extended sources were those objects viewed close to the plane of the sky, and that therefore their compact core components were not Doppler boosted. Also, the brightest flat spectrum sources were the small of fraction of objects (from among a larger population of intrinsically fainter extended sources) whose nuclear flux density was enhanced by Doppler effects. They then predicted that the compact sources ought to be surrounded by radio-emitting halos of steep spectrum and low surface brightness.

Scheuer & Readhead (1979) proposed an alternative unifying scheme involving flat radio spectrum sources. They proposed that the flat spectrum sources were oriented close to the line of sight, and that their nuclear components were relativistically beamed (just as Blandford & Königl did) . When turned close to the plane of the sky, they suggested that these objects would masquerade as the "radio-quiet" QSOs, (i.e., those which emitted very faint radio emission, if detected at all). With regard to the steep radio spectrum objects, they argued that no case could be made for Lorentz factors > 2.

Data of high dynamic range obtained from aperture synthesis instruments showed that around the bright compact radio sources of flat spectrum, there indeed were extended halos of steep spectrum (e.g., Perley *et al.*, 1980; Browne *et al.*, 1982a), just as the unified interpretation of Blandford & Königl had predicted. This bit of evidence went contrary to the unifying suggestion of Scheuer & Readhead (1979). The radio flux densities of the halos were much larger than the measured faint flux densities (if at all) of radio-quiet quasars, and therefore they could not be intrinsically the same as the compact, core-dominated radio quasars.

Thus, if ubiquitous bulk relativistic motion is invoked in the centres of radio quasars, core-dominated quasars (CDQs) and lobe-dominated quasars (LDQs) are intrinsically the same kind of object. Observed differences between them are then due to orientation effects alone.

1.4 The unified scheme—statistical tests

Kapahi & Saikia (1982) tested the unified scheme using a sample of 78 radio

quasars for which maps of high resolution were available. Since the scheme postulates that the flux density observed from the nuclear component is enhanced at inclinations close to the line of sight by Doppler effects, they took the fraction of radio emission from the core, f_c, to be a statistical measure of the angle of inclination to the line of sight. They then looked for correlations of this observed parameter with others that are also expected to depend on orientation. They found that f_c was inversely correlated with the overall projected linear size of the extended emission, and was directly correlated with the observed degree of misalignment away from a collinear radio structure. The first correlation was interpreted to represent foreshortening of the objects at orientations close to the line of sight. The second was ascribed to the fact that at inclinations close to the line of sight, any small intrinsic misalignments would be amplified for most lines of sight. Thus, the correlations they found were consistent with the predictions of the relativistic beaming model.

Orr & Browne (1982) assumed a quasar to consist of a compact relativistically beamed core component with radio spectral index $\alpha = 0$ ($\alpha \equiv \frac{\partial \log S}{\partial \log \nu}$) and unbeamed lobes of spectral index $\alpha = -1$. They used this to predict the proportion of sources with flat radio spectrum in flux-density-limited samples selected at different frequencies. It was known that higher the selection frequency at which the survey is made, larger is the proportion of radio sources with flat spectrum in the resulting sample. Given the quasar model of Orr & Browne (1982), this fraction for a given selection frequency depended on the core Lorentz factor γ. Orr & Browne found that a value of ~ 5 for γ gave satisfactory agreement with the observations.

The model was also used to predict the number/flux density counts of flat spectrum quasars, given this (observed) number for steep spectrum quasars. Once again they obtained consistency of the observations with γ values of ~ 5. Since this value was consistent with that obtained independently from the observed superluminal motions in some quasars, Orr & Browne (1982) concluded that the statistical properties of quasars were entirely consistent with the predictions of the simple relativistic beaming model.

1.5 Relativistic beaming—the present work

Clearly, the evidence for bulk relativistic motion in the environs of AGN is overwhelming. The data on radio-powerful quasars are consistent with the supposition that the prominence of the radio nuclear component is a statistical measure of the angle of inclination to the line of sight. In view of the inherent simplicity of the relativistic beaming scenario, it is important to push the hypothesis as far as it can go, and to test it against different data. It may be pointed out that *radio-powerful* AGN provide the best possible case for testing the relativistic beaming hypothesis for two reasons. Firstly, superluminal motion can be directly observed in these objects. Secondly, unlike emission at other wavelengths, the radio emission almost certainly arises from a single emission mechanism, and therefore, if aspect dependent, provides a neat handle on the orientation.

Several tests that confront the relativistic beaming hypothesis form the focus of this thesis. The main issues examined are outlined below. Radio imaging data at high angular resolutions, obtained in the process of this work and gleaned from the literature, are central to the analyses undertaken.

1.5.1 Bulk relativistic motion on a large scale

While radio-emitting effluents may move outward at relativistic velocities when they are close to the nucleus, what happens further on? Do these speeds continue right up to the ends of the "beams", which are often several hundred kiloparsecs from the nucleus? An attempt to answer this question is the focus of Chapters 2, 3 and 4.

It is the general belief that the extraordinary velocities in the radio jets are confined to the intimate surroundings of the active galactic nucleus, and do not persist beyond. However, Scheuer & Readhead (1979) did suggest that in the case of quasars showing extended radio lobes on one side of the nucleus only, this extended structure might be moving with substantially relativistic bulk speeds. The absence of a second lobe on the opposite side of the nucleus could then be ascribed to the large asymmetry in the intensity of the two outer lobes as a result of Doppler enhancement of the approaching lobe.

Kapahi (1981a) sought to test for relativistic speeds on a large scale for the case of the "one-sided" sources. He investigated the properties of a sample of all the one-sided RPAGN then known. His main finding was that their core components were of higher relative strengths as compared to quasars of two-sided radio structure.

However, Kapahi's data had been obtained with relatively low angular resolution and dynamic range. If the second outer component was missing because it was much fainter, then observations of higher dynamic range would detect it. The asymmetry of the outer components could then be determined, and the question as

to whether this parameter behaves as predicted by the relativistic beaming hypothesis can be examined. Higher resolutions were also desirable in order to determine the prominence of the nuclear radio component reliably. This exercise was therefore undertaken. The constitution of the sample chosen for radio imaging, an outline of the techniques used, and a description of the observations are given in Chapter 2. Radio images of the objects from the sample of Kapahi (1981a) were obtained using the Very Large Array, which is an appropriately powerful instrument both in terms of angular resolution and sensitivity. Its polarimetric capabilities yield data that provide additional insight into the questions at hand. The radio images obtained, along with other data compiled for each programme object are presented in Chapter 3, and the interpretative analysis is given in Chapter 4.

1.5.2 What can radio polarimetry of the nuclei tell us?

In chapter 5, the question of nuclear scale misalignments away from structural collinearity is investigated. Readhead *et al.* (1978) had pointed out that if a radio quasar were oriented with its radio structure axis close to the line of sight, then any small intrinsic misalignments away from collinearity would be amplified for most such lines of sight. Using data from VLBI, they had found that in the case of RPAGN with large projected linear sizes, there was a high degree of alignment between the radio structural features very close to the nucleus and those far out. But for the more compact objects (of flat overall radio spectrum), they found a range of orientations of structures on different scales. Their sample was, however, small and it is important to verify the result for a larger sample of objects.

VLBI on large samples of objects is difficult to perform. A way out was to use radio polarimetry to infer the orientation of the nuclear structure. Polarimetry with the sensitivity of the VLA was available for several quasars studied as part of the exercise described in section 1.5.1. These data were combined with similar data in the literature to enable fairly strong conclusions to be drawn regarding nuclear misalignments.

1.5.3 Is the optical continuum from AGN aspect dependent?

It has been widely assumed that in most AGN, the optical continuum emission observed from the nucleus is isotropic. But the need for consistency of the apparent optical magnitudes of quasars with the relativistic beaming scenario for the radio emission led Browne & Wright (1985) to propose that the optical continuum may also be aspect dependent. This question is explored in Chapter 6 of this thesis. Data on a sample of quasars surveyed by the Bologna radio telescope and imaged by the VLA has been used to test for aspect dependence of the optical continuum. A further test of this hypothesis is applied using optical imagery of quasars. Evidence that might distinguish between the different possible causes for such a phenomenon is looked for. The various implications of anisotropy of the optical continuum are then discussed.

In the final chapter, the current evidence in favour of the hypothesis, and arguments against it are summarised in conjunction with the results presented in this thesis.

1.6 Assumptions, terminology, disclaimers

Throughout this work, the redshifts of quasars are assumed to be of cosmological origin. The standard Friedmann-Robertson-Walker cosmology is used. The value of the Hubble constant is assumed to be 50 km s^{-1} Mpc^{-1}, and that of the deceleration parameter q_0 to be 0.5, except when stated otherwise.

It is assumed that the synchrotron process is the emission mechanism giving rise to the radio power in the objects considered. The standard twin-beam model for extended radio sources is also taken as given. The radio spectral index $(\frac{\partial \log S}{\partial \log \nu})$ is assumed to be 0 for the core components and -1 for the extended radio structure, unless otherwise stated.

The prototype of RPAGN was described in section 1.1. The terms "core", "core component", "nucleus", "nuclear component" and "central component", qualified by the adjective "radio" when necessary, are all used interchangeably to mean the component that is associated with the optical "parent" object. The term "optical nucleus" is used to denote the parent object. The lobes of radio emission are alternatively referred to as "outer components", "extended structures", "large scale extensions", and "kiloparsec-scale extensions". By the largest angular size (LAS) is meant the angular separation between the outermost peaks of radio surface brightness. This projected angular size, when converted to linear dimension, is referred to as projected linear size or simply as linear size. By "surface brightness ratio" is meant the ratio of the surface brightness of the peaks of the outer radio components on either side of the nucleus (> 1 by convention). By "separation ratio"

is meant the ratio of the separation of the brighter outer-component peak from the nucleus to that of the fainter outer-component peak. Having briefly dealt with the unified scheme of Scheuer & Readhead (1979) in section 1.2, by "unified scheme" or "unified interpretation" will hereinafter be meant the one first suggested be Blandford & Königl (1979), unless stated otherwise.

It was pointed out that RPAGN provide the best case for testing the relativistic beaming hypothesis for these objects. However, in the case of those identified with galaxies (as opposed to Quasi Stellar Objects), the evidence for ubiquitous bulk relativistic motion is less clear. Especially in radio galaxies that are of Fanaroff-Riley type I (Fanaroff & Riley, 1974), it is very likely that the bulk velocities of the radio-emitting effluents are subrelativistic. The parent galaxies themselves are of different kinds with possibly differing physical conditions prevailing in the environs of their nuclei (e.g., Hutchings, 1987). It is thus clear that they cannot all fit simply into the unified scheme. It is important to make the distinction because radio galaxies are sometimes of comparable radio luminosities as quasars, and are most often of steep radio spectrum. Blind tests of the unified interpretation between objects of steep and flat spectra without reference to the AGN type could thus be misleading. (At the same time, certain kinds of galaxies may not be physically different from quasars.) Radio galaxies are therefore dealt with occasionally here, but radio quasars are the main focus of the thesis.

It should be emphasized that it is unreasonable to suppose that any single theory can capture completely the richness of properties actually observed in AGN. The goal of the present work is therefore not to seek quantitative agreements of the

relativistic beaming model with observed data. The spirit of the exercise is to demonstrate that bulk relativistic motion is ubiquitous in radio-loud quasars, and therefore that aspect is certainly an important parameter in the case of the radio emission, and perhaps at other wavelengths as well. Hence, only qualitative consistency of the data with the model is sought. Indeed, it has been demonstrated from the theoretical point of view that quantitative tests of the model as it stands may not even be physically meaningful, given the possibility of oblique shocks in radio jets (e.g., Blandford, 1984; Lind & Blandford, 1985). The implications of this are that superluminal motion probably pertains to the shock patterns in the jet, while flux density enhancements are due to relativistic velocities of the underlying flow that may differ from the velocity of the pattern.

Chapter 2

IMAGING OF RADIO-POWERFUL ACTIVE GALACTIC NUCLEI WITH ONE-SIDED STRUCTURE—THE METHOD

The first question investigated with respect to relativistic beaming in this thesis is whether relativistic motion might occur out to several hundred kiloparsecs. The possibility is examined in the case of radio-powerful active galactic nuclei (RPAGN) with suspected one-sided structure, using high resolution radio imaging data. In this chapter, the sample of radio quasars selected for high resolution imaging is described. This is followed by an outline of the techniques and tools used for the imaging, and a brief description of the observations.

2.1 Radio-powerful AGN with one-sided structure—what are they ?

Most powerful radio galaxies and quasars (with radio luminosities $\gtrsim 10^{23}$ W Hz^{-1} at 408 MHz) appear to have radiatively dissipating plasma squirted out as twin beams from their central regions. These beams manifest as radio-emitting regions that extend out to hundreds of kiloparsecs on both sides of the central regions. However, a significant number of these objects show such extensions on only one side of the nucleus. Quasars with one compact radio component coincident with the optical QSO and a second outer component of much steeper spectrum were designated by Miley (1971) as of the "D2" type and recognized as a possibly different category of sources. This class of radio sources has been selected to test for possible relativistic velocities on scales of several

kiloparsecs.

It is important to point out that these sources are quite different from those with the other sort of "one-sided" morphology seen in extragalactic radio sources, viz., the so called "head-tail" type of structure. Objects of the latter kind are relatively nearby radio galaxies, of low radio luminosity ($\lesssim 10^{26}$ W Hz^{-1} at 178 MHz), and are known to occur in clusters of galaxies. It has been hypothesized that the ram pressure due to the motion of galaxies without a significant interstellar medium through the dense intracluster medium, bends the radio-emitting twin beams away from the direction of motion immediately after ejection. Structures that are bent to the extreme, appear as a single 'tail' to the nuclear component (the 'head') in low resolution images. Alternatively, it has been conjectured that if one of the beams is ejected directly into the direction of motion, it is disrupted (O'dea & Owen (1985b) and references therein). "Head-tail" objects are not included in the present analysis.

The one-sidedness in quasars of the "D2" type can arise in several ways:

(a) The twin beams are not ejected collinearly from the nucleus; at certain viewing angles, the extended structure on one-side could hide that on the other side, resulting in an apparently one-sided source.

(b) The effluent is ejected from the nucleus one side at a time only, and the one-sided sources are those where the second ejection (on the other side) has not yet occurred. (It may be noted that 'real' one-sidedness is unlikely to be merely a consequence of non-dissipativeness of one of the twin beams, because it is expected that the beam cannot but *eventually* dissipate to form a terminal hot spot.)

(c) The one-sided sources are merely objects with a high degree of asymmetry in the surface brightness of their outer components, so that with imaging of limited dynamic range, the fainter component is missed.

It is possible that explanation (a) is true in a very small number of individual cases. But it cannot be the general explanation for the phenomenon of one-sidedness, because its prevalence to the extent observed requires that significantly non-collinear ejection be a wide-spread characteristic, and this is contrary to fact.

If the one-sided sources are objects with a large surface brightness ratio of their outer components (possibility (c)), one would like to address the following question: is the observed asymmetry merely the extreme tail-end of a distribution of intrinsic asymmetry in quasars? Or is it only apparent and due to the radio-emitting regions moving at relativistic speeds, so that at small viewing angles the approaching component is enhanced relative to the receding one by Doppler effects, which manifests as one-sidededness in extreme cases?

If the one-sided sources are imaged with high dynamic range so that the missing outer component (if any) is detected, then the behaviour of the asymmetry in relation to other parameters of the quasar can be studied. The morphology could yield clues that might help distinguish between possibilities (b) and (c). Further, if the asymmetry is due to Doppler enhancement of the observed emission from the approaching component, then the asymmetry would be expected to be related to other parameters that are affected by relativistic beaming.

The basis for the study undertaken here is the sample of 49 sources with suspected one-sided structure compiled by Kapahi (1981a). He found that the one-

sided sources in this sample were characterized by strong central components, and that this was qualitatively consistent with the relativistic beaming interpretation. This conclusion was, however, reached using observations mostly by the Westerbork, Cambridge and NRAO-Green Bank interferometers; the angular resolutions that obtain are not fine enough to delineate the nuclear radio component with sufficient accuracy in many cases. Higher dynamic range is clearly called for to derive the asymmetry in the surface brightness of the outer components. Therefore, these sources were observed with the Very Large Array of the National Radio Astronomy Observatory, U.S.A. This instrument is characterized by high angular resolution, sensitivity and dynamic range capabilities that are appropriate to the problem at hand. Moreover, the instrument can also image the polarized radiation at the same resolutions, which gives supplementary information on the nature of the objects under study.

2.2 The sample of sources observed with the VLA

The sample of sources selected for imaging with the VLA was chosen mostly from the list of Kapahi (1981a). Those AGN in Kapahi (1981a) for which high resolution maps had already been published were omitted; these have been listed in Table 2.1, along with references to their radio images in the literature. To the remaining sources were added the following:

0232-042 : was excluded by Kapahi (1981a) because the classification as "one-sided" by Miley & Hartsuijker (1978) was tentative.

1007+417 : found one-sided by Kapahi (1981b), but two-sided by Miley &

Table 2.1 Objects from Kapahi(1981a) that were excluded from the present observations.

Source	Alternate Name	Reference to already available high-resolution image
0836+710	4C71.07	Perley et al.(1980)
0945+408	4C40.24	Perley et al.(1980)
1226+026	3C273	Browne et al.(1982b); Perley et al.(1980)
1350+316	3C293	Bridle et al.(1981)
1641+399	3C345	Browne et al.(1982b); Perley & Johnston(1979)
1642+690	4C69.21	Perley et al.(1980)
1800+440	OU401	Perley et al.(1982)
2037+511	3C418	Perley & Johnston(1979)
2251+158	3C454.3	Browne et al.(1982b)
1807+698	3C371	Browne et al.(1982b); Perley & Johnston(1979)
1828+487	3C380	Wilkinson (1982)

Hartsuijker (1978).

0717+170 : suspected to have one-sided structure by Joshi (1981).

2325+269 : found to be one-sided by Miley & Hartsuijker (1978) and two-sided by Potash & Wardle (1979).

The list of objects imaged, compiled in the manner described above, is given in Table 2.2.

2.3 Imaging radio sources in the sky

The interferometric technique of aperture synthesis, which is the result of the quest for higher angular resolutions, is briefly outlined below.

A two-element interferometer on earth of a given projected spacing as seen by a celestial source measures the "complex visibility" of the source. This is a single

Table 2.2 List of sources observed with the VLA. Optical objects: Q:quasar; BSO:Blue stellar object; Gxy: galaxy; ?: the present observations call into question the optical identification (Chapter 3).

Source	Alternate Name	Optical Object	Apparent Magnitude	Redshift
0003-002	3C2	Q	19.4	1.037
0051+291	4C29.01	Q	17.8	1.828
0115+027	4C02.04	Q	17.5	0.672
0232-042	4C-04.06	Q	16.5	1.436
0241+622	4U	Q	12.2	0.044
0309+411	NRAO128	Gxy	18.0	
0409+229	4C22.08	Q	18.7	1.215
0615+578	4C57.12	Q?	18.0	
0717+170	3C176	Gxy?		
0740+380	3C 186	Q	17.6	1.063
0742+376	4C37.19	BSO	20.0	
0814+201	OTL	Q?	20.0	
0821+394	4C39.23	Q	18.5	1.216
0836+195	4C19.31	Q	17.6	1.691
0919+218	4C21.25	Q	18.5	1.421
0932+022	4C02.27	Q	17.4	0.659
1007+417	4C41.21	Q	16.5	0.611
1012+232	4C23.24	Q	17.5	0.565
1040+123	3C 245	Q	17.3	1.029
1047+096	4C09.37	Q	17.9	0.786
1055+018	4C01.28	Q	18.3	0.890
1055+201	4C20.24	Q	17.1	1.110
1132+303	4C30.22	Q	18.2	0.614
1136-135	PKS	Q	16.1	0.554
1203+109	4C10.34	Q	17.3	1.088
1222+216	4C21.35	Q	17.5	0.435
1320+299	4C29.48	Q	20.0	
1347+539	4C53.28	Q	17.3	0.976
1354+195	4C19.44	Q	16.0	0.720
1415+463	4C46.29	Q	17.9	1.552
1419+315	4C31.45	Q	20.9	1.547
1433+177	4C17.59	Q	18.2	1.203
1509+158	4C15.45	Q	18.2	0.828
1547+309	4C30.29	Gxy?	17.3	0.111
1636+473	4C47.44	Q		0.740
1637+574	OS 562	Q	17.0	0.745

Table 2.2 (contd.)

Source	Alternate Name	Optical Object	Apparent Magnitude	Redshift
1729+501	4C50.43	Q	17.7	1.107
1741+279	4C27.38	Q	17.7	0.372
1842+681	JB	Q	18.0	
2041-149	OTL	Gxy?	20.5	
2251+134	4C13.85	Q	19.3	0.673
2325+269	4C27.52	Q	17.5	0.875

Fourier component of the source brightness distribution in the sky. Since cosmic radio sources are incoherent, the cross-correlation of the radiation fields measured by the interferometer depends only on the interferometer spacing or baseline. Thus, with several interferometer baselines a radio image of the source may be reconstructed using the measured Fourier components. A "single aperture" may thus be "synthesized".

Since this "aperture" would necessarily have several "holes", in practice the unmeasured Fourier components are estimated and "restored" into the image in an iterative process. In all the radio imaging done as a part of this thesis, the CLEAN algorithm (Högbom, 1974), as modified by Clark (1980) for the Fast Fourier Transform Algorithm, has been used for the "restoration".

During astronomical observations, the phase of the measured complex visibility is often disturbed by instrumental and ionospheric effects. However, images of good quality can be produced by recovering the phase using the technique of "self-calibration" (Pearson & Readhead, 1984). The technique uses the principle that part

of the phase information may be obtained if three or more antennas are correlated, and if the source brightness distribution is positive everywhere. The theory and practice of aperture synthesis imaging have been discussed in detail in Perley *et al.* (1986).

All the radio images presented in this thesis were obtained from the Very Large Array (VLA). This is a synthesis telescope consisting of twenty-seven correlated antennas, each of 25m diameter, arranged in a Y-shape. The VLA is operated in four different configurations (A, B, C and D) of differing maximum and minimum baselines. (See Thompson *et al.* (1980) for a detailed description of the instrument.) The first three configurations were used for the present observations.

2.4 The VLA observations

The 42 sources from the sample chosen for imaging were observed at the VLA in its C, B and A configurations at three different epochs between 1980 and 1983. The wavelength bands of λ20, 6 and 2 cm were variously used. Those previously known to have angular sizes of ~15 arcsec or greater were mostly observed in the C configuration; higher resolution configurations were used for the objects of smaller angular sizes.

In the case of the C-array observations, each source was observed at typically three different hour angles for about 10 minutes each. In the case of the B- and A-array observations, each source was observed for about 10 minutes.

Standard astrometric calibrators for the VLA were used to calibrate the phase of the observed visibilities. They were observed about every 25 minutes during

observations with the C-array, and before and after each scan on a programme source for observations with the B-and A-arrays. The positions of these calibrators are known to an accuracy of ~0.02 arcsec. The amplitude of the visibilities was calibrated using the primary calibrator. 3C 286 was the primary flux density and polarization calibrator. The flux densities adopted for the primary calibrator set the amplitude scale of the visibility to that of Baars *et al.* (1977).

The polarization calibration was done using 3C 286 as the calibrator. There is no evidence that any significant Faraday rotation effects occurred during the course of any of the observations at the wavelength of λ20 cm. Such Faraday rotation

Table 2.3 Centre frequencies and Dates of Observation.

VLA Configuration	A	B	C
Centre frequency (MHz)	1465	1465	-
	4885	4885	4885
	-	14965	15035
Dates of Observation	25 Nov. 1983	11 Aug., 7 & 12 Sept. 1982	13 & 14 July, 1980

effects are unimportant at λ6 and 2 cm.

The centre frequencies and the dates of the observations are listed in Table 2.3. The bandwidth used was 50 MHz in all cases. Since the observations made in the C configuration were among the first to be made with the completed

Table 2.4a Parameters of the VLA C-configuration.

Waveband	λ 6cm	λ 2cm
Frequency (MHz)	4885	15035
Bandwidth (MHz)	50	50
System temperature (K)	60	300
Typical HPBW (arcsec)	5	1.5
Typical largest structure "visible" (arcsec)	125	40
Typical number of antennae available	23	22

Table 2.4b Values adopted for the primary calibrators for the C-array observations.

Frequency	Total Flux Density	Degree of Polarization	PA of Polarization
4885 MHz	7.41 Jy	11.3 %	33°
15035 MHz	3.48 Jy	11.6 %	33°

Table 2.4c Flux densities of the secondary calibrators for the C-array observations.

Calibrator	Flux Density (Jy)	
	4885 MHz	15035 MHz
0316+161	2.95	0.71
0316+413	57.00	51.30
0711+356	1.10	0.47
0839+187	0.97	0.53
1404+286	2.90	1.41
1739+522	0.92	1.05

VLA, some of the (now standard) parameters for these observations are listed in **Tables 2.4a, b and c.**

The raw visibility data were edited and calibrated for amplitude, phase, instrumental polarization and polarization position angle using the standard VLA DEC-10 calibration programmes. They were then self-calibrated, Fourier transformed, deconvolved and post-processed using the Astronomical Image Processing System (AIPS) package of the National Radio Astronomy Observatory. In the case of the C-array observations, polarimetry could not be done with all the baselines that were used for total intensity imaging. Therefore, to derive accurate estimates of the fractional polarization, a second set of total intensity maps were made using only those baselines for which polarization information was available.

Chapter 3

THE RADIO IMAGES AND RADIO SPECTRA

The radio images obtained from the VLA using the procedures described in the previous chapter are presented in this chapter. For each observed object, the integrated radio spectrum for the whole source and the component spectra over as wide a radio frequency range as possible have been compiled, which are also presented. A description of each source, incorporating not only data obtained from the images presented herein but also extensive data from the literature, is given.

3.1 The VLA radio images

The images are presented in Figs. 3.1 to 3.38. The contours represent loci of constant surface brightness, on which are superposed the polarization data. The length of the superposed line segments at each pixel represents the polarized flux density in the case of the C-array images and the degree of fractional polarization in the case of the B- and A-array images unless stated otherwise. The orientation of the line segments represents the orientation of the polarization E-vectors. The Gaussian beams used in the deconvolution are plotted as hatched ellipses. In those cases where the present observations detect only an unresolved component, no image is presented. The position of the associated optical object is marked by a cross in each case.

The radio data obtained from the VLA measurements on individual objects are presented in **Table 3.1**, which is arranged as follows :

Column 1: source name.

Column 2: VLA configuration used (A, B or C), and radio wavelength band (cm).

Columns 3-5: Half Power Beam Width of the synthesized beam: major and minor axes, and position angle respectively.

Columns 6,7: r.m.s. noise levels of the total power and polarization images respectively.

Column 8: designation of the radio component (Opt for the optical object; N for north, NE for northeast, etc.).

Columns 9-14: positions of the components. Radio positions are from the present VLA measurements. Optical positions are taken from the literature in a majority of the cases, and measured directly from POSS prints for the rest.

Columns 15,16: peak surface brightness and radio flux density for each component.

Column 17: largest angular size (LAS) of the source

Columns 18,19: fractional polarization and position angle of the E-vector at the position of the peak of surface brightness.

Column 20: code indicating reference to the optical position measurement.

3.2 The radio spectra

The overall radio spectra between ~10 MHz and ~90 GHz are presented in Fig. 3.39. Where possible, the spectra of the individual components are also shown. The total flux densities have been compiled mostly from the flux density catalogues

Table 3.1 The radio sources observed with the VLA.

Source	VLA Array & Waveband (cm)	synthesised beam (HPBW) major (")	minor (")	PA (°)	r.m.s. noise total (mJy/beam)	polarized		Radio position(1950) of Peak Right Ascension h	m	s	Declination (°)	(')	(")	Peak Surface Brightness (mJy/beam)	Flux density (mJy)	Polarization LAS (")	%	PA (°)	Ref.
[1]	[2]	[3]	[4]	[5]	[6]	[7]	[8]	[9]	[10]	[11]	[12]	[13]	[14]	[15]	[16]	[17]	[18]	[19]	[20]
0003-002	B, 2	0.49	0.40	163	1.05		Opt	00	03	48.86	-00	21	06.4			4.8			D86
							N			48.86			05.5	361	460				
							C			48.85			06.3	94	95				
							S			48.76			10.0	15	105				
0051+291	B, 6	0.66	0.47	67	1.5		Opt	00	51	02.08	29	08	51.1			2.8			PW
							NE			02.25			52.3	29	65				
							C			02.06			51.2	138	140				
0115+027	B, 6	1.35	1.32	138	0.22	0.11	Opt	01	15	43.61	02	42	19.7			13.1			C83
							W1			43.30			17.9	50			17	7	
							W1+W2			43.47			18.2	55	225				
							C			43.64			19.6	140			2.5	165	
							E1			43.89			21.5	25			7	176	
							E1+E2			44.13			21.9	57	200				
0232-042	C, 6	5.24	3.94	171	2.3	0.3	Opt	02	32	36.55	-04	15	10.2			13.2			C83
							W[g]			35.97			09.4	184	184		10.8	30	
							C+E			36.65			09.7	226	285		≤ 0.13		
	C, 2	1.77	1.42	19	1.7	3.4	W[g]			35.92			09.7	33	75		≤ 11.2		
							C[g]+E			36.59			10.1	120	159		≤ 2.9		
							E			36.80			09.4	12			≤ 23.1		
0241+622	B, 2	0.63	0.41	61	1.34	0.68	Opt	02	41	00.62	62	15	27.2			3.9			TSMB
							C			00.68			27.6	894	957		0.7	90	
	A, 20	3.35	1.43	61	0.32		C			00.68			27.4	183	192		≤ 1		
							SE			01.19			25.9	43	49		≤ 2		
	A, 6	0.99	0.43	63	0.19		C			00.67			27.4	322	322		0.1	55	
							SE			01.15			25.9	6	8				
	A, 2	0.31	0.13	64	0.39		C			00.69			27.52	188	200		0.3	95	

Table 3.1 (Contd.)

Source	VLA Array & Waveband (cm)	synthesised beam (HPBW) major (")	minor (")	PA (°)	r.m.s. noise total (mJy/beam)	polarized (mJy/beam)		Radio position(1950) of Peak Right Ascension h	m	s	Declination (°)	(')	(")	Peak Surface Brightness (mJy/beam)	Flux density (mJy)	Polarization LAS (")	%	PA (°)	Ref.
[1]	[2]	[3]	[4]	[5]	[6]	[7]	[8]	[9]	[10]	[11]	[12]	[13]	[14]	[15]	[16]	[17]	[18]	[19]	[20]
0309+411	C, 6	4.96	3.88	72	1	0.2	Opt	03	09	44.81	41	08	47.9			26.8			pr
							C[g]			44.82			48.9	337	337		2.2	30	
	C, 2	1.65	1.27	71	2.3	2.2	C[g]			44.78			48.8	465	465		2.1	39	
	B, 20	5.94	3.84	94	0.72		NW			43.00		09	06.0	7					
							C[g]			44.78		08	49.2	289	304				
0409+229	A, 20	1.55	1.40	69	0.36	0.25	Opt	04	09	44.70	22		27.8			4.5			PW
							NW			44.52			29.1	410	504		6.8	94	
							C			44.67			27.6	198	249		6.9	133	
							NE			44.82			29.4	75	97		1.2	91	
0615+578	A, 20	1.33	1.16	152	0.3	0.16	unidentified									8.0			
							NW	06	15	51.54	57	53	19.4	237	582		0.1	172	
							C?			51.99			15.5	20			0.4	29	
							SE			52.26			14.6	24	87		4.5	48	
	A, 6	0.38	0.32	152	0.12	0.16	NW			51.54			19.6	37	43		7.5	129	
							C?			52.02			15.2	1.6					
							SE			52.22			14.7	1.3	8				
0717+170	C, 6	5.36	4.28	55	0.4	0.6	unidentified									105.7			
							W[g]	07	17	34.24	17	04	07.3	99	197		17	45	
							C?[g]			36.87			22.1	4	9		≤ 16.6		
							E[g]			40.98			50.1	15	30		10.2	140	
	C, 2	1.68	1.51	70	1.7	2.4	W			34.24			07.5	12	158		≤ 20.9		
0740+380	C, 6	5.00	3.96	95	0.9	0.2	Opt	07	40	56.82	38	00	31.0			100.4			C83
							C[g]			56.8			30.8	213	229		0.6	24	
							E1[g]		41	00.03	37	59	05.4	8					
							E1+E2[g]		41	00.39	37	58	59.8	28	39		≤ 0.8		
	C, 2	1.7	1.33	92	1.2	2.4	C[g]		40	56.78	38	00	31.0	30	78		≤ 8.5		
							E2		41	00.42	37	58	59.9	≤ 3.5					

Table 3.1 (Contd.)

Source	VLA Array & Waveband (cm)	synthesised beam (HPBW) major (")	minor (")	PA (°)	r.m.s. noise total (mJy/beam)	polarized		Radio position(1950) of Peak Right Ascension h	m	s	Declination (°)	(')	(")	Peak Surface Brightness (mJy/beam)	Flux density (mJy)	Polarization LAS (")	%	PA (°)	Ref.
[1]	[2]	[3]	[4]	[5]	[6]	[7]	[8]	[9]	[10]	[11]	[12]	[13]	[14]	[15]	[16]	[17]	[18]	[19]	[20]
0742+376	C, 6	5.21	3.98	95	0.8	0.2	Opt	07	42	22.63	37	38	33.6			62.3			pr
							W1			18.69		39	14.7	44			10.6	75	
							W1+W2			18.98		39	11.2	78	126		3.9	143	
							C[g]			22.60		38	33.2	60	60		4.6	175	
	C, 2	1.77	1.36	95	1.4	2.1	W1			18.46		39	15.8	8	103	≤	38.2		
							W2			19.00		39	11.0	10		≤	27.6		
							C			22.60		38	33.2	49	52	≤	6.4		
0814+201	A, 20	1.36	1.26	175	0.13	0.13	Opt?	08	14	12.35	20	08	04.4			unresolved			S79
							C			11.51			01.9	281	283		4	124	
	A, 6	0.39	0.36	170	0.17	0.22	C			11.51			01.9	180			1.4	100	
0821+394	C, 6	4.59	4.32	82	6.4	0.4	Opt	08	21	37.26	39	26	28.0			24.0[k]			PW
							C[g]			37.34			28.1	1036	1247		1.4	120	
	C, 2	1.96	1.4	100	8.1	2.5	C[g]			37.31			28.2	992	1270		0.6	116	
0836+195	C, 6	4.72	4.37	98	0.3	0.2	Opt	08	36	15.00	19	32	24.4			31.2			MH
							SW[g]			14.75			07.1	3	7	≤	5.0		
							C[g]			14.98			24.9	74	77		3.6	109	
							NE[g]			15.31			37.3	68	88		7.7	95	
	C, 2	1.53	1.48	75	1.1	1.6	C[g]			14.97			25.0	28	38	≤	5.7		
							NE[g]			15.30			37.8	11	18	≤	21.9		

Table 3.1 (Contd.)

Source	VLA Array & Waveband (cm)	synthesised beam (HPBW) major (")	minor (")	PA (°)	r.m.s. noise total (mJy/beam)	r.m.s. noise polarized (mJy/beam)		Radio position(1950) of Peak Right Ascension h	m	s	Declination (°)	(')	(")	Peak Surface Brightness (mJy/beam)	Flux density (mJy)	Polarization LAS (")	%	PA (°)	Ref.
[1]	[2]	[3]	[4]	[5]	[6]	[7]	[8]	[9]	[10]	[11]	[12]	[13]	[14]	[15]	[16]	[17]	[18]	[19]	[20]
0919+218	A, 20	1.38	1.24	179	0.12	0.12	Opt	09	19	53.07	21	49	33.5			11.2			SN
							SW			52.74			30.6	9		≤ 3			
							C+NE1+SW			53.04			34.0	63	231		2.6	8	
							NE2			53.32			38.4	157	278		5.9	66	
	A, 6	0.41	0.4	11	0.10	0.12	SW			52.95			33.2	1.4	30				
							C			53.03			33.6	19	23	≤ 3			
							NE1			53.06			34.6	15	30		21	138	
							NE2			53.34			38.5	38	45		25	42	
0932+022	C, 6	6.15	4.75	116	0.6	0.2	Opt	09	32	42.93	02	17	39.6			44.8			MH
							W[g]			40.95			16.1	51	137		15.4	159	
							C[g]+E			43.00			41.2	82	143		1.1	125	
							E			43.26			44.6	45			5.7	115	
	C, 2	1.65	1.34	30	1.2	2.6	C[g]			42.94			41.1	76	93	< 3.9			
							E			43.30			44.8	11	25	< 22.2			
1007+417	C, 6	4.84	3.95	104	0.9	0.2	Opt	10	07	26.13	41	47	24.4			32.0			C77
							SW[g]			25.91			05.6	302	454		8.8	160	
							C[g]			26.10			25.3	149	189		3.2	108	
							NE[g]			26.33			36.6	21	38		4.2	106	
	C, 2	1.57	1.29	85	1.4	2.3	SW[g]			26.00			05.2	52	183	≤ 9.9			
							C[g]			26.11			25.3	70	111	≤ 4.8			
							NE[g]			26.28			37.0	7	20				
1012+232	A, 20	1.34	1.28	174	0.44	0.24	Opt	10	12	00.50	23	16	12.3			18.0			W76
							N			00.50			18.1	15	40	≤ 4			
							C			00.50			12.1	659	719		3.2	73	
							S			00.57			00.7	62	300		13.8	33	
	A, 6	0.41	0.39	177	0.4	0.15	C			00.50			12.1	1083	1220		0.6	179	
							S			00.58			00.6	9	35		7.9	164	

Table 3.1 (Contd.)

Source	VLA Array & Waveband (cm)	synthesised beam (HPBW) major (")	minor (")	PA (°)	r.m.s. noise total (mJy/beam)	polarized		Radio position(1950) of Peak Right Ascension h	m	s	Declination (°)	(')	(")	Peak Surface Brightness (mJy/beam)	Flux density (mJy)	Polarization LAS (")	%	PA (°)	Ref.
[1]	[2]	[3]	[4]	[5]	[6]	[7]	[8]	[9]	[10]	[11]	[12]	[13]	[14]	[15]	[16]	[17]	[18]	[19]	[20]
1040+123	A, 20	1.43	1.32	171	0.54	0.19	Opt	10	40	06.02	12	19	15.1			7.4			W76
							W1			05.67			15.5	470	653		13.2	108	
							C+W2			05.99			15.1	1710	2045		9	86	
							E			06.18			14.7	170	413		4	100	
	A, 6	0.41	0.39	85	0.36	0.13	W1			05.67			15.4	130	177		15.6	90	
							W2			05.90			15.4	20			22.2	15	
							C			06.00			15.1	1150	1205		10.4	24	
							E			06.20			15.1	7	17		≤ 10		
1047+096	C, 6	4.67	4.14	175	0.3	0.3	Opt	10	47	48.95	09	41	47.7						MH
							W[g]			45.11		42	12.3	11	21		3.8	157	
							NW[g]			48.59		42	01.6	5	13		9	48	
							C			49.02		41	44.7	29			7.3	1	
							C+SE[g]			49.14		41	42.1	56	117		4.4	85	
	C, 2	1.53	1.37	17	1.1	1.9	C[g]+SE			48.92		41	47.0	16	112		≤ 27.5		
							SE[g]			49.15		41	41.1	7			≤ 22.4		
1055+201	C, 6	4.37	4.01	16	3.1	0.3	Opt	10	55	37.59	20	07	55.3			21.2			MH
							NW[g]			37.12		08	15.3	510	690		3.2	125	
							C[g]			37.55		07	54.9	846	959		0.1	93	
	C, 2	1.48	1.31	176	6.6	2.5	NW[g]			37.16		08	15.7	103	277		≤ 2.8		
							C[g]			37.56		07	55.3	832	889		5.4	175	
1055+018	A, 6	0.46	0.41	168	0.62		Opt	10	55	55.33	01	50	03.4			unresolved			W76
							C			55.32			03.5	2670	2680		4.1	109	
	A, 2	0.16	0.13	167	1.2		C			55.316			03.45	4120	4135		4.3	134	

Table 3.1 (Contd.)

Source	VLA Array & Waveband (cm)	synthesised beam (HPBW) major (")	minor (")	PA (°)	r.m.s. noise total (mJy/beam)	polarized (mJy/beam)		Radio position(1950) of Peak Right Ascension h	m	s	Declination (°)	(')	(")	Peak Surface Brightness (mJy/beam)	Flux density (mJy)	Polarization LAS (")	%	PA (°)	Ref.
[1]	[2]	[3]	[4]	[5]	[6]	[7]	[8]	[9]	[10]	[11]	[12]	[13]	[14]	[15]	[16]	[17]	[18]	[19]	[20]
1132+303	A, 20	1.30	1.22	24	0.31	0.13	Opt	11	32	16.25	30	22	02.3			15.5			PW
							NW			16.00		22	07.9	22	218		4.4	23	
							C+SE1			16.22		22	02.2	227	316		5.6	75	
							SE2			16.72		21	56.4	92	562		1.5	78	
	A, 6	0.42	0.42	46	0.17	0.11	NW			15.95		22	07.7	1.1	67				
							C+SE1			16.23		22	02.5	72.4	138		6.1	88	
							SE1			16.26		22	01.4	21.8			3.8	46	
							SE2			16.73		21	55.9	5.6	130		≤ 1		
1136-135	B, 6	4.93	4.24	152	3.83		Opt	11	36	38.51	-13	34	05.9			16.0			MH
							NW			37.74			00.9	332	490		8	30	
							C+SE			38.39			06.7	521	1055				
	A, 20	1.84	1.25	17	1.6	0.39	NW			37.92			01.1	730	1541		10.1	177	
							C			38.52			06.0	570	570		1.6	140	
							SE1+S			38.74			10.8	250	1478		5.6	34	
	A, 6	0.56	0.38	10	0.24	0.14	NW			37.90			01.1	129	522		7.8	31	
							C			38.52			06.0	444	462		1.8	13	
							SE1			38.75			10.8	13			12	46	
							SE1+SE2			38.80			07.8	22	606		22.2	101	
1203+109	A, 20	1.43	1.31	171	0.24	0.1	Opt	12	03	22.62	10	59	35.4			5.6			WWD
							NW			22.48			38.0	17	31		5.9	115	
							N			22.63			36.9						
							C			22.61			35.8	98	206		6.4	95	
							S			22.66			33.5	47	94		3.5	57	
	A, 6	0.45	0.41	175	0.1	0.1	NW			22.47			38.2	2	8				
							N			22.63			37.1	17	39		9.1	75	
							C			22.59			35.6	54	60		0.9	130	
							S			22.65			33.5	6	20		8	87	

Table 3.1 (Contd.)

Source	VLA Array & Waveband (cm)	synthesised beam (HPBW) major (")	minor (")	PA (°)	r.m.s. noise total (mJy/beam)	r.m.s. noise polarized (mJy/beam)		Radio position(1950) of Peak Right Ascension h	m	s	Declination (°)	(')	(")	Peak Surface Brightness (mJy/beam)	Flux density (mJy)	Polarization LAS (")	%	PA (°)	Ref.
[1]	[2]	[3]	[4]	[5]	[6]	[7]	[8]	[9]	[10]	[11]	[12]	[13]	[14]	[15]	[16]	[17]	[18]	[19]	[20]
1433+177	B, 6	2.02	1.93	48	0.29	0.2	Opt	14	33	36.12	17	42	36.5			10.0			WWD
							N			36.09			42.0	18	27		10	21	
							C			36.08			36.8	302			5	61	
							SE			36.19			32.5	192	246		4	89	
	A, 6	0.41	0.41	139	0.22	0.21	N			36.09			42.2	11	25		10.2	12	
							C+jet			36.09			36.7	228	250		3.3	58	
							SE			36.20			32.2	92	231		1.7	124	
1509+158	B, 6	2.22	2.11	47	0.38		Opt	15	09	52.47	15	51	39.2			9.0			pr
							W			51.95			36.3	128	184		17	73	
							C+E			52.45			39.0	117	203		4	0	
	A, 20	1.44	1.39	148	0.24	0.15	W1			51.95			36.4	298	343		17.5	87	
							W2			52.00			39.9	34	116		10.3	177	
							C+W3			52.45			39.3	99	155		6.1	165	
							E			52.57			39.0	72	214		$\leq$ 0.8		
	A, 6	0.42	0.41	138	0.23	0.22	W1			51.94			36.6	99	130		18	74	
							W3			52.38			39.0	5.2	30		15.2	172	
							C			52.43			39.3	80	90		2.2	165	
							E			52.56			38.4	8	85		$\leq$ 8		
1547+309	B, 6	1.6	1.1	104	0.14	0.16	unidentified									15.3			
							NW	15	47	11.92	30	56	22.2	64	235				
							C?			12.57			17.9	9					
							SE			12.97			14.9	37	85				
1636+473	C, 6	4.32	3.77	97	0.8	0.2	Opt	16	36	19.17	47	23	28.7			20.0			pr
							C[g]			19.17			28.8	500	500		1.6	53	
							NE1+NE2			19.45			46.0	48	150		1.5	164	
							NE2			19.99			47.0				11.8	179	
	C, 2	1.61	1.22	70	2.9	1.6	C[g]			19.15			28.5	914			1.3	53	
							NE1[g]			19.34			45.6	13	991				
							NE2[g]			19.89			46.4	13					

Table 3.1 (Contd.)

Source	VLA Array & Waveband (cm)	synthesised beam (HPBW) major (")	minor (")	PA (°)	r.m.s. noise total (mJy/beam)	polarized		Radio position(1950) of Peak Right Ascension h	m	s	Declination (°)	(')	(")	Peak Surface Brightness (mJy/beam)	Flux density (mJy)	Polarization LAS (")	%	PA (°)	Ref
[1]	[2]	[3]	[4]	[5]	[6]	[7]	[8]	[9]	[10]	[11]	[12]	[13]	[14]	[15]	[16]	[17]	[18]	[19]	[20]
1320+299 (contd.)	A, 6	0.37	0.36	35	0.25		Ac+Ae			40.50		57	23.54	210	260		5.5	132	
							Ae			40.81		57	22.80	3					
							Bw+Be			42.15		57	11.76	75	250		18.5	105	
							Be							6					
							C			43.77		56	53.74	24	80		9.5	4	
	A, 2	0.12	0.11	34	0.39		Ac							140	160		5.5	125	
1347+539	C, 6	4.88	3.84	106	1.8	0.2	Opt	13	47	42.66	53	56	08.0			5.3[op]			C77
							C[g]			42.61			08.5	836	891		1.8	13	
	C, 2	1.66	1.27	125	2.6	3.9	C[g]			42.58			08.4	611	666		4.5	50	
1354+195	C, 6	4.40	4.24	175	2.7	0.6	Opt	13	54	42.09	19	33	43.9			43.7			C83
							NW[g]			41.73			59.2	60			3.4	178	
							C[g]+NW+SE			42.10			44.1	1292	1761		4.8	70	
							SE[g]			42.43			16.6	73			14.3	50	
	C, 2	1.56	1.41	2	4.5	3.7	C[g]			42.07			43.9	944	1048		3.4	55	
1415+463	A, 20	1.54	1.42	56	1.1	0.23	Opt	14	15	13.47	46	20	55.5			13.2			C77
							SW1			12.23			52.1	82	252		7.1	115	
							SW2			12.3			54.1	91			8.7	142	
							C			13.43			55.6	567	567		1.5	9	
	A, 6	0.44	0.42	49	0.28	0.15	SW1			12.24			52.0	6					
							SW1+SW2			12.30			54.1	23	81		10.4	123	
							C			13.43			55.6	647	647		0.4	132	
1419+315	C, 6	4.42	3.91	63	0.8	0.2	Opt	14	19	19.39	31	32	43.7						F79a
							W[g]			18.82		32	38.8	17			10.9	157	
							C[g]			19.36		32	43.5	54	140		1.6	13	
							E			19.84		32	37.8	28			11.6	108	
							SE[g]			23.37		30	38.1	54	54	≤	0.9		
	C, 2	1.51	1.35	50	1.1	1.9	W			18.86		32	38.8	4					
							C[g]			19.33		32	43.4	38	89	≤	7.4		
							E[g]			19.83		32	37.1	9					

Table 3.1 (Contd.)

Source	VLA Array & Waveband (cm)	synthesised beam (HPBW) major (")	minor (")	PA (°)	r.m.s. noise total (mJy/beam)	polarized (mJy/beam)		Radio position(1950) of Peak: Right Ascension h	m	s	Declination (°)	(')	(")	Peak Surface Brightness (mJy/beam)	Flux density (mJy)	LAS (")	Polarization %	PA (°)	Ref.
[1]	[2]	[3]	[4]	[5]	[6]	[7]	[8]	[9]	[10]	[11]	[12]	[13]	[14]	[15]	[16]	[17]	[18]	[19]	[20]
1433+177	B, 6	2.02	1.93	48	0.29	0.2	Opt	14	33	36.12	17	42	36.5			10.0			WWD
							N			36.09			42.0	18	27		10	21	
							C			36.08			36.8	302			5	61	
							SE			36.19			32.5	192	246		4	89	
	A, 6	0.41	0.41	139	0.22	0.21	N			36.09			42.2	11	25		10.2	12	
							C+jet			36.09			36.7	228	250		3.3	58	
							SE			36.20			32.2	92	231		1.7	124	
1509+158	B, 6	2.22	2.11	47	0.38		Opt	15	09	52.47	15	51	39.2			9.0			pr
							W			51.95			36.3	128	184		17	73	
							C+E			52.45			39.0	117	203		4	0	
	A, 20	1.44	1.39	148	0.24	0.15	W1			51.95			36.4	298	343		17.5	87	
							W2			52.00			39.9	34	116		10.3	177	
							C+W3			52.45			39.3	99	155		6.1	165	
							E			52.57			39.0	72	214		≤ 0.8		
	A, 6	0.42	0.41	138	0.23	0.22	W1			51.94			36.6	99	130		18	74	
							W3			52.38			39.0	5.2	30		15.2	172	
							C			52.43			39.3	80	90		2.2	165	
							E			52.56			38.4	8	85		≤ 8		
1547+309	B, 6	1.6	1.1	104	0.14	0.16	unidentified									15.3			
							NW	15	47	11.92	30	56	22.2	64	235				
							C?			12.57			17.9	9					
							SE			12.97			14.9	37	85				
1636+473	C, 6	4.32	3.77	97	0.8	0.2	Opt	16	36	19.17	47	23	28.7			20.0			pr
							C[g]			19.17			28.8	500	500		1.6	53	
							NE1+NE2			19.45			46.0	48	150		1.5	164	
							NE2			19.99			47.0				11.8	179	
	C, 2	1.61	1.22	70	2.9	1.6	C[g]			19.15			28.5	914			1.3	53	
							NE1[g]			19.34			45.6	13	991				
							NE2[g]			19.89			46.4	13					

Table 3.1 (Contd.)

Source	VLA Array & Waveband (cm)	synthesised beam (HPBW) major (")	minor (")	PA (°)	r.m.s. noise total (mJy/beam)	polarized		Radio position(1950) of Peak Right Ascension h	m	s	Declination (°)	(')	(")	Peak Surface Brightness (mJy/beam)	Flux density (mJy)	Polarization LAS (")	%	PA (°)	Ref.
[1]	[2]	[3]	[4]	[5]	[6]	[7]	[8]	[9]	[10]	[11]	[12]	[13]	[14]	[15]	[16]	[17]	[18]	[19]	[20]
1637+574	B, 6	1.54	1.36	121	0.74	0.13	Opt	16	37	17.33	57	26	16.2			4.0			C77
							C[g]+W			17.43			15.9	1604	1678		3.4	111	
1729+501	C, 6	4.44	3.87	71	1	0.6	Opt	17	29	49.26	50	09	44.3			20.4			C77
							C[g]			49.27			44.2	39	43		5.5	50	
							E[g]			50.71			29.3	352	414		18.2	48	
	C, 2	1.43	1.23	68	1.3	1.8	C[g]			49.28			44.1	18	23	≤	10.7		
							E[g]			50.74			29.3	93	142		10.2	43	
1741+279	A, 6	0.38	0.41	102	0.25	0.22	Opt	17	41	57.97	27	54	04.8			10.1			H84
							N			57.91			10.4	17	84		6.5	147	
							C			57.89			04.8	178	194		6.4	71	
							S			58.02			01.0	3	28				
1842+681	A, 20	2.49	1.21	99	0.28	0.22	Opt	18	42	43.36	68	06	19.2			4.0			C77
							C			43.50			19.7	636			1.7	92	
							C+NW							636	726				
	A, 6	0.75	0.37	100	0.29	0.21	C			43.49			19.6	1320	1321		1.4	37	
2041-149	B, 20	5.67	3.91	178	0.69		Opt?	20	41	29.17	-14	56	32.8			30.5			S79
							W			29.08			33.6	186	280				
							E			31.08			43.0	125	205				
	B, 6	1.56	1.23	159	0.13	0.1	W			29.09			33.7	47	76		1.5		
							E			31.09			43.1	21	61		18	18	

Table 3.1 (Contd.)

Source	VLA Array & Waveband (cm)	synthesised beam (HPBW) major (")	minor (")	PA (°)	r.m.s. noise total (mJy/beam)	r.m.s. noise polarized (mJy/beam)		Radio position(1950) of Peak Right Ascension h	m	s	Declination (°)	(')	(")	Peak Surface Brightness (mJy/beam)	Flux density (mJy)	LAS (")	Polarization %	Polarization PA (°)	Ref.
[1]	[2]	[3]	[4]	[5]	[6]	[7]	[8]	[9]	[10]	[11]	[12]	[13]	[14]	[15]	[16]	[17]	[18]	[19]	[20]
2251+134	B, 6	1.30	1.25	172	0.46	0.5	Opt	22	51	51.93	13	25	49.1			6.6			W79
							SW			51.69			46.0	80	170		4	68	
							C			51.88			48.9	397			2	90	
							NE			51.98			50.9	110	180		1.5		
2325+269	B, 6	1.29	1.21	35	0.25	0.2	Opt	23	25	28.60	26	59	23.0			7.4			MH
							NW			28.41			24.8	198	331				
							C			28.54			21.4	53					
							SE			28.68			18.3	22	85				

Legend: g: the position is derived from a Gaussian fit to the image. k: LAS is from the image of Kapahi (1981b); op: LAS is from Owen & Pucshell (1984).

References to the optical position: C77: Cohen et al. (1977); C83:Clements (1983); D86:Downes et al. (1986); F79a:Fanti et al. (1979a); H84: Hintzen (1984); MH:Miley & Hartsuijker (1978); PW:Potash & Wardle (1979); pr:present work; S79:Singal et al. (1979); SN:Stannard & Neal (1977); TSMB:Tzanetakis et al. (1978); W76:Wills (1976); WWD:Wills et al. (1973); W79:Wills (1979).

Table 3.2 Sources of radio flux density measurements.

Reference	Frequency
Abraham et al. (1984)	22, 44 GHz
Amirkhanyan (1981)	8.7, 14.4 GHz
Artyukh et al. (1969)	86 MHz
Artyukh & Vetukhnovskaya (1981)	102 MHz
Barthel (1984)	5 GHz
Binette et al. (1981)	5 GHz
Braude et al. (1978)	14.7,16.7,20,25 MHz
Braude et al. (1979)	14.7,16.7,20,25 MHz
Braude et al. (1981)	14.7,16.7,20,25 MHz
Bridle & Purton (1968)	10 MHz
Condon et al. (1982)	1.41 GHz
Dixon & Kraus (1968)	1415 MHz
Ehman et al. (1974)	1415 MHz
Fitch et al. (1969)	1415 MHz
Gear et al. (1984)	150, 300, 350 GHz
Gregorini et al. (1984)	408 MHz
Hoglund (1967)	750 MHz
Large et al. (1981)	408 MHz
Lawrence et al. (1983)	4.76 GHz
Rinsland et al. (1974)	1415 MHz
Roger et al. (1986)	22 MHz
Salonen et al. (1983)	37 GHz
Scheer & Kraus (1967)	1415 MHz
Seilstad et al. (1983)	10.8 GHz
Simard-Normandin et al. (1980)	1.59,1.721 GHz
Simard-Normandin et al. (1981b)	1.6,14.8 GHz
Simard-Normandin et al. (1981c)	2.7,8.1 GHz
Simard-Normandin et al. (1982)	10.5 GHz
Singal et al. (1979)	327 MHz
Spangler & Cotton (1981)	0.43, 1.4 GHz
Sutton et al. (1974)	408 MHz
Willson et al. (1972)	408,1407 MHz
Windram & Kenderdine (1969)	408 MHz
Wright et al. (1982)	2.7, 5 GHz

listed in Kühr *et al.* (1979) and Kühr *et al.* (1981). Other references used and not listed by Kühr are given in Table 3.2. Estimates of the flux densities from aperture synthesis instruments have sometimes been included to provide information where none is available from single-dish measurements. All the flux densities have been converted to the scale of Baars *et al.* (1977). A linear ($a + b \log \nu$) or parabolic ($a + b \log \nu + c \log^2 \nu$) least-squares fit to the spectra (that includes weighting by errors) has been overlaid on the plots. In the case of the components, an error in the flux densities of 10 percent is assumed unless the quoted errors are higher. The fits should not, however, be taken too literally, especially beyond the frequency range where good measurements are unavailable.

3.3 Description of the individual sources

A description of each of the objects for which VLA images were obtained is given below. An extensive survey of the literature was made for information on the objects at radio wavelengths, and the descriptions here include the data thus compiled, with focus on multifrequency morphology, spectral characteristics, radio variability and polarization characteristics. Whenever a spectral index has been quoted, it has been obtained by a linear least-squares fit to the flux density measurements. Whenever Faraday rotation measures (RMs) are given, they are obtained from linear-least-square fits to the measurements, taking into account the errors.

The source 1320+299 was studied in somewhat greater detail than the rest of the objects. The apparently very large angular size of the source was an embarrassment to the relativistic beaming scenario. Moreover, the source

characteristics, especially those of the polarized emission, were interesting in themselves. It was therefore imaged very extensively with the VLA, and a discussion of the results is given.

0003–002 : Lyne (1972) pointed out that this source was one-sided. The lunar occultation observations with the Ooty Radio Telescope at 327 MHz (Joshi, 1981) showed the 'core-component' to consist of two compact components. But, due to the uncertainties in their positions, it was not clear as to which of these was associated with the QSO. The VLA image at $\lambda 2$ cm presented in Fig. 3.1 confirms the radio structure inferred from the Ooty observations. Now that a good optical position is available (Downes *et al.*, 1986), it is clear that the southern component is the core, and the source is two-sided with a very asymmetric separation ratio. The optical position is also plotted in the figure.

The source is a triple with a steep overall spectrum ($\alpha \sim -0.77 \pm .004$). The projected linear size of the source is ~41 kpc. It is thus a Compact Steep Spectrum (CSS) quasar. (Saikia *et al.* (1987a) discuss it in detail.)

0051+291 : This source was classified as one-sided from the observations of Potash & Wardle (1979). In the VLA B-array image (Fig. 3.2), it still appears one-sided. However, its integrated spectrum (Fig. 3.39) is steep ($\alpha \sim -0.56 \pm .03$), and its projected linear size is ~ 23 kpc; it is thus a CSS source. Swarup *et al.* (1986) discuss further details.

0115+027 : A two-sided source, though with a somewhat asymmetric separation

ratio of 1.4:1 (Fig. 3.3). (Earlier Westerbork observations of Miley & Hartsuijker (1978) did not resolve the western component from the core, and it appeared one-sided. In the VLA image here, there are suggestions of a curving jet towards the eastern component, and the polarization E-vectors appear to be systematically aligned perpendicular to the jet and following the bends in it.

The overall spectrum of the source is steep ($\alpha \sim -0.9 \pm .01$). Using the peak flux densities from this map and the λ20 cm map of Hintzen *et al.* (1983), the spectral index of the nuclear component is ~ -0.08. The VLB Interferometric position measured at 2.29 GHz by Morabito *et al.* (1982) agrees within errors with the photometric position determined by Clements (1983). Wehrle *et al.* (1984) measure a VLBI correlated flux density of 60 ± 10 mJy for the core at 2.3 GHz .

The spectral indices of the western (W1 + W2) and eastern (E1 + E2) components are ~ -1 and -0.8 respectively. The integrated RM of the quasar has been reported to be 9.8 ± 2.4 rad m^{-2} with the intrinsic polarization position angle, ψ, of 8 ± 6 (Tabara & Inoue 1980) and 9 ± 11 rad m^{-2} with ψ of 6 ± 5 (Simard-Normandin *et al.*, 1981a).

0232−042 : This is an asymmetric source where the λ2 cm surface brightness ratio of the outer components is 2.8 and the separation ratio is 3.3 (Fig. 3.4c). The total intensity and polarization maps at λ6 cm are presented in Figs. 3.4a and b respectively. Miley & Hartsuijker (1978) did not separate the eastern component from the core. No evidence is found here or in the λ20 cm VLA map of Hintzen *et al.* (1983) for the component Miley & Hartsuijker (1978) suggested 28 arcsec to

the west. Hintzen *et al.* (1983) have found a bridge of emission connecting the western component to the core.

The overall spectrum of the source is straight below ~ 2 GHz (α = −0.83 ± 0.06); it appears to flatten at higher frequencies. The nuclear component has an α of −0.38 ± 0.06. The VLBI position of Morabito *et al.* (1983) agrees within errors with the optical position of Clements (1983). The QSO is optically variable (e.g., Tritton & Selmes, 1971).

For the extended components, α_{west} ~ −1.05 ± 0.08 and α_{east} ~ −1.0 ± 0.1. The RM of the quasar has been reported to be 4.6 ± 1.2 rad m^{-2} with ψ of 34 ± 3° by Tabara & Inoue (1980) and 5 ± 1 rad m^{-2} at 32 ± 3° by Simard-Normandin *et al.* (1981a). The polarization at 5 GHz integrated over the source gives a PA consistent with the above values, although the PAs for the eastern and western components differ by ~ 40°. The central component is unpolarized.

0241+622 : The radio image of Tzanetakis *et al.* (1978) showed that this nearby x-ray quasar, which is in the Galactic plane (b = 2°.4), has radio emission only on one side of its nucleus. Hutchings *et al.* (1982) confirmed this with better VLA observations at λ6 and 20 cm. The A-array maps at λ20 and 6cm (Figs. 3.5a and b) (though made with a very elongated u-v coverage) confirm the structure reported by Hutchings *et al.* (1982). The B-array observations detect only the nuclear component. Both the overall and the nuclear spectra are flat with α ~ 0.3 ± 0.1. The source has been reported to be a variable at 10.7 GHz (Feldman 1979; Feldman *et al.* 1981). The large range in the flux densities seen wherever multiple

measurements at a single frequency are available also suggests that the quasar is variable. From VLBI observations at 10.7 GHz, Geldzahler & Shaffer (1979) find that ~ 70 per cent of the flux density is from a core of size 0.55 ± 0.1 mas, while the remaining 30 per cent is from a more extended structure of size $\geq$ 26 mas. They remark that interstellar scattering may be affecting the observed angular structure.

The spectral index of the outer component using the measurements below ~ 3 GHz is ~ −0.7 ± 0.2. The 5 GHz flux density of Hutchings *et al.* (1982) and of the present VLA observations appear to have been underestimated.

It must be pointed out that this object is of relatively low radio luminosity, and is detectable at radio wavelengths only because it is nearby. At a higher redshift where quasars usually are, it would have been classified as belonging to the 'radio-quiet' category. Indeed, from spectroscopy and V, B and R band imaging, Romanishin *et al.* (1984) infer that the elliptical nebulosity underlying the QSO is probably a spiral galaxy. (Radio-loud quasars are now believed to reside mostly in elliptical galaxies; e.g., Malkan, 1984; Fried, 1986).

0309+411 : The observations of Kapahi (1979) with the WSRT had shown this source to have a one-sided north-westerly extension to the compact component that was identified with a faint galaxy. Gisler & Miley (1979), from their results at 610 MHz which showed similar structure, suggested that it could be a head-tail source, though unlikely to be associated with the Perseus cluster in whose direction it lies.

While the VLA data with the C-configuration do not show any extension to the

compact source, the B-array observations here barely detect the extension to the north-west at a peak surface brightness level of ~ 7 mJy/beam. O'dea & Owen (1985a) also detected it with the VLA A-array at λ20cm. The position of their peak surface brightness for this component is closer to the core than that of Kapahi (1979), as is that of the B-array image presented here (Fig. 3.6). But this is not necessarily inconsistent since it is clear that this component has a very diffuse structure. Indeed, WSRT observations at 327 MHz by de Bruyn (1985) with very high dynamic range have shown that the radio source is in fact two-sided, with an angular extent of ~ 9 arcminutes.

The overall spectrum of the source is presented in Fig. 3.39. The spectrum is flat/inverted at frequencies $\gtrsim$ 2 GHz and appears to steepen at lower frequencies. This is clearly consistent with the existence of the diffuse extension to the north-west, which is expected to have a very steep spectrum. The spread in the multiple measurements of flux density and also flux density monitoring at 10.8 GHz (Seilstad *et al.* 1983) clearly suggest that the source is variable.

The degree of polarization is similar at λ6 and 2 cm and the measured PAs imply an RM of about −50± 25 rad m^{-2}. The PAs derived by the measurements presented here are not compatible with the value of 83° ± 8° of Simard-Normandin *et al.* (1982) at 10.5 GHz, although the degree of polarization is in agreement. Earlier, Simard-Normandin *et al.* (1981b) had reported a fractional polarization of 6.5 ± 0.6 percent at a PA of 13 ± 2° at 1660 MHz. It seems very likely that the source is also a polarization variable.

The position of the compact radio component measured by VLBI at 2.29 GHz (Morabito *et al.* 1982) coincides with the position of the identified optical object within the errors. Van Breugel *et al.* (1981) measure a correlated flux density of ~ 400 mJy at 5 GHz for the compact component.

0309+411 appears to be associated with a galaxy of apparent magnitude 18^m (and unknown redshift) in the direction of the Perseus cluster (redshift = 0.018). It is not clear if the optical object is physically located in the Perseus cluster or is a background galaxy. It has a structure somewhat suggestive of 'head-tail' morphology. But curiously, most of the flux density is concentrated in the component with flat radio spectrum, which is fairly highly polarized (~ 2 percent at $\lambda 6$ cm) and is variable, probably in both total radio flux density and polarization.

0409+229 : From the displacement inferred between the radio centroids at 2.7 and 8.1 GHz, Potash & Wardle (1979) conjectured that this quasar was one-sided. The VLA A-array images presented here (Fig. 3.7) show that it a triple source with very misaligned extended components. Perley (1982) also found it to be a strongly bent triple.

The overall spectrum is steep up to ~ 1 GHz, and flattens at higher frequencies (Fig. 3.39). The core component spectrum is inverted. With VLBI at 2.29 GHz, Wehrle *et al.* (1984) measured a correlated flux density of 0.21 ± 0.04 Jy for the core component. The associated QSO is extremely red ($\alpha_{optical} \sim -3 \pm 0.5$; Smith & Spinrad 1980). The fractional polarization and its orientation determined here are consistent with the data of Perley (1982) at $\lambda 20$ cm. Simard-Normandin *et al.*

(1981a) report an overall RM of -4 ± 4 rad m^{-2} with ψ of $80° \pm 4°$. Using the same data but assuming a rotation of ~ 180° between the PAs at $\lambda 6$ and $\lambda 21$ cm (which gives a better correlation), Tabara & Inoue (1980) derive an RM of 80 ± 10 rad m^{-2} and a ψ of $36° \pm 14°$. The direction of the source is not one of high RM in the sky (Simard-Normandin & Kronberg, 1980). Observations at closely spaced wavelengths and of similar resolution are required to clarify the ambiguity.

0615+578 : Based on data from Owen *et al.* (1978), this source was tentatively classified by Kapahi (1981a) as of the one-sided type; the radio component coincident with the QSO proposed as the identification had a steep radio spectrum between 2.7 and 8.1 GHz. Subsequently, this and another proposed optical identification (Cohen *et al.*, 1977 and Wills, 1976) have both been found to be stars (Wills & Wills, 1976 and Walsh *et al.*, 1979).

The present image at $\lambda 20$ cm (Fig. 3.8a) clearly shows that the object is a triple source. There is a hint of a jet from the nuclear component to the north-western lobe, visible more clearly in the $\lambda 6$ cm image (Fig. 3.8b). The jet is polarized at $\lambda 6$ cm, and the polarization orientation indicates that the projected magnetic field is aligned along the jet, and then changes into a circumferential configuration at the terminal hot spot. The integrated spectrum of the source is straight with $\alpha \cong -0.87 \pm 0.09$, and the northwest component has an α of -1.2 ± 0.1. It is quite likely that this object is a quasar, though only a deep search for the associated optical object can confirm this.

0717+170 : This source was found to be one-sided by Joshi (1981), and it was included here to confirm or otherwise his tentative suggestion that it is a head-tail source in a cluster. From lunar occultation scans at 327 MHz with the Ooty Radio Telescope, Joshi (1981) concluded that the object has a 'head' (containing ~ 75 percent of the total flux density) and a 'tail' with a weak secondary component at the end. He found a red galaxy close to the 'head' of the source and suggested it as possible identification.

The present data at $\lambda 6$ cm confirm the radio structure of Joshi (1981). But the morphology (Figs. 3.9a and b) is strongly reminiscent of FR Type II objects (Fanaroff & Riley, 1974). The polarization data also suggest that the two outer components represent the lobes of a typical triple radio source. Moreover, the western component has an extremely relaxed structure at $\lambda 2$ cm (Fig. 3.9c) with no evidence of any compact component coincident with the galaxy of 18^m (which is marked in the figure). It must be noted that the signal–to–noise was insufficient to permit self-calibration of the image at $\lambda 2$ cm.

A search near the central component revealed no new candidate for the optical identification above the limit of the Palomar Observatory Sky Survey (POSS) prints. The other galaxies in the field are marked in Fig. 3.9a. It seems likely from the above arguments that the proposed identification of Joshi (1981) is a chance superposition. The source is presently classed as unidentified.

The overall radio spectrum of the source is straight between 80 MHz and 5 GHz (spectral index $\alpha = -0.81 \pm 0.04$). The two-point spectral index for the western component is -0.85 ± 0.05 between 327 and 4885 MHz. Since the south-

west component is very faint at $\lambda 2$ cm, the flux density as determined from the aperture synthesis image is uncertain. Therefore, the derived flux density excess seen relative to the spectrum between 327 and 4885 MHz is unlikely to be significant.

0740+380 : Data at 5 GHz from the Cambridge 5-km telescope (Riley & Pooley, 1975) showed that this quasar had a single outer component, though ~ 100 arcsec away to the south-east. The VLA C-array image at $\lambda 6$ cm shows a similar picture (Fig. 3.10). Wilkinson *et al.* (1974) and Schilizzi *et al.* (1982) showed that the northwestern source was a double at position angle 132°. The map of Cawthorne *et al.* (1986) delineates the nuclear component between the double, which is coincident with the optical QSO. While the double structure *is* oriented towards the southeastern component implying a possible relation between the two, there is no evidence of any emission bridging the two sources in any of the data, nor even in the observations of Conway *et al.* (1983) at 962 MHz with the Jodrell Bank interferometer. It is therefore possible that the two sources are physically distinct objects; indeed, Conway *et al.* (1983) arrived at the same conclusion. A search therefore was made on the POSS prints for a separate optical identification for the southeastern component, but none was found. The accurate QSO position is coincident within errors with the position of the peak at $\lambda 2$ cm (inset, Fig. 3.10).

The spectrum of the "whole" source is straight above 100 MHz with $\alpha = -1.24 \pm 0.02$, but appears to turn over at lower frequencies. The spectrum of the northern triple (the plot is in a separate figure) is also steep

(α = -1.21 ± 0.02). With a VLB Interferometer between Westerbork and Effelsburg, Kapahi & Schilizzi (1979) measured a correlated flux density of 291 mJy at 1417 MHz from the northeastern source, which is ~ 22 percent of its total flux density. But because there is no evidence for the presence of a flat spectrum component in the spectrum of the northeastern source, they concluded that the correlated flux density that they measure is unlikely to come from a nuclear component with flat radio spectrum. If the northeastern source is a separate object, then it would be of projected linear size 14 kpc. This, together with the steep radio spectrum, would imply that it is a CSS source.

Measurements > 2σ among those quoted by Tabara & Inoue (1980) and the VLA data presented here obtain an RM of ~ 30 rad m^{-2} and a ψ of ~ 15°.

0742+376 : This source appears to be one-sided with an angular size of ~ 62 arcsec (Figs. 3.11a, b and c), consistent with the structure reported by Katgert-Merkelijn *et al.* (1980) and Machalski *et al.* (1982). The integrated spectrum is straight (α = -1.0 ± 0.02). The index for the core is ~ 0.1 ± 0.1 between 5 and 15 GHz. The 15 GHz flux density of the western component ($\alpha_{1.4}^{5GHz}$ = -1.2 ± 0.1) is unreliable due to its low brightness. It is interesting that the PA of the $\lambda 6$ cm polarization changes by ~ 70° between components W1 and W2.

Although the northwestern double is aligned with the southwestern component, there is no evidence for any emission connecting them in either the images presented here or the VLA data at 1465 MHz of Machalski *et al.* (1982). However, no optical object was found on the POSS prints at the position of the northwestern

component. It is not clear whether the two components are related.

0814+201 : From lunar occultation data obtained using the Ooty Radio Telescope at 327 MHz, and the Optimum Deconvolution (ODM) algorithm for the deconvolution (Subrahmanya, 1979), Subrahmanya & Gopal-Krishna (1979) inferred that this object, which is in the direction of the Cancer cluster, has a double structure. Although the present VLA observations at $\lambda 20$ and $\lambda 6$ cm detect only an unresolved single component, its position is well within the error window of the *western component* of Subrahmanya & Gopal-Krishna (1979). No images are presented for this object. No radio emission is detected from the region of the eastern component of Subrahmanya & Gopal-Krishna, down to a peak surface brightness of 0.13 mJy/beam and 0.53 mJy/beam at $\lambda 20$ and $\lambda 6$ cm respectively. It is this latter component that was found by them to be identified with a 20^m red object. The unresolved compact source thus remains unidentified (unless it is taken to be related to the weaker object; but the source would then consist of a nuclear component of very steep radio spectrum and an outer component of flat spectrum which is unlikely). Imaging at a low frequency is required to determine the nature of the connection between the two components detected by Subrahmanya & Gopal-Krishna (1979).

The source has an α of $\sim -0.35 \pm 0.06$ (including the fluxes measured by the VLA).

0821+394 : Kapahi (1981b) detected a single secondary component to the south-west of the nuclear component of this object (Westerbork observations at 5 GHz)

and thus classified it as one-sided. Stannard & Neal (1977) had also reported a one-sided structure for this object, though the position of their outer component is ~ 16 arcsec away from that of Kapahi (1981b). They, however, cautioned against possible uncertainties due to the proximity of 0822+394, which is 6.2 arcminutes distant at 60° (Bridle *et al.*, 1972). Potash & Wardle (1979) did not detect the secondary component at either 2.7 or 8.1 GHz. There is no evidence for the presence of the secondary component in the C-array data presented here. At both λ6 and 2 cm, the object appears unresolved. (No image is presented.)

However, the integrated spectrum of the source (Fig. 3.39: only those flux density measurements that are believed to be unaffected by confusion due to 0822+394 are plotted) speaks for there being significant extended emission: there is definite indication of steepening at lower frequencies. Imaging that is sensitive to diffuse radio structure is required to determine the nature of this object. Note that the spread in the flux density measurements at the higher frequencies implies that the source is probably a variable at these frequencies. The VLBI position measured by Morabito *et al.* (1982) coincides within errors with the position of the QSO.

The RM is 14 ± 5 rad m^{-2} with a ψ of 119° ± 7° (Simard-Normandin *et al.*, 1981a). The PAs derived from the present measurements, viz., 116° and 120° at λ2 and 6 cm respectively, are similar to the intrinsic value.

0836+195 : This quasar was believed to be of the one-sided kind from several previous observations (Jenkins *et al.*, 1977; Miley & Hartsuijker, 1978; Subrahmanya & Gopal-Krishna, 1979). It is a triple source (Fig. 3.12a and b) with

a prominent core component and a large surface-brightness ratio for the outer components (23:1 at λ6 cm). The flux density of the south-west component of 7 mJy is consistent with the upper limit of 10 mJy of Miley & Hartsuijker (1978), and is lower than the noise level of Jenkins *et al.* (1977). This component has been missed in the VLA (A-array, λ6 cm) image obtained by Barthel *et al.* (1988) as well. It has possibly been detected by Douglas *et al.* (1980) at 365 MHz; they deduced that the angular size of the source was 28 ± 1 arcsec along a PA of 9° ± 3°, which is in broad agreement with the value of 31 arcsec along a PA of ~ 15° derived from the present measurements.

The overall spectrum of the source is straight (α = −0.94 ± 0.02). The spectral index of the north eastern component appears to be rather steep (~ −1.4) but more accurate flux densities are required to ascertain this. For the nuclear component, α = −0.58 ± 0.07 between 2.7 and 15 GHz.

The RM of the source is 10 ± 1 rad m^{-2}, with a ψ of 98° ± 4° (Simard-Normandin *et al.*, 1981a), which is consistent with the measurements here at λ6 cm. Transatlantic VLBI at 5 GHz (Barthel *et al.*, 1984) detected a faint nucleus with a correlated flux density of $55 \lesssim S_{correlated} \lesssim 70$ mJy.

0919+218 : This quasar has a triple structure (Figs. 3.13a and b), but with a very asymmetric surface brightness ratio for the outer components. For this reason, it [illegible] in the data of Potash & Wardle (1979). Even Hintzen *et al.* (1983), from their λ20 cm VLA image, only tentatively classify it as a triple source. The λ6 cm image clearly shows a jet from the nucleus towards the north

eastern component, with the E-vectors aligned perpendicular to the jet and turning circumferential in the terminal hot spot.

The overall spectrum of the object is steep ($\alpha = -0.88 \pm 0.02$). The nuclear component is weak, and does not flatten the spectrum at higher frequencies. The spectrum of the northeastern component is also steep ($\alpha = -0.90 \pm 0.08$).

0932+022 : The outer components are very asymmetrically located (separation ratio ~ 0.2 (Figs. 3.14a and b). The eastern component was not resolved from the core by Miley & Hartsuijker (1978). On the western side of the nucleus, there is weak component (~ 3.5 arcsec from the core, with $\alpha \sim -1$ and $S_{1413} \sim 9$ mJy) in addition to the normal edge-brightened lobe at ~ 40 arcsec from the core (Hintzen *et al.* (1983); Swarup *et al.*, 1984), which has not been detected in the $\lambda 2$ cm image.

The spectral index of the entire source is -0.78 ± 0.02; the indices for the western and eastern lobes and the core between 1.4 and 15 GHz are -0.99 ± 0.05, -0.76 ± 0.03, and -0.11 ± 0.09 respectively. From long-baseline interferometric observations at Jodrell Bank, Bentley *et al.* (1976) detected a flux density of 150 ± 50 mJy at 1666 MHz from a component of size < 0.1 arcsec. Since both the outer hot spots appear to be resolved by the VLA with a 0.5 arcsec beam at $\lambda 6$ cm (Swarup *et al.*, 1984), this component is possibly the core. Within the quoted errors, its flux density at 1666 MHz is consistent with the core spectrum.

From VLBI observations, Preston *et al.* (1983) quote an upper limit to the correlated flux density of 110 mJy at 2.3 GHz. Barthel *et al.* (1984) measure a

correlated flux density of 90 mJy at 5 GHz from a component of $\lesssim$ 1 mas size.

1007+417 : Though absent from the list of Kapahi (1981a), this source was included here because of the high ratio of the flux densities of the outer components reported by Owen *et al.* (1978). The images are presented in Figs. 3.15a, b and c. Kapahi (1981b) did not detect the component to the north.

The source has a straight spectrum (α = -0.68 ± 0.01). The spectral indices of the northern and southern lobes and the core are -0.51 ± 0.1, -0.72 ± 0.04, and -0.44 ± 0.13 respectively. The presence of the jet (imaged by Owen & Puschell, 1984 and by Saikia *et al.*, 1986) appears to steepen the core's spectrum.

1012+232 : This was classified as one-sided from the observations of Potash & Wardle (1979). Later observations of Hintzen *et al.* (1983) with the VLA at λ20 cm also did not detect the northern outer component of low surface brightness that is seen in the image here at λ20 cm (Fig. 3.16a).

The peak surface brightness of the northern component is comparable to the noise level of the image of Hintzen *et al.* (1983) (10 mJy/beam), while the noise level in the present map is 0.4 mJy/beam. The two data sets are therefore not inconsistent. The source is thus a triple, very asymmetric, with a separation ratio of ~ 2, and surface brightness ratio of ~ 4 at λ20 cm. The northern component remains undetected in the λ6 cm data (Fig. 3.16b).

There are suggestions of the beginnings of a curving jet-like feature that starts out at a position angle of ~ 138° (cf. Fig. 3.16b) and then bends southwards (cf.

Fig. 3.16a). The polarization E-vectors at λ6 cm align perpendicular to the jet structure. The overall spectrum of the quasar is steep at low frequencies ($\lesssim$ 1 GHz) and then flattens towards higher frequencies. The spread in the multiple measurements of flux density that are available at some frequencies suggests that the source is a variable at $\gtrsim$ 1 GHz, and especially at 11 GHz. The nuclear component (α = 0.23 $\pm$ 0.05) has been reported to vary at 8 GHz by Potash & Wardle (1979).

The southern component has a steep spectrum (α = – 0.35 $\pm$ 0.3). The derived flux density of the southern component by both Potash & Wardle (1979) (8 GHz) and the present λ6 cm data appear to be underestimates.

source (– 308 $\pm$ 32 rad m^{-2}), with ψ of 81° $\pm$ 21°. There are no other sources in their list that are local to that region of the sky for which they derive such a large negative RM.

1040+123 : This a very well studied 3CR object (3CR245). It appeared one-sided in the Cambridge 5-km map of Jenkins *et al.* (1977). However, from lunar occultation observations at 240, 408 and 1420 MHz, Lyne (1972) found that there are extended components on both sides of the nuclear component, though very asymmetric in their separation from it (see also Kapahi, 1981a). Indeed, the re-analysis of the data of Jenkins *et al.* (1977) data using the brighter component as the phase reference (Laing, 1981) shows the three components of the source.

The present VLA images at λ20 and 6 cm (VLA A-array: Figs. 3.17a and b)

show the triple source very clearly. The $\lambda 6$ cm image and shows the jet from the nucleus towards the western component (also clearly seen in the MERLIN image by Foley and Davis at 1666 MHz; cited in Hough, 1986). The polarization E-vectors align in the familiar "perpendicular" configuration. The images are consistent with previously published maps of the object (including Davis *et al.*, 1983; Hintzen *et al.*, 1983).

The overall spectrum of the source is steep up to ~ 5 GHz, and flattens out at higher frequencies. Below 5 GHz, α is -0.67 ± 0.002. The western and eastern components have a steep spectrum ($\alpha = -0.95 \pm 0.06$ and -1.2 ± 0.4 respectively). It appears that the 5 GHz flux density determined by the present VLA observations is a gross underestimate.

The multiple flux density measurements available at the same frequency indicate that the nuclear component is variable at frequencies $\gtrsim$ 5 GHz. While Bennett *et al.* (1984) do not classify the object as strongly variable from their monitoring at 5 GHz, Seilstad *et al.* (1983) find a significant variation in 1982 at 10.7 GHz; Wehrle *et al.* (1984) report a change in the correlated flux density measured by VLBI at 2.29 GHz between 1980 and 1982. The variability at 10.8 GHz is associated with structural changes on milliarcsecond scales (Hough 1986). Hough (1986) also cites variability detected at 8 GHz and 15 GHz.

Barthel *et al.* (1984) measured a correlated VLBI flux density of ~ 400 mJy for the milliarcsecond-scale nuclear component, and also detected structure on a scale of ~ 10 mas. The latter was confirmed by the VLBI observations of Hough (1986). From multi-epoch VLBI observations, Hough & Readhead (1988)

derive a superluminal expansion velocity in the nucleus of ~ 3c.

The integrated RM of the object is ~ 30 ± 2 rad m^{-2} with ψ of 22° ± 1°.

1047+096 : This source was suspected to be one-sided from the observations of Miley & Hartsuijker (1978). They suggested (on the basis of evidence they found for a bridge of emission) that the extreme western component, ~ 60 arcsec from the central component was related to it. The present VLA observations clearly indicate that the central component of Miley & Hartsuijker (1978) is itself a triple source with largest angular size of ~ 21 arcsec. Hintzen *et al.* (1983) did not detect the northern lobe of this triple. The flux density of the northern component (Fig. 3.18) measured here is ~ 13 mJy at λ6 cm (with a size of 4.9 ± 3.6 arcsec along a PA of 1°), consistent with its non-detection at 1413 MHz to a limit of ~ 4 mJy/beam by Hintzen *et al.* (1983). The triple in the image of Hintzen *et al.* (1983) shows a curved structure, which is also reflected in the polarization structure imaged here.

There appears to be no evidence for any connecting jet linking the two extreme radio sources in any of the data. In fact, the extreme northwestern component itself appears as a double source (Hintzen *et al.*, 1983). A possible optical identification for this was looked for, but none was found above the limit of the POSS prints. Presently it is suggested that the northwestern source is unrelated to the QSO.

The spectrum of the entire complex appears straight between ~ 16 MHz and 5 GHz (α ~ −0.98 ± 0.03). It presently appears that the flux density of Wardle & Miley (1974) at 8GHz may be an underestimate. A single dish measurement at

15 GHz would be useful to determine if the spectrum flattens at frequencies > 5 GHz. The spectral index of the western (possibly unrelated) source is -0.6 ± 0.1 between 1.4 and 8 GHz, while that of the triple associated with the quasar is -1.02 ± 0.07 between ~ 0.6 and 8 GHz. The flux density of the western source at 610 MHz appears to be overestimated and has not been used in evaluating the spectral index. Barthel *et al.* (1984) report a marginal detection by VLBI, with a correlated flux density of ~ 25 mJy at 5 GHz.

Reliable measurements of the integrated polarization are not available to determine the RM.

1055+201 : This source appears one-sided in the present images (Figs.3.19), and also in the maps of Hintzen *et al.* (1983). There is a suggestion of extended structure on the opposite side of the core from the observations of Douglas *et al.* (1980) at 365 MHz, who find the source to be an asymmetric double with a flux density ratio of ~ 8.5 and largest angular size of ~ 50 arcsec. But the PA of $-78° \pm 2°$ for their model fit is not consistent with the data presented here. That the source is two-sided has now been confirmed (e.g., Hooimeyer *et al.* 1987).

The integrated spectrum of the source is straight below ~ 1 GHz ($\alpha = -0.69 \pm 0.02$) but flattens at higher frequencies. The spectral index of the extended component is -0.76 ± 0.04 between 1.4 and 15 GHz. The core has an inverted spectrum ($\alpha = 0.52 \pm 0.12$) between 1.4 and 15 GHz. The present VLA measurement of the flux density of the core is higher that that of Miley & Hartsuijker (1978) at the same frequency by ~ 60 per cent, suggesting that the core

may be variable. The position of the milliarcsecond-scale nuclear component at 2.29 GHz determined by Morabito *et al.* (1982) is consistent with the position of the QSO within errors. Barthel et al. (1984) measure a correlated flux density of 950 mJy at 5 GHz with VLBI. Hooimeyer *et al.* (1987) infer the structure of the nuclear component on milliarcsecond scales to be one-sided, pointing towards the larger structure.

The source has an RM of -22.8 ± 2.2 rad m^{-2} and ψ of $123° \pm 5°$ (Tabara & Inoue, 1980). The PA derived here at $\lambda 6$ cm is consistent with this value.

1055+018 : Lunar occultation observations with the Ooty Radio Telescope at 327 MHz (Singal *et al.*, 1979) implied a double structure for this source, with a separation of ~ 1.5 arcsec and flux density ratio of 1:3 and with the QSO proposed as identified with the brighter component. (It may be worth noting that the object is in the direction of the Abell cluster 1139 (Owen *et al.*, 1982). Perley (1982) detected an outer component at $\lambda 20$ cm, but this is 4 arcsec away from the nucleus. The present observations do not detect any extended structure to the quasar, either at $\lambda 6$ or at $\lambda 2$ cm. However, Wardle *et al.* (1981) find evidence for a "halo"-like structure of size ~ 11 arcsec around the compact object at 2.7 GHz, and VLA imaging by Browne & Perley (1986) at $\lambda 6/20$ cm shows that the object has emission on *both* sides of the nucleus, with a largest angular size of 29 arcsec and surface brightness ratio of ~ 2. The object is an inter-planetary scintillator at 327 MHz (Banhatti *et al.*, 1983)

The overall spectrum of the object (Fig. 3.39) is flat. A linear fit to the quasi-

simultaneous flux density measurements of Owen *et al.* (1980) which are marked by open circles in the figure, gives an α of -0.17 ± 0.01. The variability of the object is well established at both high frequencies (Medd *et al.*, 1972; Dent *et al.*, 1974; Bennett *et al.*, 1984) and low frequencies (Fanti *et al.*, 1981; Spangler & Cotton, 1981). The correlated VLBI flux has also been found to vary (Wehrle *et al.* 1984). Further, Slee (1984) observed an extremely strong outburst at 80 and 160 MHz, which is poorly understood. Gopal-Krishna *et al.* (1984) argue that it is very unlikely that slow interstellar scintillations are causing this outburst, and that if it is due to relativistic beaming, singularly large Doppler factors are implied. VLBI imaging at 1.667 GHz has shown milliarcsecond-scale extensions to the north west and north east (Romney *et al.* 1984). Two-epoch VLBI observations have led Padrielli *et al.* (1986) to conclude that, while marginally significant size variations occur on milliarcsecond scales, the expansion rate predicted by the relativistic beaming model for the low frequency variability is too low to be measured with their resolutions.

The polarization of the nuclear component measured here at $\lambda 6$ and 2 cm is consistent with the measurements of Rudnick *et al.* (1985). The fractional polarization at $\lambda 6$ cm is twice that measured by Perley (1982). The latter values are, however, consistent with those of de Pater & Weiler (1982). The integrated RM of Simard-Normandin *et al.* (1981a) is -45 ± 1 rad m^{-2} with ψ of $124° \pm 1°$.

1132+303 : This is a triple source but with a very asymmetric surface brightness ratio (Figs 3.20a and b). Potash & Wardle (1979) missed the fainter northwestern

component, and the source was therefore designated as one-sided. A jet extends out from the central component towards the brighter southwestern lobe. The overall spectrum of the quasar is steep ($\alpha = -0.94 \pm 0.01$). The northwestern and southeastern components also have steep spectral indices of -0.99 ± 0.1 and -1.2 ± 0.1 respectively.

the earlier data of Miley & Hartsuijker (1978). This is almost so even in the B-array image presented here (Fig. 3.21a). But the A-array images at λ20 and 6cm (Fig. 3.21b and c) clearly show both the outer components with a separation ratio of 1.7:1. In the northwestern component, the polarization data suggest a highly ordered magnetic field along its elongation. The largest angular size measured here

& Moffet (1971) at λ21cm, by MacDonald & Miley (1971) or by Wilkinson *et al.* (1974) at λ11cm.

The position of the VLBI component detected by Morabito *et al.* (1982) agrees with that of the QSO. The integrated spectrum of the source is straight ($\alpha = -0.7 \pm 0.03$). The spread in the total flux density values at 10 GHz suggests that the source may be variable at this frequency. The total flux density at λ6 cm

al. (1981) suggesting that the source might be variable at 5 GHz as well. The RM has been found to be $\sim -25.6 \pm 2.1$ rad m^{-2} with ψ of $49° \pm 5°$ by Tabara & Inoue (1980) and -26 ± 1 rad m^{-2} with ψ of $51° \pm 2°$ by Simard-Normandin *et al.* (1981a).

1203+109 : Miley & Hartsuijker (1978) found an outer component of 8 mJy and a core component of 149 mJy at 5 GHz (the latter being associated with the QSO). It appears from the present observations (Figs 3.22a and b) and also the image of Hintzen *et al.* (1983) at λ20cm that this 'core' component is a triple source of rather complex structure. No component appears at the position of the outer component of Miley & Hartsuijker (1978) either in the image of Hintzen *et al.* (1983) or in the present observations. The polarization E-vectors in the jet are aligned perpendicular to it and bend with it.

Barthel *et al.* (1984) detect a correlated flux density of 50 mJy at GHz with European VLBI, possibly from a milliarcsecond-scale core. The overall spectrum of the source is steep ($\alpha = -0.77 \pm 0.02$). The southern component has an α of $\sim -1.3 \pm 0.1$. The resolution of the image at λ20cm here or in Hintzen *et al.* (1983) is insufficient to delineate the other component, so no spectrum has been determined.

1222+216 : The early observations of MacDonald & Miley (1971), Miley & Hartsuijker (1978) and Potash & Wardle (1979) did not detect the second outer component of low surface brightness. This component is severely misaligned with respect to the jet that extends to the eastern outer component (Figs. 3.23a and b). Note that the southern outer component in the B-array image is ~ 17 times the noise level in the image. The A-array image shows the curved jet with the aligned polarization E-vectors also curving.

Multiple flux density measurements at 5 GHz suggest that the source is

variable. VLBI on the core at 5 GHz (Barthel *et al.*, 1984) shows a component of size < 1 mas with a flux density of ~ 600 mJy. Hooimeyer *et al.* (1987) report a one-sided milliarcsecond scale structure that is extended in the direction of the outer lobe. The total spectrum of the source is straight (α = –0.55 ± 0.02). α is –0.94 ± 0.11 for the southern component and –0.5 ± 0.2 for the eastern component.

1320+299 : This radio source is associated with a quasar of 20th magnitude. It was first mapped at radio wavelengths using the Westerbork Synthesis Radio Telescope (Fanti *et al.* 1977, Fanti *et al.*, 1979a) at λ20 and 6cm. The object showed a very peculiar one-sided structure: two components (B and C) on the same side of the component coincident with the quasar (A) and at separations ~ 25 and 50 arcsec respectively from A. It was one of the most extended among the then known one-sided sources (Kapahi, 1981a).

Feretti *et al.* (1982) confirmed the one-sidedness using the WSRT, and showed steepening of the radio spectral index outwards from component A. The orientation of the magnetic field (as inferred from the polarization orientation—the deduced value of the external RM was low) was found to differ significantly from one component to another. Applying the model of Burn (1966), they inferred from the fractional polarization values that the magnetic field in all the three components was rather irregular. Further, from a comparison of its optical images on the POSS print and a Palomar plate taken by Bracessi in 1967, they inferred that the nuclear component was variable in the optical. The source did seem a typical one-sided quasar in that it had a very prominent nuclear component and optical variability.

But given its inferred size (largest angular size = 50 arcsec), Feretti *et al.* (1982) concluded that relativistic effects were unlikely to be the cause of the asymmetry.

The VLA radio images made here are presented in Figs. 3.24a to g. There is no emission connecting the three well separated components. Component A has a one-sided radio structure with a prominent core. The spectral index is -0.42 ± 0.05. Clearly, there is very little depolarization for component A. The RM is also low ($\sim$ 5 rad m^{-2}). Component B has an interesting asymmetric structure, with a high brightness 'head', and a 'tail' bending towards the north-east and extending to $\sim$ 3 arcsec. The polarization at λ6 cm appears to be perpendicular to the elongation and follows the bend in the structure. There appears to be considerable depolarization between λ6 and 20 cm. Component C shows a slight extension towards the north-west. No significant depolarization is indicated. The RM inferred from the λ20cm (A-array) and λ6 cm (B-array) data is $\sim$ 5 rad m^{-2}.

The spectra of components A, B, and C are shown in Fig.3.39. The spectral indices of the components have been evaluated using the lowest resolution VLA images at λ20, 6 and 2cm. Component A has a flat spectrum while B and C have steep spectra.

A CCD image of the field of 1320+299 (3.2 arcmin x 1.9arcmin) was obtained at the f/15 Cassegrain focus of the 1.0m Jacobus Kapteyn Telescope, La Palma on August 3, 1986 (Fig. 3.24h). A 1500 second exposure was taken through an R band interference filter. The seeing was $\sim$ 1 arcsec, and the zenith extinction coefficient 0.11 mag. R magnitude of the QSO is 19.95. Any other object that might be coincident with or be in between radio components B and C has an R

magnitude fainter than 21.5 mag (which is five times the r.m.s. of the image).

Are the three components A, B and C physically related and part of the same object? The probability of three unrelated sources so aligned by chance is extremely low, but there is no evidence from the radio data alone of any physical association. Component A has a radio structure that is typical of core-dominated radio quasars mapped with limited dynamic range, and its QSO might even be a variable. Although component B is reminiscent of low radio luminosity 'head-tail' sources usually found in clusters of galaxies, since any associated galaxy is fainter than 21.5 mag and hence would certainly be further than redshift ~ 0.5, the implied radio luminosity is very high for a head-tail source (cf. O'dea & Owen 1985b). On the other hand, B and C could be the outer components of a single radio source.

1347+539 : Owen *et al.* (1978) detected a marginally resolved component with a flux density of 50 ± 18 mJy at 2695 MHz at a distance of ~ 31 arcsec from the core of this quasar, which suggested a possible one-sided structure. The present observations do not detect this component to a limit of ~ 1.8mJy/beam with a beam of ~ 4.9 x 3.8 arcsec. Recent VLA observations with the A-array at λ6 cm (Perley, 1982); Owen & Puschell, 1984) show one-sided emission extending up to ~ 5 arcsec to the north west of the core. They do not detect any component at the position of the outer component of Owen *et al.* (1978).

The overall spectrum of the quasar is flat at high frequencies and shows signs of steepening at low frequencies. The source appears to vary at 10.8 GHz (Seilstad *et al.*, 1983). The position of the nuclear component detected by VLBI at 2.29 GHz

agrees well with that of the QSO.

1354+195 : This is a core dominated triple source (Figs. 3.25a and b). The jet towards the southern component that is suggested in the figures is seen clearly in the λ18cm image of Rusk & Rusk (1986). The outer components are asymmetrically located (separation ratio = 1.8). The southeastern component was not detected by Miley & Hartsuijker (1978) and MacDonald & Miley (1971), and the quasar was thereby was included in the list of Kapahi (1981a). The A-array observations of Perley (1982) also missed the southern component.

The quasar has long been known to be radio variable (Medd *et al.*, 1972; Altschuler & Wardle; 1976). Kesteven *et al.* (1976) and Wardle *et al.* (1981) found it to variable at 2.7 GHz, while monitoring by Bennett *et al.*, 1984 showed mild variability at 5 GHz. The optical QSO is also known to be mildly variable (Pica *et al.*, 1980). VLBI observations at 10.7 GHz (Marscher & Broderick, 1983) indicate extensions of up to ~ 7 mas. The most compact structure is an equal double (separation ~ 0.75 mas) along a PA of 151°, close to the axis of the entire source.

From transatlantic VLBI at 5 GHz, Zensus *et al.* (1984) find 53 percent of the total flux density in a compact component of size ~ 0.5 mas. U.S. VLBI at 5 GHz by Rusk & Rusk (1986) shows a milliarcsecond secondary component ~ 8 arcsec southeast of the brighter compact component.

The radio spectrum is steep below 2 GHz ($\alpha = -0.65 \pm 0.04$) but flattens above it. If the weaker component detected by Wilkinson *et al.* (1974) is assumed to be the core, then the core spectrum turns over around 1-2 GHz. The spectral

index of the north-west component is -1.04 ± 0.05.

The reported RMs of this source are 4.2 ± 0.8 rad m^{-2} with ψ of $72° \pm 1°$ (Tabara & Inoue, 1980) and 5 ± 1 rad m^{-2} with ψ $69° \pm 2°$ (Simard-Normandin *et al.*, 1981a). The polarization orientations obtained here are consistent with these values.

1415+463 : Kapahi (1981b) found this to one-sided. The model fit of Owen *et al.*(1978) had indicated that the nuclear component was a double at 2.7 GHz. The present data (Figs 3.26a and b) do not corroborate this, nor do subsequent published data (Perley, 1982); Perley *et al.*, 1982; Owen & Puschell, 1984); the quasar still appears one-sided. Imaging with better sensitivity is needed to detect any jet from the core component towards the western double. There is mild suggestion of it in the λ20cm image here and also in the polarization data of Owen & Puschell (1984).

The nuclear component appears to be mildly variable at frequencies $\geq$ 1 GHz. Monitoring at 10.8 GHz does indicate variability (Seilstad *et al.*, 1983). The overall spectrum is flat with signs of steepening at frequencies lower than ~ 2 GHz. The spectrum of the nuclear component appears to turn over at ~ 3 GHz. The spectrum of the western double is steep with an index of -0.88 ± 0.08. With VLBI at 2.29 GHz, Morabito *et al.* (1982) detect a milliarcsecond component which agrees well in position with that of the QSO.

1419+315 : Fanti *et al.* (1977) and Fanti *et al.* (1979a) first suggested that this quasar was one-sided. While the core component appeared resolved in their observations, the outer component located ~ 130 arcsec to the south-east appeared

unresolved. In the present observations (VLA C-array: Fig. 3.27a, b and c), the S-E component still appears unresolved, but the core component is resolved into three components misaligned by about 80°. The quasar is coincident with the central one of the three, which is also the most weakly polarized and has a flat spectrum ($\alpha \sim -0.31 \pm 0.11$). The polarization E-vectors appear to follow the bends in the overall structure.

The spectral index of the northern triple is -0.6 ± 0.1 between 1.4 and 15 GHz. The spectrum of the entire complex appears straight between 178 and 5000 MHz with $\alpha \sim -0.69 \pm 0.04$. The monitoring of Seilstad *et al.* (1983) did not show any variability of the quasar at 10.8 GHz between 1979 and 1982. (See Saikia *et al.*, 1987b for a detailed study.)

There is no evidence in any of the data for any emission linking the northern triple with the southern component, and an examination of the POSS prints showed no possible identification. It is presently suggested that the two are unrelated objects. It has a steep radio spectrum ($\alpha = -0.8 \pm 0.1$ between 1.4 and 5 GHz) and is probably a CSS object.

1433+177 : This quasar is a slightly misaligned triple source (misalignment angle of ~ 20°) with a highly asymmetric surface brightness ratio of ~ 8:1 (Figs. 3.28a and b). The weak and fairly diffuse northern component that also appears in the map of Hintzen *et al.* (1983) was not detected by the earlier observations of Wills (1979), and therefore the source was categorized as of the one-sided kind. Hintzen *et al.* (1983) also detected possible further emission trails to the north.

The presence of a jet that is suggested by the polarization in the B-array image is clearly manifest in the A-array $\lambda 6$ cm image (Fig. 3.28b). This image also reveals a highly polarized extension to the compact core which is unresolved by the B-array map.

The source has a steep overall spectrum with index $\alpha \sim -0.7 \pm 0.01$ below ~ 1 GHz but flattens at higher frequencies. The spectrum of the core component appears to turn over at ~ 2 GHz. The core flux density plotted at 2.7 GHz (Wills, 1979) is probably dominated by emission from the extension to the core referred to above. The northern and southern components have steep spectra ($\alpha = -0.7 \pm 0.1$ and -0.8 ± 0.1 respectively).

1509+158 : This quasar appeared one-sided in the observations of Wills (1979), but this has turned out to be due to the very asymmetric separation ratio of its outer components. The eastern component that is coincident with the QSO appears to have extensions in both the image (Figs. 3.29a, b and c), and the two-sided nature of the source is explicit in the A-array image at $\lambda 6$ cm.; it reveals a compact component coincident with the QSO, well separated from the eastern lobe.

The westward extension to the eastern component in the lower resolution images and in the orientation pattern of the polarization suggests the presence of a jet connecting the two components. This is manifest in the A-array image, though at a low surface brightness level.

The source has a steep overall spectrum ($\alpha = -0.83 \pm 0.05$). The eastern and western components have more or less steep spectra above ~ 1 GHz

(α = −0.6 ± 0.1 and ~ −0.8 ± 0.1 respectively).

1547+309 : The map of Rudnick & Adams (1979) at 8 GHz showed this object to be a connected double source with a galaxy coincident with the northwestern component. Katgert-Merkelijn *et al.* (1980) also found a similar structure with the WSRT at 5 GHz. The object was therefore classified as one-sided.

The source has a steep spectrum (α = −0.97 ± 0.01). The VLA B-array image from the present observations (Fig. 3.30) clearly shows a typical edge-brightened triple morphology. It is therefore presently suggested that the optical identification is a chance association. (See Saikia *et al.* (1986) for details.)

1636+473 : The observations of Kapahi (1981b) first showed this source to be one-sided. The lobe to the north of the core component (Figs. 3.31a, b and c) is quite odd; it is elongated along an axis that is at ~ 70° to the line joining the core and the lobe's eastern peak. An image with MERLIN at better resolution is presented by Browne *et al.* (1982a) and Wilkinson (1982). The data of Perley (1982) and Perley *et al.* (1982) are consistent with all of the above. A map at 2.7 GHz with the Cambridge 5-km telescope by Pooley has also been quoted as having the same general features (Browne *et al.* 1982a).

The northern lobe appears somewhat similar to a normal double/triple radio source. An optical identification for it was therefore looked for on the POSS prints, but no likely candidates were found. It is interesting that from VLBI observations Porcas (personal communication) finds the core to be extended by ~ 0.5 mas in the north-south direction.

The position of the milliarcsecond core component detected by Morabito *et al.* (1982) with VLBI at 2.29 GHz agrees well with that of the QSO. The overall spectrum of the source flattens at high frequencies and possibly rises above ~ 10 GHz. Although the 90 GHz datum has large errors it shows that the spectrum must steepen again between 10 and 90 GHz. While the spectrum of the core appears to be curved, that of the extended emission is straight between 408 MHz and 15 GHz ($\alpha = -0.72 \pm 0.03$). The source is a variable at 10.8 GHz (Seilstad *et al.*, 1983). The PAs in the core are similar at $\lambda 6$ and 2cm. Assuming Faraday rotation to be small at $\lambda 6$ cm, the projected magnetic field of the extended component would be along its axis.

1637+574 : Observations with the NRAO interferometer at $\lambda 11$cm showed that this quasar consists of a core and a secondary component at a separation of ~ 9 arcsec towards the south-west (Owen *et al.*, 1978). This secondary component is not found in the present observations (Figs. 3.32). However, there is evidence for weak extended emission towards the north and north-west. This structure is consistent with the observations of Perley (1982) and Rudnick & Jones (1983).

The quasar has a complex spectrum. There is a large spread in the flux density values where multiple measurements are available, indicating that the source is definitely variable. (Seilstad *et al.* (1983) have detected variability at 10.8 GHz.) From VLBI observations at 5 GHz, Pearson & Readhead (1981) find the core flux density to be ~ 810 mJy. Morabito *et al.* (1982) measured a VLBI position for the milliarcsecond component that agrees well with that of the QSO. The spectral index derived from a straight fit to the quasi-simultaneous flux density measurements of

Landau *et al.* (1986) is 0.03 ± 0.004.

From their VLA observations at λ18 and 20cm, Rudnick & Jones (1983) find the RM of the compact component to be 22 ± 42 rad m^{-2}. Using their VLA measurements at λ6 and 2cm as well, the RM is 13 ± 5 rad m^{-2}.

1729+501 : This object was first shown to be one-sided by Owen *et al.*(1978). No second outer component has been detected in the images given here (Figs. 3.33a, b and c). The quasar has a relatively weak core component contributing only ~ 10 percent of the total flux density at λ6 cm. Hintzen *et al.* (1983) and Owen & Puschell (1984) also find the source to be one-sided from VLA observations at λ20 and 6cm respectively.

The core spectrum appears to flatten below ~ 5 GHz. The integrated spectrum appears straight between 26 MHz and 15 GHz (α = −0.73 ± 0.03). The 26 MHz flux density has been estimated by subtracting the extrapolated flux density of the confusing source, 1729+491 (4C 49.29). For the extended component to the east, α is −0.73 ± 0.03 between 1.4 and 15 GHz.

1741+279 : The southern outer component of low surface brightness was missed in the earlier observations of Potash & Wardle (1979), and the source was therefore included in the list of Kapahi (1981a). The present A-array image at λ6 cm (Fig. 3.34) shows the two (slightly non-collinear) outer components to the north and south of the nucleus. The surface brightness ratio is ~ 6:1 at λ6 cm. The image here also shows a jet extending from the nucleus to the outer component.

The source has a steep overall spectrum (α = −0.63 ± 0.02). Spangler & Cotton (1981) tentatively suggest that it may be a low frequency variable, though they remark that it is singular in having a steep overall radio spectrum to boot.

Using data from Hintzen *et al.* (1983), the spectral indices of the northern and southern components are −0.69 ± 0.11 and −0.81 ± 0.11 respectively. The nucleus is not delineated well enough there to permit determination of its spectrum.

1842+681 : This quasar appears to have a faint one-sided extension to the north-west at λ20cm (Fig. 3.35). Only the nuclear component is detected at λ6 cm. No image is therefore presented. Owen *et al.*(1978) had found a secondary component to north of the core at λ11cm.

The overall spectrum of the quasar is complex. A straight fit gives an index of 0.08 ± 0.01. The spread in the flux density values suggests that the source is variable. Kapahi (1981b) measured a change of ~ 30 percent in the flux density at 5 GHz over ~ 3 months. It is also variable at 10.8 GHz (Seilstad *et al.*, 1983).

The spectrum of the nuclear component as derived from the peak surface brightness values of the present VLA images is inverted (α = 0.45 ± 0.08). The position of the compact component detected by Morabito *et al.* (1982) with VLBI at 2.29 GHz agrees with that of the QSO.

2041−149 : The lunar occultation observations of Singal *et al.* (1979) detected two components at 327 MHz, one of which was coincident with a red object on the POSS plates. The structure obtained by the present maps at λ6 and 20cm (Figs 3.36a and b), broadly confirm this. However, the more detailed morphology

(particularly at λ20cm) is strongly reminiscent of a double radio source with a weak, undetected core. Both the components have steep spectra (α is -0.94 ± 0.1 and -0.98 ± 0.003 for the western and eastern components respectively) and the λ20cm image shows a bridge of emission between them. The source as a whole has an α of -0.94 ± 0.02. It is possible that the coincidence between the western component and the red object is by chance. The POSS plates were searched for an object in between the two radio components, but none was found.

A deep optical observation, as also more sensitive radio observations at high frequencies that might reveal a possible core, would be of interest. In any case, the source cannot really be classed as "one-sided" since the component coincident with the supposed optical identification is not of flat spectrum.

2251+134 : Perley (1982) has shown this to be a triple source. The maps presented in Fig. 3.37 confirm this. Wills (1979) had detected two components for this source, one coincident with the QSO and the other to the north west at a position angle of ~ 40°. This had led to its inclusion in the list of Kapahi (1981a). But the northwestern component has not been detected in the maps presented here, nor by Perley (1982).

The source has a separation ratio of ~ 1.6:1. Both the total intensity distribution and the polarization pattern at λ6 cm suggest a curved jet bridging the core and the southern component.

Morabito *et al.* (1982) measured a position for a milliarcsecond-scale component with VLBI AT 2.29 GHz that agrees with that of the QSO. Hooimeyer

et al. (1987) have determined the milliarcsecond-scale structure at 5 GHz, and find a one-sided extension that points to the outer lobe.

The source has a steep spectrum below ~ 5 GHz (α = −0.6 ± 0.03) which appears to flatten slightly at higher frequencies. The nuclear component appears to have a flat spectrum (α = 0.03 ± 0.06).

2325+269 : This quasar was included here because though Potash & Wardle (1979) found it to be two-sided, Miley & Hartsuijker (1978) and Katgert-Merkelijn *et al.* (1980) found only one-sided extensions to the component coincident with the optical QSO. The images shown here (Fig. 3.38) confirm its triple structure (though the positions of the surface brightness peaks of each component are systematically displaced by 1-2 arcsec from those of Potash & Wardle (1979) at 8 GHz).

The overall spectrum of the source is steep (α = −0.83 ± 0.02). The outer components have surface brightness ratio of ~ 9:1 at λ6 cm. They appear to be linked to the core by curved bridges in an overall S-shaped structure. The polarization patterns also suggest the presence of a curved jet.

3.4 Summary

Of the 42 objects observed with the VLA, for three of the objects (0717+170, 1547+309 and 2041−149) the new observations suggest that the sources have a triple structure and the optical identification is probably incorrect: the radio component coincident with the proposed identification is probably a chance coincidence. For 0615+578, and 0814+201, the optical identification has been found

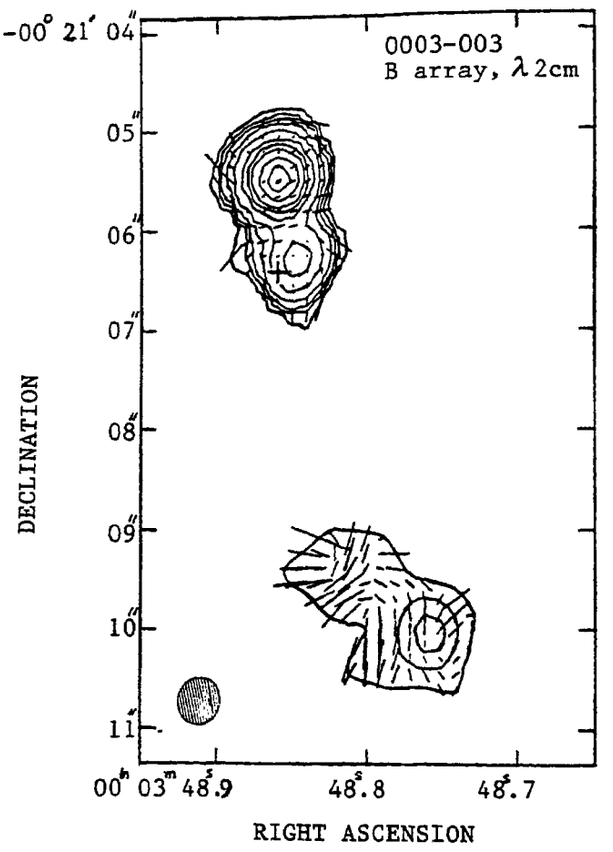

Fig. 3.1 Contour levels: 3.6 x (-1, 1, 2, 3, 5, 10, 20, 30, 40, 60, 80) mJy/beam. Polarization: 1 arcsec = 1.25 ratio.

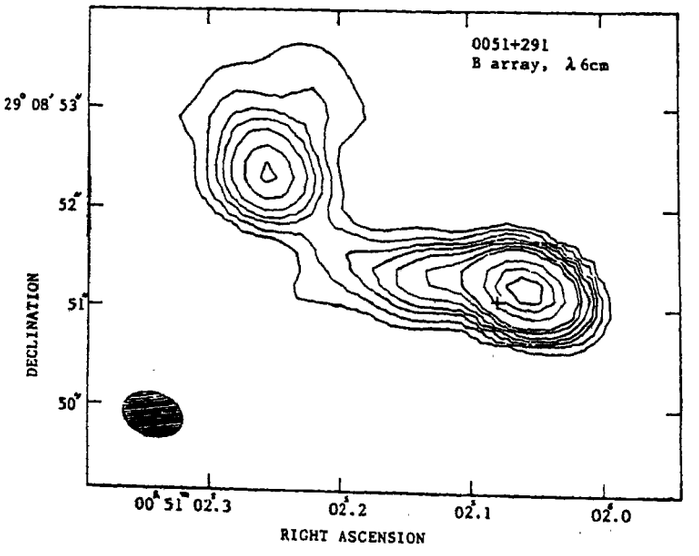

Fig. 3.2. Contour levels: 1.4 x (-1.5, 1.5, 3, 5, 7, 10, 15, 20, 40, 60, 80) mJy/beam.

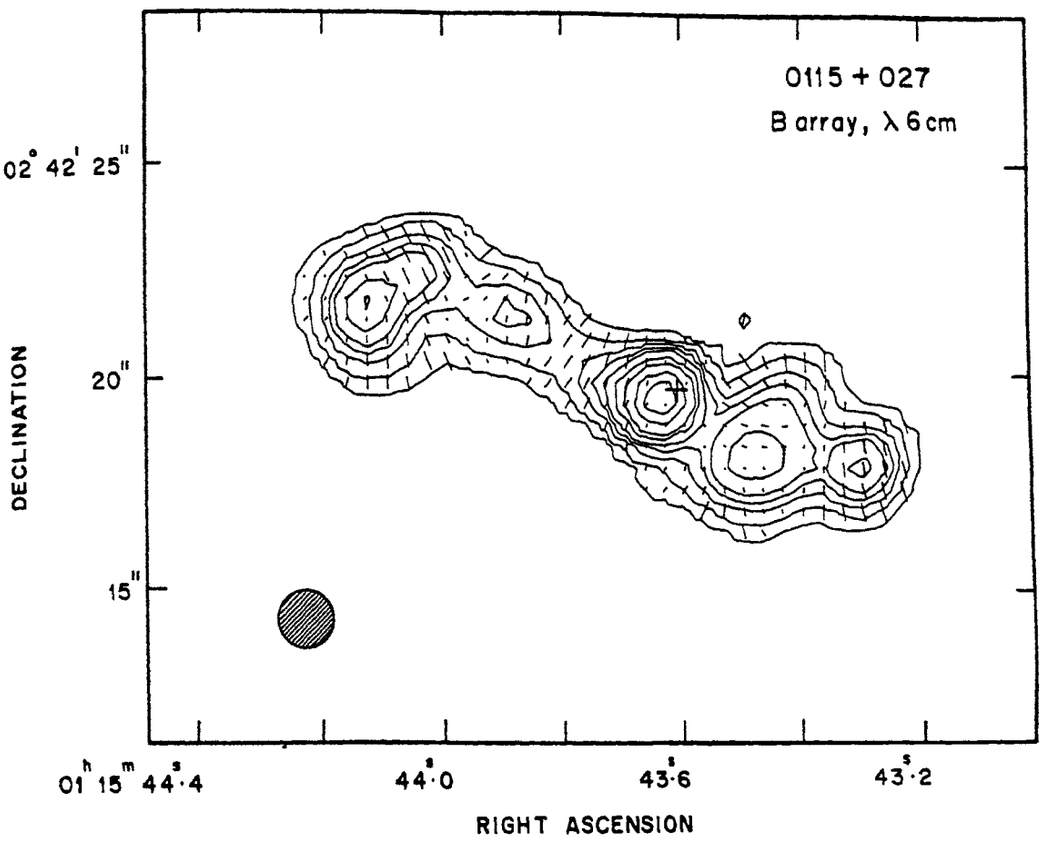

Fig. 3.3 Contour levels: 1.4 x (-2, 2, 5, 10, 15, 20, 30, 40, 60, 80)mJy/beam. Polarization: 1 arcsec = 0.468 ratio.

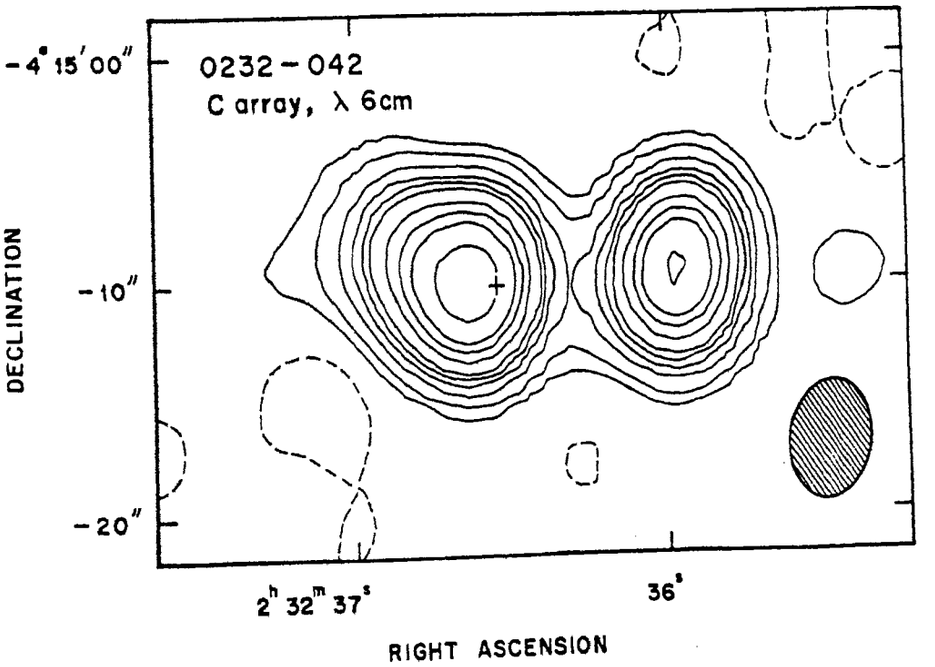

Fig. 3.4a. 230 x (-0.04, -0.02, 0.02, 0.04, 0.08, 0.12, 0.16, 0.2, 0.3, 0.4, 0.5, 0.75) mJy/beam.

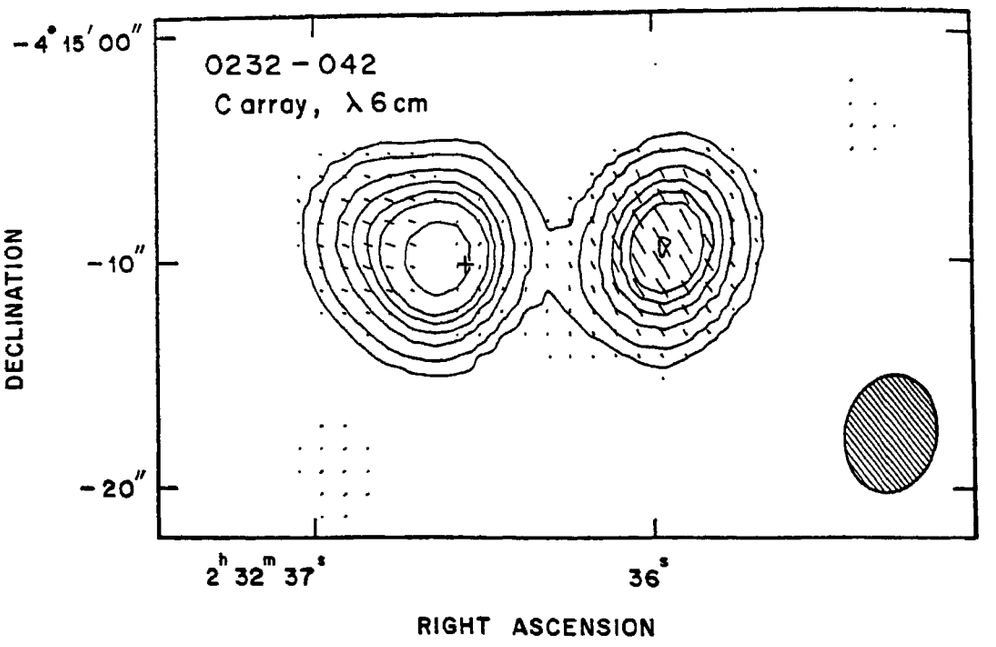

Fig. 3.4b. Contour levels: 240 x (-0.01, -0.05, 0.05, 0.1, 0.2, 0.3, 0.4, 0.5, 0.75) mJy/beam.

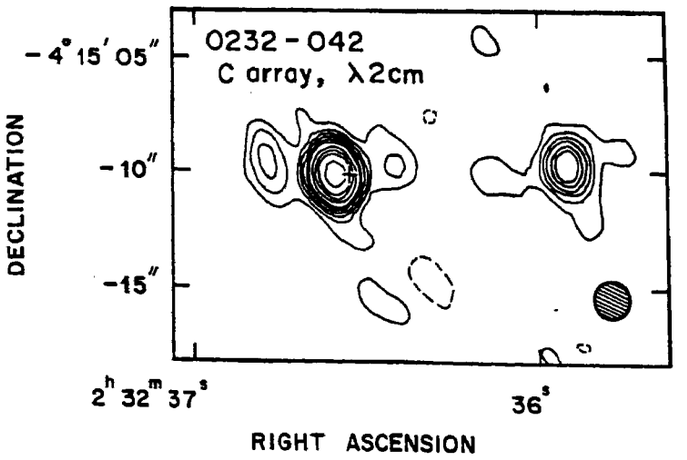

Fig. 3.4c. Contour levels: 121 x (-0.06, -0.03, 0.03, 0.06, 0.09, 0.12, 0.16, 0.2, 0.3, 0.4, 0.5, 0.75) mJy/beam.

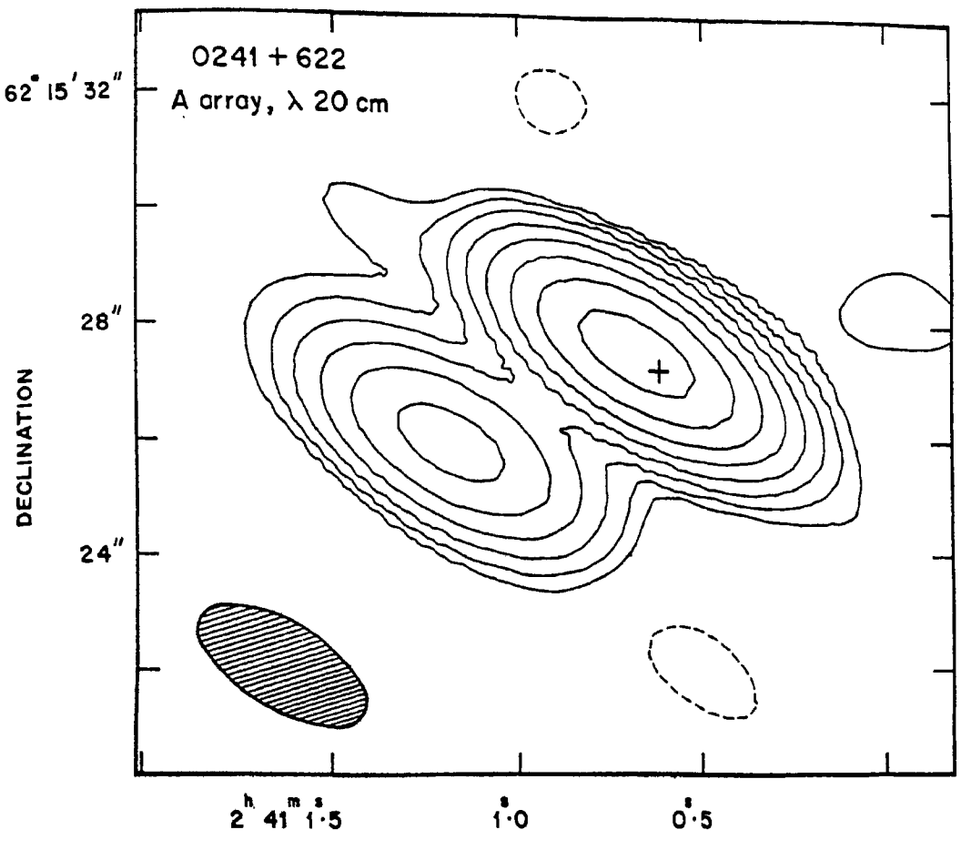

Fig.3.5a. Contour levels: 1 x (-4, -2, -1, 1, 2, 4, 8, 16, 32, 64, 128, 256, 512, 1024, 2048) mJy/beam. Polarization: 1 arcsec = 0.081 ratio.

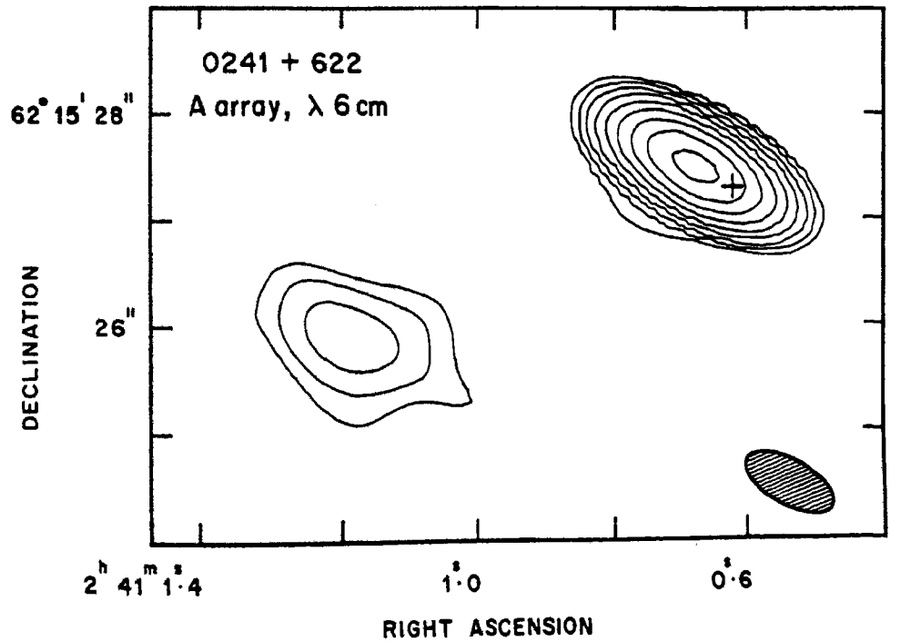

Fig.3.5b. Contour levels: 1 x (-4, -2, -1, 1, 2, 4, 8, 16, 32, 64, 128, 256, 512, 1024, 2048) mJy/beam. Polarization: 1 arcsec = 0.269 ratio.

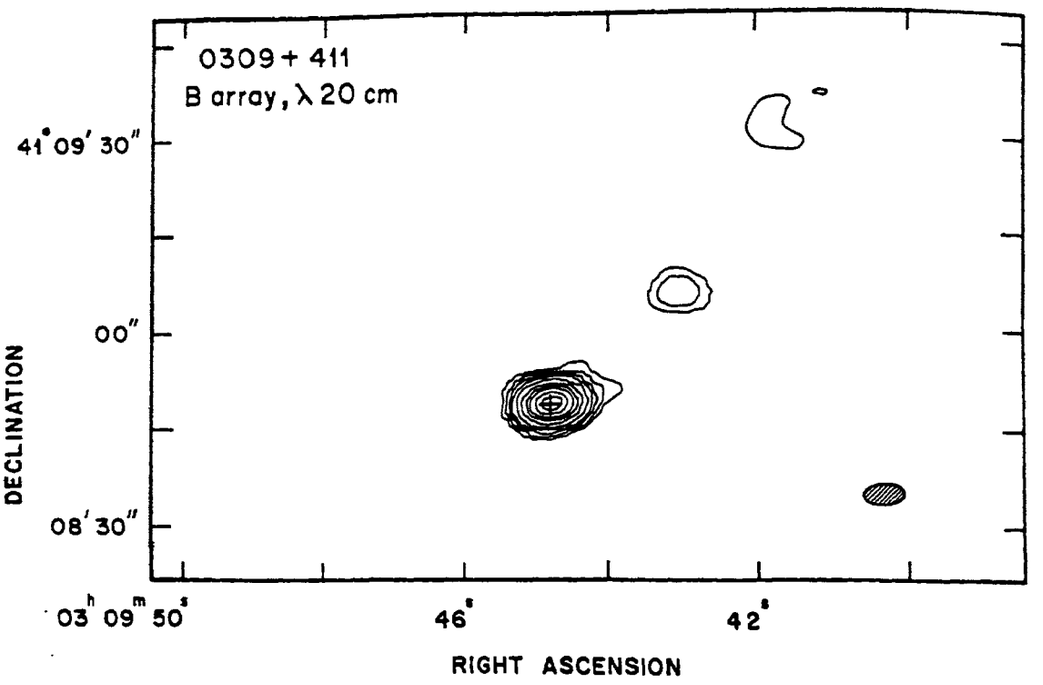

Fig. 3.6. Contour levels: 2.7 x (-0.8, 0.8, 1.5, 3, 5, 10, 20, 40, 60 80) mJy/beam.

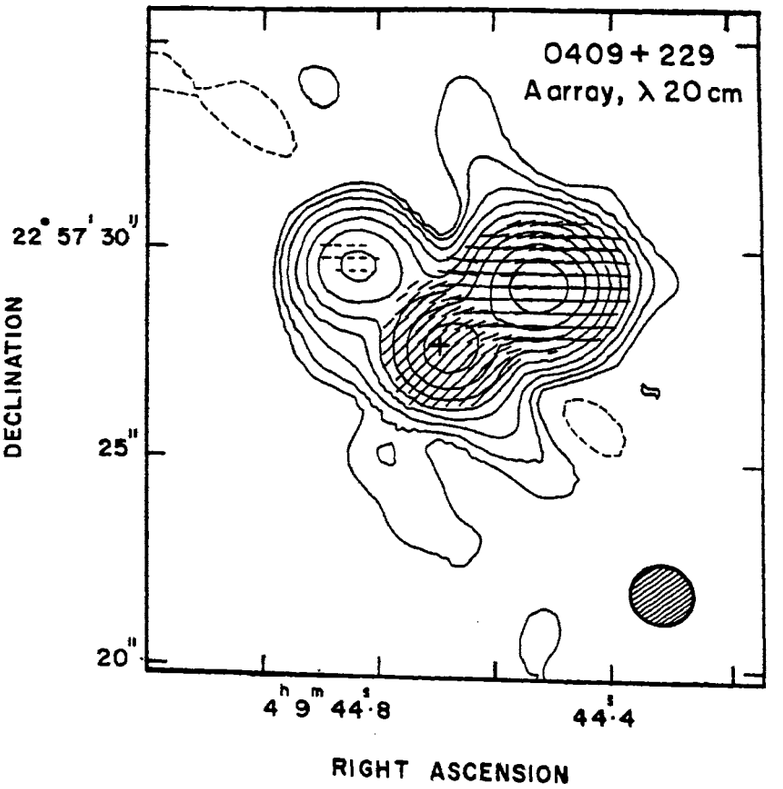

Fig. 3.7. Contour levels: 1 x (-4, -2, -1, 1, 2, 4, 8, 16, 32, 64, 128, 256, 512, 1024, 2048) mJy/beam. Polarization: 1 arcsec = 0.126 ratio.

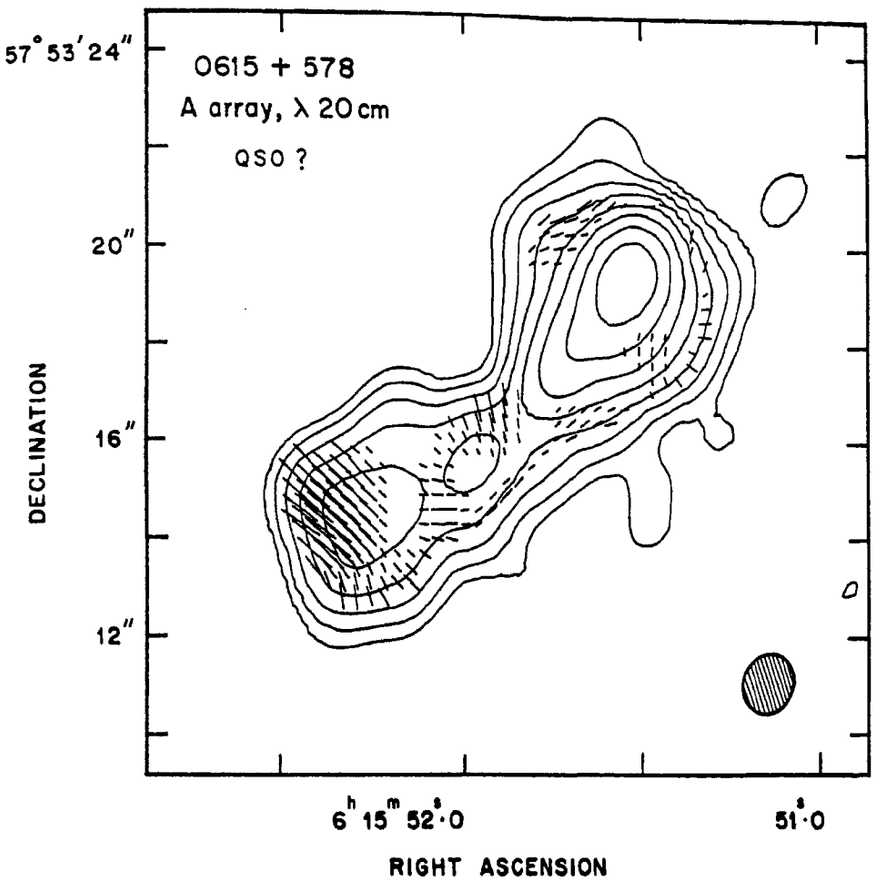

Fig.3.8a. Contour levels: 1 x (-4, -2, -1, 1, 2, 4, 8, 16, 32, 64, 128, 256. 512, 1024, 2048) mJy/beam. Polarization: 1 arcsec=0.086 ratio.

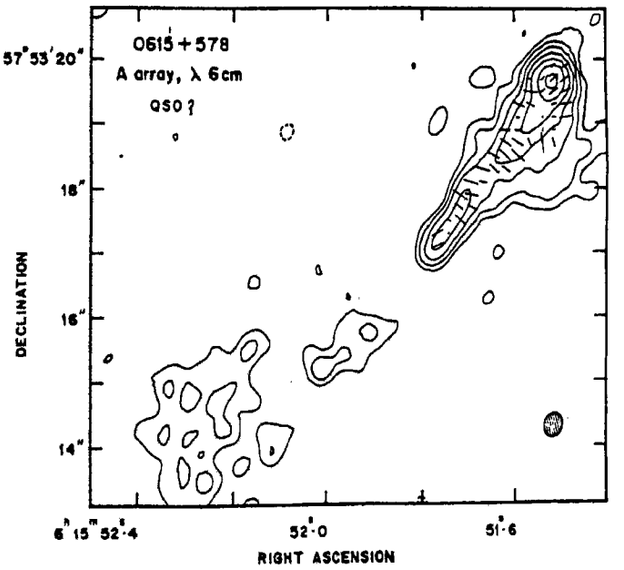

Fig.3.8b. Contour levels: 0.5 x (-4, -2, -1, 1, 2, 4, 8, 16, 32, 64, 128, 256, 512, 1024, 2048) mJy/beam. Polarization: 1 arcsec= 0.417 ratio.

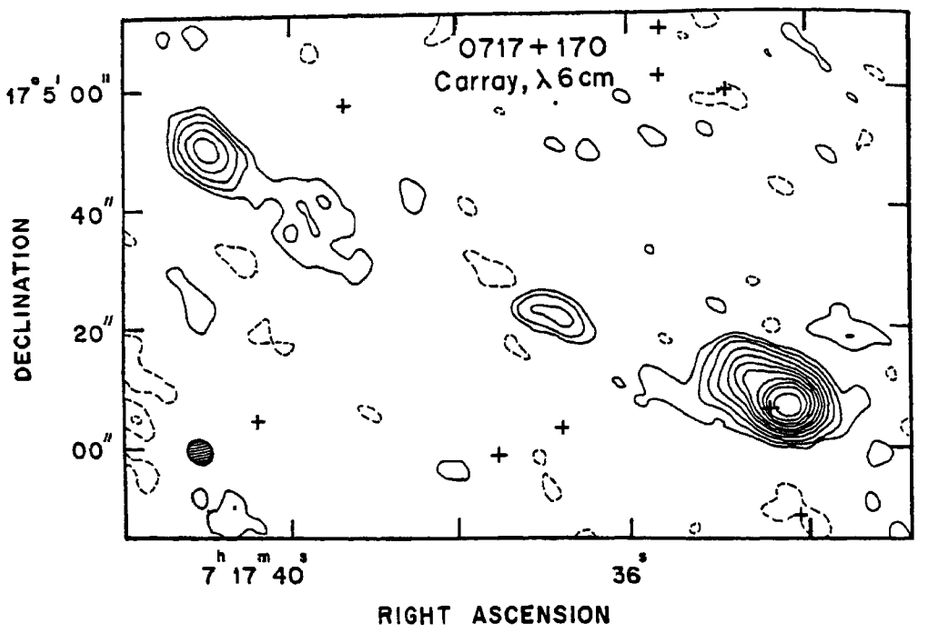

Fig.3.9a. Contour levels: 101 x (-0.015, -0.0075, 0.0075, 0.015, 0.03, 0.06, 0.1, 0.15, 0.2, 0.3, 0.4, 0.5, 0.75) mJy/beam.

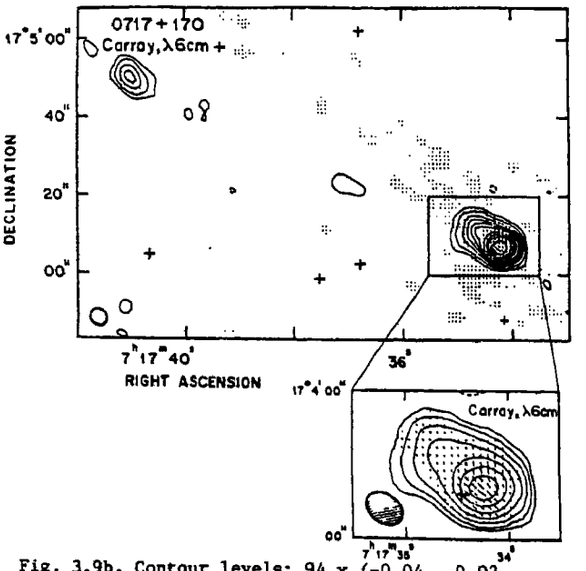

Fig. 3.9b. Contour levels: 94 x (-0.04, -0.02, 0.02, 0.04, 0.08, 0.12, 0.16, 0.2, 0.3, 0.4, 0.5, 0.75) mJy/beam. Inset: 94 x (-0.02, -0.01, 0.02, 0.04, 0.08, 0.16, 0.3, 0.5, 0.75)mJy/beam.

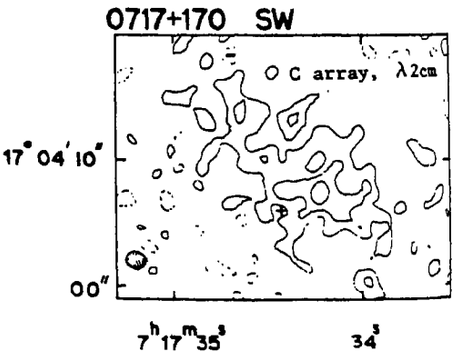

Fig. 3.9c.Contour levels: 12 x (-0.5,-0.25 0.25, 0.5, 0.75) mJy/beam.

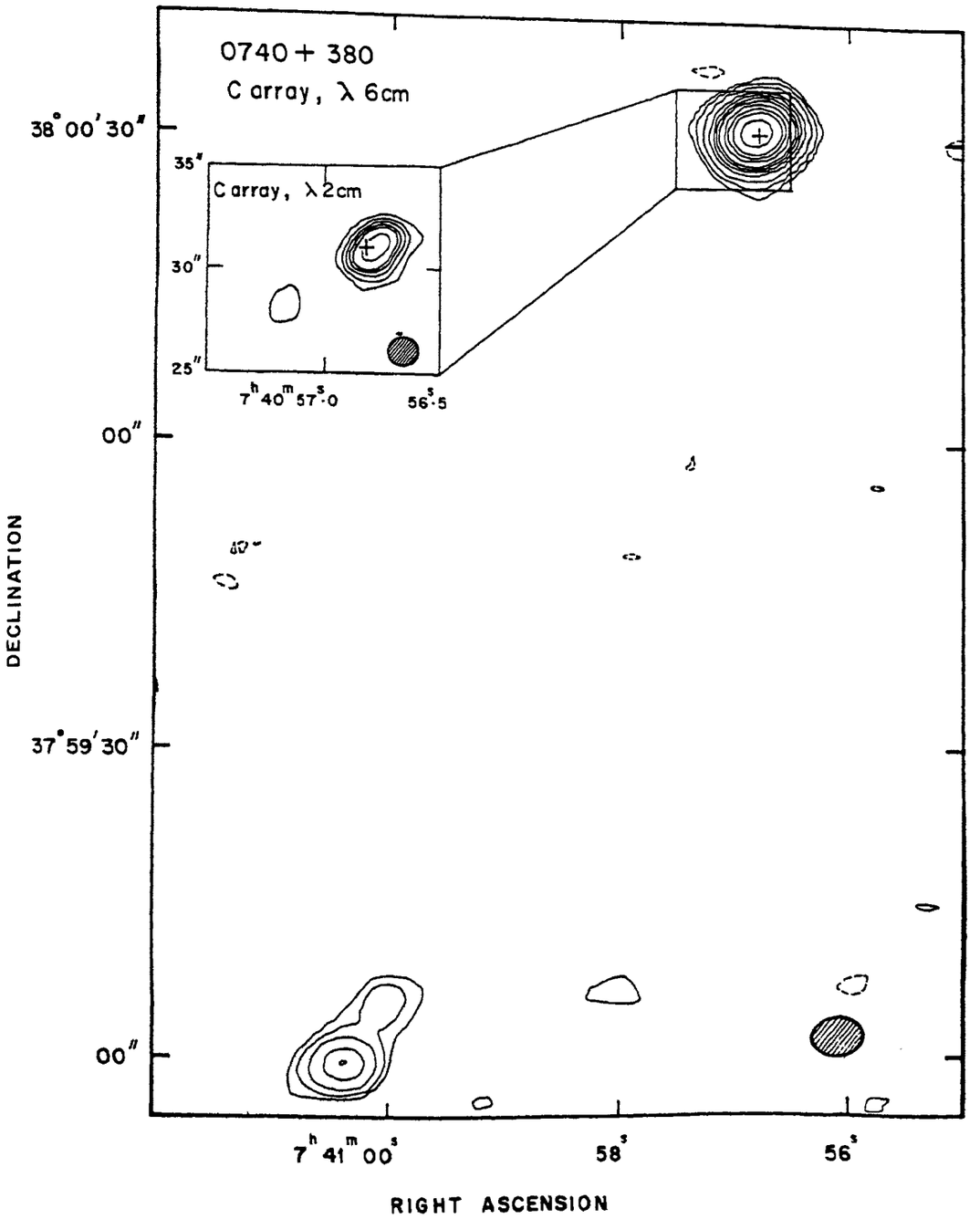

Fig.3.10. Contour levels: 210 x (-0.02, -0.01, 0.01, 0.02, 0.04, 0.08, 0.12, 0.16, 0.2, 0.3, 0.4, 0.5, 0.75) mJy/beam. Inset: 29 x (-0.2, -0.1, 0.1, 0.2, 0.3, 0.4, 0.5, 0.75) mJy/beam.

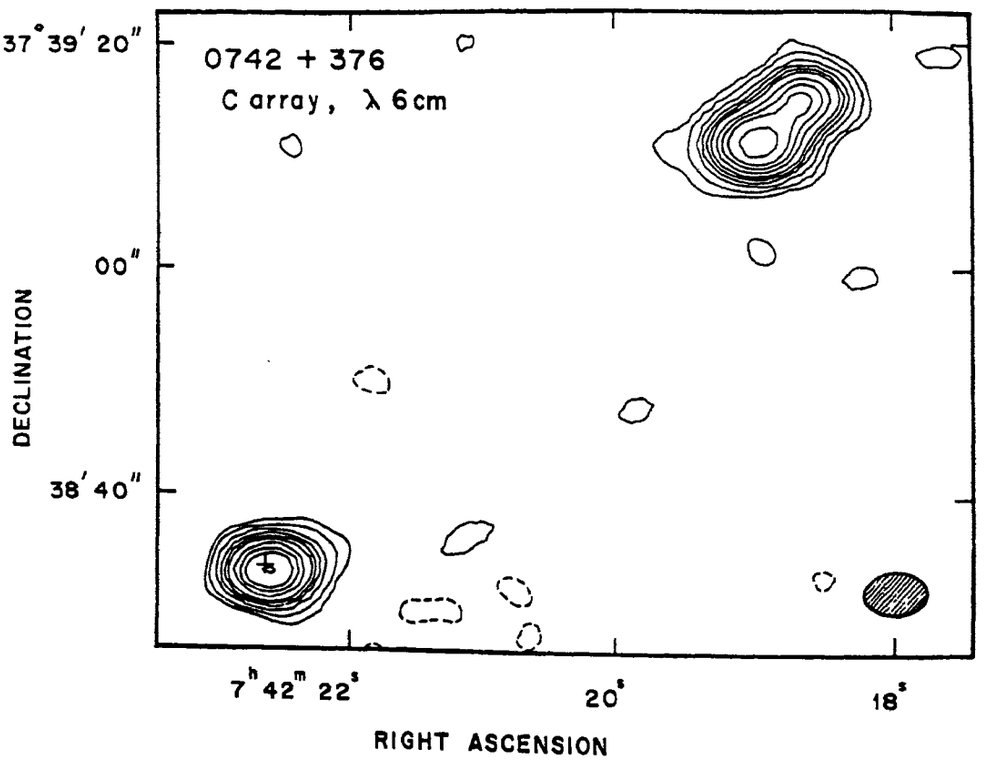

Fig.3.11a. Contour levels: 76 x (-0.04, -0.02, 0.02, 0.04, 0.08, 0.12, 0.16, 0.2, 0.3, 0.4, 0.5, 0.75) mJy/beam.

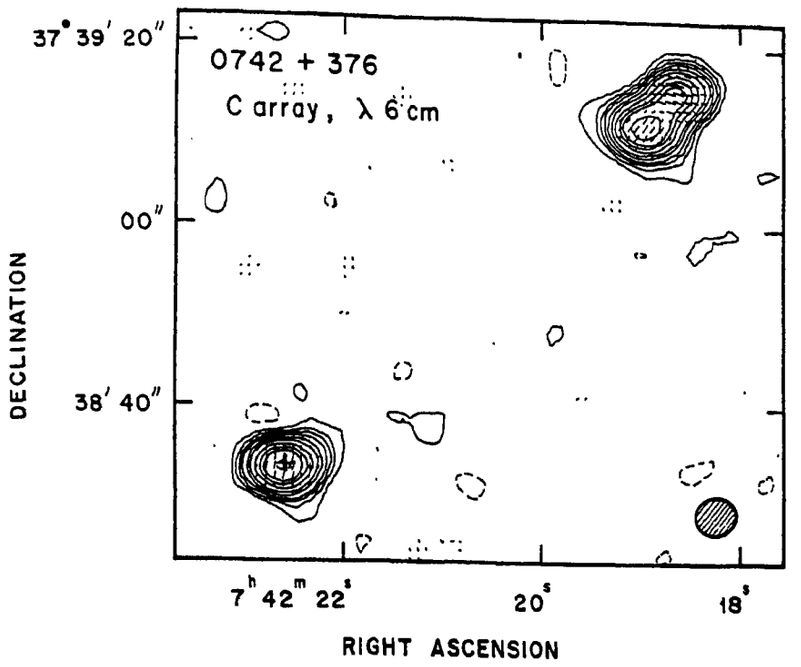

Fig.3.11b. Contour levels: 72 x (-0.05, -0.025, 0.025, 0.05, 0.075, 0.1, 0.15, 0.2, 0.3, 0.4, 0.5, 0.75) mJy/beam.

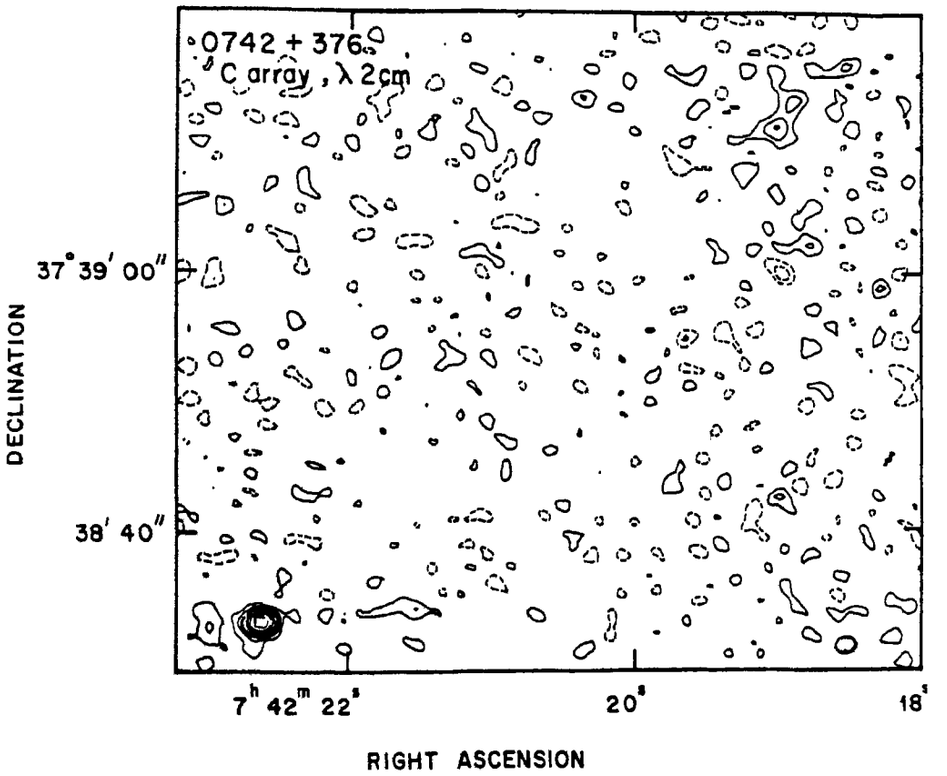

Fig. 3.11c. Contour levels: 47 x (-0.1, -0.05, 0.05, 0.1, 0.15, 0.2, 0.3, 0.4, 0.5, 0.75) mJy/beam.

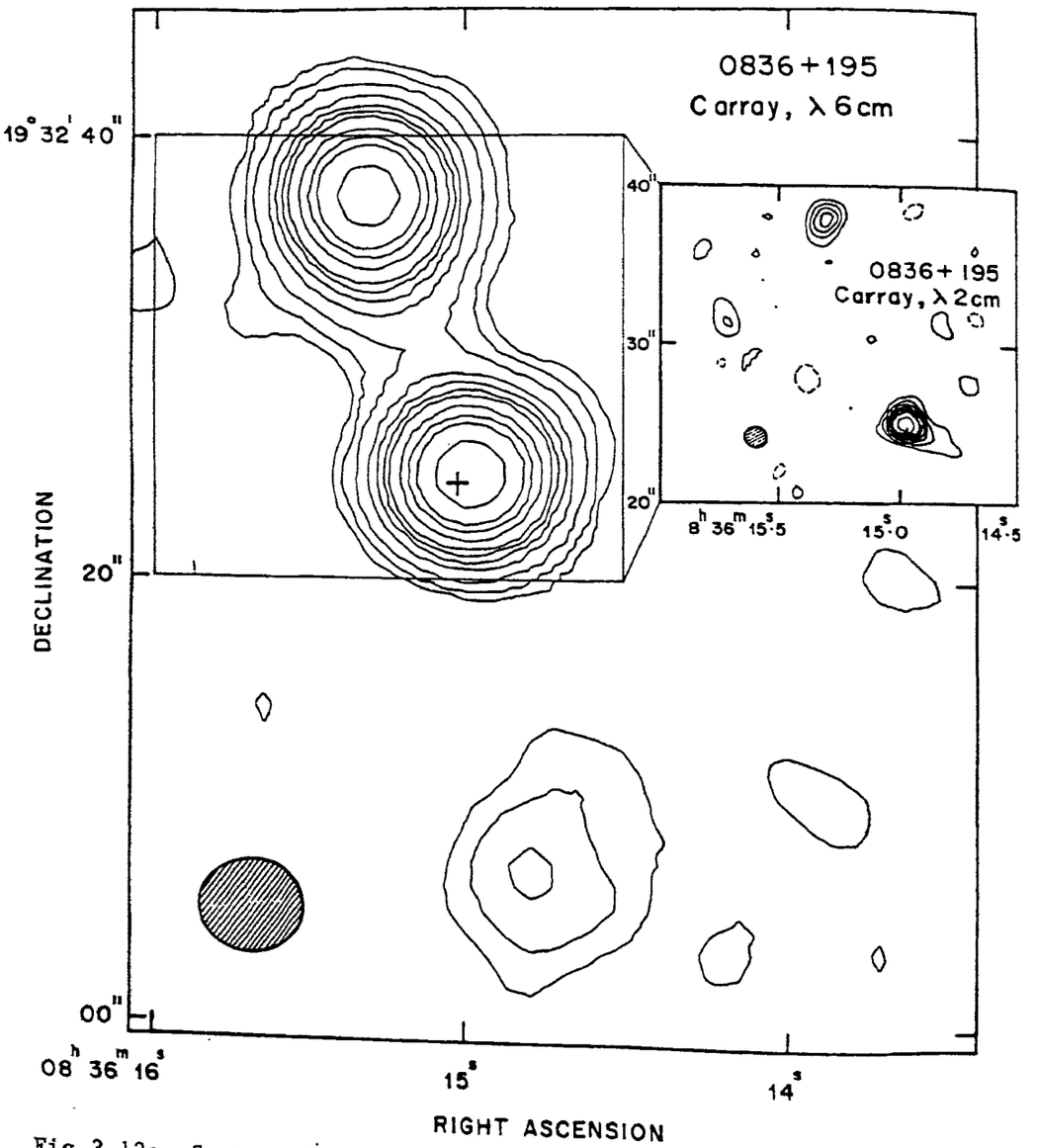

Fig.3.12a. Contour levels: 71 x (-0.02, -0.01, 0.01, 0.02, 0.04, 0.08, 0.12, 0.16, 0.2, 0.3, 0.4, 0.5, 0.75) mJy/beam. Inset: 28 x (-0.15, -0.075, 0.075, 0.15, 0.225, 0.3, 0.4, 0.5, 0.75) mJy/beam.

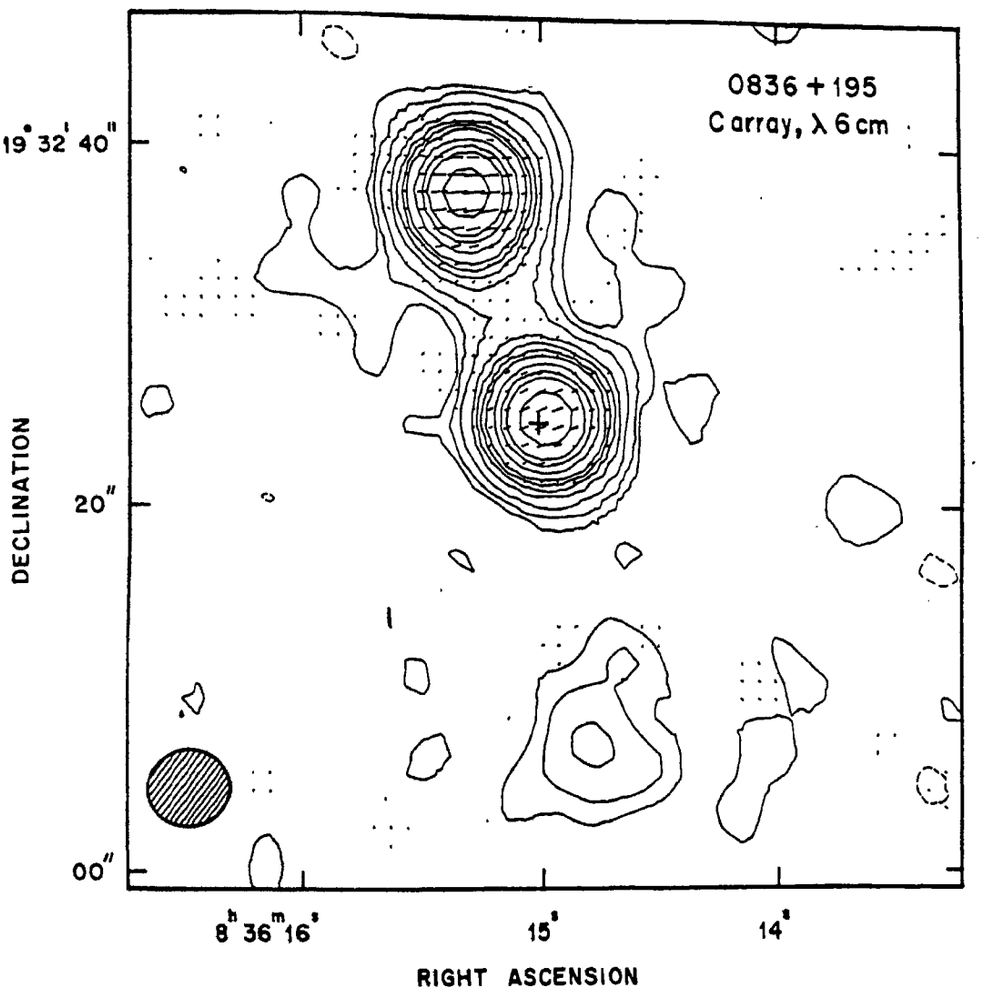

Fig.3.12b. Contour levels: 72 x (-0.02, -0.01, 0.01, 0.02, 0.04, 0.08, 0.12, 0.16, 0.2, 0.3, 0.4, 0.5, 0.75) mJy/beam.

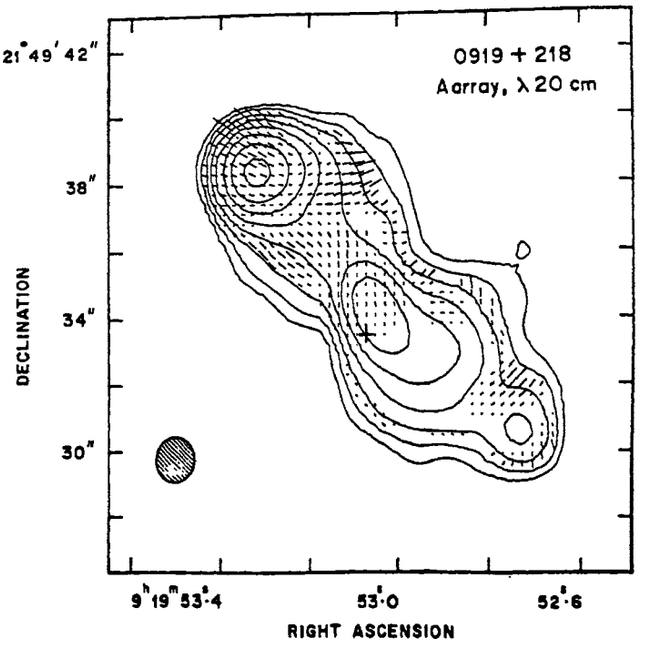

Fig.3.13a. Contour levels: 1 x (-4, -2, -1, 1, 2, 4, 8, 16, 32, 64, 128, 512, 1024, 2048) mJy/beam. Polarization: 1 arcsec = 0.245 ratio.

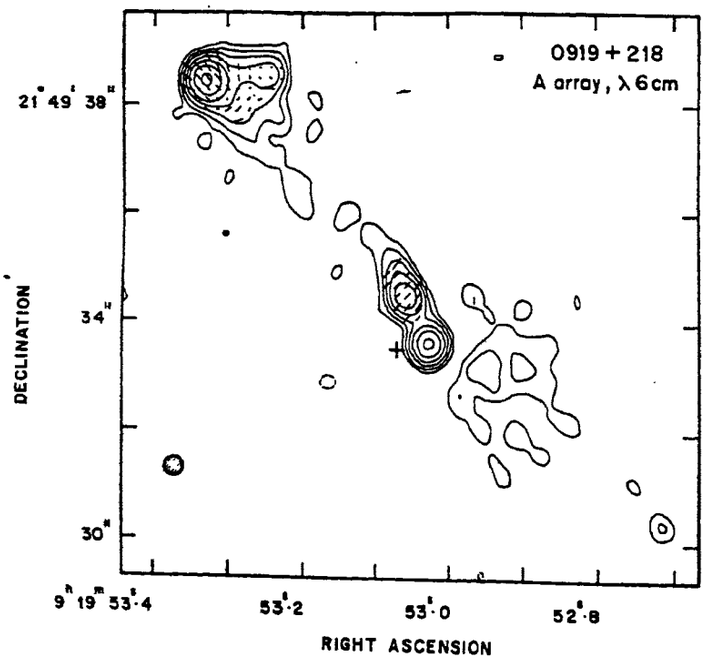

Fig.3.13b. Contour levels: 0.5 x (-4, -2, -1, 1, 2, 4, 8, 16, 32, 64, 128, 256, 512, 1024, 2048) mJy/beam. Polarization: 1 arcsec = 1.34 ratio.

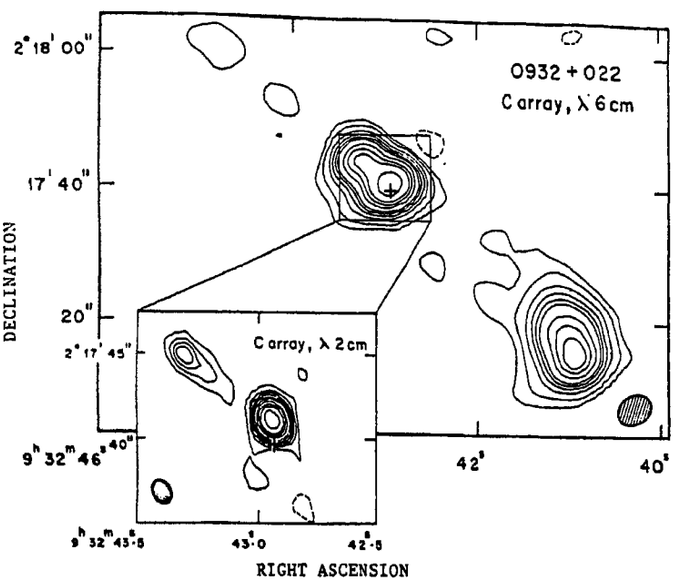

Fig.3.14a. Contour levels: 82 x (-0.04, -0.02, 0.02, 0.04, 0.08, 0.12, 0.16, 0.2, 0.3, 0.4, 0.5, 0.75) mJy/beam. Inset: 72 x -0.06, -0.03, 0.03, 0.06, 0.09, 0.12, 0.16, 0.2, 0.3, 0.4, 0.5, 0.75) mJy/beam.

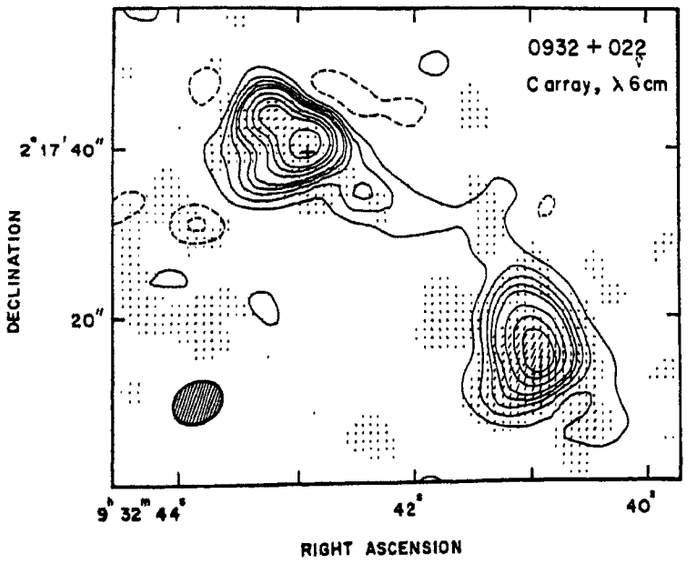

Fig.3.14b. Contour levels: 72 x (-0.08, -0.04, 0.04, 0.08, 0.12, 0.16, 0.2, 0.3, 0.4, 0.5, 0.75) mJy/beam.

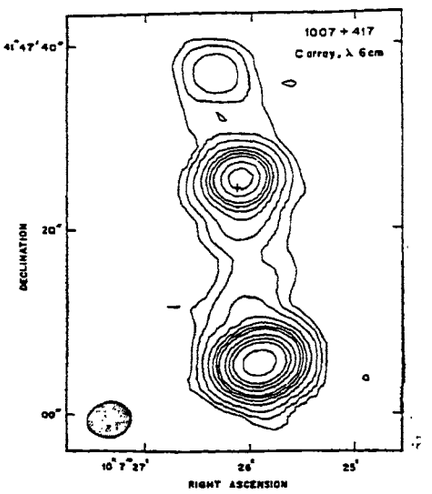

Fig.3.15a. Contour levels: 304 x (-0.02, -0.01, 0.01, 0.02, 0.04, 0.08, 0.12, 0.16, 0.2, 0.3, 0.4, 0.5, 0.75) mJy/beam.

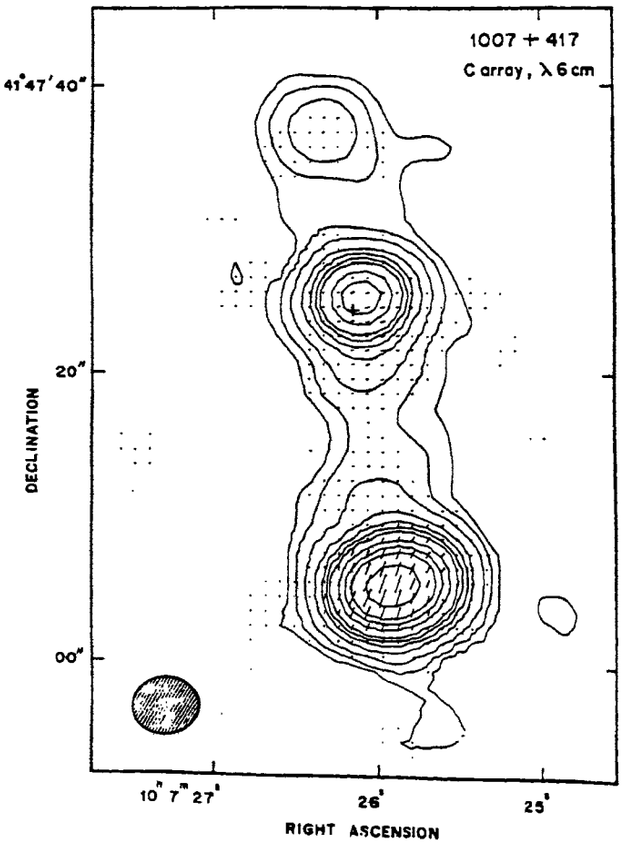

Fig. 3.15b. Contour levels: 302 x (-0.02, -0.01, 0.01, 0.02, 0.04, 0.08, 0.12, 0.16, 0.2, 0.3, 0.4, 0.5,0.75) mJy/beam.

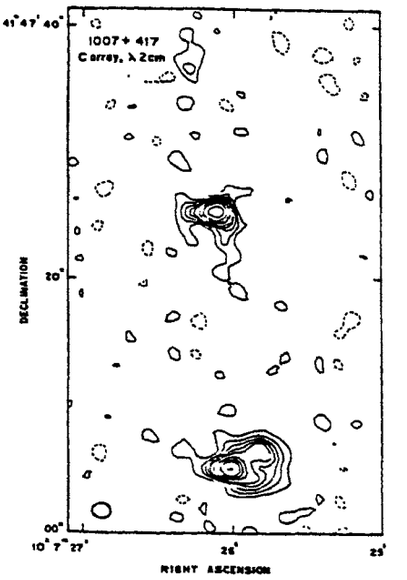

Fig. 3.15c. Contour levels: 67 x (-0.08, -0.04, 0.04, 0.08, 0.12, 0.16, 0.2, 0.3, 0.4, 0.5, 0.75) mJy/beam.

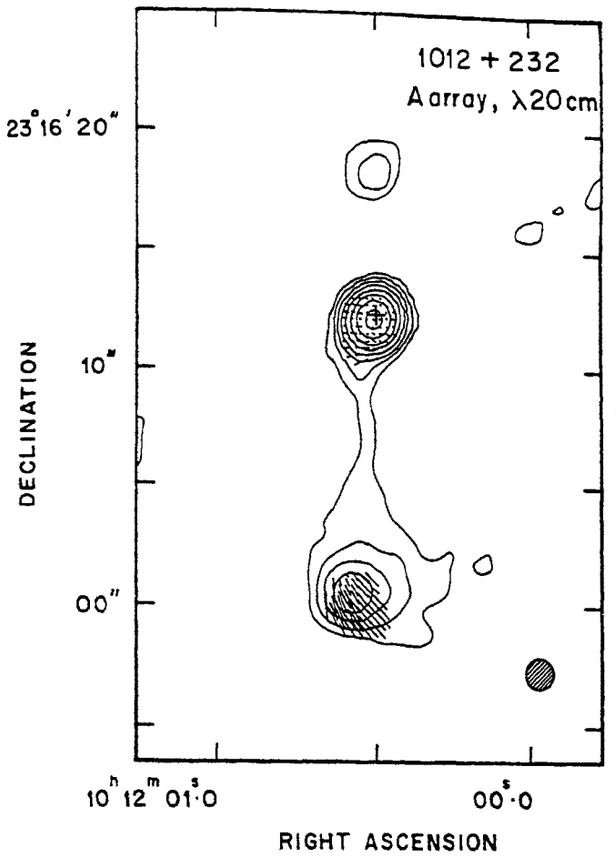

Fig.3.16a. Contour levels: 2 x (-4, -2, -1, 1, 2, 4, 8, 16, 32, 64, 128, 256, 512, 1024, 2048) mJy/beam. Polarization: 1 arcsec = 0.242 ratio.

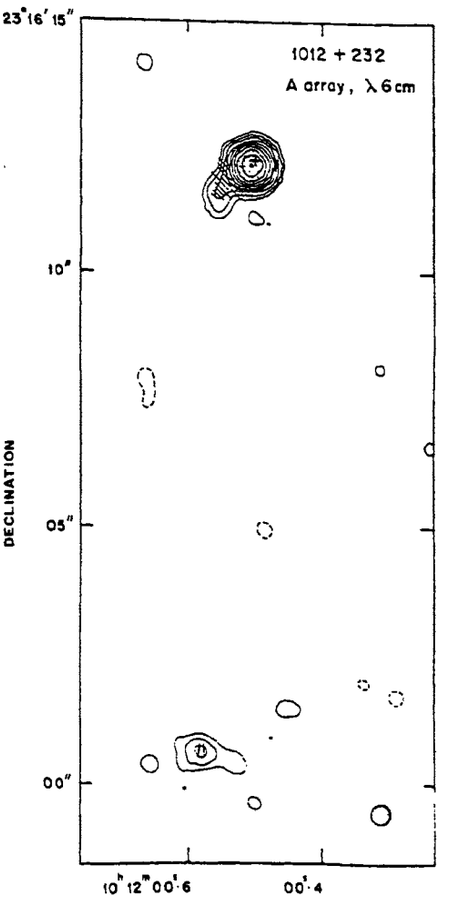

Fig.3.16b. Contour levels: 2 x (-4, -2, -1, 1, 2, 4, 8, 16, 32, 64, 128, 256, 512) mJy/beam. Polarization: 1 arcsec = 0.343 ratio.

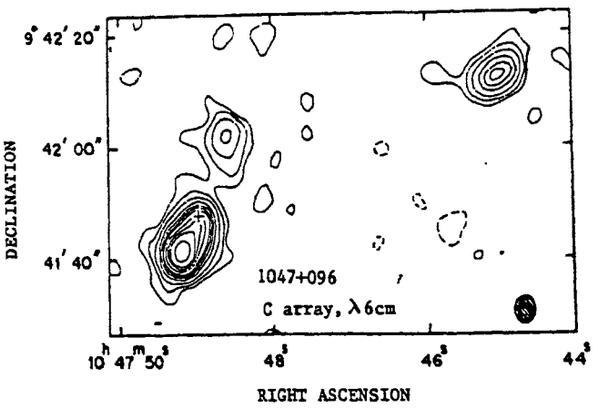

Fig.3.18a. Contour levels: 59 x (-0.02, -0.01, 0.01, 0.02, 0.04, 0.08, 0.12, 0.16, 0.2, 0.3, 0.4, 0.5, 0.75) mJy/beam.

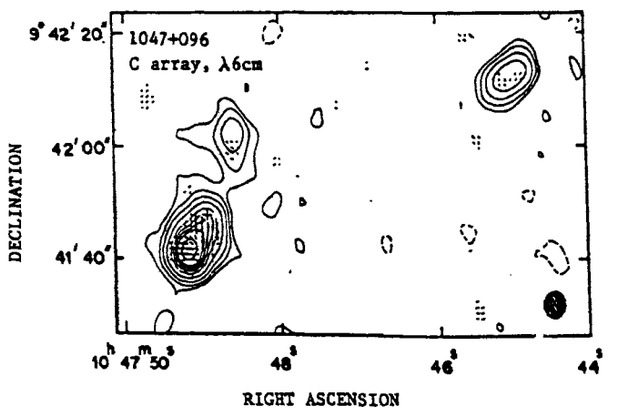

Fig.3.18b. Contour levels: 58 x (-0.025, -0.0125, 0.0125, 0.025, 0.05, 0.1, 0.2, 0.3, 0.4, 0.5, 0.75) mJy/beam.

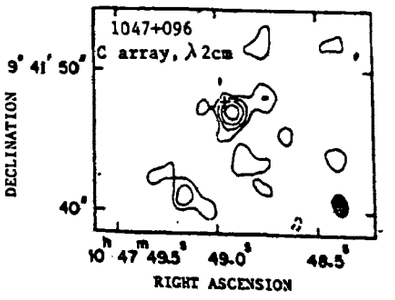

Fig.3.18c. Contour levels: 16 x (-0.3, -0.15, 0.15, 0.3, 0.5, 0.75) mJy/beam

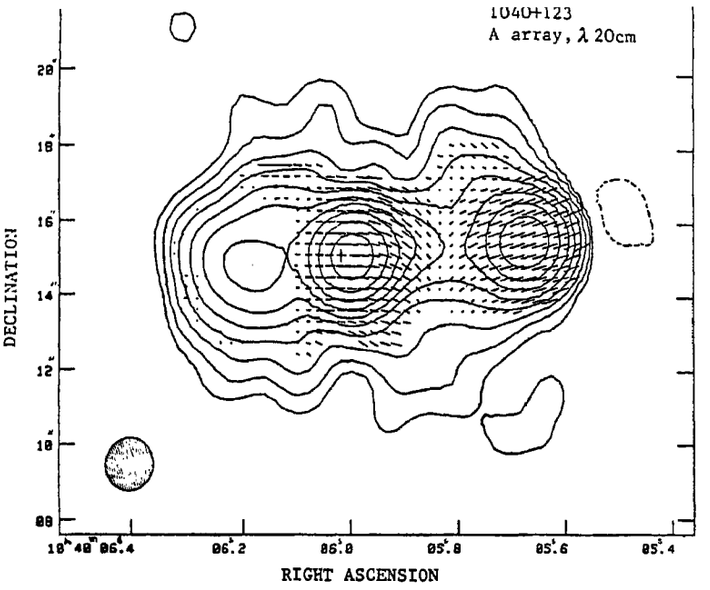

Fig.3.17a. Contour levels: 2 x (-4, -2, -1, 1, 2, 4, 8, 16, 32, 64, 128, 256, 512) mJy/beam. Polarization: 1 arcsec = 0.321 ratio.

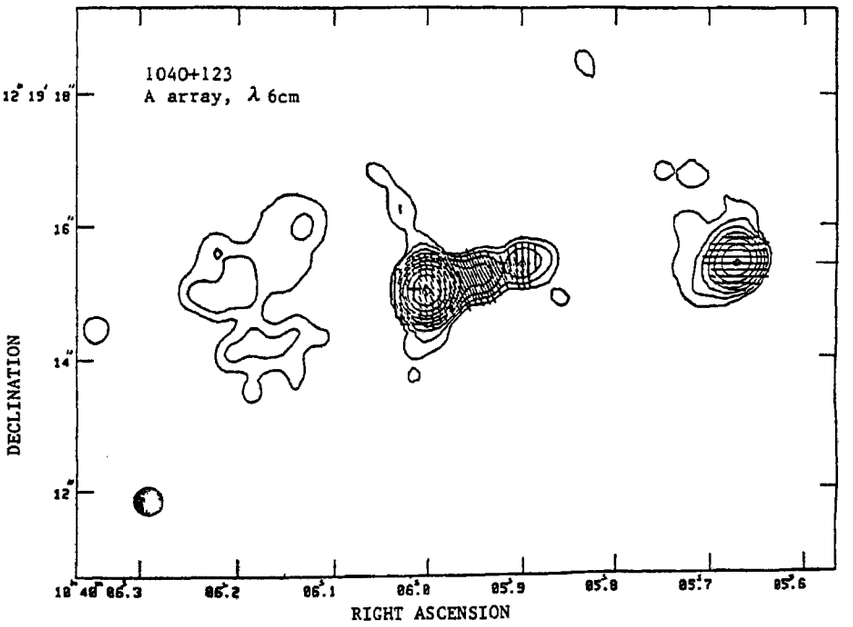

Fig.3.17b. Contour levels: 2 x (-4,-2, -1, 1, 2, 4, 8, 16, 32, 64, 128, 256, 512) mJy/beam. Polarization: 1 arcsec = 0.967 ratio.

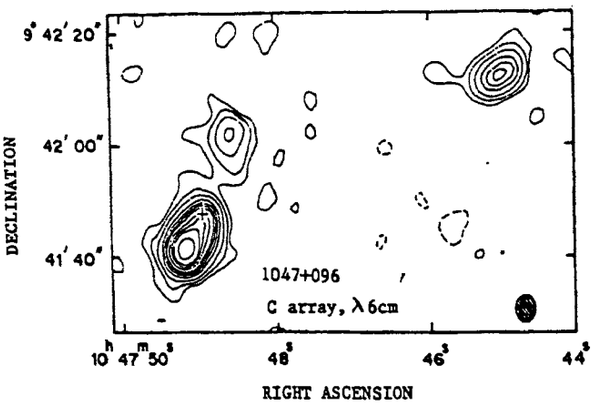

Fig.3.18a. Contour levels: 59 x (-0.02, -0.01, 0.01, 0.02, 0.04, 0.08, 0.12, 0.16, 0.2, 0.3, 0.4, 0.5, 0.75) mJy/beam.

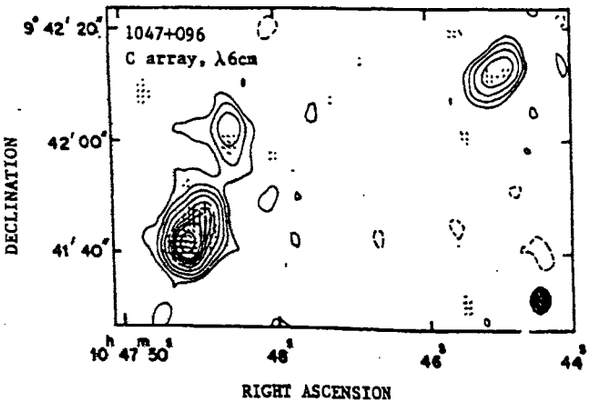

Fig.3.18b. Contour levels: 58 x (-0.025, -0.0125, 0.0125, 0.025, 0.05, 0.1 0.2, 0.3, 0.4, 0.5, 0.75) mJy/beam.

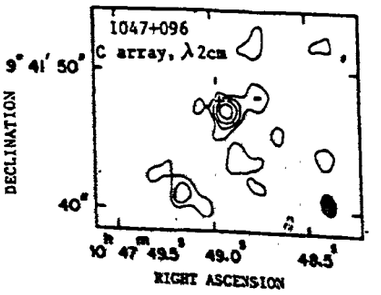

Fig.3.18c. Contour levels: 16 x (-0.3, -0.15, 0.15, 0.3, 0.5, 0.75) mJy/beam

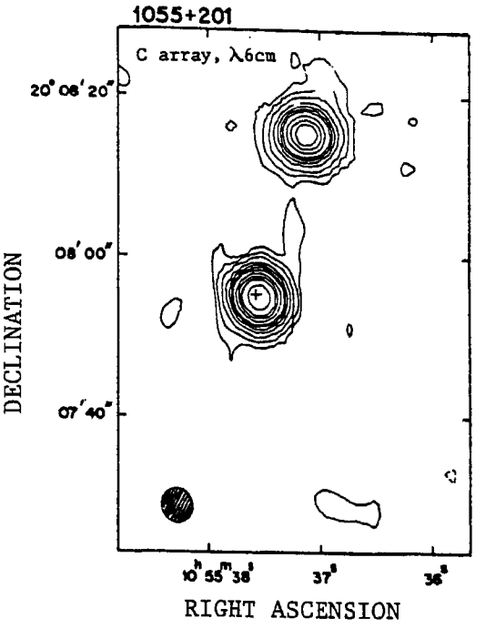

Fig.3.19a. Contour levels: 792 x (-0.02, -0.01, 0.01, 0.02, 0.04, 0.08, 0.12, 0.16, 0.2, 0.3, 0.4, 0.5, 0.75) mJy/beam.

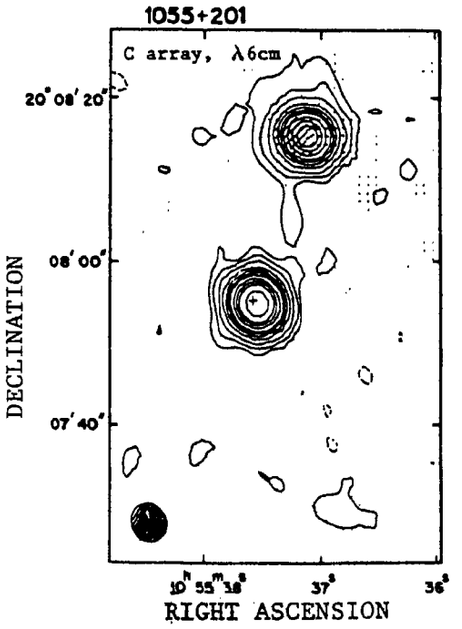

Fig. 3.19b. Contour levels: 787 x (-0.02, -0.01, 0.01, 0.02, 0.04, 0.08, 0.12, 0.16, 0.2, 0.3, 0.4, 0.5, 0.75) mJy/beam.

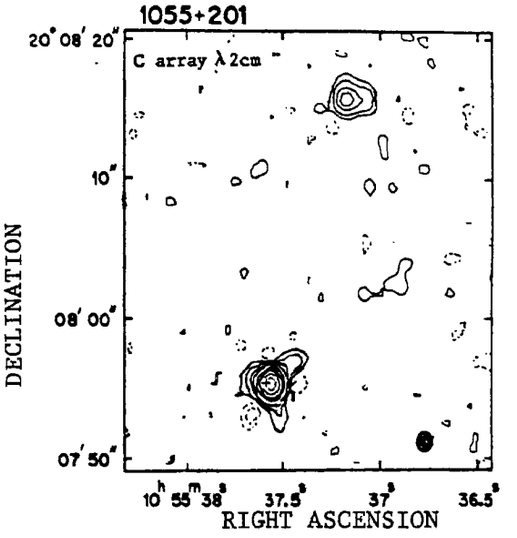

Fig. 3.19c. Contour levels: 819 x (-0.03, -0.015, .015, 0.03, 0.06, 0.09, 0.2, 0.3, 0.5, 0.75) mJy/beam.

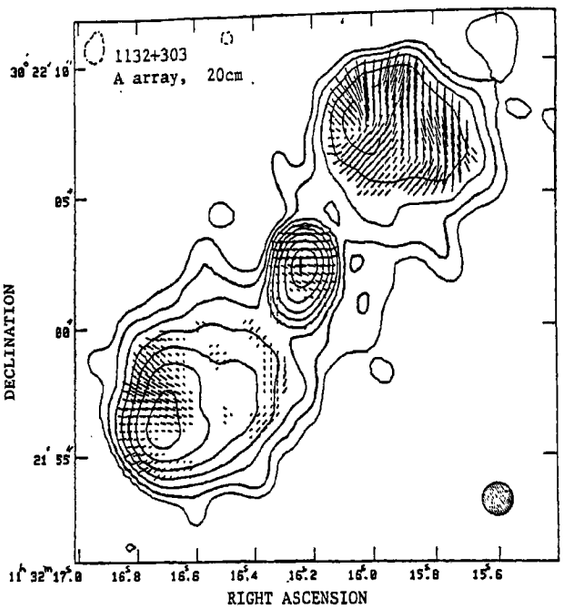

Fig. 3.20a. Contour levels: 1 x (-4, -2, -1, 1, 2, 4, 8, 16, 32, 64, 128) mJy/beam. Polarization: 1 arcsec = 0.147 ratio.

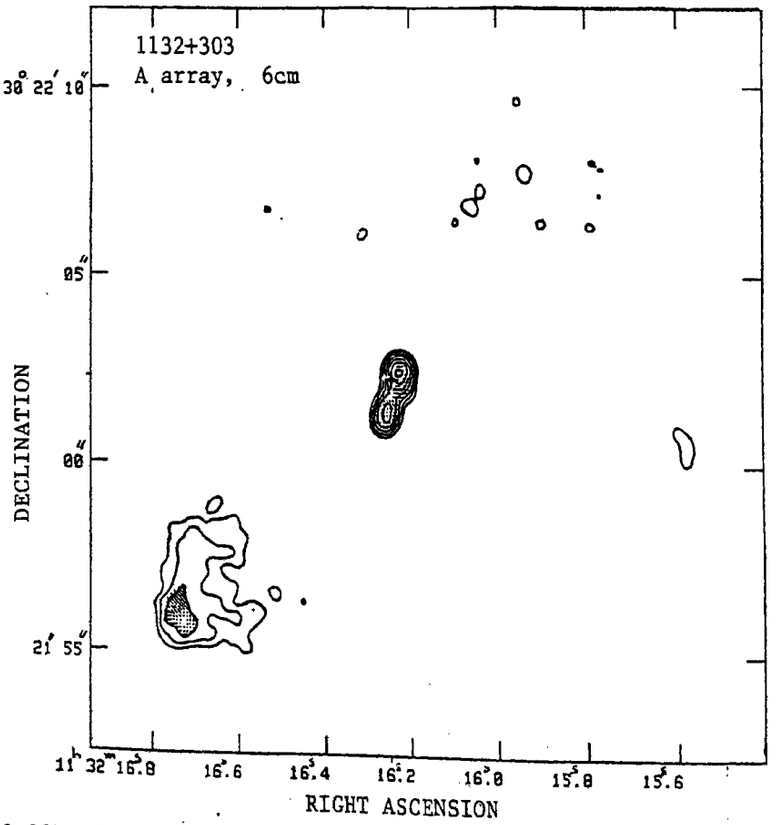

Fig. 3.20b. Contour levels: 1 x (-4, -2, -1, 1 2, 4, 8, 16, 32, 64)mJy/beam. Polarization: 1 arcsec = 0.686 ratio.

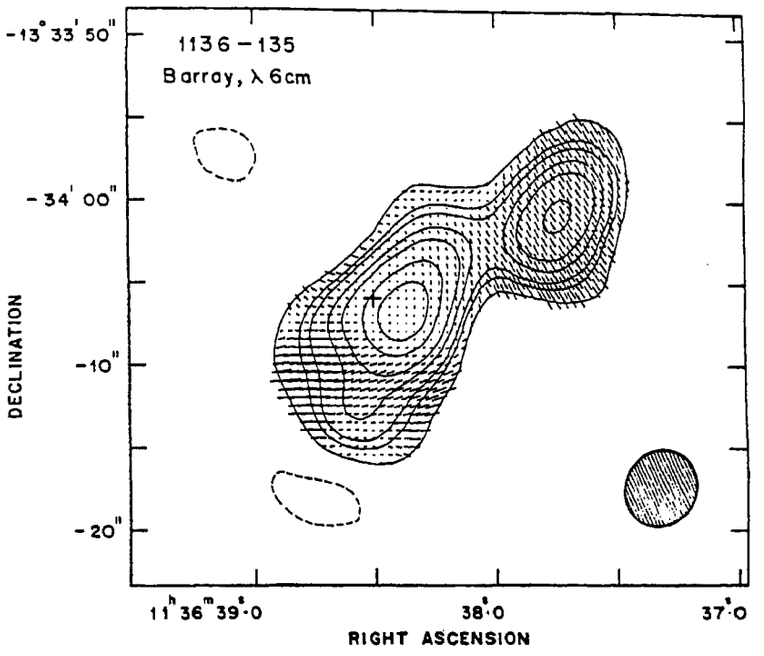

Fig.3.21a: Contour levels: 5.3 x (-7, 7, 15, 20, 30, 40, 60, 80) mJy/beam. Polarization: 1 arcsec = 0.132 ratio.

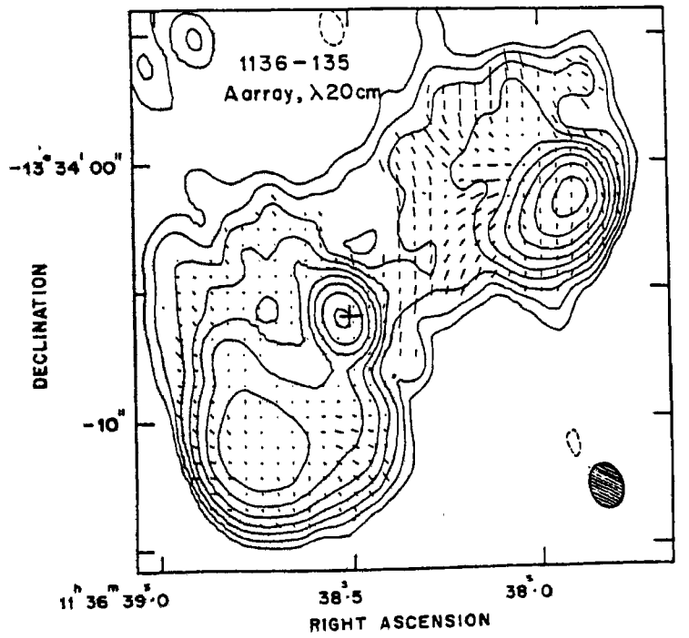

Fig.3.21b. Contour levels: 2 x (-4, -2, -1, 1, 2, 4, 8, 16, 32, 64, 128, 256, 512) mJy/beam. Polarization: 1 arcsec = 0.48 ratio.

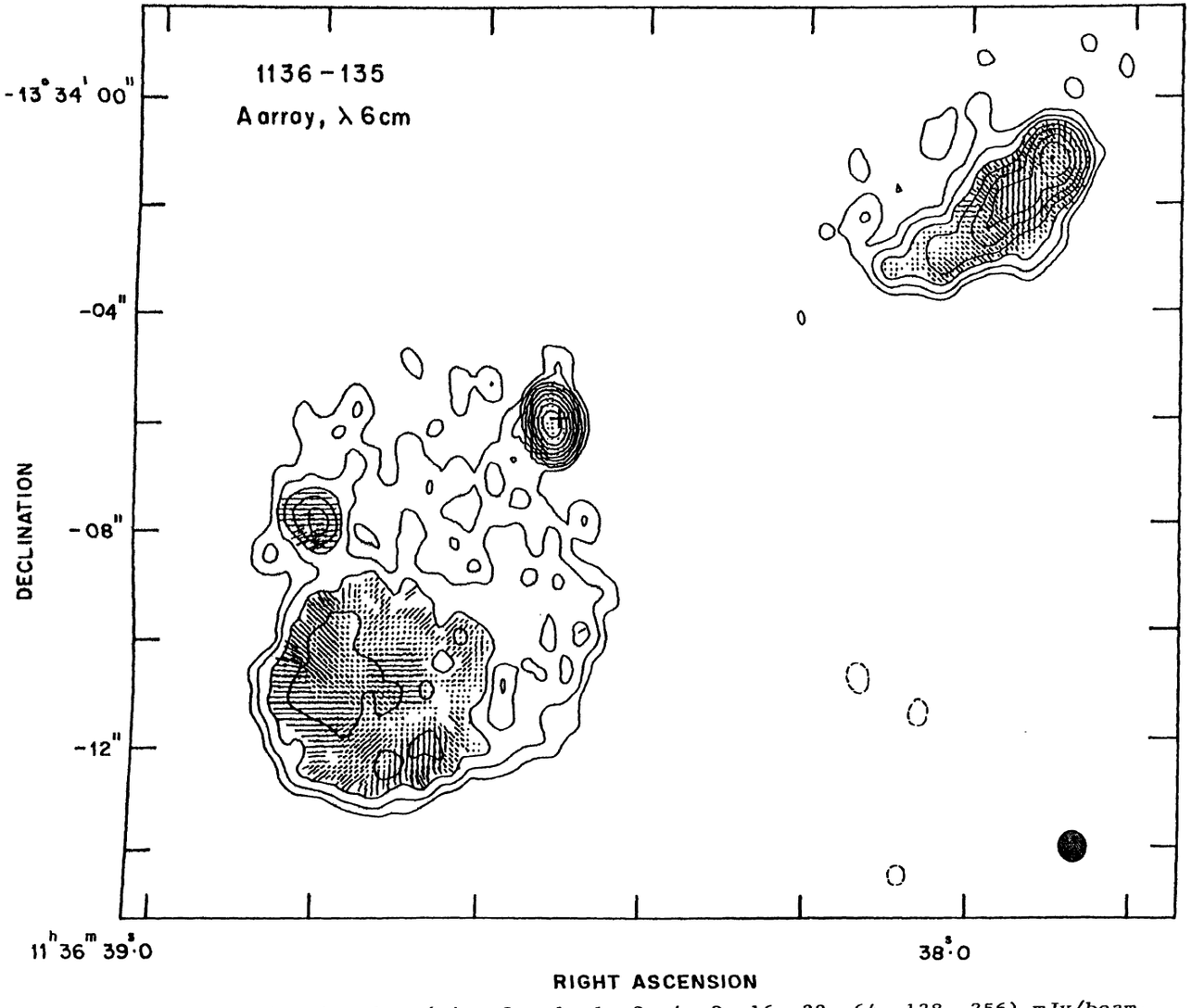

Fig.3.21c. Contour levels: 1 x (-4, -2, -1, 1, 2, 4, 8, 16, 32, 64, 128, 256) mJy/beam.
Polarization: 1 arcsec = 1.04 ratio.

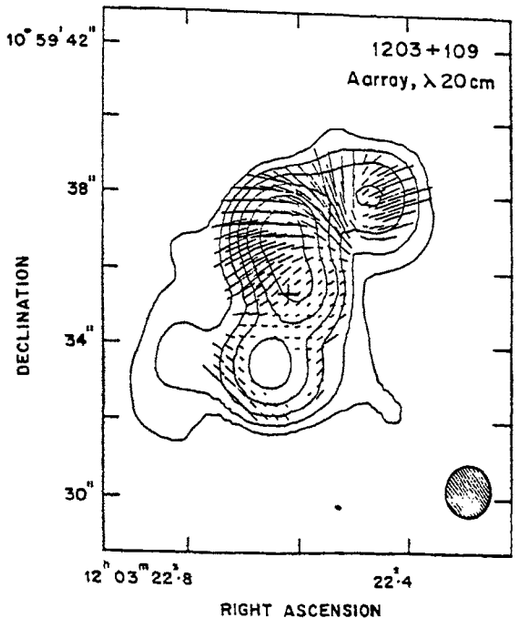

Fig.3.22a. Contour levels: 1 x (-4, -2, -1, 1, 2, 4, 8, 16, 32, 64) mJy/beam. Polarization: 1 arcsec = 0.12 ratio.

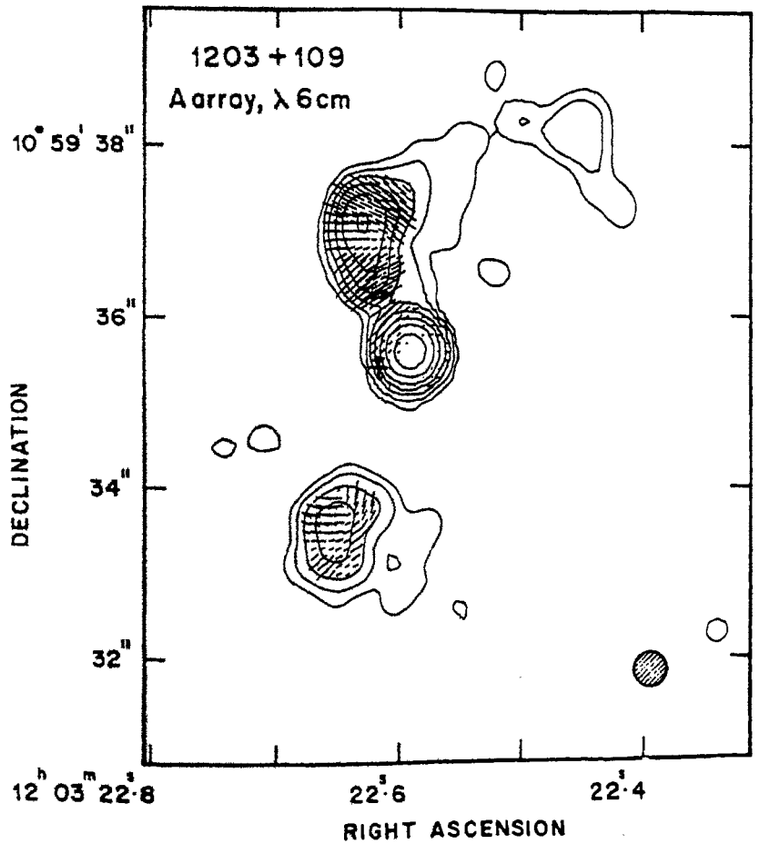

Fig.3.22b. Contour levels: 0.5 x (-4, -2, -1, 1, 2, 4, 8, 16, 32, 64) mJy/beam. Polarization: 1 arcsec = 0.652 ratio.

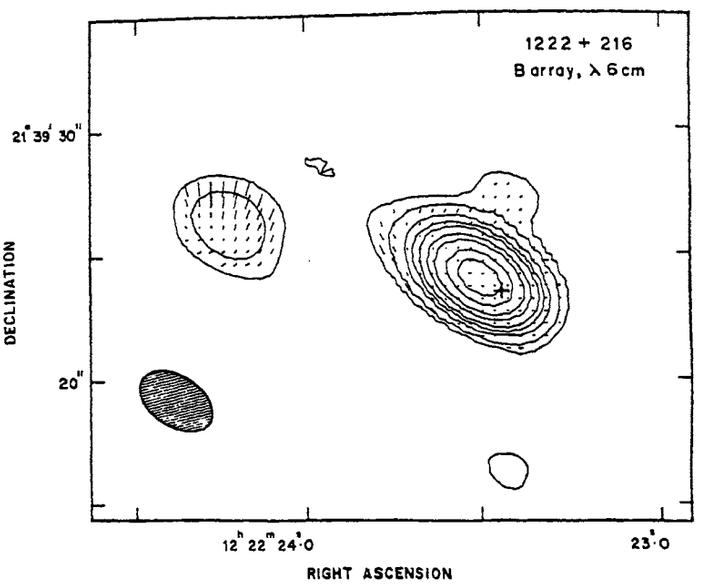

Fig.3.23a. Contour levels: 8.5 x (-2.5, 2.5, 5, 10, 15, 20, 30, 40, 60, 80) mJy/beam. Polarization: 1 arcsec = 0.246 ratio.

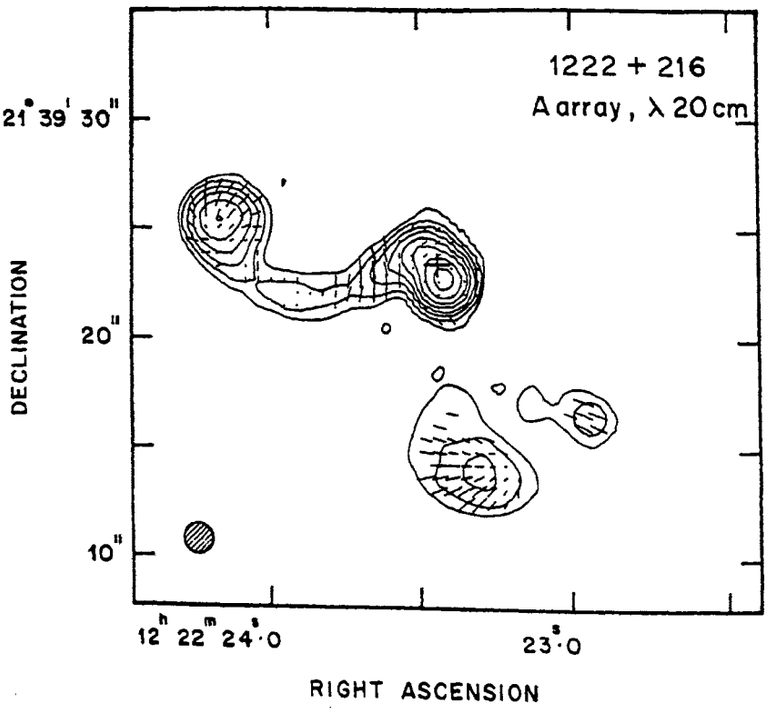

Fig.3.23b. Contour levels: 1 x (-4, -2, -1, 4, 8, 16, 32, 64, 128, 256, 512) mJy/beam. Polarization: 1 arcsec = 0.337 ratio.

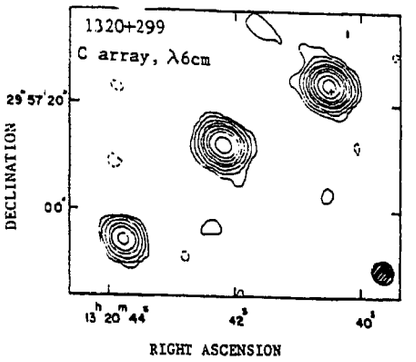

Fig. 3.24a. Contour levels: 277 x (-0.02, -0.01, 0.01, 0.02, 0.04, 0.08, 0.12, 0.2, 0.3, 0.5, 0.75) mJy/beam.

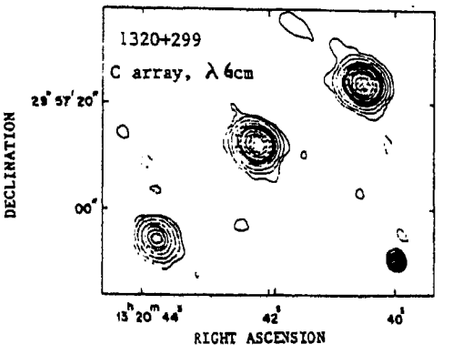

Fig. 3.24b. Contour levels: 277 x (-0.02, -0.01, 0.01, 0.02, 0.04, 0.08, 0.12, 0.16, 0.2, 0.3, 0.4, 0.5, 0.75) mJy/beam.

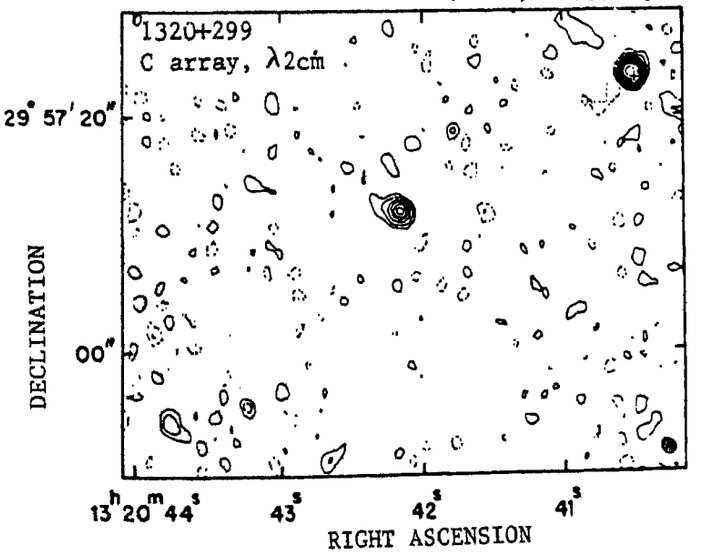

Fig. 3.24c.Contour levels: 156 x (-0.04, -0.02, 0.02, 0.04, 0.08, 0.12, 0.16, 0.2, 0.3, 0.5, 0.75) mJy/beam.

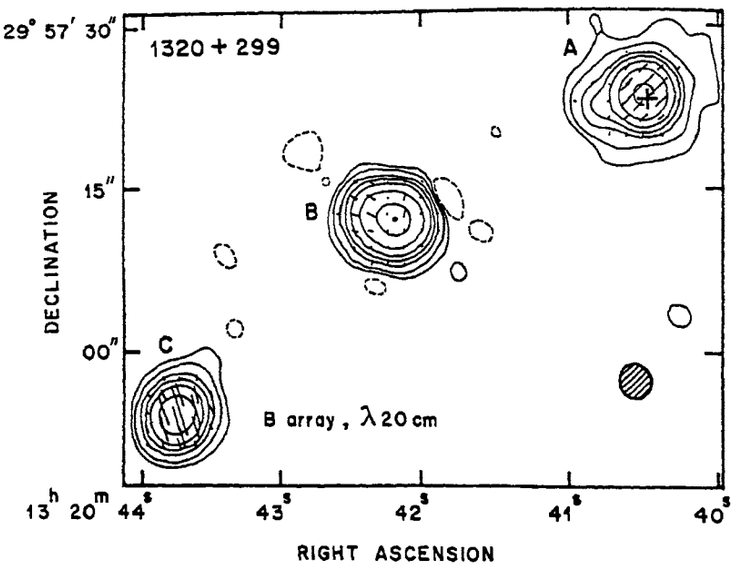

Fig. 3.24d. Contour levels: 1 x (-1, 1, 3, 10, 20, 40, 100, 300, 500) mJy/beam. Polarization: 1 arcsec = 4.5 mJy/beam.

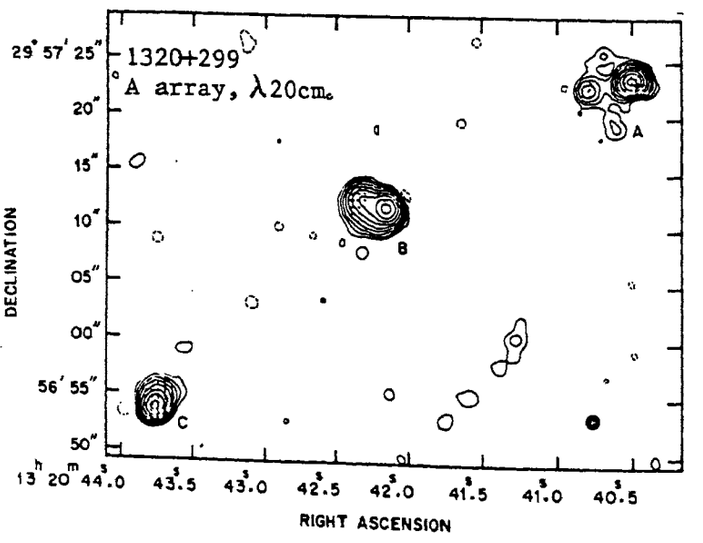

Fig. 3.24e. Contour levels: 1 x (-4, -2, -1, 1, 2, 4, 8, 16, 32, 64, 128, 256) mJy/beam. Polarization: 1 arcsec = 0.26 ratio.

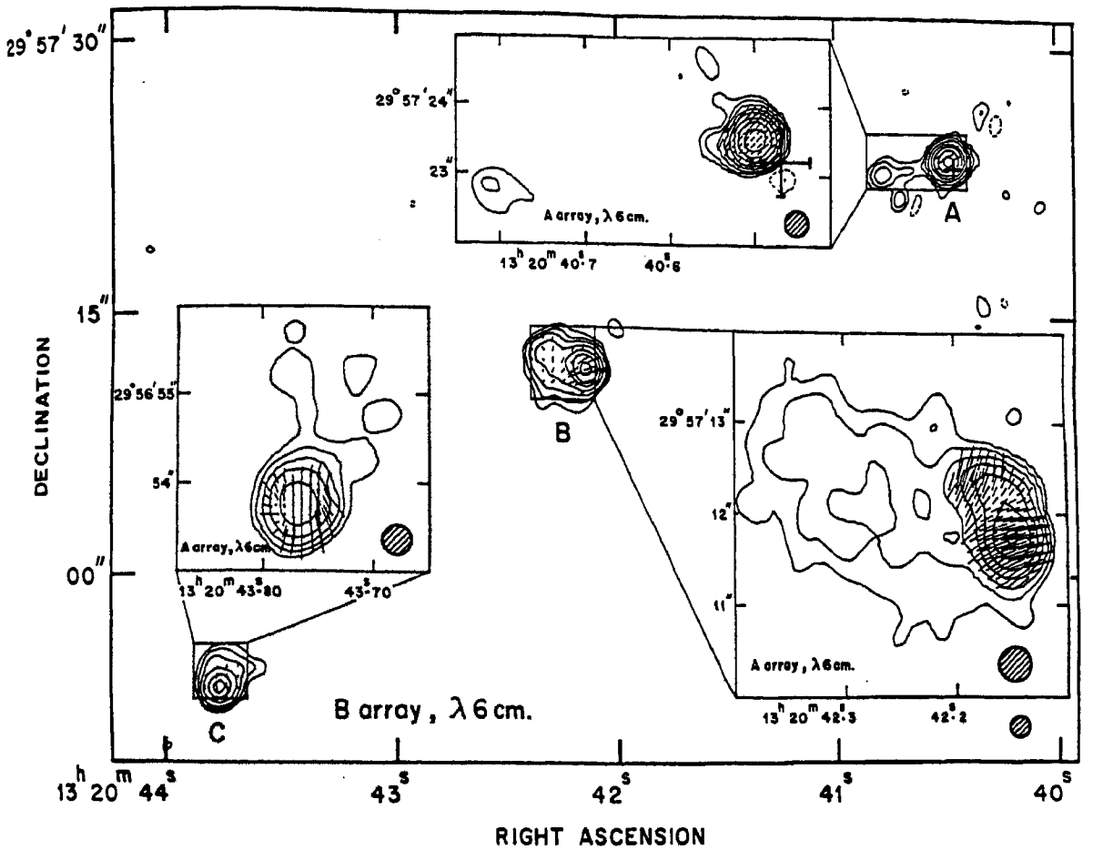

Fig. 3.24f. Contour levels: 1 x (-0.7, 0.7, 1.4, 3, 8, 20, 40, 100, 200) mJy/beam. Polarization: 1 arcsec = 9.1 mJy/beam. Insets: Contour levels: 1 x (-4, -2, -1, 1, 2, 4, 8, 16, 32, 64, 128) mJy/beam. Polarization: 1 arcsec = 0.61 ratio.

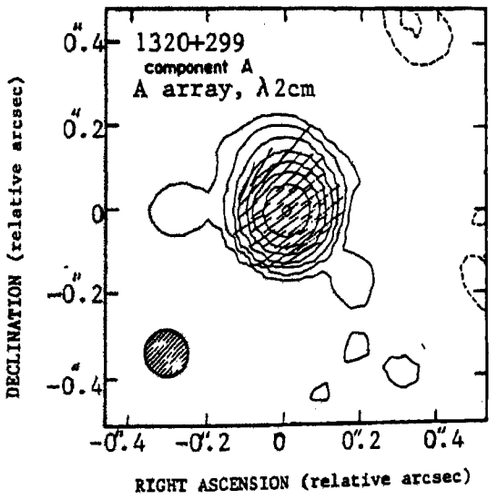

Fig. 3.24g. Contour levels: 1 x (-4, -2, -1, 1, 2, 4, 8, 16, 32, 64, 128)mJy/beam. Polarization: 1 arcsec = 0.8 ratio.

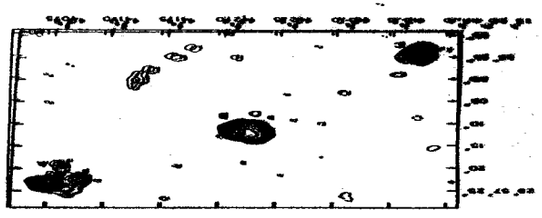

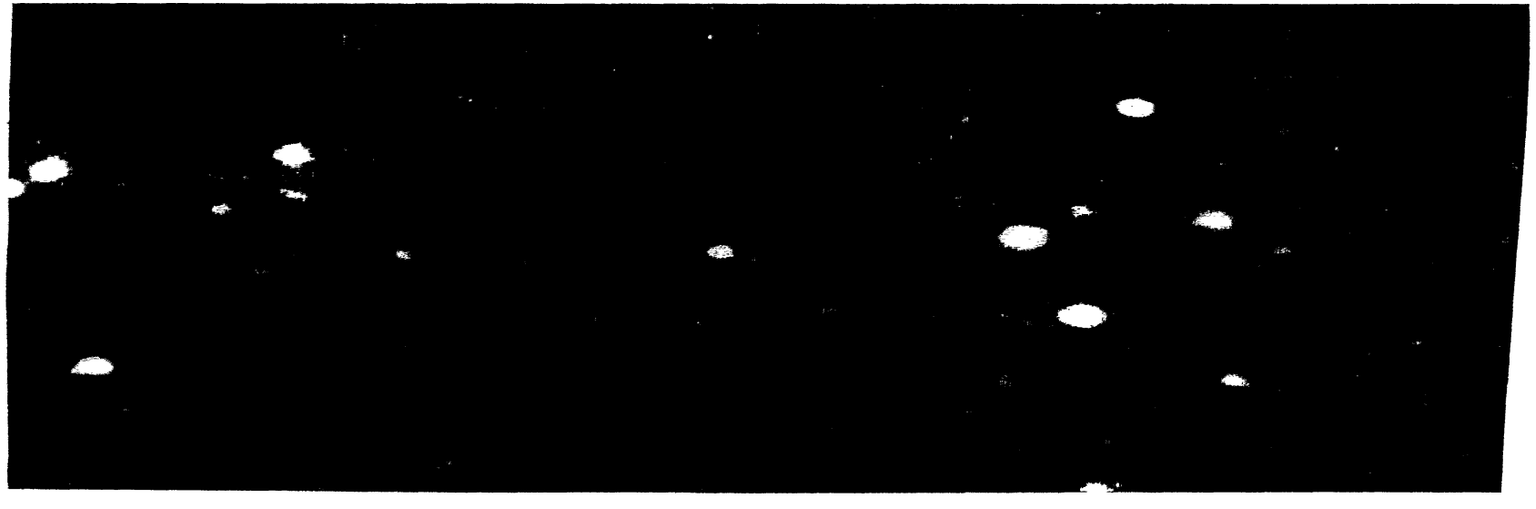

Fig. 3.24h. The R band CCD image of the field of 1320+299. Overlaid is the A-array radio image at 6.0cm

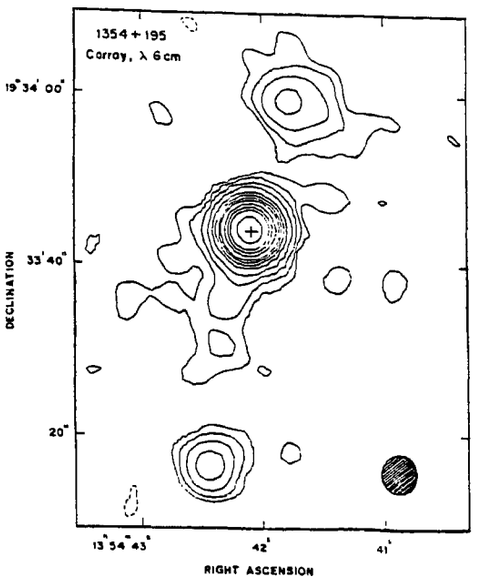

Fig.3.25a. Contour levels: 1230 x (-0.01, -0.005, 0.005, 0.01, 0.02, 0.04, 0.08, 0.12, 0.16, 0.2, 0.3, 0.4, 0.5, 0.75) mJy/beam.

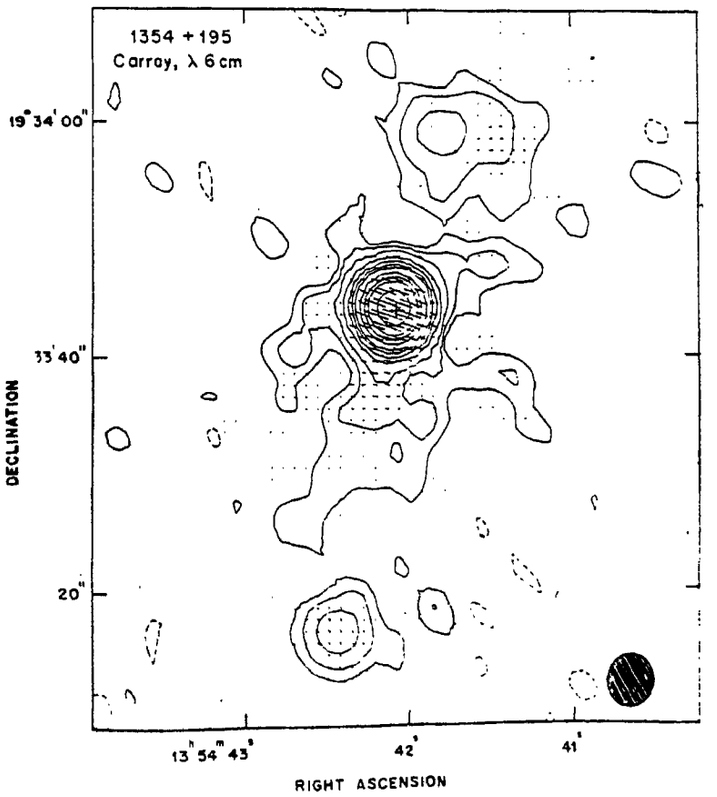

Fig.3.25b. Contour levels: 1202 x (-0.02, -0.01, 0.01, 0.02, 0.04, 0.08, 0.12, 0.16, 0.2, 0.3, 0.4, 0.5, 0.75) mJy/beam.

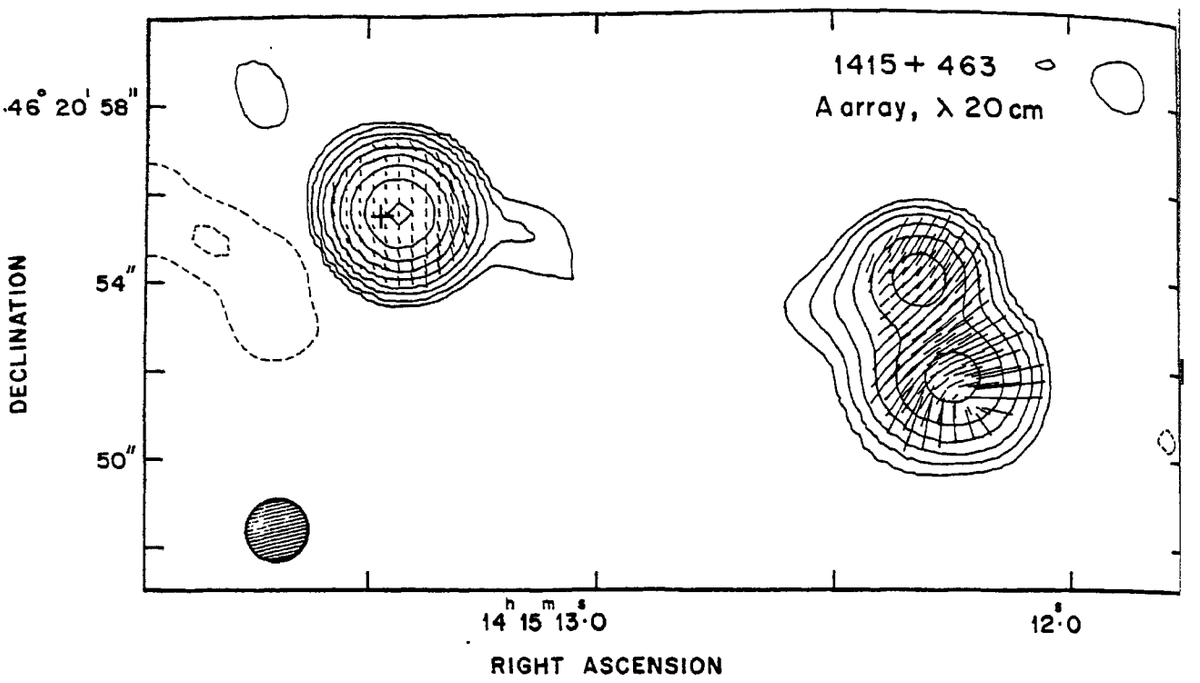

Fig.3.26a. Contour levels: 2 x (-4, -2, -1, 1, 2, 4, 8, 16, 32, 64, 128, 256) mJy/beam. Polarization: 1 arcsec = 0.127 ratio.

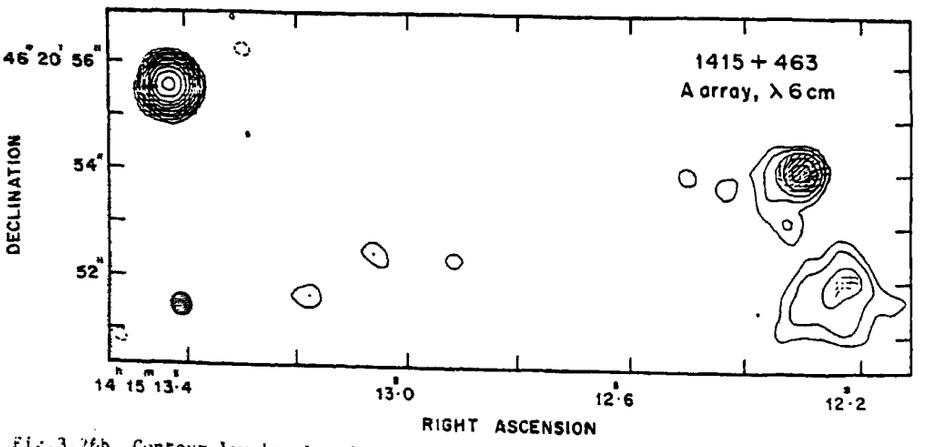

Fig.3.26b. Contour levels: 1 x (-4, -2, -1, 1, 2, 4, 8, 16, 32, 64, 128, 256, 512) mJy/beam. Polarization: 1 arcsec = 0.544.

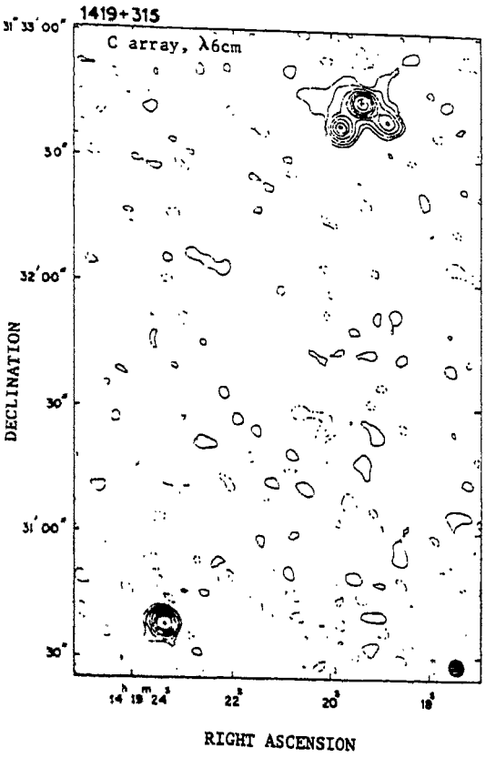

Fig. 3.27a. Contour levels: 55 x (-0.06, -0.03, 0.03, 0.06, 0.12, 0.2, 0.3, 0.4, 0.5, 0.75) mJy/beam.

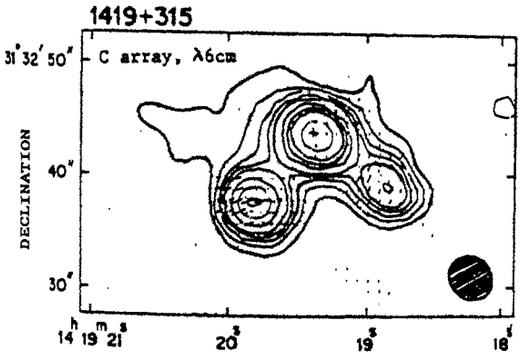

Fig. 3.27b. Contour levels: 54 x (-0.08, -0.04, 0.04, 0.08, 0.12, 0.16, 0.2, 0.3, 0.4, 0.5, 0.75) mJy/beam.

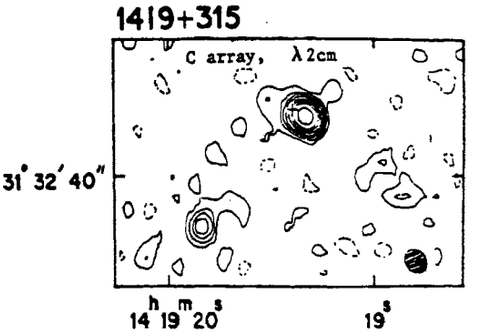

Fig. 3.27c. Contour levels: 36 x (-0.1, -0.05, 0.05, 0.1, 0.2, 0.3, 0.3, 0.4, 0.5, 0.75)mJy/beam.

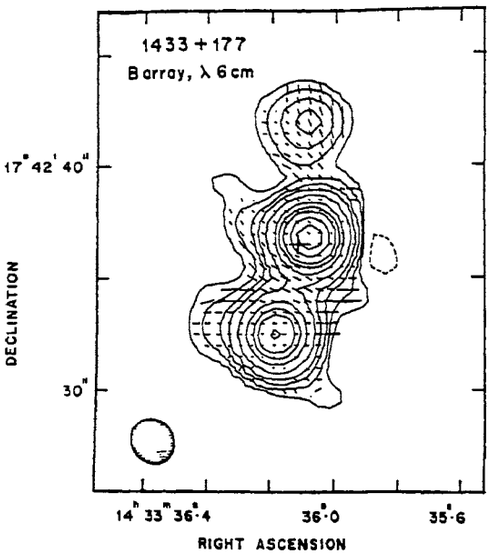

Fig.3.28a. Contour levels: 3 x (-0.7, 0.7, 1.5, 3, 5, 10, 20, 30, 40, 60, 80) mJy/beam. Polarization: 1 arcsec = 0.303 ratio.

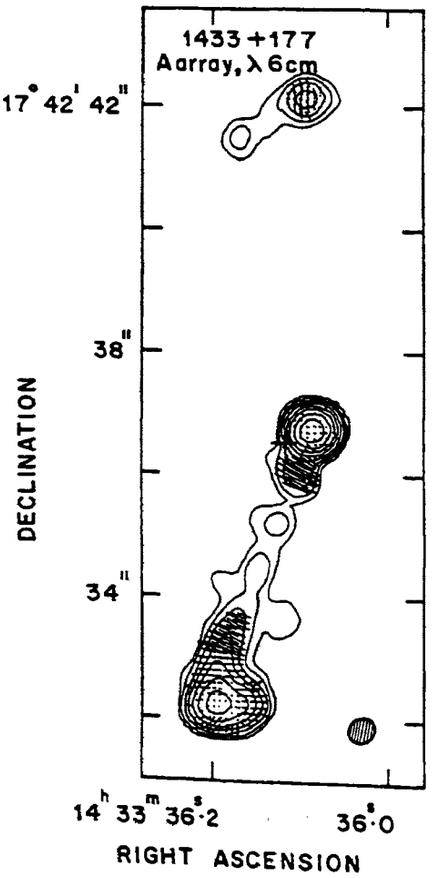

Fig.3.28b. Contour levels: 1 x -4, -2, -1, 1, 2, 4, 8, 16, 32, 64, 128) mJy/beam. Polarization: 1 arcsec = 0.919 ratio.

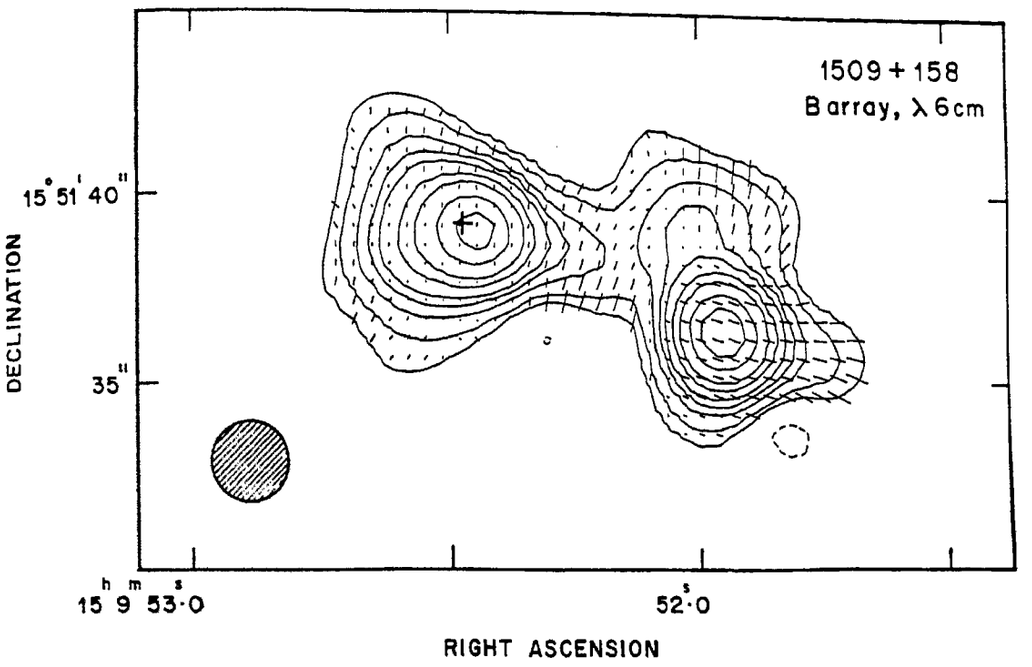

Fig. 3.29a. Contour levels: 1.3 x (-2.5, 2.5, 5, 10, 15, 20, 30, 40, 60, 80) mJy/beam. Polarization: 1 arcsec = 0.469 ratio.

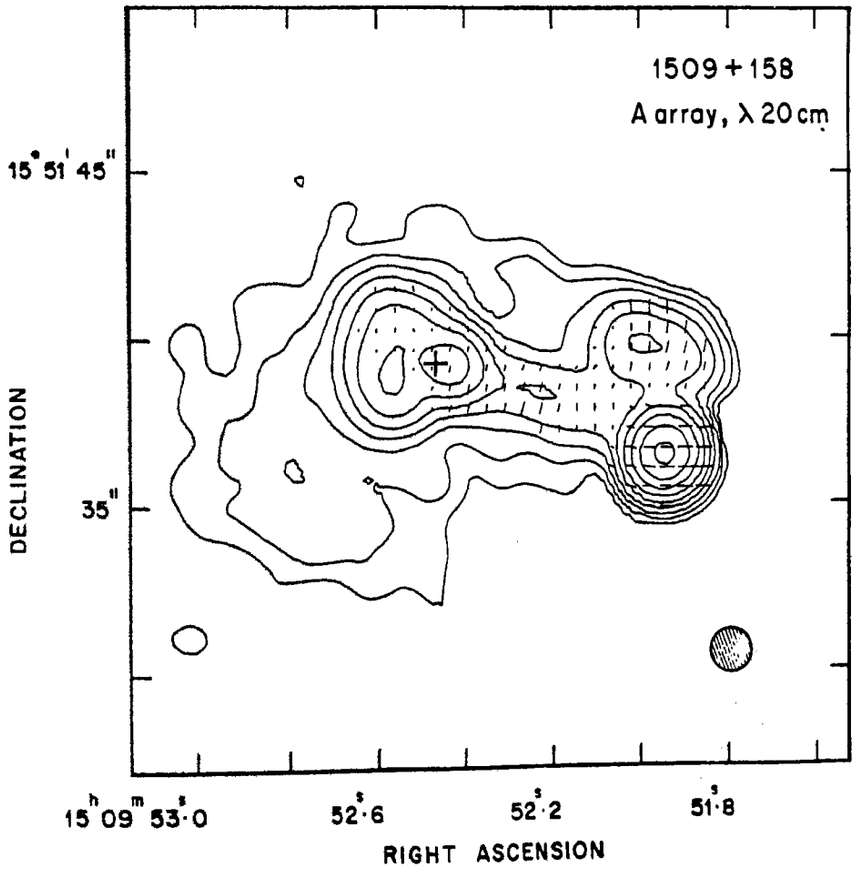

Fig. 3.29b. Contour levels: 1 x (-4, -2, -1, 1, 2, 4, 8, 16, 32, 64, 128, 256) mJy/beam.

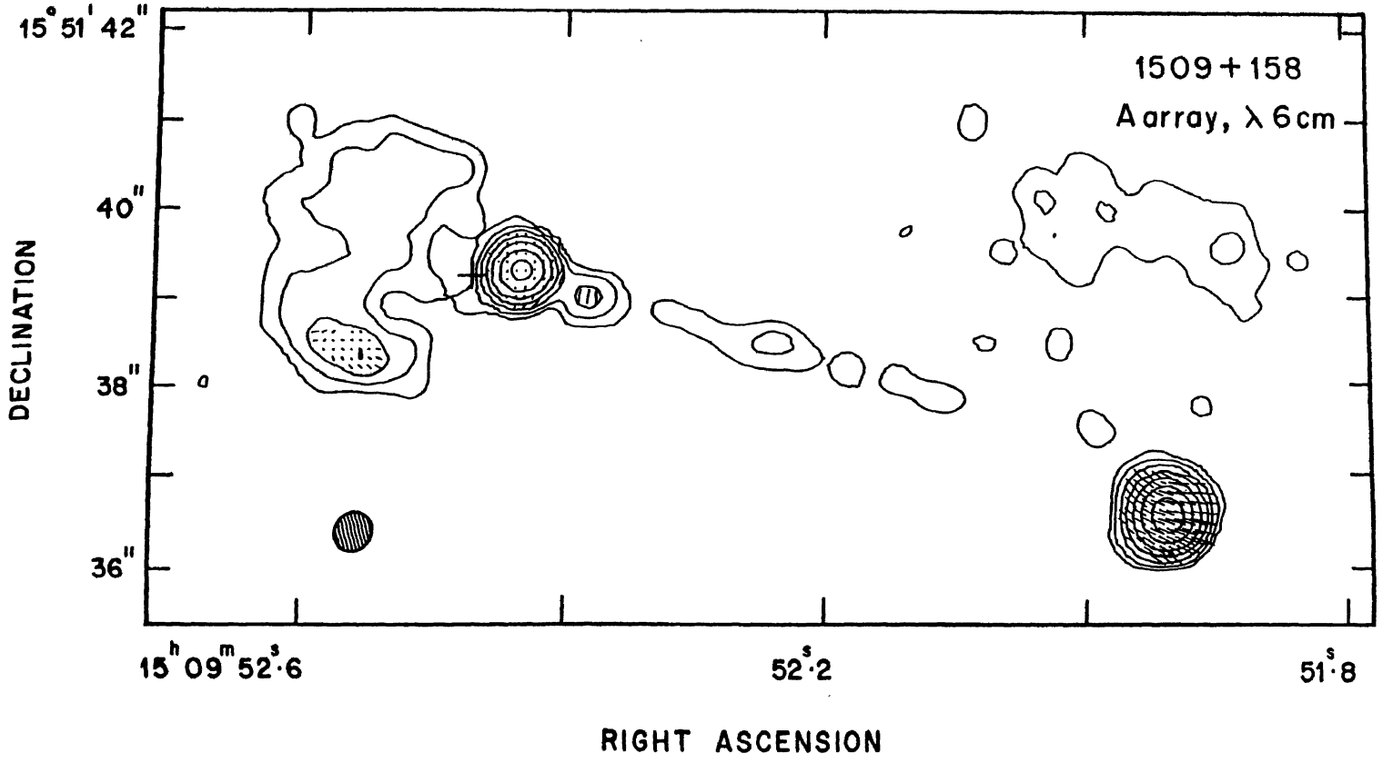

Fig. 3.29c. Contour levels: 1 x (-4, -2, -1, 1, 2, 4, 8, 16, 32, 64) mJy/beam.
Polarization: 1 arcsec = 0.962 ratio.

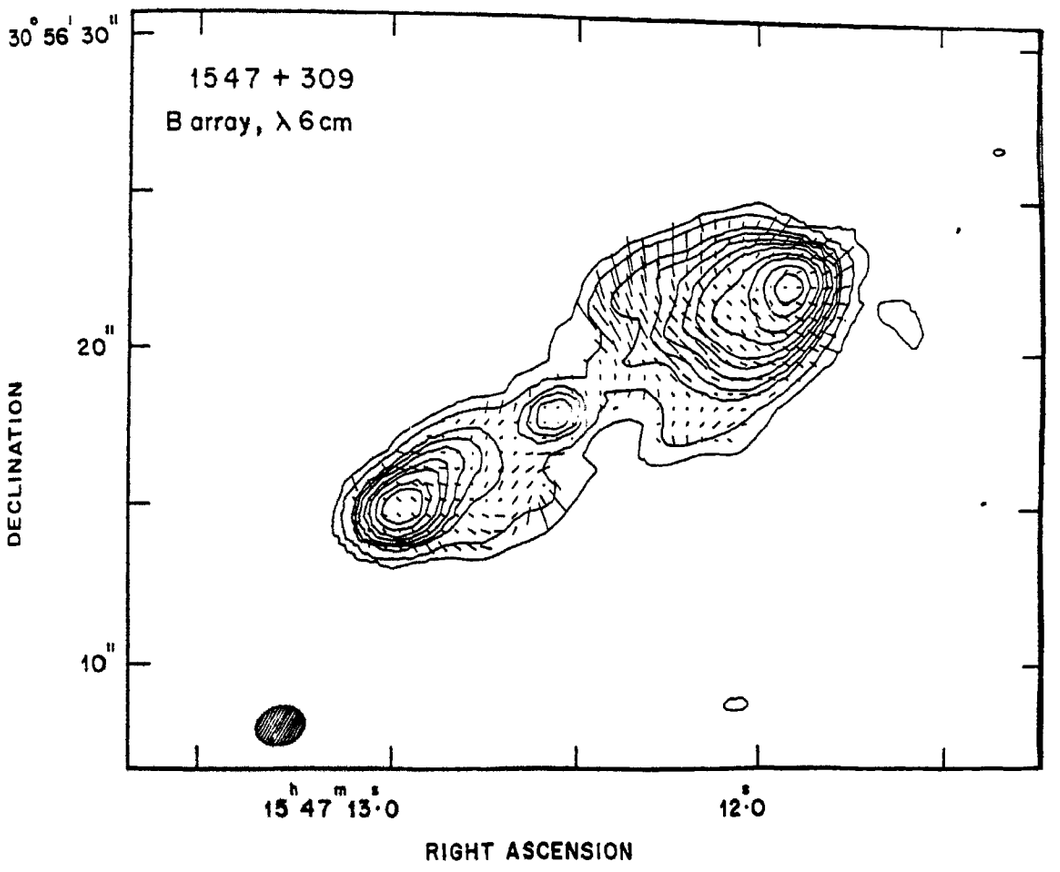

Fig. 3.30. Contour levels: 0.64 x (-0.8, 0.8, 2, 5, 7, 10, 15, 20, 30, 40, 60, 80) mJy/beam. Polarization: 1 arcsec = 0.464 ratio.

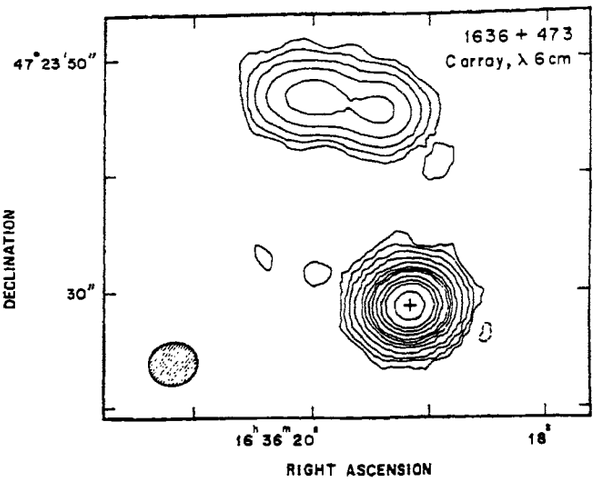

Fig. 3.31a. Contour levels: 492 x (-0.01, -0.005, 0.005, 0.01, 0.02, 0.04, 0.08, 0.12, 0.16, 0.2, 0.3, 0.4, 0.5, 0.75) mJy/beam.

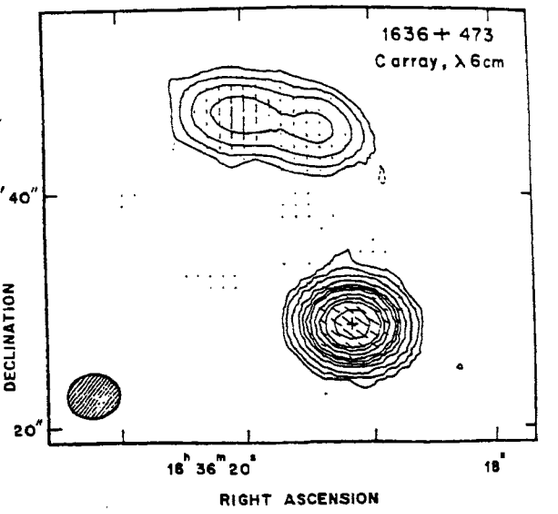

g. 3.31b. Contour levels: 494 x (-0.02, .01, 0.01, 0.02, 0.04, 0.08, 0.12, 0.16, 0.2, 0.3, 0.4, 0.5, 0.75) mJy/beam.

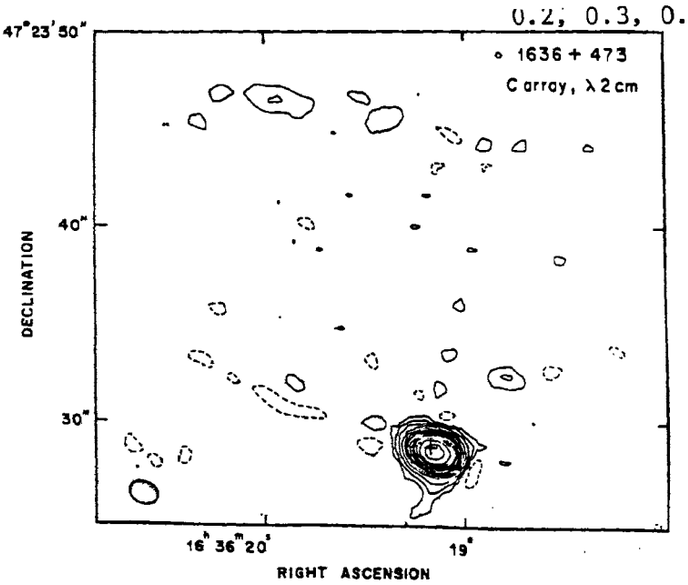

Fig. 3.31c. Contour levels: 885 x (-0.03, -0.015, -0.0075, 0.0075, 0.015, 0.03, 0.06, 0.09, 0.12, 0.15, 0.2, 0.25, 0.3, 0.4, 0.5, 0.75) mJy/beam.

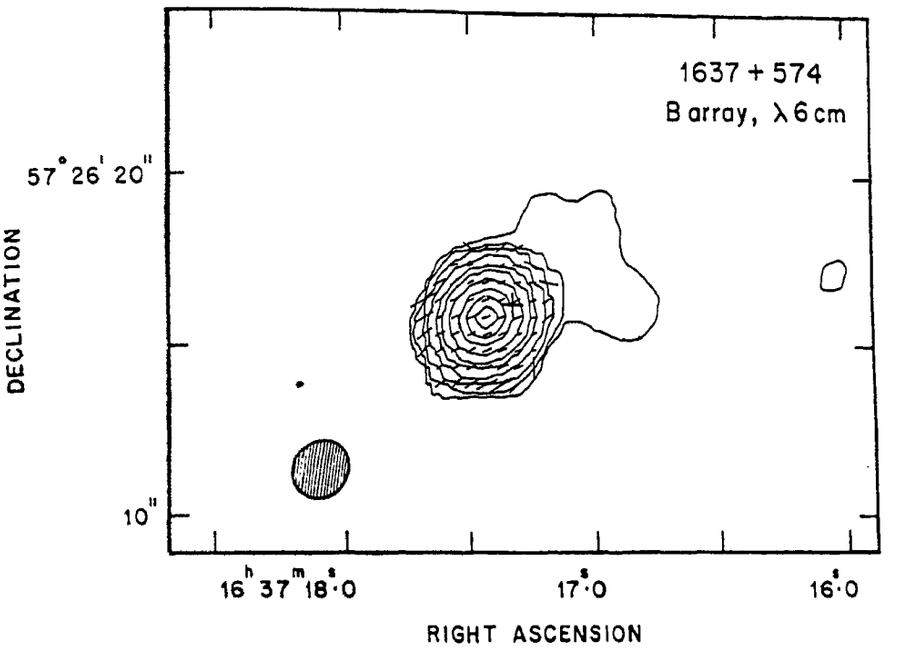

Fig.3.32. Contour levels: 1.6 x (-0.2, 0.2, 0.3, 0.7, 2, 5, 10, 20, 40, 60, 80) mJy/beam. Polarization: 1 arcsec = 0.115 ratio.

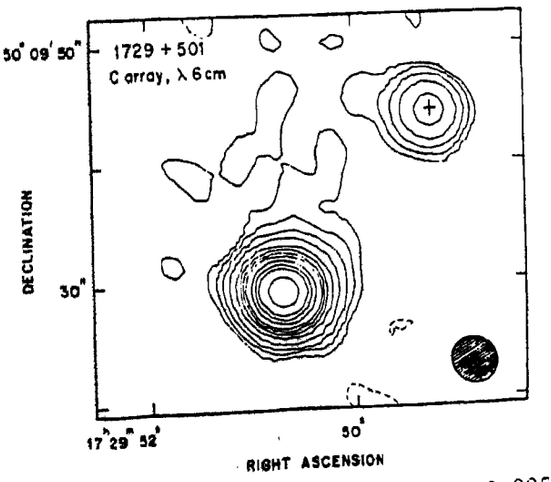

Fig.3.33a. Contour levels: 355 x (-0.01,-0.005, 0.005, 0.01, 0.02, 0.04, 0.08, 0.12, 0.16, 0.2, 0.3, 0.4, 0.5, 0.75) mJy/beam.

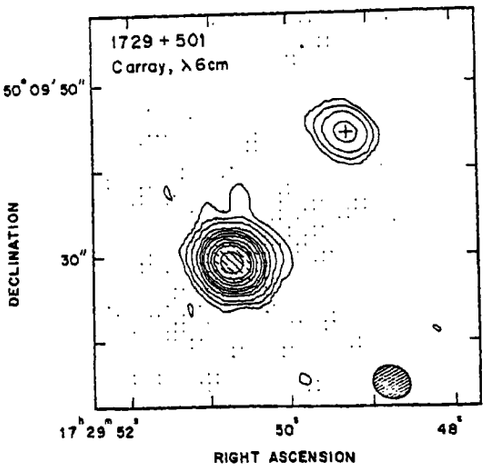

Fig.3.33b. Contour levels: 353 x (-0.02, -0.01, 0.01, 0.02, 0.04, 0.08, 0.12, 0.16, 0.2, 0.3, 0.4, 0.5, 0.75) mJy/beam

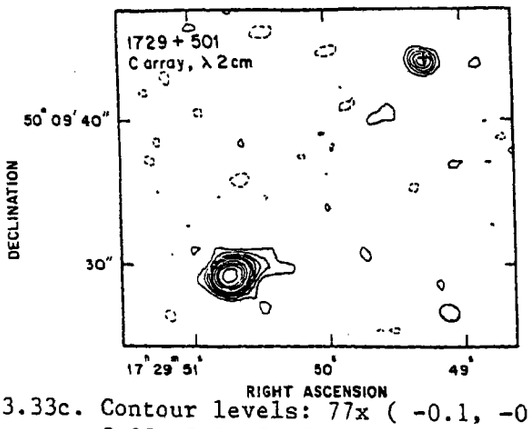

Fig.3.33c. Contour levels: 77x (-0.1, -0.05, 0.05, 0.1, 0.15, 0.2, 0.3, 0.4, 0.5, 0.75) mJy/beam.

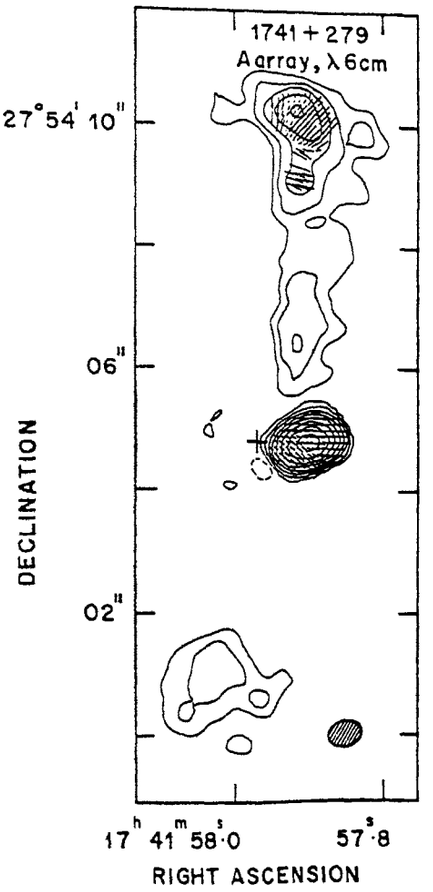

Fig.3.34. Contour levels: 1 x (-4, -2, -1, 1, 2, 4, 8, 16, 32, 64, 128) mJy/beam. Polarization: 1 arcsec = 0.479 ratio.

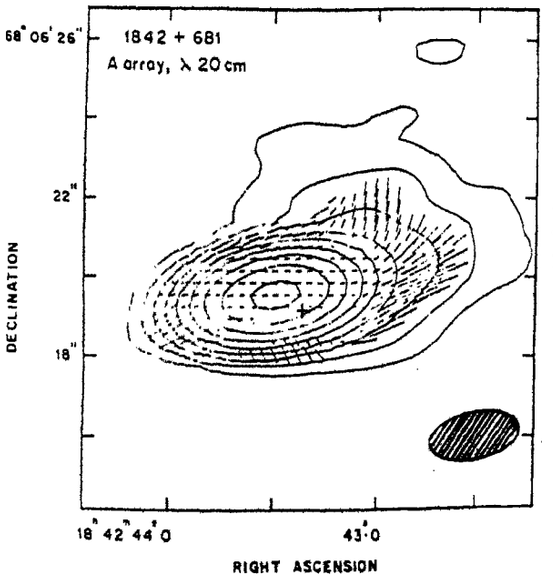

Fig. 3.35. Contour levels: 1 x (-4, -2, -1, 2, 4, 8, 16, 32, 64, 128, 256, 512) mJy/beam. Polarization: 1 arcsec = 0.11 ratio.

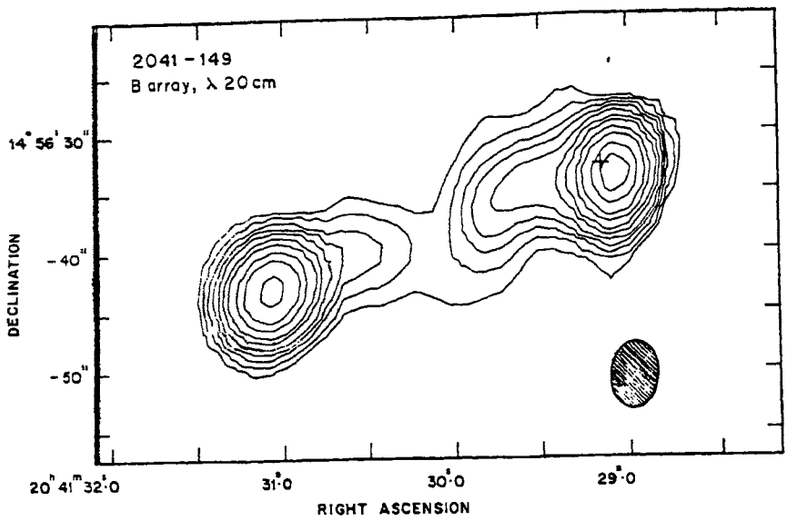

Fig.3.36a. Contour levels: 1.9 x (-1.5, 1.5, 3, 5, 7, 10, 15, 20, 30, 40, 60, 80) mJy/beam.

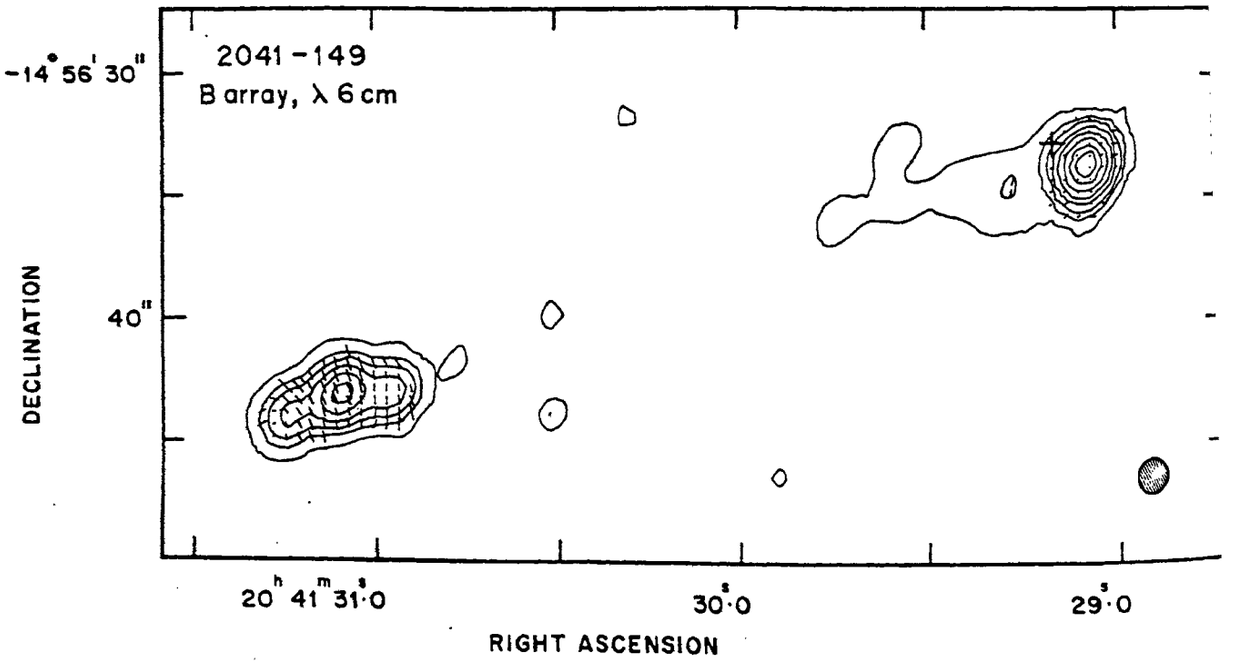

Fig.3.36b. Contour levels: 468 x (-1, 1, 4, 8, 15, 25, 40, 60, 80) mJy/beam. Polarization: 1 arcsec = 0.41 ratio.

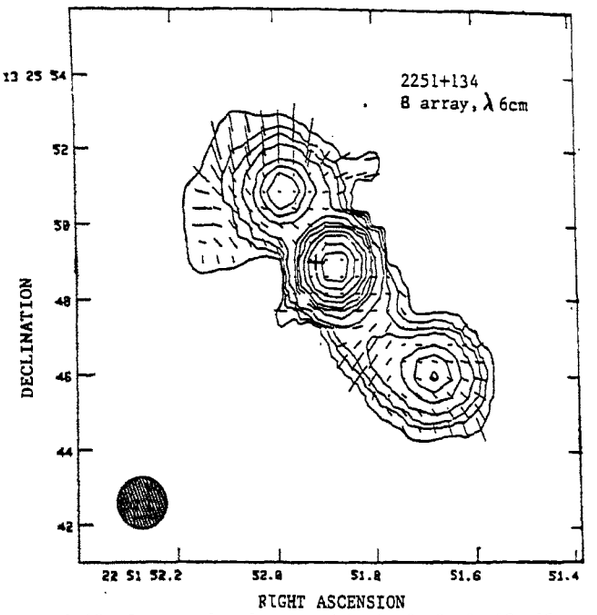

Fig. 3.37. Contour levels: 4 x (-1, 1, 2, 3, 5, 10, 15, 20, 30) mJy/beam. Polarization: 1 arcsec = 0.22 ratio.

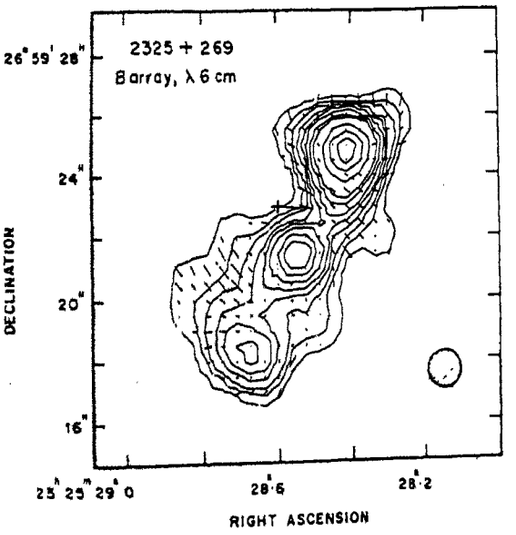

Fig.3.38. Contour levels: 1.98 x(-1, 1, 2, 3, 5, 7, 10, 15, 20, 40, 60, 80) mJy/beam. Polarization: 1 arcsec = 0.515 ratio.

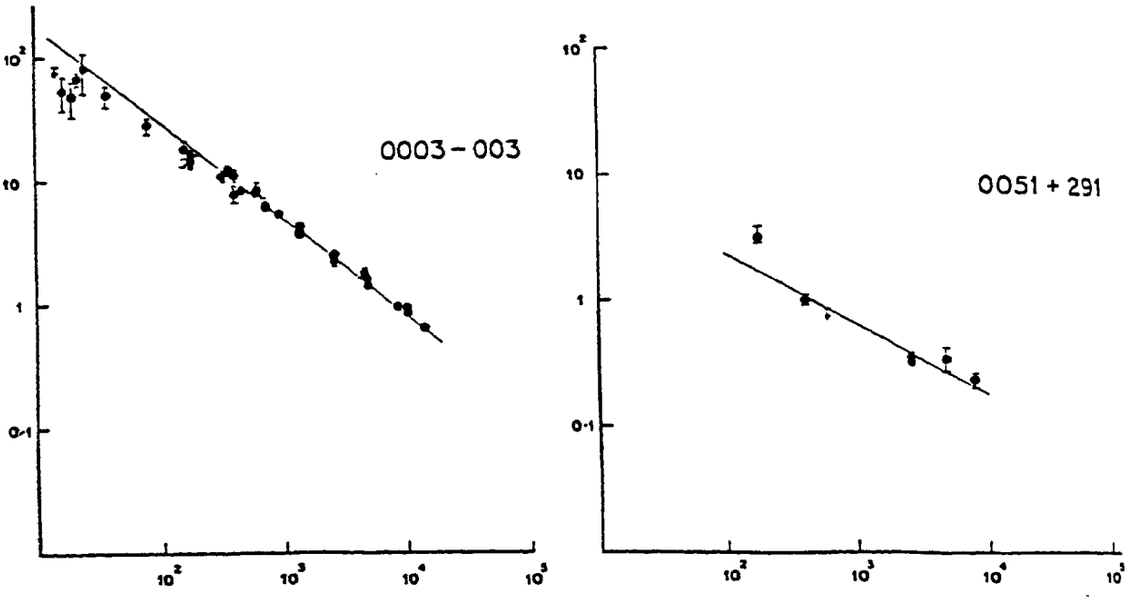

Fig. 3.39 The radio spectra of the sources along with those of their components (designated C:core, N:north, SW:south west, etc., except in the case of 1320+299:cf. description of the source, Section 3.3). Filled circles represent the flux density of the entire source; crosses represent the flux density of the core component; unfilled circles represent flux densities of the other components, except in the case of 1055+018 and 1637+574, where open circles represent simultaneously measured flux densities for the entire source. All flux densities are in Jy unless otherwise stated, and frequencies are in MHz. Solid and dashed curves represent least-squares fits to the spectra of the entire source and the components respectively.

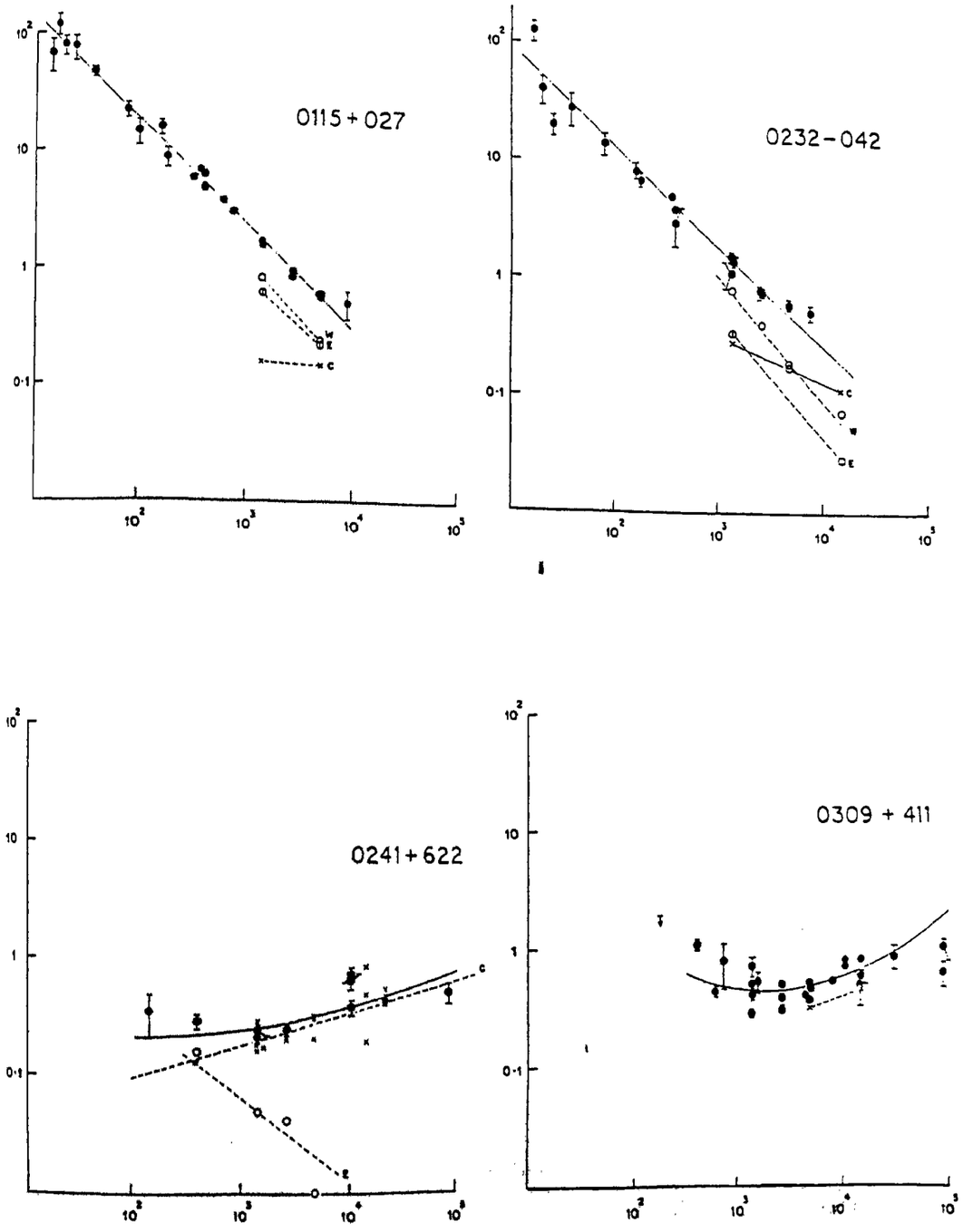

Fig. 3.39 continued.

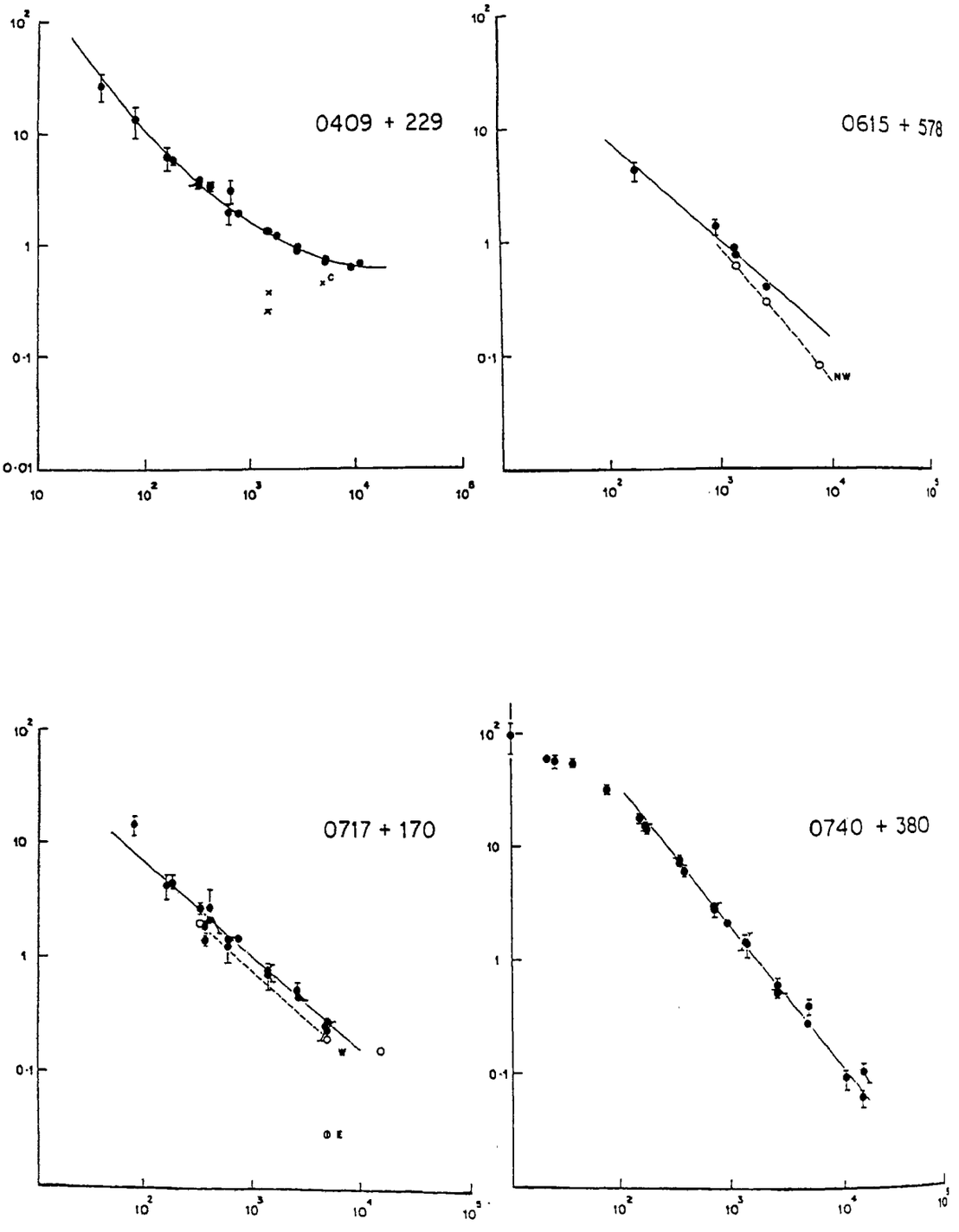

Fig. 3.39 continued.

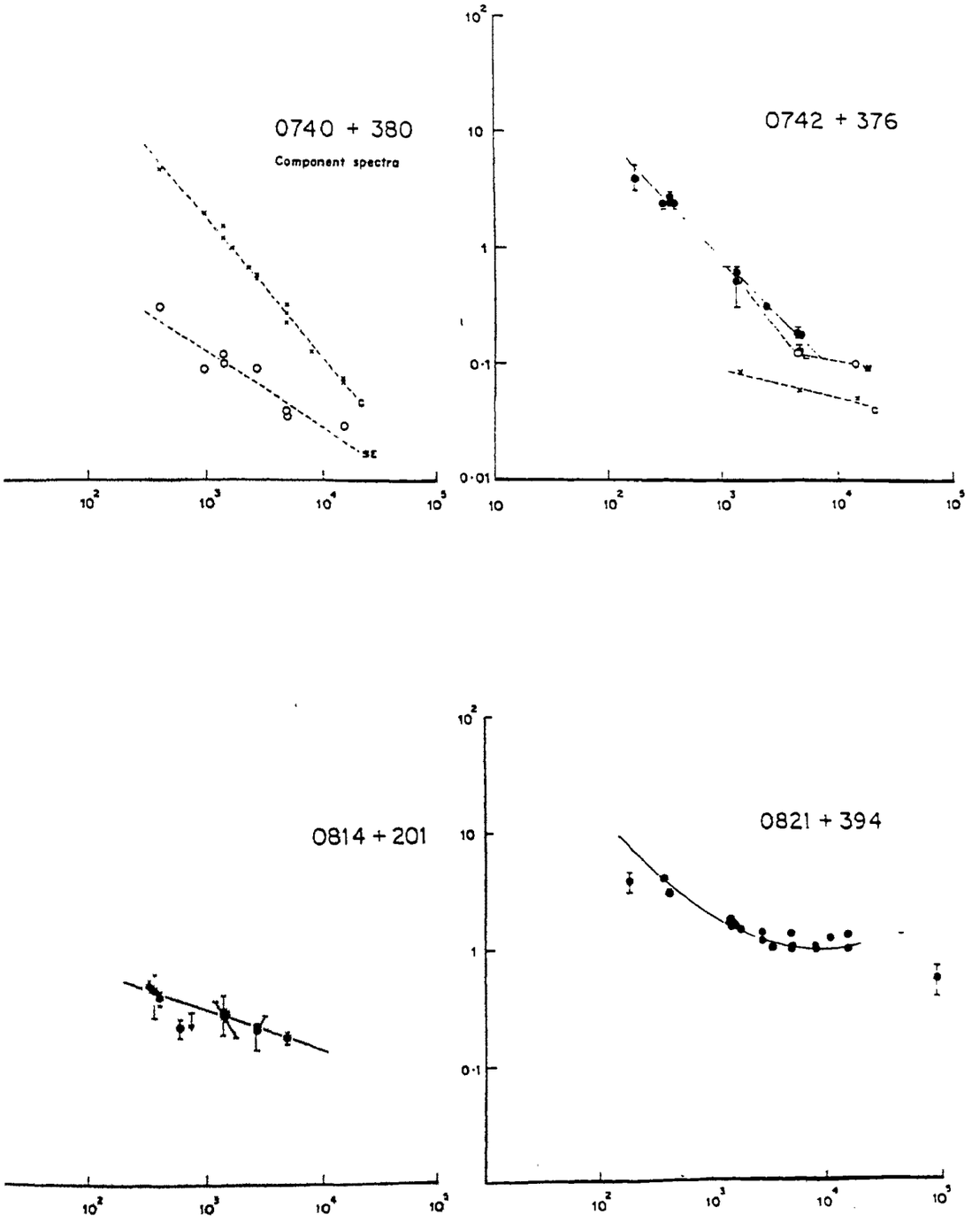

Fig. 3.39 continued.

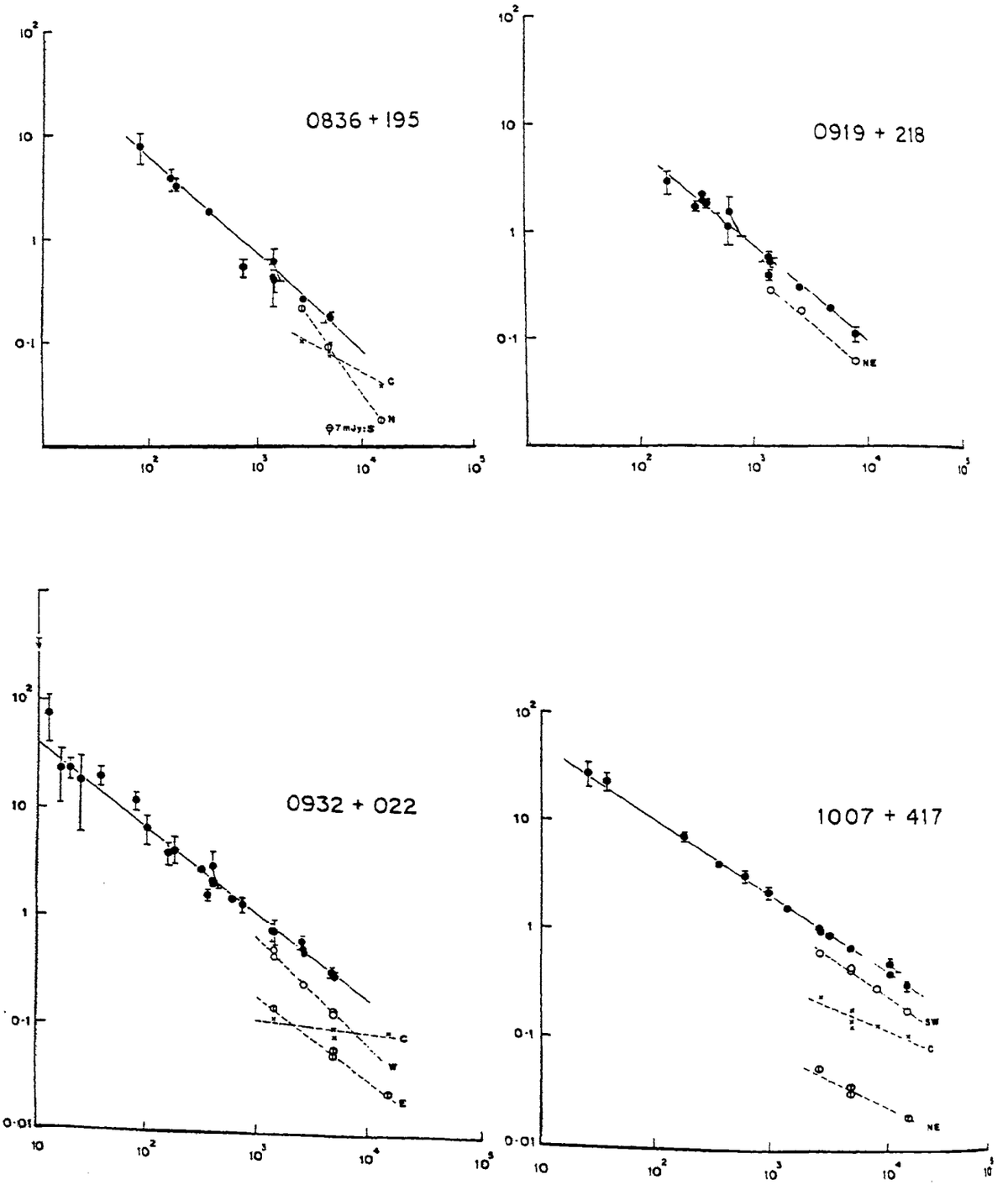

Fig. 3.39 continued.

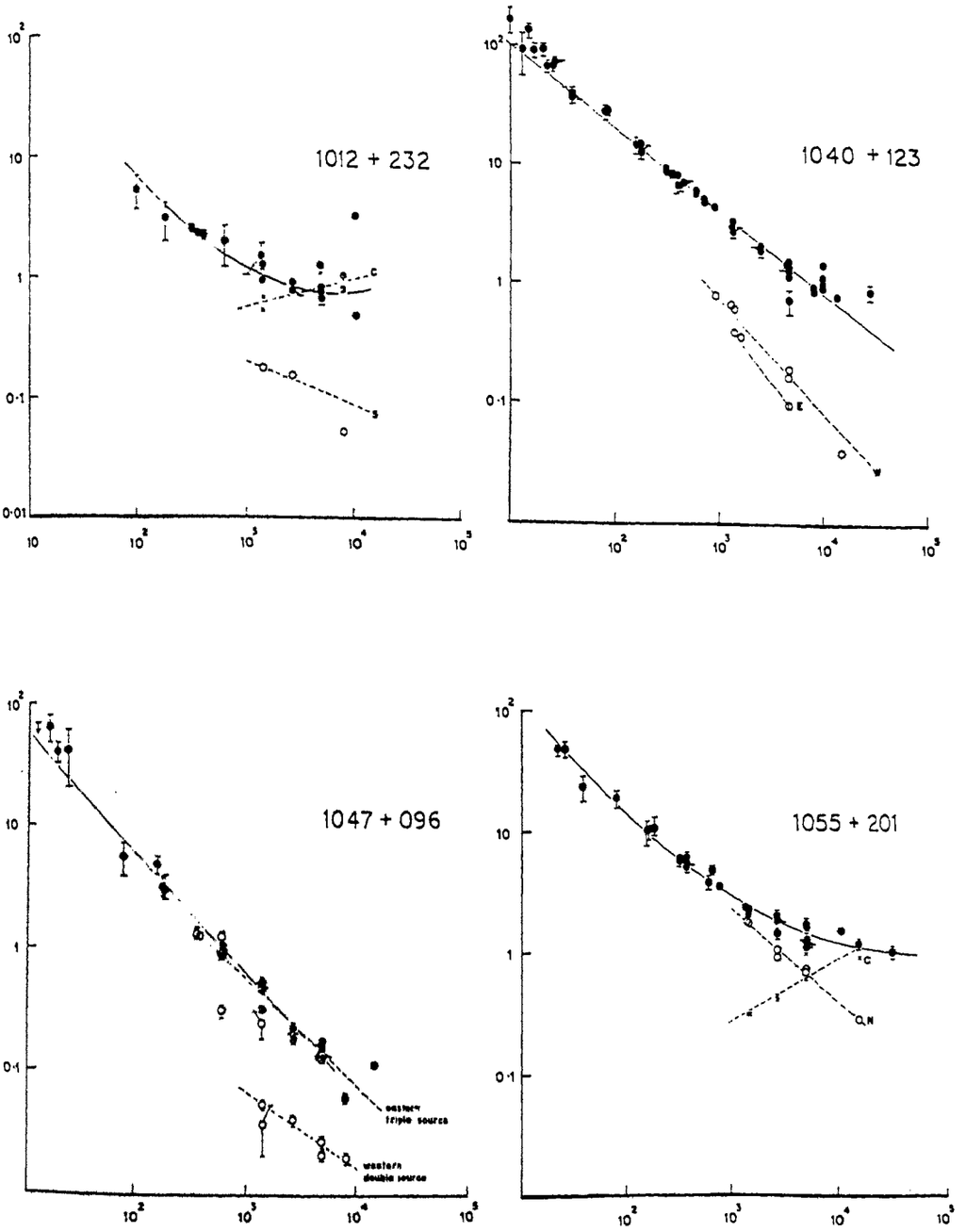

Fig. 3.39 continued.

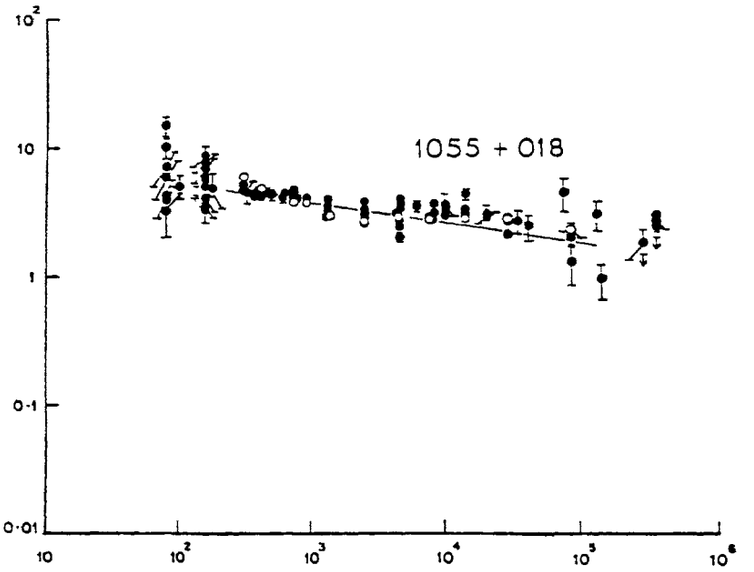

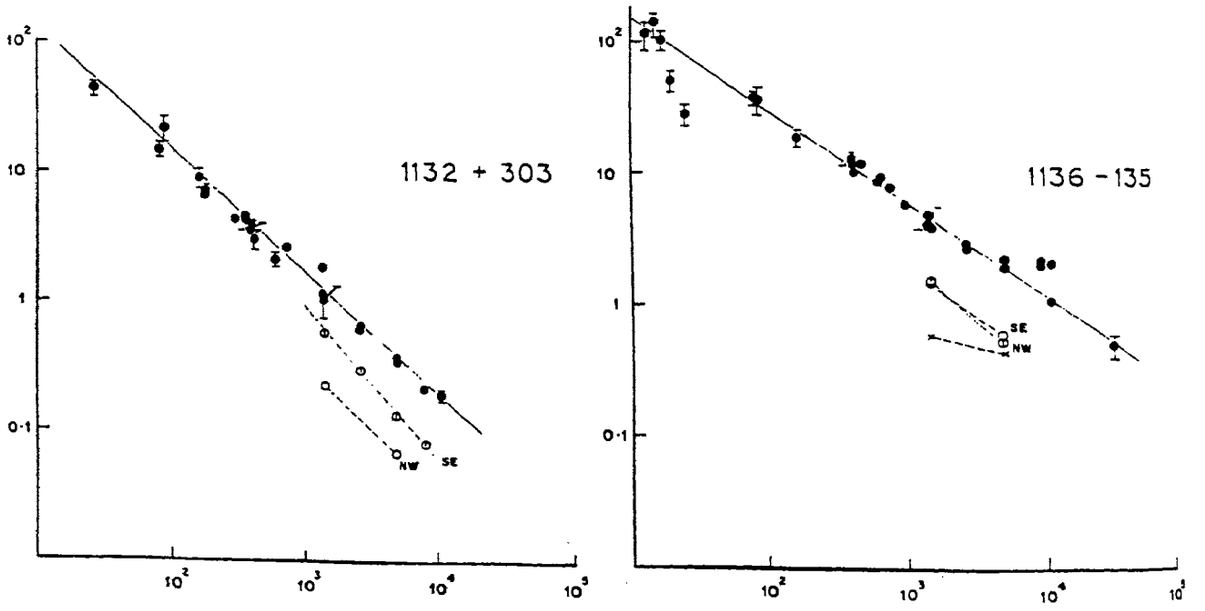

Fig. 3.39 continued

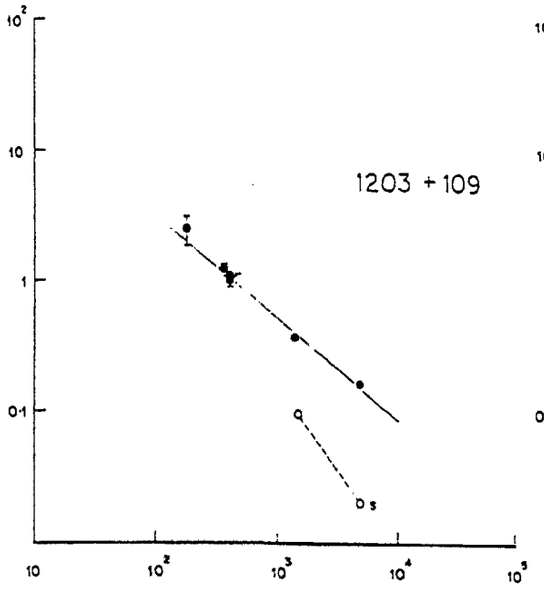

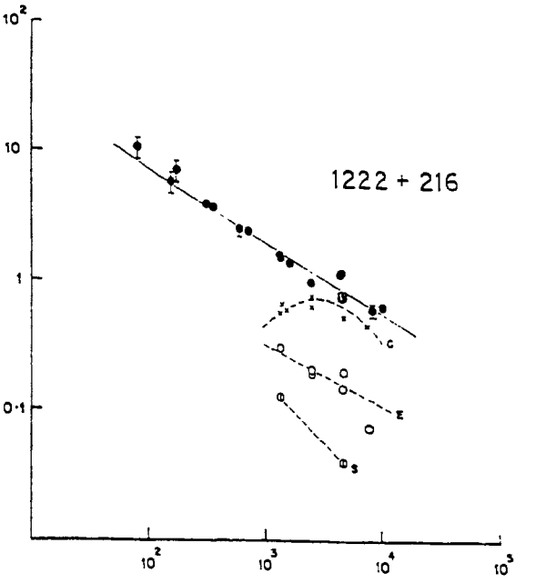

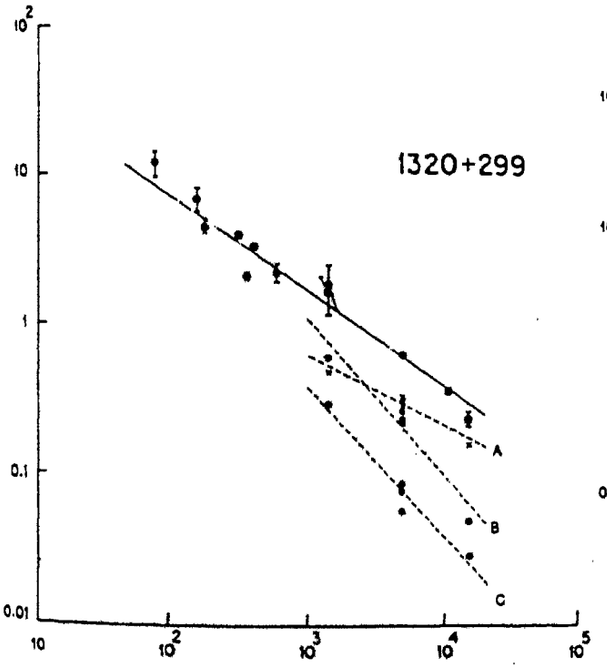

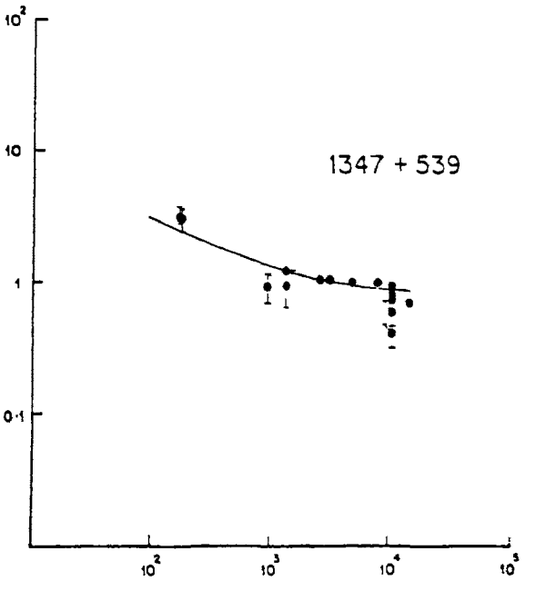

Fig. 3.39 continued.

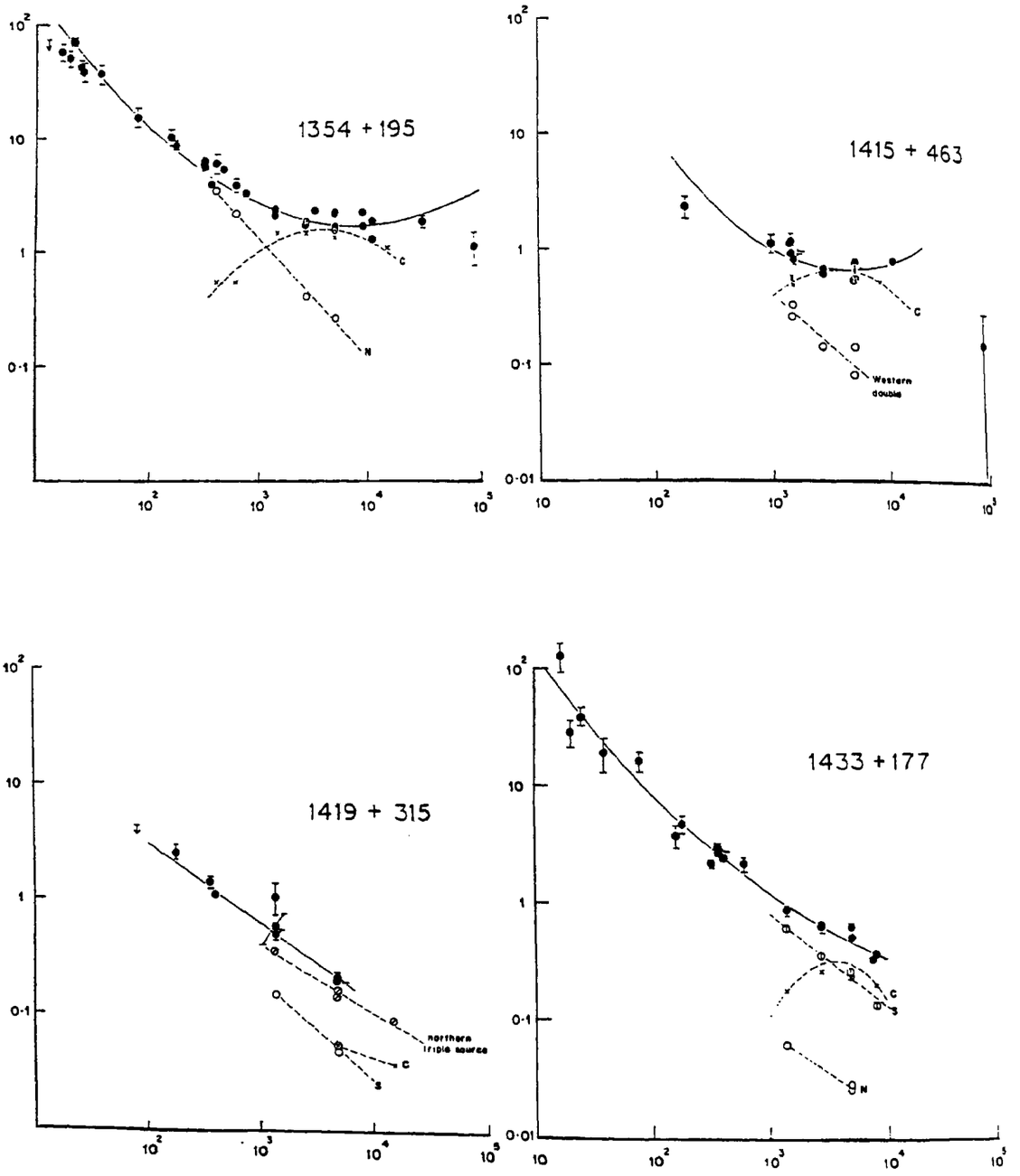

Fig. 3.39 continued.

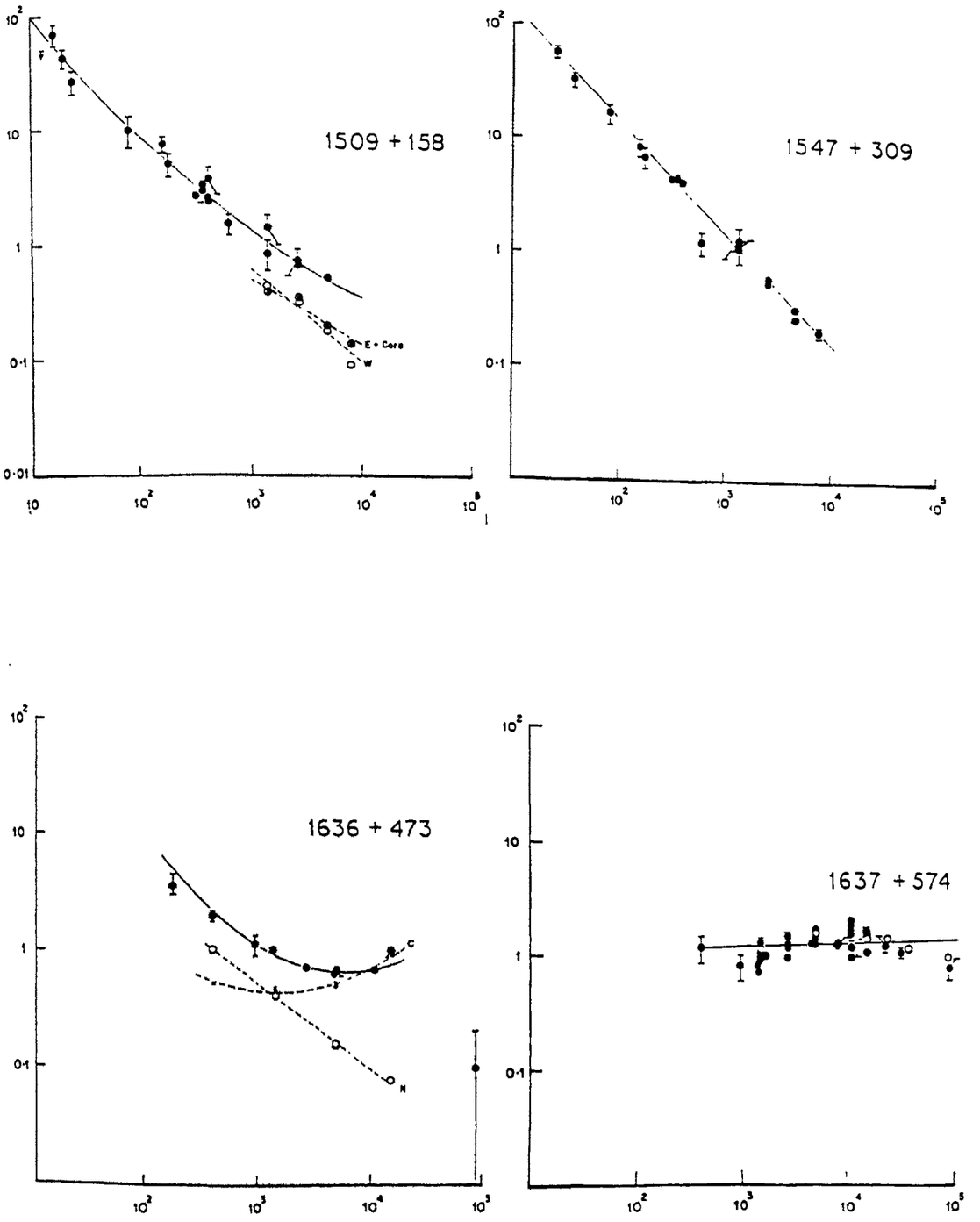

Fig. 3.39 continued.

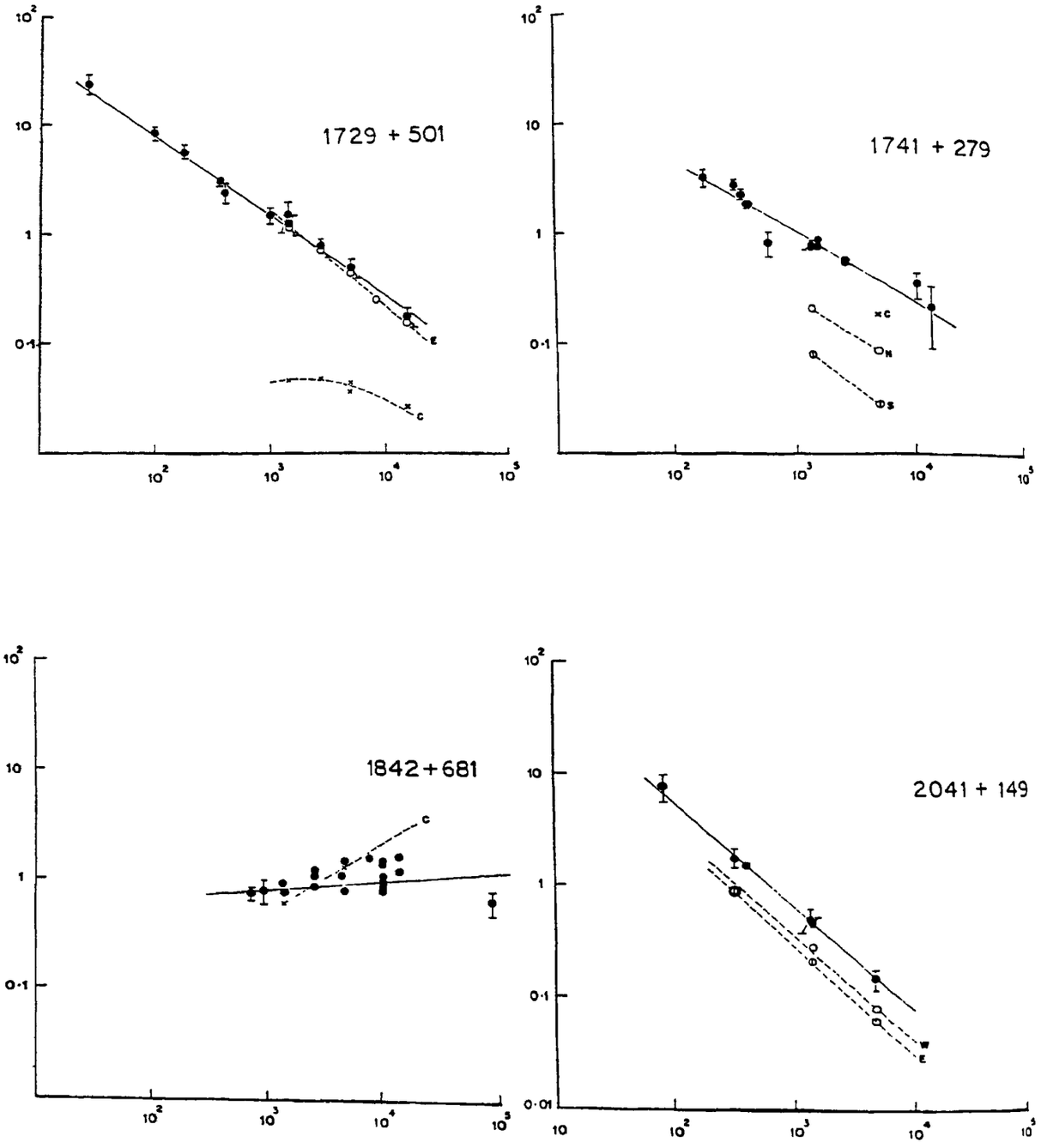

Fig. 3.39 continued.

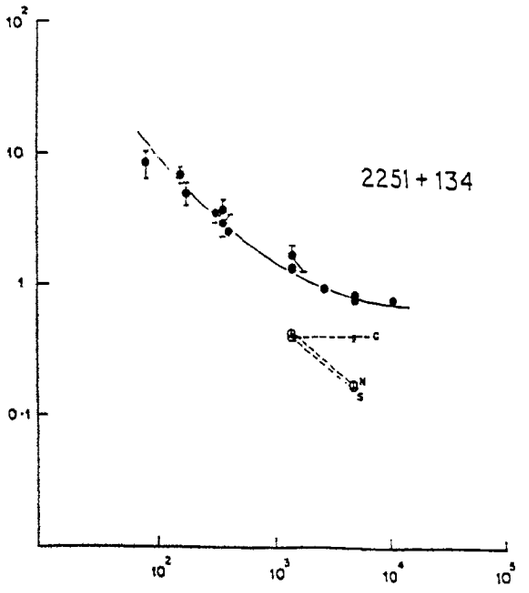

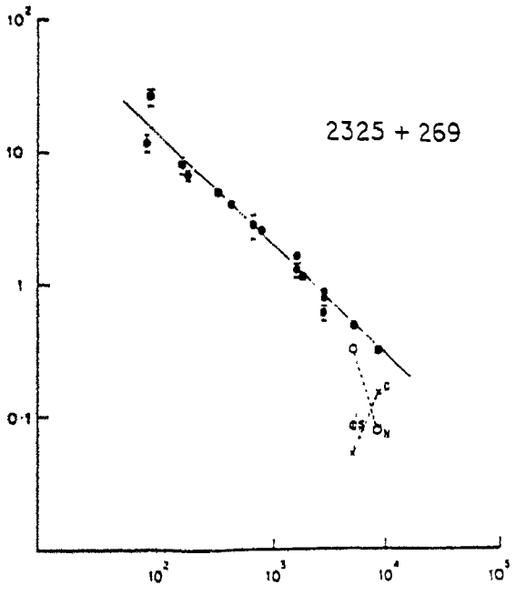

Fig. 3.39 continued.

to be wrong. Each of 0740+380, 1047+096, 1320+299 and 1419+315 is most likely to be a chance juxtaposition of two unrelated radio sources, one of which is presently unidentified. In the case of 1203+109 and 2251+134, the "outer component" of the earlier observations is probably spurious.

Of the remaining "genuinely asymmetric" objects, 11 show one-sided structure even with the high resolution and dynamic ranges obtained. (Among them, 0309+411, 1055+018 and 1055+201 have been shown to be two-sided by other authors.) Among the rest, asymmetric surface brightness ratios and separation ratios are often seen.

Radio jets between the cores and the outer components have been detected in many of the objects. The polarization E-vectors often align perpendicular to the elongation of the jet. In cases where the jet appears to bend, they appear to follow these bends. The jets are in almost every case one-sided. All these properties are consistent with what is known of quasar radio structure in general.

Chapter 4

DOES BULK RELATIVISTIC MOTION OCCUR ON A LARGE SCALE ?

Do the relativistic speeds inferred in the nuclei of radio quasars persist out to the large scale jets and hot spots that are several hundred kiloparsecs away? Kapahi (1981a) examined the conjecture that extragalactic radio sources of suspected one-sided structure were actually those with large apparent side-to-side asymmetry that arose out of relativistic Doppler effects. The data that he compiled for all such objects known at the time supported this conjecture. These sources would then be oriented close to the line of sight, and at least mild bulk relativistic motion would be implied not only in the jets but also in the hot spots.

The availability of better quality data for the sample of Kapahi (1981a) enable a more stringent test of this hypothesis, and this is the focus of the present chapter. Radio images of high angular resolution presented in Chapter 3 form the main body of data used; a systematic examination of the behaviour of asymmetry in radio morphology in the context of the relativistic beaming hypothesis has been attempted therefrom. The basic idea of the unified scheme, viz., that the prominence of the nuclear radio component (R) is a statistical measure of the angle of inclination to the line of sight (e.g., Kapahi & Saikia, 1982) is used. While there is good evidence for the occurrence of bulk relativistic motion in radio quasars, the case for radio galaxies and radio-quiet quasars is not as clear. Especially in radio galaxies that are of Fanaroff-Riley type I (Fanaroff & Riley, 1974), it is very likely that the bulk velocities of the radio-emitting effluents are subrelativistic. The analysis is therefore

restricted to radio-loud quasars.

The sample of the Kapahi (1981a) is slightly reconstituted in view of the data presented in chapter 3, and properties that are expected to be a function of orientation with respect to the line of sight are derived. These properties are then compared with those of three quasar samples selected to be both more and less extreme in their orientation with respect to the line of sight (as per the relativistic beaming scenario).

4.1 The new sample

The sample of radio sources selected for study of asymmetry in radio structure was mostly drawn from the list of Kapahi (1981a). Various facts, mostly revealed by high resolution images of these objects (either from Chapter 3 or from the literature) warrant exclusion of some sources from the analysis that follows. All additions to and deletions from the sample of Kapahi (1981a) are described below. The sample thus reconstituted shall be referred to hereinafter as the **D2 sample** (so named after the nomenclature of Miley, 1971).

The following objects, not in Kapahi (1981a), were included in the D2 sample (cf. chapter 2): 0232-042, which was tentatively classified as one-sided by Miley & Hartsuijker (1978); 0717+170, which was suspected to have one-sided structure by Joshi (1981); 1007+417, which was found one-sided by Kapahi (1981b) but two-sided by Miley & Hartsuijker (1978); 2325+269, which was found to be one-sided by Miley & Hartsuijker (1978) and two-sided by Potash & Wardle (1979). VLA images for all of these objects have been presented in chapter 3.

Objects in the list of Kapahi (1981a) whose optical identification is in doubt are not included in the D2 sample. These are: 0615+578, the original identifications for which were later found to be stars; 0717+170, 0814+201 and 2041-149, in the case of all of which the new VLA images call into question the identifications previously suggested (cf. section 3.3).

In the cases of 0740+380, 1047+096, 1320+299 and 1419+315, what had been previously regarded as the "central component" (associated with a QSO) has been revealed to be almost certainly an independent quasar. The "outer component" is in each case almost certainly a physically distinct object, juxtaposed by chance near the identified quasar. They have therefore not been included in the D2 sample.

What was regarded as the "core component" of 1203+109 and 2251+134 turns out to be an independent triple source. The "outer component" of the earlier observations remains undetected. These objects have been excluded.

All radio galaxies and radio-quiet quasars have been excluded from the D2 sample because the focus of this study is the evidence for relativistic bulk motion in radio-loud quasars. Therefore, only radio-loud quasars are included in the D2 sample. Hence, the following objects were eliminated:

* 0241+622, which actually belongs to the class of radio-quiet QSOs. It is of relatively low radio luminosity, and is detectable easily at radio wavelengths only due to its proximity to us. Also, it probably inhabits a spiral galaxy (cf. description in section 3.3), while radio loud quasars are known to usually reside in elliptical galaxies.

* 0309+411, 1350+316 and 1807+698, each of which is optically identified with an elliptical galaxy.

The 36 objects in the D2 sample are listed in **Table 4.1.**

4.2 The comparison samples

Three samples of quasars have been chosen for comparison of properties with the D2 sample. The first two are expected to have most of their objects inclined at relatively small angles to the plane of the sky, while the third is expected to consist of quasars inclined extremely close to the line of sight. The three comparison samples are described below. Their constituent objects are listed in **Tables 4.2** to **4.4** respectively.

4.2.1 The 3CR sample

This is the extremely well-known and extensively studied sample of extragalactic radio sources derived from the the 3rd Cambridge Radio survey at 178 MHz (Laing *et al.*, 1983). The sample has a flux density limit of 10 Jy at this frequency. The low survey frequency has resulted in the selection of objects that are mostly of the steep radio spectrum type, since those of flat radio spectrum are rarely bright enough at this frequency. It is expected in the unified scheme that quasars from this sample would be oriented randomly in the sky.

There are 44 quasars in the 3CR sample. Redshifts are available for all the objects. Radio images obtained with the VLA are available in the literature for most of them, and these data were used to derive their properties that are of interest here. In exceptional cases it was necessary to use lower resolution images obtained with

Table 4.1 The D2 sample of quasars: derived properties.

Source	Alternate Name	z	R	Linear Size kpc)	Surface Brightness Ratio	Separa-tion Ratio
0115+027	4C02.04	0.672	0.32	105	1.3	1.4
0232-042	4C-04.06	1.436	0.23	113	2.8	3.3
0409+229	4C22.08	1.215	1.30	39	5.5	0.9
0742+376	4C37.19		0.40	530	> 32.5	
0821+394	4C39.23	1.216	13.85	40	> 1.7	
0836+195	4C19.31	1.691	0.47	263	22.7	0.8
0836+710	4C71.07	2.160	16.52	16	> 12.0	
0919+218	4C21.25	1.421	0.07	96	27.0	1.3
0932+022	4C02.27	0.659	0.31	370	4.0	0.2
0945+408	4C40.24	1.252	2.15	35	> 4.0	
1007+417	4C41.21	0.611	0.27	245	14.4	1.7
1012+232	4C23.24	0.565	7.53	134	4.1	2.0
1040+123	3C245	1.029	3.01	63	18.6	1.7
1055+018	4C01.28	0.888	35.75	251	2.0	
1055+201	4C20.24	1.110	2.26	182	> 54.8	
1132+303	4C30.22	0.614	0.27	119	5.1	1.2
1136-135	PKS	0.554	0.28	118	5.9	1.7
1203+109	4C10.34	1.088	0.48	48	2.8	0.8
1222+216	4C21.35	0.435	1.58	112	6.1	1.2
1226+023	3C273	0.158	3.57	75	>500.0	
1347+539	4C53.28	0.976	4.04	45	> 3.0	
1354+195	4C19.44	0.720	4.85	351	1.2	1.8
1415+463	4C46.29	1.552	4.45	112	> 27.4	
1433+177	4C17.59	1.203	0.46	86	8.4	0.9
1509+158	4C15.45	0.828	0.16	69	12.4	4.0
1636+473	4C47.44	0.740	3.35	162	> 20.0	
1637+574	OS 562	0.745	36.49	32	> 1.8	
1641+399	3C345	0.595	29.78	22	> 13.0	
1642+690	4C69.21	0.751	9.33	81	> 34.0	0.7
1729+501	4C50.43	1.107	0.07	175	>117.3	
1741+279	4C27.38	0.372	0.59	63	5.7	1.3
1800+440	OU401	0.660	1.83	80	1.2	0.3
1842+681	JB	0.475	26.16	28	> 3.0	
2037+511	3C418	1.687	4.76	25	> 50.0	
2251+158	3C454.3	0.859	35.00	44	> 5.5	
2325+269	4C27.52	0.875	0.10	62	9.0	1.1

the Cambridge interferometer (Laing, 1981; Jenkins *et al.*, 1977).

4.2.2 The SSH sample

Swarup *et al.* (1984) published radio images of 31 radio-loud quasars obtained with the VLA. The quasars were selected from among those that lie close to the upper envelope of the largest-angular-size vs. redshift diagram. Thus, foreshortening due to projection would not be significant for these quasars, and they would be expected to lie close to the plane of the sky.

Swarup *et al.* (1984) remark that the radio structure of 0911+053 is uncertain, because there is lack of consistency among different data available for the object. Also, their data show that in the case of 2318+026, the association of the QSO with the central radio component is uncertain. The sample constituted after excluding these two objects thus contains 29 quasars, and is designated as the **SSH sample.**

4.2.3 The OBC sample

O'dea *et al.* (1986; 1988) have presented radio images of 16 quasars obtained with the VLA. The quasars were selected to be strongly core-dominant. In the unified scheme, these radio sources would have their radio axes oriented close to the line of sight. This sample, designated the **OBC sample**, was thus chosen to represent the opposite extreme in radio axis orientation vis-a-vis the 3CR and SSH samples.

4.3 Compact Steep Spectrum Quasars

It has recently become clear that while extragalactic sources that have flat radio

Table 4.2 The 3CR sample of quasars: derived properties.

Source	Alternate Name	z	R	Linear Size kpc)	Surface Brightness Ratio	Separation Ratio
0017+154	3C9	2.012	< 0.002	95	4.0	1.0
0033+183	3C14	1.469	0.01	198	1.3	0.5
0133+207	3C47	0.425	0.07	450	8.0	1.2
0229+341	3C68.1	1.238	<0.0003	482	48.0	0.6
0710+118	3C175	0.768	0.06	396	1.6	0.8
0758+143	3C190	1.195	0.10	58	1.3	1.7
0833+654	3C204	1.112	0.06	301	1.1	1.4
0835+580	3C205	1.534	0.02	145	1.4	1.2
0838+133	3C207	0.684	0.69	100	2.7	1.2
0850+140	3C208	1.110	0.05	110	6.3	1.1
0855+143	3C212	1.048	0.15	84	3.3	0.9
0903+169	3C215	0.411	0.06	199	2.5	0.5
0906+430	3C216	0.670	1.34	24	6.3	0.8
1040+123	3C245	1.029	3.01	63	18.6	1.7
1100+772	3C249.1	0.311	0.13	130	2.4	0.5
1111+408	3C254	0.734	0.02	107	1.2	0.1
1137+660	3C263	0.646	0.14	336	33.3	0.6
1206+439	3C268.4	1.400	0.04	88	3.8	0.9
1218+339	3C270.1	1.519	0.18	79	3.6	0.8
1241+166	3C275.1	0.557	0.14	131	1.4	1.5
1258+404	3C280.1	1.659	0.07	196	6.7	1.5
1549+628	3C325	0.860	< 0.08	145	1.6	0.5
1618+177	3C334	0.555	0.42	338	1.3	0.6
1622+238	3C336	0.927	0.03	192	1.2	2.1
1641+399	3C345	0.595	29.78	22	>13.0	
1704+608	3C351	0.371	0.01	365	2.4	0.8
1732+160	4C16.49	1.880	0.02	128	1.2	1.7
2120+168	3C432	1.805	0.01	112	1.1	0.6
2251+158	3C454.3	0.859	35.00	44	>5.5	

Table 4.3 The SSH sample of quasars: derived properties.

Source	Alternate Name	z	R	Linear Size kpc)	Surface Brightness Ratio	Separation Ratio
0118+034	3C39	0.765	0.12	360	2.0	1.0
0133+207	3C47	0.425	0.07	450	8.0	1.2
0229+341	3C68.1	1.238	<0.0003	482	48.0	0.6
0312-034	4C-3.11	1.072	0.01	361	1.8	1.1
0808+289	B2	1.910	1.55	496	4.0	1.7
0835+580	3C205	1.534	0.02	145	1.4	1.2
0901+285	B2	1.121	0.53	202	3.3	1.1
0903+169	3C215	0.411	0.06	199	2.5	0.5
0922+149	4C14.31	0.896	0.11	345	3.0	1.2
0932+022	4C02.27	0.659	0.31	370	4.0	0.2
0957+003	4C00.34	0.907	0.23	282	2.4	1.3
1004+130	4C13.41	0.240	0.04	551	2.9	1.5
1011+280	4C28.25	0.899	0.63	122	2.5	0.7
1100+772	3C249.1	0.311	0.13	130	2.4	0.5
1137+660	3C263	0.646	0.14	336	33.3	0.6
1221+186	4C18.34	1.401	0.24	203	1.1	1.4
1244+324	4C32.41	0.949	0.29	207	1.7	0.9
1248+305	4C30.25	1.061	0.02	243	4.2	1.2
1305+069	3C281	0.599	0.04	312	9.5	0.7
1435+315	B2	1.366	2.48	103	1.6	0.5
1545+210	3C323.1	0.264	0.07	358	1.8	0.7
1602-001	4C-0.63	1.625	0.43	225	1.8	2.4
1606+289	4C28.40	1.689	0.04	251	1.9	0.9
1618+177	3C334	0.555	0.42	338	1.3	0.6
1622+238	3C336	0.927	0.03	192	1.2	2.1
1704+608	3C351	0.371	0.01	365	2.4	0.8
1739+184	4C18.51	0.186	0.15	850	2.0	1.0
2131+175	4C17.87	1.215	0.16	267	1.8	1.0
2325+293	4C29.68	1.015	0.06	426	22.8	0.9

Table 4.4 The OBC sample of quasars: derived properties.

Source	Alternate Name	z	R	Linear Size kpc)	Surface Brightness Ratio	Separation Ratio
0224+671			13.07	255	7.5	
0333+321	NRAO140	1.263	50.19	69	3.1	1.8
0605-085		0.870	22.01	46	> 7.0	
0735+178			37.24	17	> 2.0	
0836+710		2.160	16.52	16	> 12.0	
0859-140		1.327	49.05	103	> 2.5	
1055+018	4C01.28	0.888	35.75	251	2.0	
1116+128		2.118	5.97	24	> 50.0	
1510-089		0.361	15.52	55	> 4.0	
1624+416			32.65	9	> 16.0	
1633+382		1.814	162.04	100	> 1.2	
1642+690	4C69.21	0.751	9.33	81	> 34.0	0.7
1749+701			123.46	3	> 2.5	
1807+698	3C371	0.051	56.78	394	> 25.0	
1823+568		0.664	7.27	118	> 66.7	
2037+511	3C418	1.687	4.76	25	> 50.0	

Table 4.5 Compact Steep Spectrum quasars in the 3CR sample.

Source	Alternate Name	z	R	Linear Size (kpc)
0127+233	3C43	1.459	4.75	21
0134+329	3C48	0.367		8
0518+165	3C138	0.759		5
0538+498	3C147	0.545	3.38	10
0725+147	3C181	1.382	0.01	50
0740+380	3C186	1.063	0.03	14
0802+103	3C191	1.956	0.04	40
0809+483	3C196	0.871	0.00	48
1328+254	3C287	1.055		1
1328+307	3C286	0.849	3.83	22
1458+718	3C309.1	0.905	1.46	18
1634+628	3C343	0.988	58.75	9
1828+487	3C380	0.692	0.57	7
2249+185	3C454	1.757		5
2252+129	3C455	0.543	0.12	24

spectrum over a large frequency range are almost invariably of small projected linear sizes, those with steep radio spectrum, while usually large, *are sometimes also of small linear dimensions* (Kapahi, 1981b; Peacock & Wall, 1982; van Breugel *et al.*, 1984a). These latter have been termed Compact Steep Spectrum (CSS) sources, and they include both radio galaxies and radio-loud quasars. Van Breugel *et al.*, 1984a argued that the combination of compactness and steepness of spectrum in the CSS objects was due to strong interaction of the radio emitting effluents with the (gas rich) interstellar medium. Thus, they are almost certainly a class of objects that is physically distinct from the CDQs and the LDQs. If the interactions with the surrounding medium are indeed significant, they could well intensify the intrinsic radiative dissipation from the radio emitting material, instead of (or in addition to!) relativistic bulk motion enhancing the apparent emission.

More recent VLBI studies have shown that the nuclear radio structures in CSS quasars are often complex (Fanti *et al.*, 1988; Nan *et al.*, 1988), suggestive of interaction of the twin-beams with the interstellar medium. If so, the prominent nuclear radio components sometimes seen in CSS quasars could be a reflection of this interaction, in which case *R would no longer be a statistical measure of the angle of inclination of the radio axis to the line of sight.* It may be noted that the CSS quasars could then fortuitously contribute to the correlation of R with projected linear size (l), and also to the correlation of R with misalignment of radio structure (since the strong interaction with the interstellar medium is likely to produce relatively large intrinsic bends in the jets). It is therefore not appropriate to include

the CSS quasars in analyses that test the unified scheme for samples of quasars.

The following operational definition of a CSS quasar has been adopted hereinafter. A radio quasar that has most of its radio flux density in a component of steep radio spectrum (i.e., $\alpha < -0.5$) in the radio frequency range between 1 and 15 GHz, and has a projected linear size < 50 kpc is regarded as a CSS quasar. The cutoff values chosen for α and l are necessarily somewhat arbitrary, but the intention is to include objects of steep radio spectrum over a reasonably wide frequency range, and of subgalactic linear dimension. It may be noted that deep and high resolution imaging at optical wavelengths have revealed that the host galaxies of radio-loud quasars have sizes of about 40 to 80 kpc for H_0 of 50 km s^{-1} Mpc^{-1} and q_0 of 0.5 (e.g., Hutchings, 1987: 25 to 60 kpc for H_0 of 100 km s^{-1} Mpc^{-1} and q_0 of 0).

In the case of the D2 sample, 0003-003, 0051+291 (both described in Chapter 3) and 1828+487 (Pearson *et al.*, 1985) qualify as CSS quasars under the above definition and have been excluded from the analysis. In the case of the 3CR sample, 15 quasars are CSS objects (Table 4.5); they have been excluded. Note that of the 11 for which the image resolutions are sufficient to delineate the core and determine R, six have R > 0.5. Neither the SSH nor the OBC sample contain any CSS quasars.

4.4 The derived properties of quasars

To do the comparative analysis of the four samples of quasars, the prominence of the nuclear radio component R_{emit}, the projected linear size l, the ratio of surface

brightness of the peaks of the outer components, and the ratio of the angular separation of these peaks from the nuclear component have been evaluated for each quasar. The definitions of these parameters and the methods by which they are calculated are given below. The parameter values for the four samples are listed in Tables 4.1 to 4.4.

4.4.1 The prominence of the nuclear component

The prominence of the nuclear radio component R_{emit}, is defined as the ratio of the radio emission from the nuclear component to that from the extended structure, evaluated at an emitted frequency of 8 GHz (in the rest frame of the quasar). It is more accurate to use the frequency of emission in the rest frame rather than the observed frequency of emission because the nuclear and outer components usually have very different spectral indices. The emitted frequency was chosen to be 8 GHz to minimize errors due to the fact that the exact spectral indices of the components are unknown (most of the flux densities are measured near 5 GHz).

The radio spectral indices of the components actually need to be derived from multi-frequency images of comparable resolution, which are unavailable in most of the cases. Therefore, it has been assumed here that the nuclear components have a spectral index of 0 and the extended outer components have a spectral index of -1. The former is the median value of spectral indices for the quasars observed by Perley (1982) between wave bands of $\lambda 6$ and 20cm. The latter is the median value of spectral indices for the extended components of the 3CR quasars (Laing & Peacock, 1980). Thus,

$$R_{emit} = \left[\frac{S^{nuc}}{\left(S^{tot} - S^{nuc}\right)}\right]\left[\frac{8.0}{\nu^{tot}(1+z)}\right],$$

where S^{nuc} and S^{tot} are the nuclear and total radio flux densities respectively, and ν^{tot} is the observing frequency at which the total flux density was measured.

The flux densities of the nuclear components have been measured in the $\lambda 6$ cm band in all cases, except 0232–042 (where it is measured at 15 GHz) and 1222+216 (where it is measured at 1.4 GHz). Both these objects belong to the D2 sample. Most of the total flux densities have been measured at $\lambda 6$ cm too, unless unavailable, in which case values at $\lambda 11$ or 18 cm, have been used. Single-dish measurements have been used for the total flux density except where unavailable, in which case interferometric measurements are used. The derived values of R_{emit} for the quasars in the four samples are listed in column 4 of the Tables 4.1 to 4.4.

4.4.2 The projected linear size

The projected linear size l of each of the quasars is given by

$$l = \left\{(LAS)\frac{c}{[H_0 q_0^2(1+z)^2]}\right\}\left\{zq_0 + (q_0-1)[-1 + (2q_0 z + 1)^{1/2}]\right\}$$

where LAS, the largest angular size, is the angular separation between the outermost surface brightness peaks of radio emission of the quasar. H_0 is assumed to be 50 km s^{-1} Mpc^{-1} and q_0 to be 0.5. The calculated values of l are listed in column 5 of Tables 4.1 to 4.4.

4.4.3 The surface brightness ratio of the outer components

The ratio of the radio surface brightness of the peaks of the outer components on either side of the core component (estimated with the value of the brighter peak in the numerator by convention) is taken to be a measure of the asymmetry in side-to-side emission. This parameter will hereinafter be referred to as the surface brightness ratio. In the case of the D2 sample, the estimates have mostly been made using the VLA data presented in Chapter 3. In all other cases, data from the literature have been used, and if the values of the surface brightness of the peaks are not themselves listed, they have been estimated from the published radio images. In most of these cases, the data are from the VLA. Data from the Cambridge interferometer were used for the exceptions, which are 0710+118, 1549+628 (both from Jenkins *et al.*, 1977) and 0833+654 (Laing, 1981). (All three objects are from the 3CR sample.)

The surface brightness ratio has been evaluated at $\lambda 6$ cm wavelength, and if unavailable, then at $\lambda 11$ or 20 cm. In cases where an outer lobe has been detected on only one side of the nuclear component, a lower limit to the surface brightness ratio has been evaluated, using three times the quoted r.m.s. value of the image, or the lowest/second lowest contour of surface brightness plotted. The values of this parameter are listed in column 6 of Tables 4.1 to 4.4.

4.4.4 The separation ratio of the outer components

The ratio of the angular separation of the brightest peak of the extended radio emission to the separation of the brightest peak on the opposite side of the core

component (hereinafter referred to as the "separation ratio") has been adopted as a measure of the asymmetry of projected separation of the outer components. Thus, for equidistant outer components the value is unity; if the component with a higher peak surface brightness is closer to the core, the value is, by convention, taken to be less than unity and vice versa. The values for each individual quasar are listed in column 7 of Tables 4.1 to 4.4.

4.5 The results—general consistency with the unified scheme

As was mentioned in section 4.2, the 3CR and SSH comparison samples were chosen to provide sets of quasars expected to be generally oriented closer to the plane of the sky than the D2 sample, and the OBC comparison sample is expected to be a set of quasars inclined close to the line of sight, perhaps even closer than the D2 sample. The results of the analysis are presented and discussed in this section.

4.5.1 The behaviour of surface brightness ratio and R

Fig 4.1a to d show the distribution of surface brightness ratio for the quasars in the 3CR, SSH, D2 and OBC samples respectively. (It may be noted that in the case of the OBC quasars, most of the values are lower limits because only one outer component has been detected.) The distributions for the D2 and OBC quasars show evidence for a large number of objects with very asymmetric surface brightness ratio. On the other hand, the distributions for the 3CR and SSH quasars peak at a much lower value and contain far fewer objects of large asymmetry. The distribution for the SSH quasars peaks at a marginally higher value than the 3CR quasars.

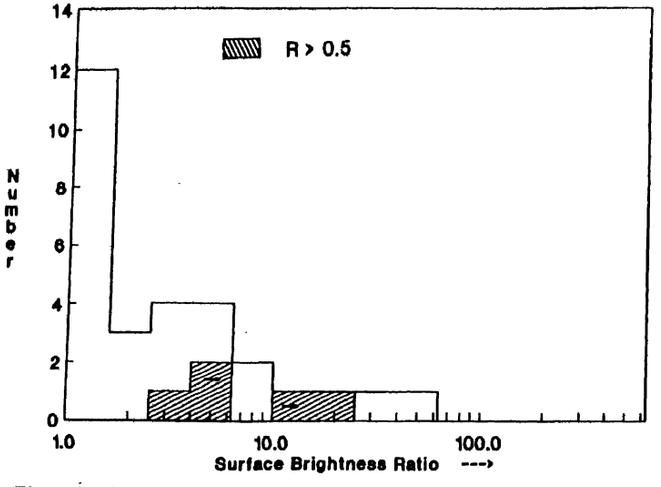

Fig.4.1a Distribution of surface brightness ratio for 3CR quasars

Fig.4.1b Distribution of surface brightness ratio for SSH quasars

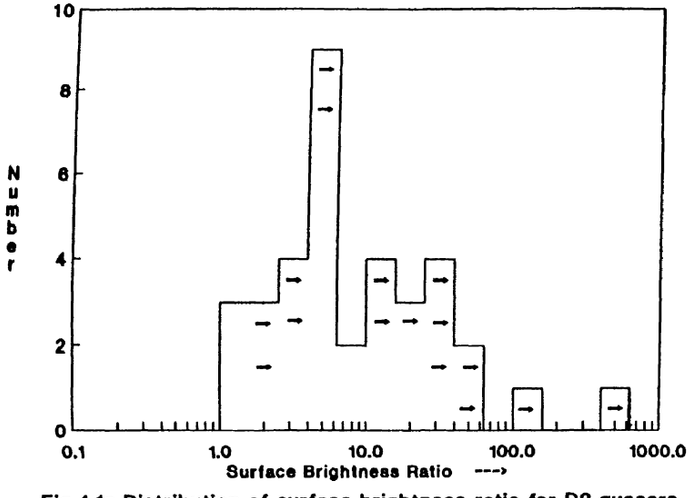

Fig.4.1c Distribution of surface brightness ratio for D2 quasars

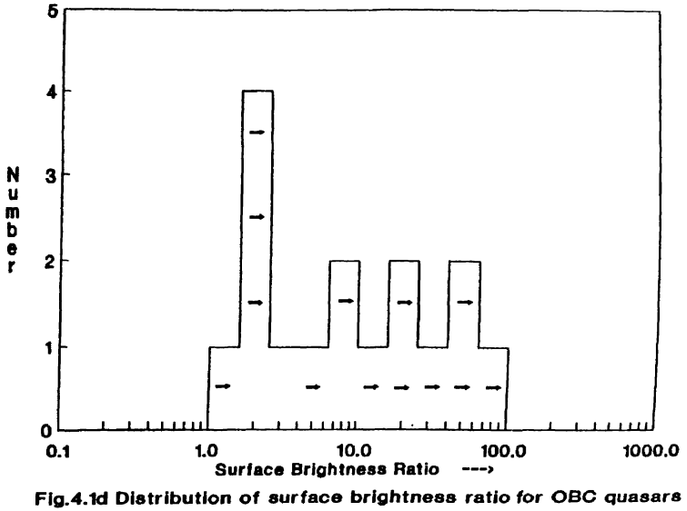

Fig.4.1d Distribution of surface brightness ratio for OBC quasars

Is the asymmetry related to the orientation inferred from the value of R? The distribution of R_{emit} for each of the samples is shown in Figs. 4.2a to d. The peak and median values of the distributions shift to larger values of R_{emit} as one moves from Fig.4.2a through to d, which parallels the trend in the distributions of surface brightness ratio. The median values of the distributions of R_{emit} and the surface brightness ratio for the four samples are given in Table 4.6. It is worth pointing out that there are a few objects in the 3CR sample with $R_{emit} > 0.5$. These have been marked hatched in the distribution of surface brightness ratio, and it turns out that four out of five of the objects are of surface brightness ratio > 4. *Thus the results are broadly consistent with the supposition that the hot spots at least mildly relativistic*, so that Doppler beaming plays a significant role in determining the side-to-side asymmetry.

Table 4.6 Median values of the distributions.

Sample of Quasars	R_{emit}	Projected Linear Size (kpc)	Surface Brightness Ratio	Separation Ratio
3CR	0.07	130	2.5	0.8
SSH	0.12	312	2.4	1.0
D2	2.0	84	6.0	0.5
OBC	27	62	7.3	-

4.5.2 Caveats

Ideally, to test if the outer hot spots are relativistically beamed, the *flux densities* of the hot spots need to be determined. For this, sufficient angular resolutions are required that will delineate what might be identified as the physical

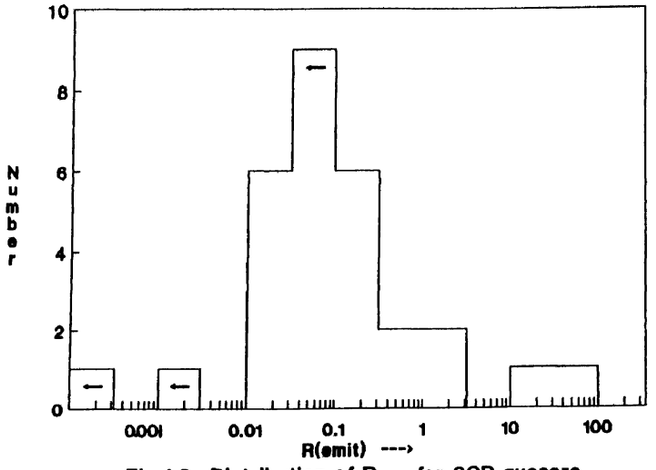

Fig.4.2a Distribution of R_{emit} for 3CR quasars

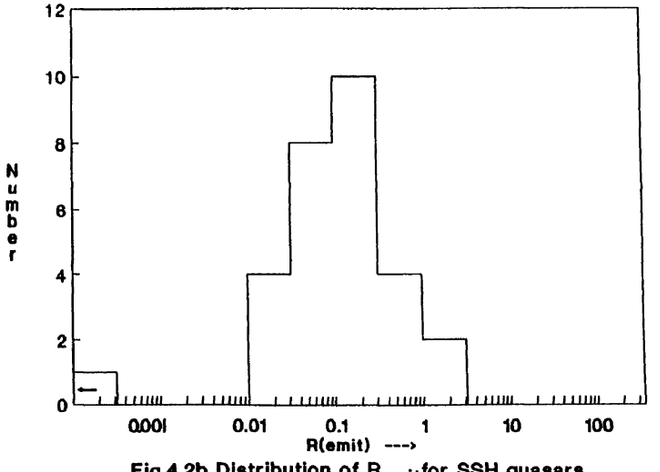

Fig.4.2b Distribution of R_{emit} for SSH quasars

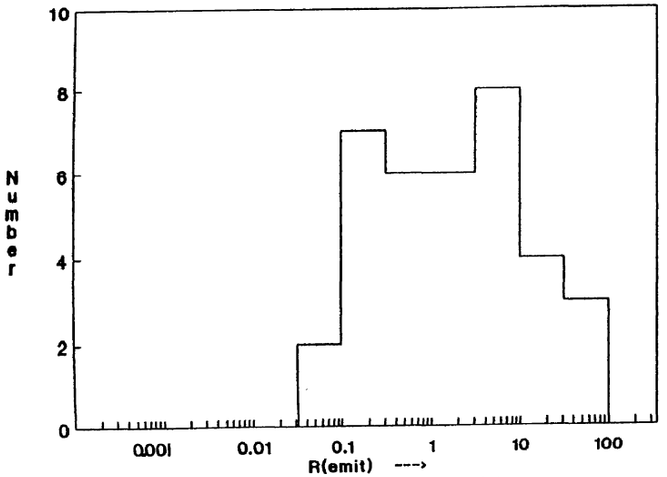

Fig.4.2c Distribution of R_{emit} for D2 quasars

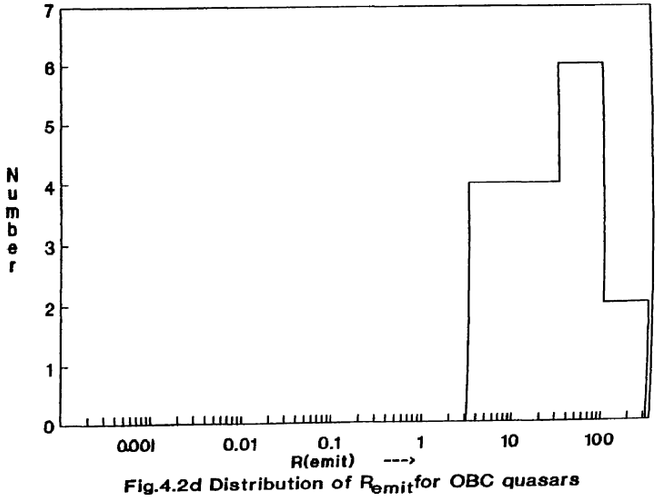

Fig.4.2d Distribution of R_{emit} for OBC quasars

hot spot, which is important because the surrounding (more diffuse) emission (from material which has emerged from the hot spot—e.g., Begelman *et al.*, 1984) is not expected to be relativistically beamed. But since the angular resolutions obtained for the body of data analyzed here are insufficient to determine these flux densities, the surface brightness ratio has been adopted as the next best measure of the side-to-side asymmetry in intensity.

The uncertainties in an analysis of this sort should be kept in mind. The value of the surface brightness ratio inferred would depend on the restoring beam-width used in the image. (Ideally, beam widths that are uniform for all the objects when converted to the linear scale should be used.) Further, even if flux densities of the hot spots *were* used, there is another complication. The two hot spots on the opposite sides are observed at different ages because of the light-travel-time between them, and therefore differences in hot-spot characteristics due their time-evolution could contribute to the observed asymmetry. It is interesting that despite these complications that could potentially mask any systematic effects, the adopted measure of the surface brightness asymmetry appears to show a gradation with R_{emit}.

4.5.3 The distribution of *l*

The distributions of projected linear size for the four samples respectively are plotted in Figs. 4.3a to d. The quasars in the SSH sample, which consists of objects of large angular size, have the largest projected linear sizes; those from the OBC sample have the smallest. The median values of these distributions are also listed in Table 4.6. The qualitative trend is roughly consistent with what was found by

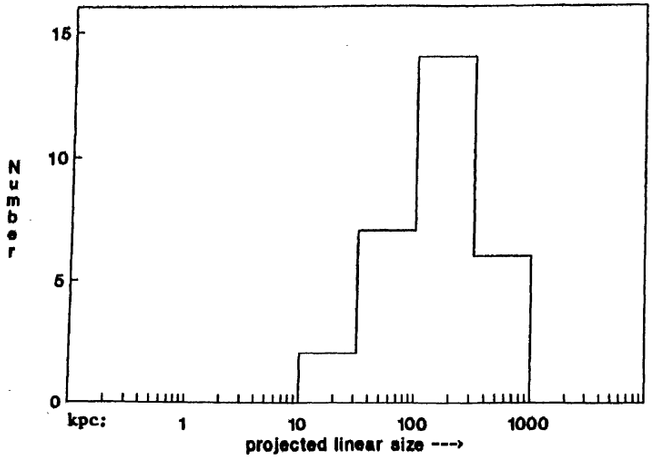

Fig.4.3a Distribution of projected linear size: 3CR quasars

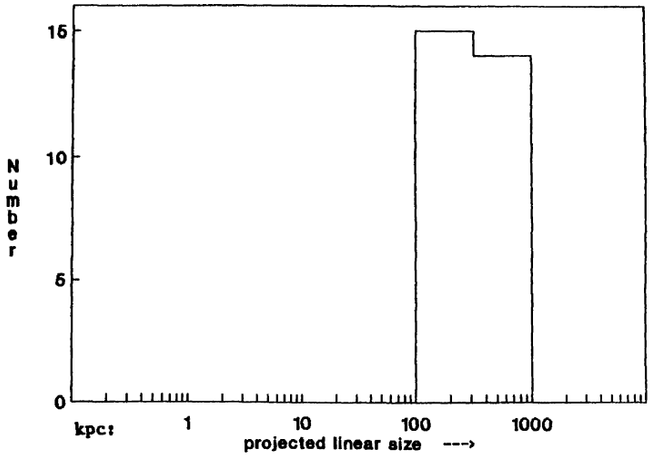

Fig.4.3b Distribution of projected linear size: SSH quasars

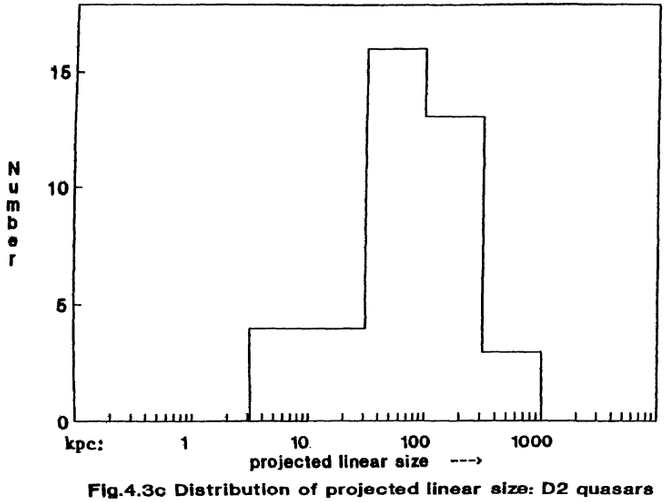

Fig.4.3c Distribution of projected linear size: D2 quasars

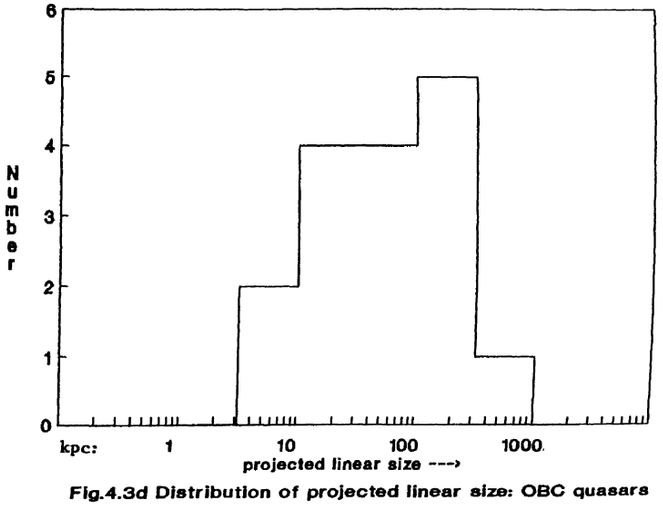

Fig.4.3d Distribution of projected linear size: OBC quasars

Kapahi & Saikia (1982), viz., that *the prominence of the nuclear component is inversely correlated with the projected linear size.*

Note that the 3CR quasars are expected to be randomly oriented in the sky. The quasars in the SSH sample, on the other hand, have been chosen to have the largest sizes, as indeed Fig. 4.3b shows. It is therefore expected that they are the least foreshortened objects, or, the ones closest to the plane of the sky. But this is not borne out by the R distributions; that for the SSH sample has higher values of peak and median than the 3CR distribution. Two possible factors could contribute to this apparent inconsistency. Firstly, the intrinsic linear size could be correlated with the Lorentz factor for the nuclear jets (e.g., Browne, 1987), in which case the largest quasars would have more prominent nuclear components. Secondly, the SSH quasars had to necessarily have a measured redshift, and redshifts are usually preferentially measured for the optically brighter objects. And if, as has been elaborated upon in Chapter 6, the Doppler boosting of the radio emission from the nuclear component is accompanied by enhancement of the optical continuum, there might well be a slight bias in the SSH sample of quasars towards objects with their nuclear jets inclined not so closely to the plane of the sky.

4.5.4 The separation ratio

The distributions of separation ratio for the 3CR, SSH and D2 samples are plotted in Figs. 4.4a to c. In the case of the OBC sample, outer components on both sides of the core component have been detected for only two objects, and therefore no distribution has been plotted. The D2 quasars show a marginally broader distribution than the other two samples, i.e., relatively larger deviations from unity

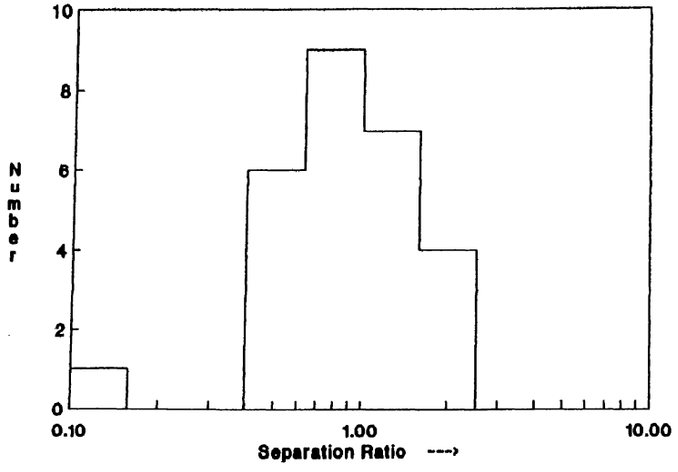

Fig.4.4a Distribution of separation ratio for 3CR quasars

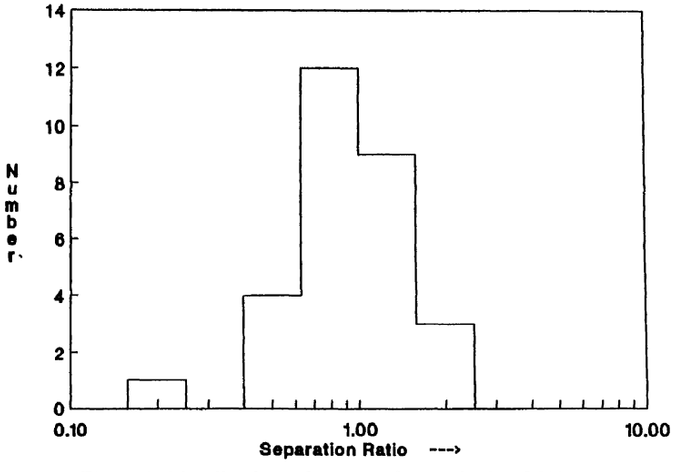

Fig.4.4b Distribution of separation ratio for SSH quasars

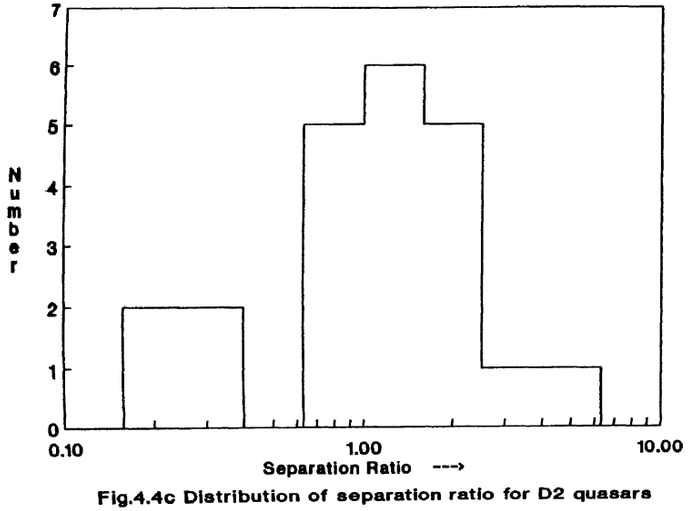

Fig.4.4c Distribution of separation ratio for D2 quasars

in both directions. The median values do not differ significantly across the four samples (see Table 4.6).

If the D2 quasars are relativistically beamed, then there are two reasons to expect the apparent separation ratio of an intrinsically symmetric quasar to differ from the value of unity. Firstly, the approaching outer component of a straight, intrinsically symmetric source would be observed at a later time and hence larger separation from the nucleus as compared to the receding outer component, due the light-travel-time difference. The observed separation ratio is thus given by

$$\frac{(1 + \beta\cos\theta)}{(1 - \beta\cos\theta)} ,$$

where βc is the velocity of advancement of the peaks of emission, and θ is the angle of inclination of the direction of motion to the line of sight. If the asymmetry in the surface brightness ratio is a consequence of differential Doppler beaming, then the brighter component is the approaching one, and the separation ratio would be greater than unity. Since the separation ratio increases with decrease in inclination angle θ, quasars inclined close to the line of sight would show large separation ratios (Kapahi & Saikia, 1982). Separation ratios of ~ 1.4 obtain for β of 0.2 (and ~ 2.5 for β of ~ 0.5). Secondly, if any non-collinear ejection bends the approaching radio jet towards the line of sight, the separation ratio observed otherwise would be reduced, since the projected angular separation would then decrease relative to that of the receding component (Saikia, 1984a). Clearly, the two are opposing effects.

Further, whether or not relativistic beaming occurs, light-travel-time differences may be masked by differences in the characteristics of the interstellar/intergalactic

medium on either side of the nucleus. Differences in the surrounding media on either side could cause separation ratios to differ from unity.

4.5.5 Jet detectability accompanied by hot spot enhancement

Among the 20 quasars of the D2 sample for which two-sided emission has been detected, in 17 certain cases and 2 likely cases, the jet points towards the brighter of the two outer components. The exception to this trend is 0932+022. If the detectably high surface brightness of the jets were not due Doppler enhancements but due to high dissipativeness, one would expect that most of the bulk kinetic energy would be radiated away and therefore the terminal hot spot would in fact be fainter than on the side where no jet (and therefore no dissipation of kinetic energy) is seen. *The observed trend is thus consistent with the supposition that the jets and hot spots are both at least mildly relativistic.*

Of course, if the outflow were intermittent, then the jet could point to the brighter (newer) hot spot with neither the jets nor the hot spots needing to be Doppler enhanced. But then the correlation of jet detectability with R (e.g., Saikia, 1984b), or tendency of larger R quasars to have larger surface brightness ratios (Section 4.5) are not explained.

4.6 The flip-flop model

It is fairly common in the case of radio quasars, that the separation ratio shows marked departures from the symmetric value of unity. One of the hypotheses that has been advanced to explain this is that ejection of effluents from quasar nuclei occurs on only one side at a time (Rudnick & Edgar, 1984). If that is the case, the

"one-sided" quasars best exemplify such a phenomenon.

The primary motivation for advocating this "flip-flop" hypothesis was the phenomenon of "preferential avoidance" of radio structures of high surface brightness at the same angular separation from the nucleus. One way in which Rudnick & Edgar (1984) demonstrated this was by pointing out a "dip" at the value of unity in the distribution of separation ratios of quasars from their sample.

While the data presented here cannot be used to disprove the flip-flop hypothesis, Figs.4.4a to d show that none of the four samples of quasars considered here (which *do* satisfy the selection criteria of Rudnick & Edgar, 1984), show any evidence for the presence of a "Rudnick dip". Indeed, Kapahi & Saikia (1982) had pointed out that the bias in the sample of Rudnick & Edgar (1984) against objects with weak core components together with measurement errors could well be the causes of the "Rudnick dip". It may be noted that the trend for large separation ratios to occur in quasars with large values of R_{emit} does not find an explanation in the Rudnick & Edgar scenario. Nor does the trend that samples with large asymmetry in surface brightness of the outer components show systematically larger values of R_{emit} Thus it is unlikely that one-sided ejection is a common phenomenon in quasars. However, the above statements are statistical, and individual cases to the contrary are not ruled out. A case in point is one of the objects in the D2 sample, viz., 1729+501. This is a one-sided source even with the present high dynamic range observations (Fig.3.33a, b and c, Chapter 3), and has a very weak nuclear radio component (R = 0.07). The lower limit to the ratio of surface brightness of the outer peaks of emission is very large. Therefore it does not

fit into the relativistic beaming scenario, and may well be an illustration of one-sided ejection. While examples of this type are not common, it must be pointed out that due to the fact that the radio nuclear component is weak, such sources may remain optically unidentified and therefore missed.

4.7 The excess of core components with steep spectrum

Kapahi (1981a) had found that the radio spectral indices of the central components of the quasars in his sample had a much wider distribution (0.4 to −1) than was known for "two-sided" quasars. Two possibilities had been suggested by him as causes of this difference: that the core components had "compact double" structure (known to occur in several radio galaxies) or were synchrotron self-absorbed at low frequencies, or alternatively, that these central components consisted of subcomponents of both flat and steep radio spectrum, such as a core with a jet, or a core with an outer lobe close by.

The high resolution images of chapter 3 support the latter alternative in the case of five of the total of nine sources suspected of having nuclear components of steep radio spectrum by Kapahi (1981a): 0003-003, 0919+218, 1040+123 and 1509+158. All of these objects have lobes of low surface brightness close to the nuclear components which were unresolved from the latter in the earlier observations; 1132+303 has a core and jet that are explicit in the new image. As for the remaining four quasars, in the case of 0615+578 which is a triple source, the northwestern lobe (which, of course, has a steep radio spectrum) was the component coincident with the proposed identification which has been subsequently found to be wrong. The same is probably true of 1547+309 (see Section 3.3 of this thesis). In

the case of 0740+380 and 1047+096, the new images show that what were previously regarded as the core components are actually independent quasars, and therefore their steep radio spectrum is no surprise.

4.8 The implied speeds of bulk motion

If the radiating, intrinsically symmetric twin beams of plasma are moving at relativistic speeds, then the ratio of the surface brightness of the approaching component to that of the receding one is given by

$$\left[\frac{1+\beta\cos\theta}{1-\beta\cos\theta}\right]^{2-\alpha}$$

For inclination angles $\leq 25°$, the values of β required for bulk motion to produce the observed surface brightness ratios in the D2 sample range from ~0.3 to ~0.7. These velocities are higher than what has been generally assumed or inferred for the large scale jets. They are certainly higher than the values derived from ram pressure confinement of the hot spots. However, the parameter that is deduced from the latter arguments is the speed of advance of the hot spot, and, as has been pointed by Blandford (1984) and Lind & Blandford (1986), the flow speeds of the complex shock patterns can be higher than the speeds of hot spot advancement.

4.9 Summary

The question of whether bulk relativistic motion on a scale of several hundred kiloparsecs can explain the structural asymmetry in radio quasars was explored in this chapter. It was argued that CSS quasars need to be excluded from analyses done within a simple relativistic beaming framework, because for these quasars R

may not be a good statistical measure of the angle of inclination of their jets.

It was shown that radio quasars with large side-to-side asymmetry in surface brightness tend to have more prominent radio nuclear components and smaller projected linear sizes. This is consistent with the prediction that they are inclined at small angles to the line of sight, and that the asymmetry is due to bulk relativistic motion.

Although in the simple relativistic beaming picture light-travel-time differences are expected to result in large separation ratios of the outer components for quasars oriented close to the line of sight, only a marginal effect is observed. Intrinsic misalignments and side-to-side differences in the characteristics of the interstellar medium could, however, mask the effect of light-travel-time differences.

For the quasars analyzed, the detected jet points to the brighter of the two hot spots in all but one case, implying mild relativistic velocities for not only the jets but also the hot spots. Only mild relativistic speeds are required of the hot spots to explain these results. Further, if the large scale jets and outer hot spots were as relativistic as the nuclear jets, R would not be expected to correlate with the degree of side-to-side asymmetry or jet detectability, because R is a measure of orientation *provided* there is a substantial difference in the Doppler enhancement of the nucleus as compared to the outer structure. Thus, the results presented in this chapter also suggest that extreme relativistic velocities in the outer components of quasars are ruled out.

Chapter 5

NUCLEAR RADIO POLARIZATION AND MISALIGNMENT IN RADIO STRUCTURES

Polarized radiation from regions around active galactic nuclei is a powerful probe of the physical conditions prevailing in those regions in several different ways. Its behaviour is an important diagnostic of the emission mechanism and/or the (polarizing) propagation effects along the line of sight. More fundamentally, the very existence of polarized radiation implies the absence of complete symmetry or complete disorder, either in the structuring of the emitting material or in the polarizing agents along the line of sight.

Observations at high angular resolution have shown that the radio emission from the nuclear components of radio quasars and galaxies *is* polarized, though at very low levels as compared to the degree of polarization seen in the large-scale jets and lobes. In this chapter, polarization data have been used to infer the geometry of the central regions of radio-powerful active galactic nuclei (RPAGN), and to examine how this geometry relates to the radio structure on the large scale. The results for radio quasars are discussed in the context of the relativistic beaming hypothesis. The case of radio galaxies has also been considered.

Similar investigations with *optical* polarization have been done before. It has been found that in the 'LPQs' (the QSOs that show 'low'—i.e., $\lesssim 3$ percent—optical polarization) that have double radio lobes, the position angle (PA) of the

polarization was roughly aligned with the radio structure (Moore & Stockman, 1984, and references therein). This result implies that the PA of the optical polarization must be relatively constant over the lifetime of the source, i.e., over scales of ~ 10^7years.

5.1 Misalignments in radio structure

The study of the structural alignment between the nuclear jets and the larger scale extensions in RPAGN is important because it yields estimates of the time scales over which the ejection axis of the effluent remains stable, and hence provides constraints on models for jet formation. Besides, as has been elaborated in the introductory chapter, the question of misalignment of radio structures of quasars is directly relevant to the unified scheme. At inclination angles of sources that are close to the line of sight, any intrinsic misalignments are amplified for most lines of sight; and since in the unified scheme, core-dominated quasars (CDQs) are believed to be at small angles to the line of sight, it follows that there should be larger misalignments between nuclear and large scale structure in them as compared to lobe-dominated quasars (LDQs).

5.1.1 Insights from Very Long Baseline Interferometry

The study of radio sources at angular resolutions of the order of milliarcseconds has been made possible by the introduction of Very Long Baseline Interferometry (VLBI). One of the most important conclusions reached by the early VLBI investigations of radio-powerful active galactic nuclei was the following: objects with 'symmetric' type of (large scale) radio structure (*i.e.*, the 'classical

double' sources with steep overall radio spectrum and projected linear sizes $\gtrsim$ 100 kpc) showed a high degree of alignment between the most compact and the most extended features. On the other hand, those with 'core' type of structure (*i.e.*, sources with flat overall radio spectrum, smaller projected linear sizes of $\lesssim$ 100 kpc, and the radio component coincident with the QSO dominating the emission) showed a range of orientations of their structures on different scales (Readhead *et al.*, 1978). In the sample of Readhead *et al.* (1978), there were five sources of the 'symmetric' type (all nearby radio galaxies, of redshifts < 0.1) and four of the 'core' type (all quasars, of larger redshifts). From similar VLBI data for three radio quasars with one-sided radio structure, Davis *et al.* (1978) concluded that the nuclear elongations were typically misaligned by ~ 20° with the axis of the overall radio structure. This finding is similar to that of Readhead *et al.* (1978) for the 'core'-type objects.

Readhead *et al.* (1983) enlarged the older sample to 18 objects and confirmed the earlier conclusions. Their new sample had eight objects of the 'symmetric' type (of which seven are radio galaxies of redshift < 0.1 and one is a quasar), and ten of the 'core' type (of which eight are quasars and two are nearby BL Lacertids). They concluded that the distribution of the observed angles of misalignment for the sample was consistent with the relativistic beaming model, with an assumed intrinsic bend angle of ~ 10° and Lorentz factor γ of 10. It must, however, be noted that in the context of the unified scheme, the comparison of misalignments should really be made specifically between radio *quasars* of the 'symmetric' and 'core' types. Also, the above findings need to be verified for a larger sample of

objects.

VLBI observations entail international collaborative effort; moreover, due to limitations of sensitivity, only objects with the brightest nuclear components (which usually turn out to be those with relatively more prominent nuclei) can be observed. As a result, large collections of radio structures on angular scales of milliarcseconds are not easy to come by, and particularly not for objects with a wide range in core dominance.

5.2 An alternative approach

An alternative route is adopted here to study the question of misalignment. The orientation of the nuclear jet is inferred from the PA of the polarized emission from the nuclear component, as measured at $\lambda 6$ cm with angular resolutions of $\lesssim$ 1 arcsec. (Such observations made with the VLA are available for several radio quasars). This approach entails the following assumptions:

(a) that the polarized emission observed from the central component using angular resolutions of $\lesssim$ 1 arcsec is dominated by radiation from the optically thin (unresolved) nuclear jet (cf. Fig. 5.1);

(b) that Faraday rotation at wavelengths as short as $\lambda 6$ cm is ignorable, so that the observed orientation of the E–vector of the radiation is close to the intrinsic one;

(c) that the nuclear jet is optically thin at these frequencies, so that the orientation of the observed polarized (synchrotron) radiation is perpendicular to the magnetic field in the jet; and

(d) that the direction of the magnetic field bears a fixed relation (specifically,

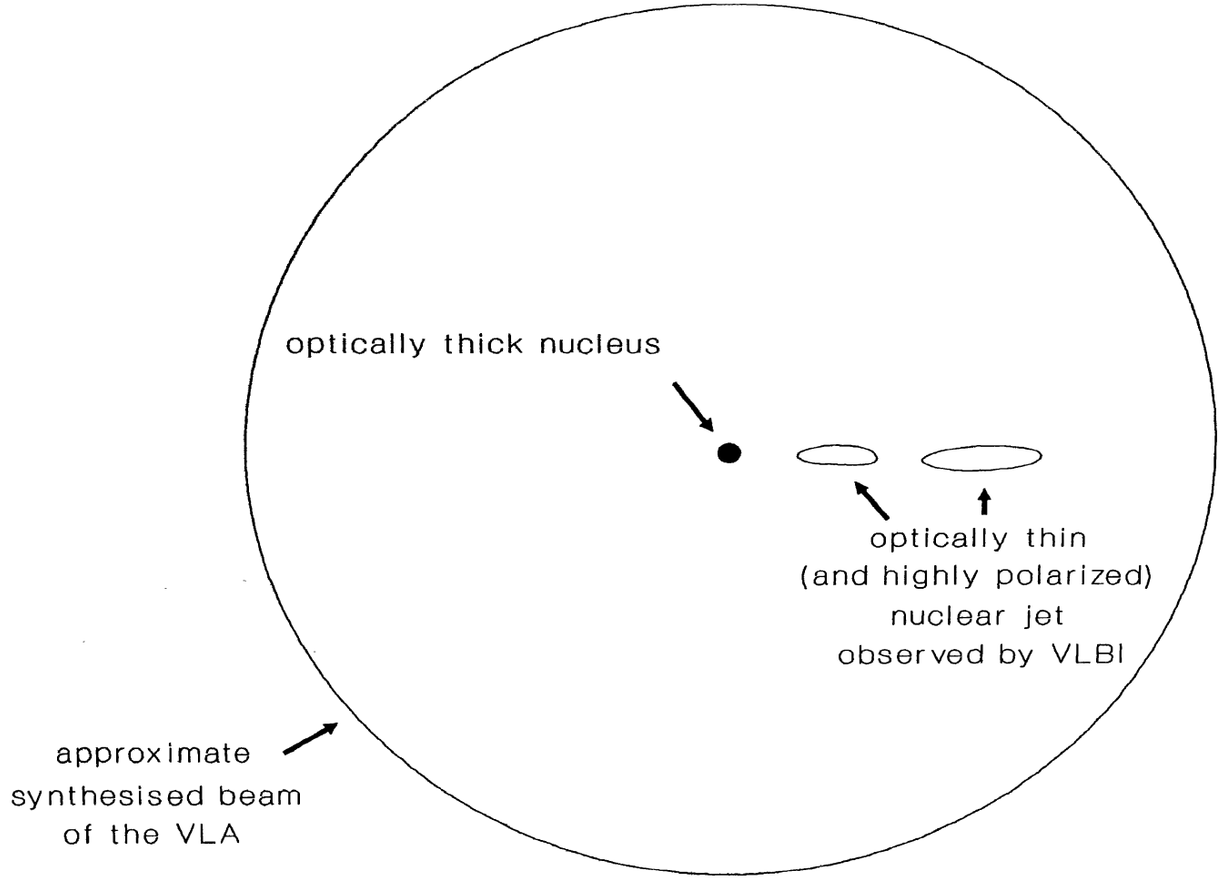

Figure 5.1. Illustration of assumption (a)

perpendicular) to the axis of the nuclear jet.

To ensure that (a) holds, the sample has been constituted from objects for which high angular resolution VLA observations are available, so that the observed polarized emission from the nuclear component is not contaminated by larger scale structure.

To ensure that (b) holds, it is important to avoid those directions in the sky where effects of propagation through our Galaxy are known to rotate the plane of polarization significantly. Simard-Normandin & Kronberg (1980) have calculated rotation measures (RMs) from linear polarization measurements made at several wavelengths for 552 extragalactic objects spanning the whole sky. The results show that directions through the Galactic plane (up to latitudes of about 15°) show large positive RM. Also, there appears to be a region below the plane around longitude of about 90° that shows a large negative RM. Candidate objects for the present study that occur in these regions have been excluded from the analysis. Fig. 5.2 shows a map of the sky with equatorial and Galactic coordinates marked. The areas of sky excluded from the present analysis are shown hatched.

Large scale jets observed in quasars and radio galaxies are known to be generally optically thin, and it is expected that the nuclear jets are qualitatively similar in this respect (premise (c)). Multifrequency VLBI maps in a few cases have shown that this is indeed so (e.g., Eckart *et al.*, 1987).

Premise (d) obtains by extrapolating from observations of large scale jets in radio quasars (Owen & Puschell, 1984), and from the following finding of Davis *et al.* (1978) for nuclear jets. For the three radio quasars in their investigation, the

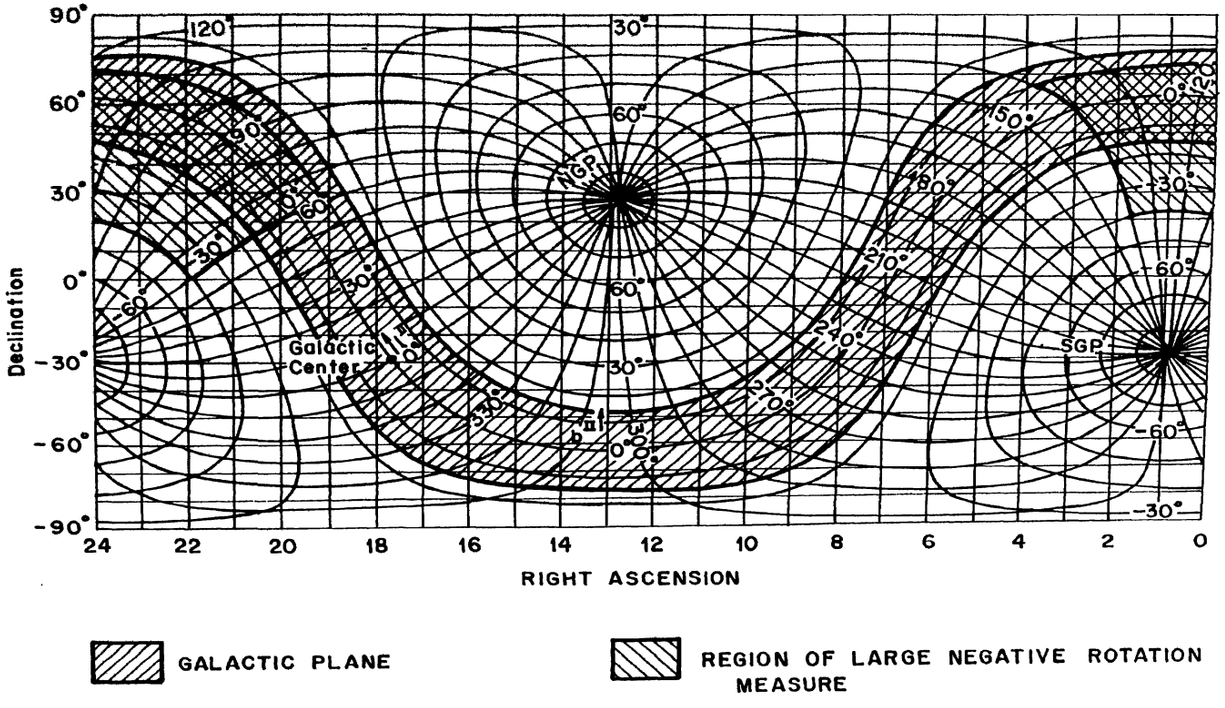

Fig. 5.2. Excluded regions of the sky.

magnetic field directions in the subcomponents (as derived from interferometric polarimetry) appeared to coincide with the structural elongations of the component. This assumption has subsequently been vindicated *for the CDQs* by several later workers (e.g., Rusk & Seaquist (1985); Jones *et al.* 1985; O'dea *et al.*, 1988; Wrobel *et al.*, 1988).

If all the above assumptions are valid, then the direction of the nuclear jet is, to a good approximation, perpendicular to the orientation of the observed polarization at $\lambda 6$ cm.

5.3 The sample and the selection criteria

The sample has been compiled by choosing from among the radio images of quasars that were presented in Chapter 3 (which have polarization data measured with the VLA) and from VLA polarization data for quasars in the literature. The latter are listed in Table 5.1.

Table 5.1 Sources of high-resolution polarimetry.

Chapter 3, this thesis	Rudnick et al. (1985)
Feigelson et al.(1984)	Rudnick et al. (1986)
Gower & Hutchings (1982)	Rudnick & Jones (1982)
Harris et al. (1983)	Rudnick & Jones (1983)
O'dea et al. (1988)	Saikia et al. (1983)
Owen & Puschell (1984)	Saikia et al. (1985)
Padrielli et al. (1988b)	Stocke et al. (1985)
Perley et al. (1980)	Swarup et al. (1982)
Perley et al. (1982)	Swarup et al. (1984)
Perley (1982)	Swarup et al. (1986)
Potash & Wardle (1980)	Wardle & Potash (1982)

The selection criteria adopted are the following:

(i) The VLA polarization data are required to be of good signal-to-noise and thus usable to estimate the orientation of the polarization. Data with estimated error in the polarization PA of more than 20° have been excluded.

(ii) Sources in the Galactic plane region (latitudes $|b| < 15°$), or lying in the Galactic region $60° < l < 140°$ and $-40° < b < 10°$, have to be excluded. The latter is a region of large negative RM (Simard-Normandin & Kronberg 1980). The RMs for $|b| \gtrsim 15°$ are usually $\lesssim 30$ rad m^{-2}.

(iii) Two-sided quasars whose large scale structure is highly bent are excluded. In these objects, a comparison of the PA of the core polarization with the line joining the outer lobes is not very meaningful. Only those sources for which the supplement of the angle formed at the nucleus by the outer lobes/hot spots is $\lesssim 25°$ are included. This 'misalignment cutoff' resulted in the exclusion of 12 objects.

The final list consists of 133 objects. Here, no attempt has been made to distinguish between quasars and BL Lacertids.

5.4 The derived parameters

The objects in the sample and their properties are listed in **Table 5.2** which is arranged as follows:

Column 1: the name of the quasar (followed by an asterisk if the polarization data are from B or C-array of the VLA; for the rest, A-array data have been used).

Column 2: the radio structure-type, *viz.*, 'two-sided' or 'one-sided'.

Column 3: the redshift.

Column 4: the projected linear size ($q_0 = 0.5$, $H_0 = 50$ km s^{-1} Mpc^{-1}).

Column 5: PA of the core polarization E–vector at $\lambda 6$ cm.

Column 6: PA of the radio structure axis.

Column 7: the angle ϕ, the difference between the two PAs above (cf. Fig. 5.3). (For the 'two-sided' quasars the radio axis is defined by the hot spots at the outer extremities of the source, while for the 'one-sided' objects, it is defined by the core and the single outer component.)

Column 8: the prominence of the radio nuclear component in the quasar rest frame, R_{emit} (emitted frequency of 8 GHz; cf. this thesis, Section 4.4.1). The few quasars that have no measured redshift have been assumed to be at a redshift of 1.

Column 9: reference codes for the sources of the polarization data and extended structure (from which the PA of the radio axis has been derived). The references are listed in **Table 5.3**.

The structure-type for some of the objects in the table has been noted as 'one-sided?', and these objects have no listed projected linear sizes. All these objects are from Perley (1982). Their structure-type and angular extents are uncertain because, in the course of the deconvolution of the images, fairly small search/CLEAN windows were used, and so one or more secondary components of a quasar may have been missed. For this reason, as noted by Perley himself, some sources listed as having only a single secondary component may actually have more components

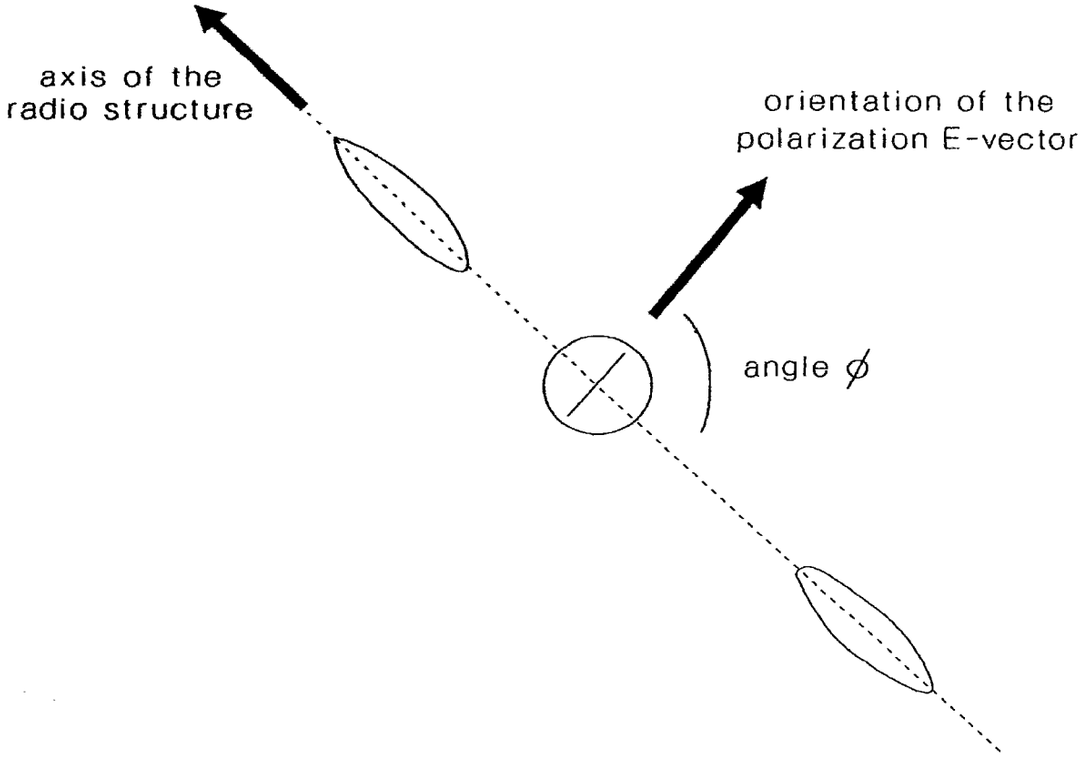

Figure 5.3 The parameter ∅

Table 5.2 The sample of quasars

Source	Structure type	Redshift	Projected linear size (kpc)	Core Polarization PA (°)	Structure PA (°)	Ø (°)	R	References
0048-097	one-sided?			55	9	46	1.02	P82
0106+013	one-sided	2.107	32.4	151	5	34	4.30	P82; BP
0112-017	one-sided	0.284	37.8	60	130	70	57.57	P82; BP
0113-118	one-sided	0.672	39.4	60	162	78	2.21	P82; BP
0115+027*	two-sided	0.672	104.8	163	73	90	0.32	present
0135-247	one-sided?	0.831		170	92	78	0.91	P82
0202-172	one-sided	1.740	111.7	116	55	61	12.94	P82; BP
0216+011	one-sided?			36	145	71	12.85	P82
0221+067	one-sided		130.3	36	101	65	3.55	P82; BP
0237+040	one-sided?	0.978		43	145	4	4.97	P82
0239+108	one-sided?			45	40	5	63.75	P82
0319+121	one-sided		106.4	67	162	85	96.75	P82; BP
0333+321	two-sided	1.263	68.9	57	146	89	50.19	P82; OB; SdB
0336-019	one-sided	0.852	43.3	155	165	10	399.52	P82; BP
0400-319	one-sided?			163	50	67	2.56	P82
0402-362	one-sided?	1.417		67	170	77	10.00	P82
0420-014	two-sided	0.915	347.0	64	10	54	206.25	P82; A
0426-380	one-sided?			110	156	46	57.84	P82
0438-436	one-sided?	2.852		19	15	4	22.58	P82
0440-003	one-sided	0.844	8.3	23	90	67	0.61	P82; BP
0451-282	one-sided?	2.559		82	170	88	1.27	P82
0511-220	one-sided?			149	120	29	2.36	P82
0514-161	one-sided?	1.278		1	55	54	9.39	P82
0528-250	one-sided?	2.765		104	80	24	2.22	P82
0539-057	one-sided?			95	50	45	3.31	P82
0609+607	one-sided?			100	90	10	90.14	P82
0707+476	two-sided	1.310	73.2	115	90	25	1.47	P82; BP
0716+714	two-sided		81.7	3	119	64	0.81	P82; PFJ80
0723+679	two-sided	0.846	128.6	172	82	90	0.40	OP
0735+178	one-sided		17.0	80	170	90	37.24	P82; BP
0742+376*	one-sided		530.4	175	132	43	0.40	present
0745+241	two-sided		127.7	27	65	38	6.71	P82
0759+183	one-sided?			65	95	30	10.49	P82
0812+367	two-sided	1.025	152.8	65	156	89	3.19	P82; PFJ82
0820+560	one-sided?	1.417		7	130	57	43.93	P82
0821+447	two-sided	0.904	220.5	52	134	82	0.07	OP

Table 5.2 (contd.)

Source	Structure type	Redshift	Projected linear size (kpc)	Core Polarization PA (°)	Structure PA (°)	Ø (°)	R	References
0821+621	two-sided	0.542	337.7	133	52	81	6.35	OP
0827+243	one-sided?	0.939		37	20	17	1.40	P82
0833+585	one-sided	2.101	94.0	170	155	15	3.50	P82; BP
0836+195*	two-sided	1.691	263.2	109	14	85	0.47	present
0836+710	one-sided	2.160	16.1	102	24	78	16.52	P82; PFJ82; OB
0850+581*	two-sided	1.322	128.5	110	145	35	1.69	RJ82; HUO
0851+202	one-sided	0.306	155.0	87	115	28	9.91	P82; dBS
0859+470	one-sided	1.462	24.8	68	150	82	14.76	P82; PFJ80; BP
0859-140	two-sided	1.327	103.3	75	162	87	49.05	OB; BP
0906+430*	two-sided	0.670	23.6	74	60	14	1.34	RJ82; WMA
0919+218	two-sided	1.421	96.1	129	46	83	0.07	present
0923+392	two-sided	0.699	30.3	176	73	77	6.35	P82; B82
0945+408	one-sided	1.252	35.3	12	35	23	2.15	P82; PFJ82; BP
0954+658	one-sided	0.368	23.4	161	25	44	1.09	P82; BP
0955+476	two-sided	1.873	165.9	58	120	62	166.67	P82
1004-018	one-sided?	1.212		29	130	79	4.70	P82
1007+417	two-sided	0.611	245.0	104	7	83	0.27	present; OP
1012+232	two-sided	0.565	134.2	179	176	3	7.53	present
1020-103	one-sided?	0.197		120	150	30	14.08	P82
1021-006	one-sided?	2.547		167	10	23	13.64	P82
1028+313*	one-sided	0.177	32.5	60	176	64	2.33	FIK
1032-199	one-sided	2.198	21.6	92	145	53	2.24	P82; BP
1040+123	two-sided	1.029	63.2	24	92	68	3.01	present
1055+018	two-sided	0.888	251.5	101	180	79	35.75	present; P82; OB; BP
1055+201	two-sided	1.110	182.0	93	165	72	2.26	present
1116+128	one-sided	2.118	24.3	120	135	15	5.97	P82; OB; BP
1132+303	two-sided	0.614	118.9	88	143	55	0.27	present
1136-135	two-sided	0.554	117.7	13	129	64	0.28	present
1147+245	two-sided		183.4	18	170	28	2.27	P82; A
1148-001	one-sided	1.982	38.6	143	30	67	14.72	P82; BP
1150+497	two-sided	0.334	90.1	123	8	65	0.85	P82; OP
1150+812	one-sided	1.250	43.1	102	80	22	43.67	P82; BP
1156+295	two-sided	0.729	31.0	120	0	60	4.78	P82; A
1213+350	two-sided	0.851	116.5	117	25	88	43.30	P82
1221+186	two-sided	1.401	202.7	44	124	80	0.24	SSH
1221+809	two-sided		26.4	147	17	50	5.20	P82; PFJ80

Table 5.2 (contd.)

Source	Structure type	Redshift	Projected linear size (kpc)	Core Polarization PA (°)	Structure PA (°)	Ø (°)	R	References
1226+023	one-sided	0.158	74.6	155	42	67	3.57	P82; P81
1236+077	one-sided?			128	65	63	10.30	P82
1237-101	one-sided	0.753	138.0	47	30	17	2.32	P82; BP
1243-072	one-sided	1.286	25.8	20	80	60	2.99	P82; BP
1252+119	one-sided	0.871	16.7	153	110	43	2.79	P82; BP
1317+520	two-sided	1.060	250.8	33	130	83	0.75	OP; HUO
1320+299	one-sided		32.2	132	101	31	3.44	present
1347+539	one-sided	0.976	45.0	13	138	55	4.04	present; P82; OP
1354+195	two-sided	0.720	350.8	67	167	80	4.85	present; P82; RR
1354-152	one-sided	1.890	23.2	130	90	40	9.40	P82; BP
1415+463	one-sided	1.552	112.5	172	83	89	4.45	present; OP
1418+546	one-sided		290.0	175	83	88	158.78	P82; A
1430-178	one-sided?	2.331		5	90	85	1.03	P82
1433+177*	two-sided	1.203	86.1	64	172	72	0.46	present
1434+235	one-sided?			92	20	72	131.02	P82
1435+315	two-sided	1.366	103.2	156	137	19	2.40	SSH; RPdR
1435+638	one-sided	2.060	122.1	156	50	74	1.15	P82; BP
1451-375	two-sided	0.314	169.4	150	60	90	4.33	P82
1502+106	one-sided	1.839	58.3	178	160	18	1.46	P82; BP
1509+158	two-sided	0.828	68.7	147	68	79	0.16	present
1510-089	one-sided	0.361	54.9	79	160	81	15.52	P82; OP; BP
1514-241	one-sided	0.049	30.1	50	98	48	485.75	P82; A
1524+101*	two-sided	1.358	92.9	128	46	82	0.75	FIK
1551+130	one-sided?	2.21		95	75	20	1.16	P82
1555+332*	two-sided	0.942	301.8	10	95	85	1.50	FIK
1616+063	one-sided?	2.086		51	45	6	8.22	P82
1636+473	one-sided	0.740	161.7	58	25	33	3.35	present; P82
1637+574	one-sided	0.745	32.4	108	98	10	36.49	present; P82
1638+398	one-sided	1.660	21.1	176	140	36	1.17	P82; BP
1642+690	two-sided	0.751	81.1	144	2	38	9.33	P82; BO81
1656+053	one-sided	0.887	18.4	176	110	66	2.14	P82; BP
1716+686	one-sided?	0.777		91	130	39	4.64	P82
1717+178	one-sided		80.9	18	6	12	9.56	P82; AU
1725+044	one-sided	0.296	27.8	15	105	90	3.75	P82; BP
1725+123	one-sided?			94	135	41	1.39	P82
1729+501	one-sided	1.107	175.1	50	137	87	0.07	present; OP

Table 5.2 (contd.)

Source	Structure type	Redshift	Projected linear size (kpc)	Core Polarization PA (°)	Structure PA (°)	Ø (°)	R	References
1739+522	one-sided	1.375	30.1	67	80	13	15.30	P82; BP
1741+279	two-sided	0.372	62.6	71	171	80	0.59	present
1743+173	one-sided?	1.702		68	35	33	10.00	P82
1751+441	two-sided	0.871	117.0	10	77	67	4.48	P82; PFJ82; BP
1800+440	two-sided	0.660	79.6	138	68	70	1.83	P82; B82; BP
1803+784	one-sided		385.2	75	14	62	3.23	P82; A
1807+279	two-sided	1.760	83.9	162	45	63	0.46	P82
1823+568	one-sided	0.664	117.8	31	97	66	7.27	P82; OB
1842+681	one-sided	0.475	27.8	37	144	73	26.16	present
1849+670	one-sided?			47	30	17	16.67	P82
1857+566	two-sided	1.595	254.9	29	135	74	0.03	S83; OP
1933-400	one-sided?			64	140	76	0.68	P82
2007+777	one-sided		223.0	68	80	12	27.11	P82; BP
2010+723	one-sided?			149	103	46	14.45	P82
2044-168	one-sided?	1.937		56	145	89	1.51	P82
2058-297	one-sided?			80	34	46	6.74	P82
2131-021	one-sided?	0.557		168	135	33	265.51	P82
2155-152	two-sided		46.8	31	0	31	2.34	P82
2210-257	one-sided?	1.833		25	10	15	59.51	P82
2216-038	one-sided	0.901	67.2	85	140	55	5.71	P82; BP
2243-123	one-sided	0.630	30.1	178	40	42	53.84	P82; BP
2251+134	two-sided	0.673	52.0	108	40	68	0.99	present; P82
2308+098	two-sided	0.432	544.5	60	143	83	0.44	S86
2318+049	one-sided	0.622	65.4	63	135	72	3.12	P82; BP
2329-162	one-sided	1.155	16.3	179	50	51	2.14	P82; BP

Table 5.3 List of References

A	Antonucci et al. (1986)	present	Chapter 3, this thesis
AU	Antonucci & Ulvestad (1985)	RJ82	Rudnick & Jones (1982)
B82a	Browne et al. (1982a)	R85	Rudnick et al. (1985)
B82b	Browne et al. (1982b)	RPdR	Rogora et al. (1986))
B87	Browne (1987)	RR	Rusk & Rusk (1986)
BP	Browne & Perley (1986)	S83	Saikia et al. (1983)
dBS	de Bruyn & Schilizzi (1986)	SSK	Saikia et al. (1985)
FIK	Feigelson et al.(1984)	SSS	Saikia et al. (1984)
HUO	Hintzen et al. (1983)	SSH	Swarup et al.(1984)
OBC	O'dea et al. (1988)	S86	Swarup et al. (1986)
OP	Owen & Puschell (1984)	SdB	Schilizzi & de Bruyn (1983)
P82	Perley (1982)	WMA	Wardle et al. (1984)
PFJ80	Perley et al. (1980)	W82	Wilkinson (1982)
PFJ82	Perley et al. (1982)		

even with his dynamic ranges and may not be 'one-sided'. For example, Perley (1982) lists only an intense feature of the jet in the two-sided quasar 0742+318. Similarly, for 1354+195, another two-sided source, only one of the outer components is listed. Quasars that are noted as having only one secondary component in Perley (1982) and with no confirmatory image elsewhere in the literature, have therefore been marked as of uncertain structure-type in Table 5.2, and no projected linear size has been listed for them.

5.5 The results

The distribution of ϕ for the quasars in the sample is plotted in Fig. 5.4. It shows, on the one hand, a large number of quasars with $\phi \gtrsim 60°$. Given the assumptions stated in section 5.2, this implies a remarkably good alignment of the

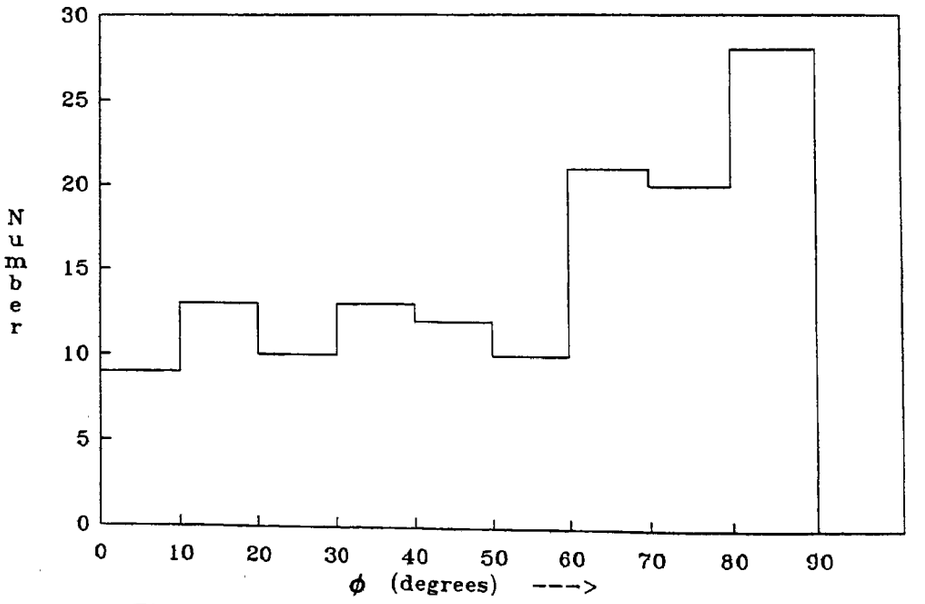

nuclear jet with the radio axis. The axis of ejection of the radio emitting effluent must thus be stable for ~ 10^7 yr. On the other hand, the distribution also shows

large misalignments for several other objects.

5.6 Are the misalignments intrinsic?

Are the above misalignments intrinsic and merely due to the presence of a bending/polarizing agent in those particular nuclei or their environs? This is indeed a possible interpretation. However, the findings of Readhead *et al.* (1983) naturally provoke one to investigate if whether this misalignment correlates with other structural properties, and whether these correlations go the way the unified scheme would predict.

5.6.1 The ϕ – R_{emit} correlation

The immediate correlation to look for is of course that of ϕ with R_{emit}. This is

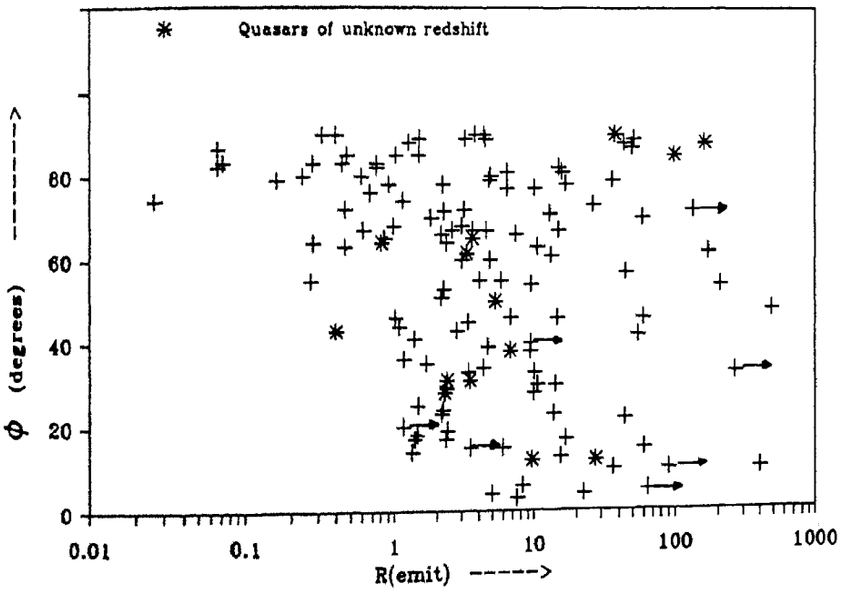

Fig. 5.5 Correlation of ϕ with R

plotted in Fig. 5.5 for the present sample of quasars. The diagram shows that ϕ ranges from ~ 10° to ~ 90° for quasars having R_{emit} >1, whereas for R_{emit} < 1, it

is almost always between 60° and 90°. There is a distinct paucity of objects with low values of R_{emit} *and* large misalignments. Thus the qualitative trend seen here is indeed what the unified scheme would predict. The distributions of ϕ for the objects of the present sample bifurcated at $R_{emit} = 1$ are shown in Figs. 5.6a and b. Formally, a Kolmogorov-Smirnov two-tailed two-sample test indicates that the probability that the two subsamples are drawn from the same parent distribution is < 0.001.

5.6.2 Could it be just selection effects?

The sample of quasars under consideration is quite eclectic and far from being statistically complete; therefore the above correlation could, in principle, arise due to selection effects.

If the polarized flux density measurements for the objects with large R_{emit} had systematically lower values and therefore larger errors of measurement of the PA of polarization, then this would be reflected as a large scatter in their ϕ values. But the distributions of the degree of polarization for the quasars of the present sample (wherever available) with high and low values of R_{emit} (Figs. 5.7a and b) show that the degree of polarization is not systematically lower for the CDQs.

Could objects satisfying the selection criteria (i) and (ii) but not (iii) (i.e., those with misaligned outer lobes) fill up the paucity in Fig. 5.5? No, because as can be seen from Table 5.4 where these objects have been listed, they all have large values of R_{emit}, as indeed would be predicted by the unified scheme. Exclusion of these objects cannot therefore create a spurious paucity of sources with low R_{emit} *and*

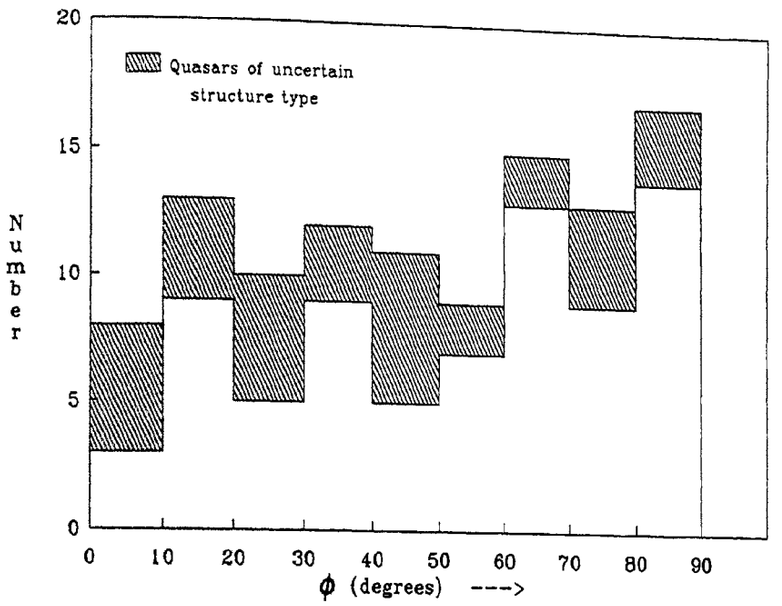

Fig. 5.6a Distribution of ϕ for quasars with R > 1

Fig. 5.6b Distribution of ϕ for quasars with R < 1

Fig. 5.7 Distribution of fractional polarization

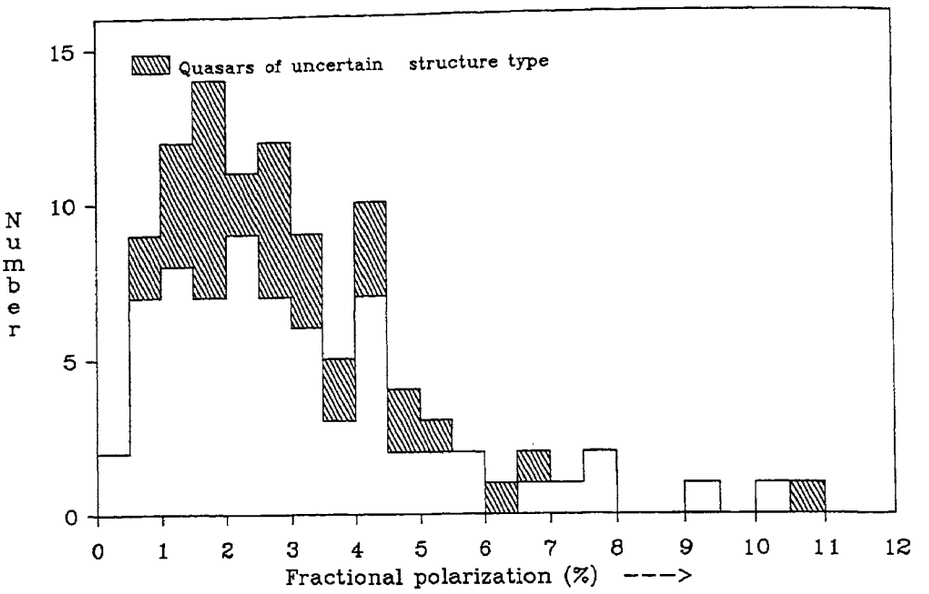

(a) Quasars with R > 1

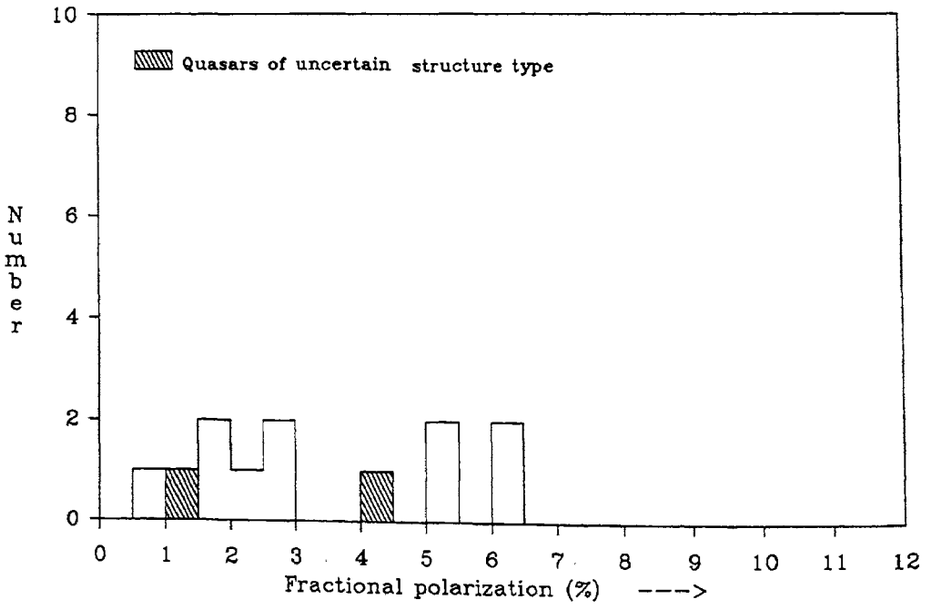

(b) Quasars with R < 1

Table 5.4 Quasars with highly misaligned outer lobes.

Source	Misalignment Angle (deg)	R	References
0119+041	49	> 4.7	P82;BP
0409+229	73	1.41	P82;present
0808+019	78	0.99	P82;AU
0814+425	85	> 8.0	P82;BP
0954+556	70	4.29	P82;B82a
1049+215	100	> 2.7	P82;BP
1253-055	57	2.54	P82;BP
1400+162	53	0.59	SSS
1641+399	53	282.78	P82;SdB
1823+568	75	7.45	P82;PFJ82
1924+507	54	6.44	OP
1928+738	35	11.06	P82;B87

large misalignments. It is hard to think of any other selection effect that would spuriously create a correlation of the kind presented in Fig. 5.5.

It must be pointed out that with better imaging, some of the quasars of uncertain radio structure in Perley (1982) might turn out to have large misalignments and would thereby have to be dropped from the sample by (criterion (iii)). But this would still not detract from the above correlation.

5.6.3 The connection with sidedness

Davis *et al.* (1978) found that, for the three 'one-sided' quasars they observed, the nuclei showed misalignments in marked contrast to 'two-sided' quasars. From this, they suggested that there may be a real connection between nuclear misalignment and the absence of a second outer component. Indeed there is. Fig. 5.8a and b present the distributions of ϕ for the quasars of the present sample bifurcated on the basis of sidedness. The objects with 'two-sided' structure clearly have a greater tendency to have nuclear and large scale structure aligned, while the

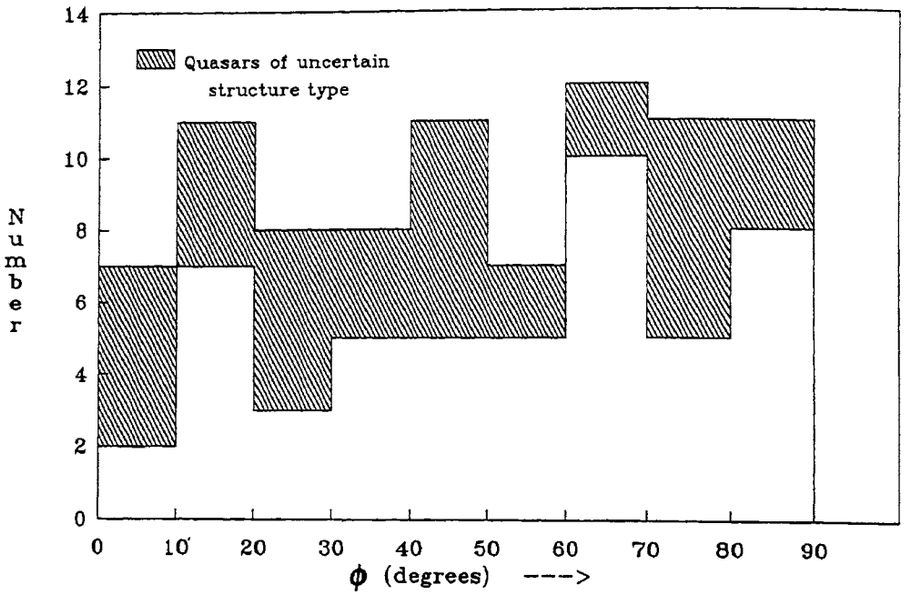

Fig. 5.8a Distribution of ϕ for one-sided quasars

Fig. 5.8b Distribution of ϕ for two-sided quasars

Fig. 5.9 Distribution of fractional polarization

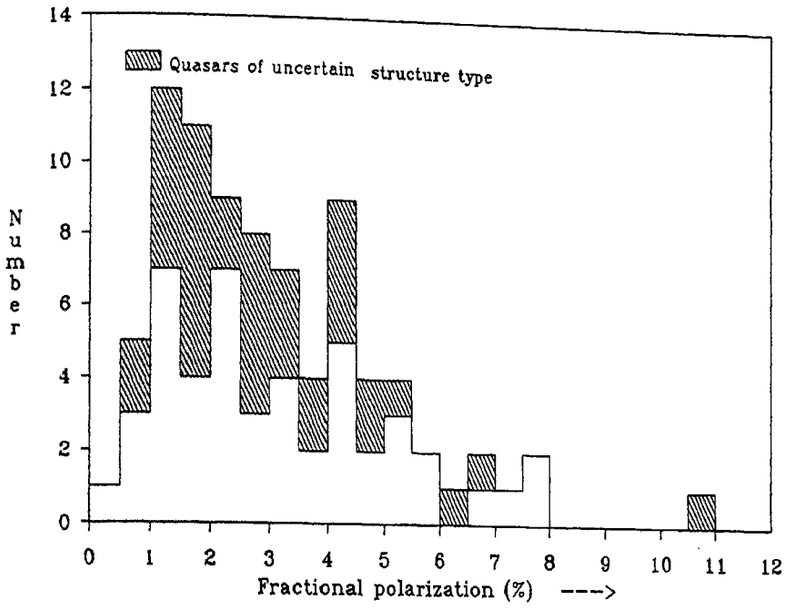

(a) One-sided quasars

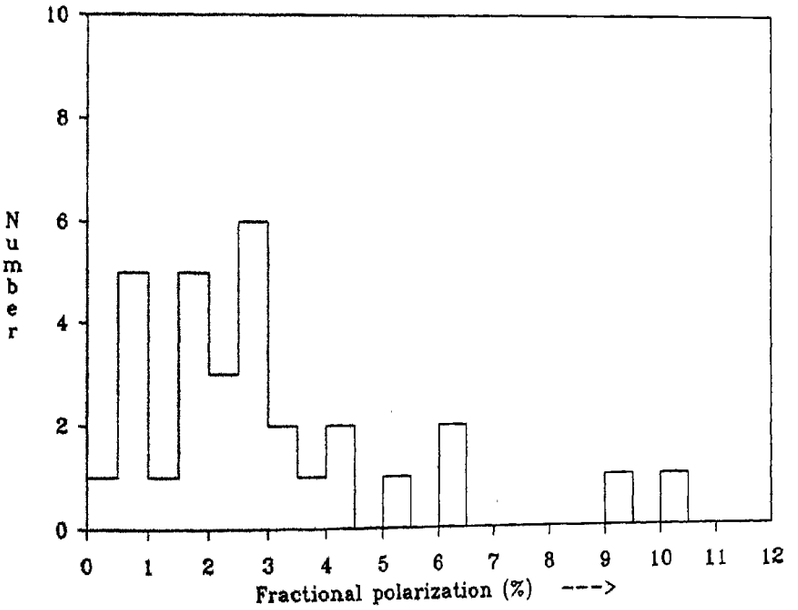

(b) Two-sided quasars

'one-sided' objects show large misalignments. A Kolmogorov-Smirnov two-tailed two-sample test shows that the probability that the two distributions are derived from the same parent distribution is <0.005. The trend is in accord with the interpretation of misalignment and of 'one-sidedness', viz., that 'one-sided' objects and misaligned objects are both sources oriented at small angles to the line of sight.

The distributions of the degree of polarization (whenever available) for the one- and two-sided objects are plotted in Figs 5.9a and b respectively. Once again it is clear that there is no systematic trend for the one-sided sources to have lower fractional polarization. This rules out the possibility that the nearly random distribution of ϕ for one-sided sources is due to larger errors in their PA of polarization.

It should be pointed out that the categorization of the sample into 'one-' and 'two-' sided sources is a very rough one, because the sample is eclectic and therefore the sensitivity and dynamic range of the radio images are not uniform; what appears as a 'one-sided' image with a certain dynamic range may well show structure on both sides of the nuclear component with finer imaging. However, the classification is not entirely meaningless, because it enables one to distinguish between objects of large and small surface brightness ratios of the outer components.

5.6.4 The ϕ–l relation

In Fig. 5.10, the projected linear size l, in kiloparsecs, is plotted against the misalignment parameter ϕ. l has been determined for a q_0 of 0.5 and H_0 of

50 km s^{-1} Mpc^{-1}. Projected linear sizes for those objects with no measured redshift were determined by assuming a redshift of 1, and these have been marked separately in the figure. It is clear from the ϕ–l relation that (for quasars with measured redshifts) almost all that have $l \gtrsim 200$ kpc have $\phi \gtrsim 60°$, while those with $l \lesssim 200$ kpc span the whole range of ϕ. This diagram is also consistent with the interpretation that quasars with a random distribution of ϕ are at small angles to the line of sight because they are then also expected to have smaller projected linear sizes due to foreshortening.

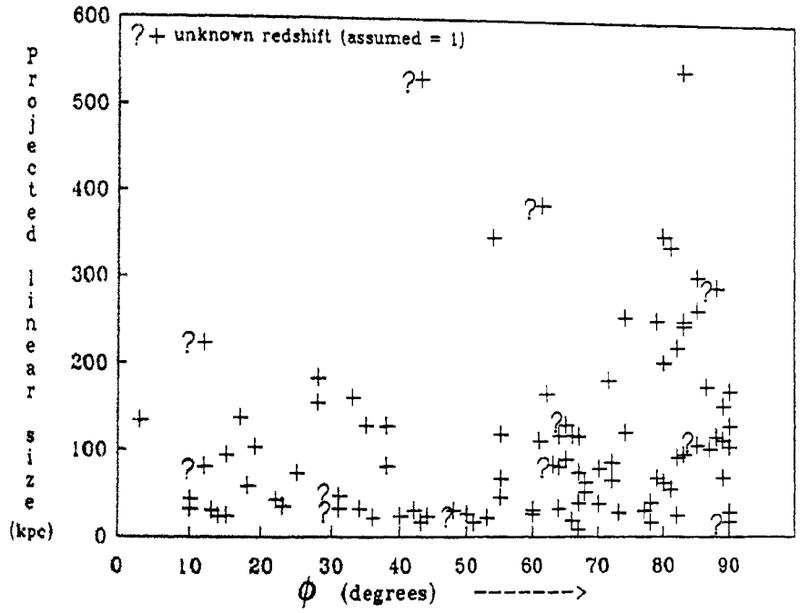

Fig.5.10 Projected linear size vs. ϕ

It should be noted that the quasars from Perley (1982) of uncertain structure-type have been excluded from this diagram. But this cannot create a spurious correlation of linear size with ϕ, because the quasars in question are, by their very selection, compact objects and of small projected linear sizes. Notably, even if their

sizes (as given by Perley, 1982) are doubled to account for any missing outer component on the other side, they are still consistent with the $\phi - l$ correlation. There is one exception to the correlation, viz., 0742+376. This is a 'one-sided' source with a large projected linear size (as derived from an assumed redshift of 1). Its large size is however consistent with its low value of R_{emit}.

5.7 The case of radio sources identified with galaxies

A limited number of polarimetric measurements at high angular resolutions are available in the literature for radio galaxies also. It is therefore interesting to investigate whether the radio galaxies too follow any systematic trend. Antonucci (1984) has carried out such an investigation for eight radio galaxies and found that the polarization generally tends to be perpendicular to the radio structure axis. Galaxies that have available radio polarimetric measurements and properties of structure and sky position that meet the selection criteria listed in section 5.4 are tabulated in **Table 5.5** (a total of 17 sources). The objects from Antonucci (1984) are also included. The distribution of the parameter ϕ is shown in Fig. 5.11. The distribution shows that most of the objects have a value of $\phi \gtrsim 60°$. Taking the cue from the case of quasars, this trend probably reflects a similar physical phenomenon, *viz.*, that the magnetic field is parallel to the elongation of the nuclear radio jet in radio galaxies. Several measurements at slightly larger distances from the nucleus (e.g., Spangler & Pogge, 1984) also suggest this.

It must be pointed out here that no attempt has been made to distinguish between different kinds of galaxies, whether by optical type (for instance, elliptical, Seyfert, etc.) or by radio type (FR type I or II; Fanaroff & Riley, 1974). This could

Table 5.5 The sample of radio galaxies

Source	Alternate Name	core polarization PA (°)	Structure PA (°)	ϕ (°)	Reference
0111+021		47	120	73	Perley (1982)
0119+115		166	20	34	Perley (1982)
0206+135	4C35.03	14	132	62	Antonucci (1984)
0305+039		80	55	25	Perley (1982)
0338-214		123	90	33	Perley (1982)
0410+110	3C109	78	143	65	Antonucci (1984)
0430+052		166	136	30	Perley (1982)
0454+066		113	50	63	Perley (1982)
1128-047		60	116	56	Perley (1982)
1323-426	Cen A	69	132	63	Burns et al. (1983)
1330+022	3C287.1	171	90	81	Antonucci (1984)
1346+268	4C26.42	103	16	87	van Breugel et al.(1984)
1417-192		127	13	66	Antonucci (1984)
1441+522	3C303	5	116	69	Kronberg (1986)
1652+397	4C39.49	152	45	73	Antonucci (1984)
1807+698	3C371	162	60	78	Perley (1982)
2349-014	4C-01.61	58	170	68	Antonucci (1984)

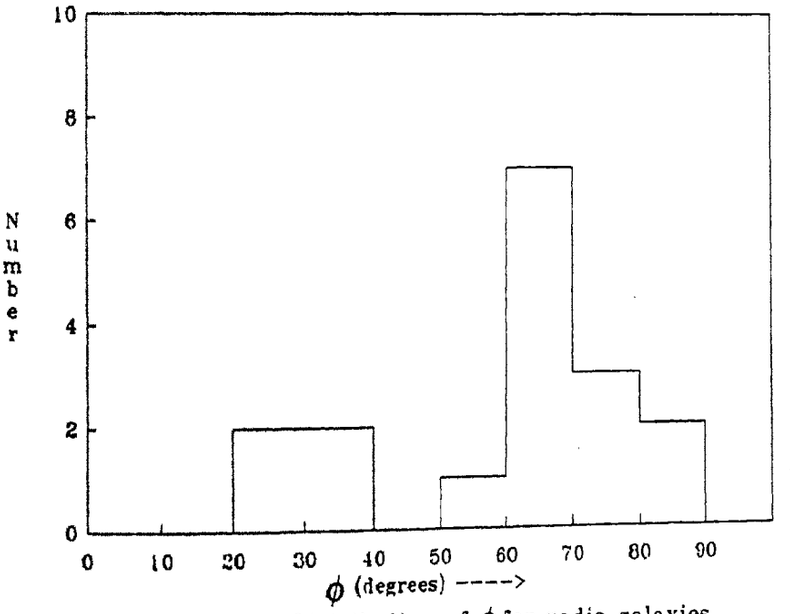

well be important, because the conditions in the nuclear regions would be different for different kinds of galaxies. Further, it would be illuminating to determine what role, if any, the nature of the optical emission line region plays in determining the nature of the observed polarized emission.

5.8 Are the RMs and depolarization dependent on orientation?

The results described in the earlier sections seem to suggest that the 'internal' RMs (due to Faraday rotation near the nuclear region) of the AGN under consideration are small. In view of the fact that sources with large R_{emit} show large misalignments of ϕ, it is important to investigate the dependence of the RM of the nuclear components on R_{emit} for quasars. Such a study is now under way. Polarimetric imaging with the VLA has been performed on a sample of radio quasars that were selected to have as large a range in R_{emit} values as possible from areas of sky with low Galactic RM (cf. Section 5.3).

Assuming that the unified scheme is valid, the above investigation is expected to lead to clues on the geometry of the Faraday rotating regions, and would thus also have a bearing on the results on quasar absorption lines that are now available. It has been suggested that the associated absorption at $z_{absorption} \approx z_{emission}$ in quasars occurs in absorbing clouds at distances of a few kiloparsecs from the QSO (Williams *et al.*, 1975). At resolutions $\lesssim$ 1 arcsec of the above polarimetric investigation, the physical regions sampled are of size similar to this at redshifts of ~ 1.5. Further, work by Foltz *et al.*(1987) on a sample of 88 radio-loud quasars has shown that strong associated absorption (within about $\pm$ 5000 km s^{-1} of the emission line redshift) was found in 22 of the objects, and there is a tendency for

the absorption to occur preferentially in sources with steep radio spectrum. It would be interesting to examine if this dichotomy in the absorption characteristics is related to the observed Faraday rotation effects of the radio polarization.

5.9 Summary

The nuclear radio polarization of quasars has been used to infer the orientation of their nuclear jets. These jets appear well-aligned with the overall radio structure in the case of the LDQs, while CDQs often show large misalignments, consistent with the predictions of the unified scheme. Radio galaxies also appear to have their nuclear jets well-aligned with their radio axes. In view of the misalignments observed in CDQs, it is important to investigate if Faraday rotation in the nuclei of quasars is aspect dependent, and whether this might shed light on why associated absorption complexes appear to be preferentially in quasars of steep radio spectrum.

Chapter 6

ASPECT DEPENDENCE OF THE OPTICAL CONTINUUM

A major criticism of the unified interpretation for radio quasars has been the analysis of the Bologna (B2) sample of quasars by de Ruiter *et al.* (1986). They showed that the R-distribution for this complete low-frequency sample differs significantly from that for the 3CR sample. They concluded that the unified scheme of Orr & Browne (1982) is not sustained, because in this scheme all complete samples of radio quasars selected at low frequencies are expected to have their constituents randomly oriented in the sky and therefore exhibit similar R-distributions.

The above inconsistency could, however, be understood if the quasar sample of de Ruiter *et al.* (1986) were biased in some manner. The aspect dependence of the optical continuum (Browne & Wright, 1985) is a potential source of such a bias. In this chapter, the possibility that the Bologna sample may be ridden with a selection effect due to the optical continuum being dependent on orientation is explored. The results appear to support this conjecture, thus not only undermining the criticisms of de Ruiter *et al.* (1986), but also provoking a deeper analysis of the phenomenon of optical aspect dependence. Further support for the idea comes from an analysis of the data on host galaxies of quasars. The possible causes of the phenomenon are then discussed, as also the implications.

6.1 The Bologna quasars—an inconsistency with the unified scheme?

In order to conduct statistical studies of extragalactic radio sources, it is important to have samples of objects that are not biased with regard to the orientation of their radio axes. Only then can phenomenologies for these objects be quantitatively tested, especially if they postulate an orientation dependence for some of the concerned properties. It is generally assumed that samples of objects selected by surveys conducted at low radio frequencies would be unbiased with respect to source orientation. For, one would then be picking up sources by their extended radio emission (of steep radio spectrum) which is not relativistically beamed (or nearly so, cf. chapter 4), rather than by the emission from the central component (of flat radio spectrum) that *is* possibly Doppler boosted. It is also implicit that the optical emission from the nucleus is not dependent on orientation, and therefore, even if all the objects in such a complete low frequency sample are not identified, the quasars that are, are taken to constitute an *unbiased* sample.

There *are*, of course, suggestions, albeit model dependent, that a fraction of the optical continuum from the nucleus of some active galactic nuclei might be synchrotron emission that is relativistically beamed, especially among BL Lacertids and OVV (optically violently variable) quasars (e.g., Wardle *et al.*, 1984). However, these objects are of flat/complex radio spectrum of the extreme sort, and are not expected to constitute more than a very small fraction of complete low frequency samples, which therefore are generally assumed to remain "unbiased". The 3CR sample was the first among such samples, and was the one used by Orr & Browne (1982) to assign a numerical value to the model parameter in their unified

scheme.

6.1.1 The Bologna sample

The B2 sample of quasars has been obtained from the Bologna radio survey that was conducted at 408 MHz (over a limited area of ~ 0.14 steradians of sky) and has a limiting radio flux density of 0.25 Jy. Those radio sources from the survey that were identifiable with stellar objects on the Palomar (POSS) plates and showed an excess of ultraviolet continuum were classified as quasars (a total of 74; Fanti *et al.*, 1975). The only purported selection effect in the sample is against objects of redshifts larger than 2.5 (because the criterion of ultraviolet excess was used). Therefore, this sample is "unbiased" as per the description given in the previous subsection, and more, has a radio flux density limit that is fainter than the 3CR sample. It is thus a sample that is doubly important in the context of relativistic beaming models; the deductions that have been made on the basis of such models (and tested on the 3CR sample) can now, in principle, be verified on an independent and fainter sample.

From VLA images obtained at 5 GHz, de Ruiter *et al.* (1986) determined the form of the distribution of $R_{observed}$ for 59 of the 74 quasars in the B2 sample. They found that it did not fit the theoretical distribution based on random orientation of the radio sources (Orr & Browne, 1982); their values of $R_{observed}$ were systematically higher by a factor of about five. They therefore stated that their data do not support the unified scheme.

It is important to confirm the result of de Ruiter *et al.* (1986) for the whole B2

sample. A more complete R distribution is shown in Fig. 6.1 (and the derivation of the values of R in it is described later in section 6.4.1). Also shown in the figure is the distribution of R for the 3CR sample (Fig. 1(a) of Orr & Browne, 1982). The peak in this updated Bologna distribution occurs somewhere between 0.1 and 1, while that for the 3CR distribution occurs between ~0.03 and 0.1. A further difference from the 3CR distribution is the significant fraction of objects with a large ($\gtrsim$ 10) value for $R_{observed}$. Thus, the observed differences are in fact even larger than was suggested by de Ruiter *et al.* (1986) on the basis of their restricted sample of 54 Bologna quasars.

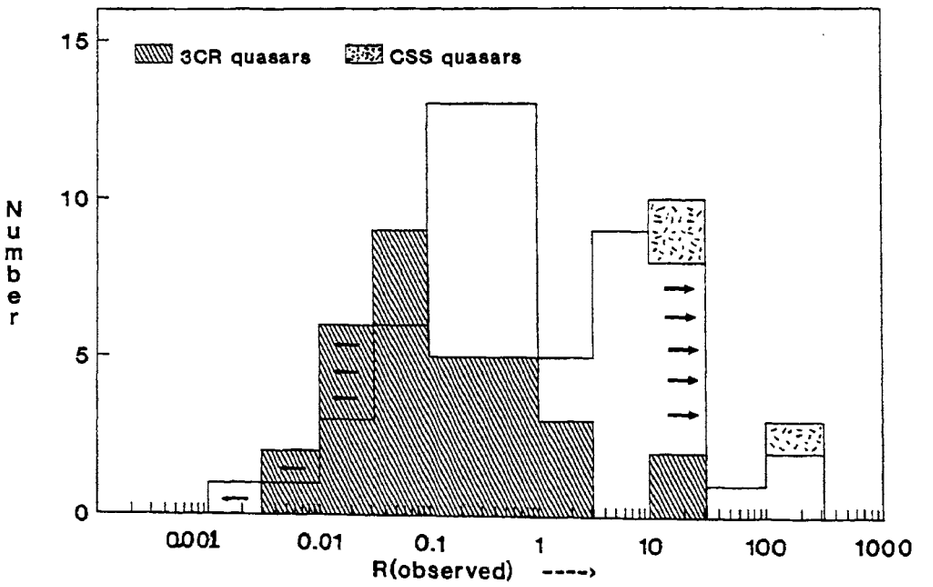

For a majority of the quasars in the B2 sample, the redshifts are unknown. Hence, the values of R cannot be determined at the emitted frequency. Some of the disparity with the 3CR distribution could arise if the Bologna quasars have significantly higher redshifts. For, they would then be seen to larger emitted

frequencies and hence the cores would appear more prominent intrinsically (due to the difference in spectral index between the cores (α typically ~ 0) and lobes (α typically ~ -1). The disparity, however, is too large to be explained by such an effect alone. Redshifts of about four would be required to explain a difference of a factor of five in the values of R.

It is thus important to examine if there are any selection effects in the B2 sample, and also if the proposition of Browne & Wright (1985) might explain the contrariety that de Ruiter *et al.* (1986) find with the scheme of Orr & Browne (1982).

6.1.2 Evidence for aspect dependence of the optical continuum

For sets of quasars of flat and steep radio spectrum from complete radio frequency samples, chosen such that these objects were *intrinsically similar* in the scheme of Orr & Browne (1982), a comparison of the apparent optical magnitude distributions has demonstrated that the distributions differ significantly (Browne & Wright, 1985). It may be noted that in unified schemes, a quasar with steep radio spectrum, if turned "end-on", would appear as one of flat radio spectrum *and* of higher radio flux density. Specifically, in the scheme of Orr & Browne, a typical lobe-dominated (steep radio spectrum) quasar (LDQ) of flux density 0.3 Jy at 408 MHz and a core-dominated (flat radio spectrum) quasar (CDQ) of flux density of 1 Jy at 5 GHz are intrinsically identical objects. Browne & Wright (1985) found that (radio-faint) LDQs appeared optically fainter than (radio-bright) CDQs. In order to reconcile this difference in the distributions of apparent magnitudes with the scheme of Orr & Browne (1982), it is necessary to invoke a dependence of the

optical continuum on aspect in the same sense as that of the radio emission. Browne & Wright (1985) suggested relativistic beaming or inclination dependent obscuration of the optical continuum at small angles to the line of sight as possible explanations for such an aspect dependence. They estimated that, for consistency, the average brightness of the continuum should change by at least 1 magnitude with orientation.

Wills & Browne (1986) also suggested that the optical continuum was aspect dependent, on the basis of evidence for an inverse correlation between equivalent widths of nuclear O[III] and H_β emission lines and the dominance of the radio core, and also between linewidth and core dominance. Relativistic beaming or thermal emission by a physically thin and optically thick disc were put forth as possibilities. In the latter case too, the amount of radiation received would differ with inclination angle, and this dependence on orientation would also be in the same sense as that of the radio emission if the disc were perpendicular to the radio jet.

6.1.3 The B2 sample—not really unbiased?

For the Bologna quasars, optical identifications have been looked for only down to the limiting apparent magnitude of the POSS plates, which is ~ 21. Now, it is well known that the distribution of apparent optical magnitude of a sample of quasars is a function of its limiting radio flux density: the median of the distribution of apparent magnitudes gets fainter with decrease in the radio flux density limit of the sample (Bolton & Wall, 1970). This effect is particularly strong for quasars selected from low-frequency catalogues, as can be seen from Fig. 1 of Browne & Wright (1985). At the flux density limit of the Bologna sample of 0.25 Jy, the peak

occurs close to the POSS plate limit, suggesting that many QSOs would be too faint to be included in the sample. Deep optical observations of a sample selected at 408 MHz and complete to 1 Jy (from, in fact, the Bologna survey) have shown directly that as many as 40% of all quasar identifications are with objects below the POSS plate limit (Allington-Smith *et al.*, 1982). The fraction could be even higher at the flux density limit of 0.25 Jy.

Now, if the optical continuum is also a function of orientation in the same sense as the nuclear radio emission, the sample will pick up many quasars that are, so to speak, "intrinsically below the plate limit", but that get included because of their favourable inclination which causes the optical emission (along with the radio emission) to appear enhanced. The resulting sample would then *not* be unbiased with respect to orientation of radio structure axes. It should be pointed out that the cut-off effect of the optical continuum would be much less important for the 3CR quasars, because at the higher radio flux density limit of this sample, the distribution of apparent magnitudes peaks well above the POSS plate limit, and almost all the sources in the 3CR sample have in any case been optically identified from deeper optical observations.

6.2 Search for aspect dependence—the B2 quasars

If an aspect-dependent optical continuum does indeed result in an orientation bias in the Bologna sample, it should be revealed in the distributions of apparent magnitudes, m_v, of quasars with large and small values of $R_{observed}$. High resolution images of the Bologna quasars, mostly available in Rogora *et al.* (1986; 1987) are used here to investigate this question.

6.2.1 The derivation of $R_{observed}$

Of the 74 Bologna quasars listed in Fanti *et al.* (1979), three (0900+294, 0923+295 and 1340+319) have been condemned as misidentifications, after VLA images at high resolution revealed a displacement of ~ 5 arcsec between the optical position and the radio source (Rogora *et al.* 1986; 1987). The remaining 71 quasars have been considered below. 1320+299, 1328+307 and 1419+315 have been imaged by the VLA before (this thesis, Chapter 3; Perley, 1982). It may be noted that in the case of 1320+299, the radio "component" associated with the QSO is almost certainly unrelated to the other components observed by Feretti *et al.* (1982) (cf. description of the source, this thesis, section 3.3). It is therefore taken to be an independent source. 1419+315 also is almost certainly a juxtaposition of two unrelated radio sources (this thesis, section 3.3); only the triple source associated with the QSO is considered here to be the quasar.

For the remaining 68 quasars, flux densities of the nuclear components used for the estimation of $R_{observed}$ have been taken from high resolution VLA imaging data available in Rogora *et al.* (1986; 1987). It turns out that in 6 cases, the resolution of the image or the accuracy of the optical position is insufficient to identify the nuclear component (although the identification of the radio source itself as a quasar is secure), and therefore the value of $R_{observed}$ cannot be determined. These objects have therefore to be excluded from the analysis. The flux densities of the extended emission have been taken from the VLA data of Rogora *et al.* whenever available. If the VLA images do not detect any extended emission, then the total flux densities measured at 5 GHz by Fanti *et al.* (1979) using the WSRT are used. In some cases,

the radio flux density has clearly varied and the flux density of the unresolved component as given by the VLA image is higher than the total flux density as measured by the WSRT. In these cases, an approximate estimate of $R_{observed}$ is made using the radio spectral index of the radio source between 1.4 and 5 GHz (Fanti *et al.*, 1979), and assuming that the radio quasar consists of a nuclear component of spectral index 0 and extended emission of spectral index −1. Since for sources with inverted spectrum this estimate is invalid, a lower limit for the value of $R_{observed}$ is estimated from the $R_{observed} - \alpha$ relation presented in Fig. 6.2. The relevant properties for the 71 Bologna quasars are presented in Table 6.1.

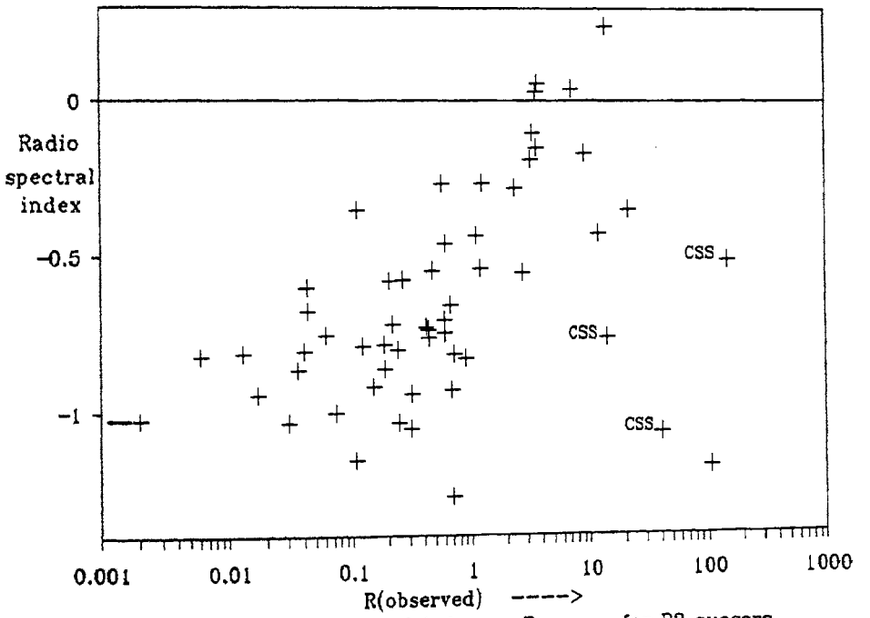

Fig. 6.2 Radio spectral index vs. $R_{observed}$ for B2 quasars

6.2.2 The B2 sample—not unbiased!

Fig. 6.3a and b show the distributions of apparent magnitudes for the two

Table 6.1 The quasars from the Bologna (B2) sample. The radio spectral index is estimated between 1.4 and 5 GHz.

Source	Apparent Optical Magnitude	Radio Spectral Index	R	Remarks
0808+289	18.8	-0.55	2.8	
0810+327	18.0	-0.10	3.4	
0816+268	18.2	-0.80	0.2	
0836+296	20.8	-0.68	0.04	
0853+291	19.1	-1.00	0.07	
0900+294		-1.15		Misidentified
0901+285	17.6	-0.26	1.3	
0906+306	18.3	-0.46	0.6	
0906+313	17.8	-0.43	1.1	
0907+280	19.5	-1.15	0.1	
0909+302	20.3	-0.76	14.2	CSS
0912+297	16.3	-0.19	3.3	
0917+294	19.7	-0.86	0.2	
0920+312	19.5	-0.95	0.02	
0920+313	18.2	-0.15	3.7	
0922+306	20.9	-1.06	0.3	
0922+316	20.0	0.04	7.3	
0923+295		-0.74		Misidentified
0928+312	18.6	-1.18	107	
0933+276	20.2	-1.03	0.03	
0937+304	18.2	-0.12	15.1	
0939+278	18.0	-0.94	0.3	
0953+307	20.2	-0.58	0.3	
0955+326	15.9	-0.43	12.0	
1002+281	20.6	-0.92	0.2	
1003+299	19.2	-0.72	0.2	
1003+328	19.0	-0.54	1.2	
1011+280	18.9	-0.27	0.6	
1015+277	19.1	-0.75	0.06	
1016+302	21.0	-0.60	0.04	
1017+318	20.3	-0.82	0.01	
1204+281	18.1	0.04	22.2	
1208+322	16.2	-0.93	0.7	
1211+284	20.0	-1.07	40.2	CSS
1213+307	19.2	-0.81	0.01	
1213+321	19.5	-0.35	21.4	

Table 6.1 (contd.)

Source	Apparent Optical Magnitude	Radio Spectral Index	R	Remarks
1215+303	15.1	-0.17	9.3	
1219+285	14.6	-0.34	3.8	
1222+320	18.1	-0.35	0.1	
1225+317	15.6	0.10	22.2	
1230+295	20.2	-0.74	0.4	
1234+268	20.5	-1.03	< 0.002	No core detected
1242+283	19.0	-1.27	0.7	
1244+324	18.2	-0.73	0.4	
1248+305	18.0	-0.87	0.04	
1254+285	20.9	-0.80	0.04	
1255+327	18.9	-0.01	156	
1308+326	19.5	0.17	22.2	
1320+299	20.7	-0.28	2.4	
1327+313	19.0	-1.09		Core position uncertain
1328+307	16.7	-0.51	148	CSS
1340+289	16.5	0.06	3.8	
1340+319		-0.76		Misidentified
1348+308	19.3	0.02	22.2	
1351+267	17.2	-0.83	0.9	
1351+318	17.4	-0.55	0.5	
1353+306	18.2	0.10	22.2	
1355+309	20.0	-0.98		Core position uncertain
1402+296	20.1	-0.79	0.1	
1410+317	20.5	-0.76	0.4	
1411+299	18.7	-0.75	0.6	
1419+315	20.0	-0.71	0.6	
1422+307	20.6	-1.03	0.2	
1425+267	15.4	-0.81	0.7	
1426+295	18.4	-0.63		Core position uncertain
1430+315	19.8	-0.87		Core position uncertain
1431+323	20.6	-0.58	0.2	
1435+315	18.0	0.03	3.7	
1443+266	18.8	-0.93		Core position uncertain
1448+301	19.5	-0.24		Core position uncertain
1451+270	19.7	0.24	14.3	
1452+301	19.0	-0.26	5.5	
1555+303	19.7	-0.66	0.7	
1620+301	19.4	-0.78	0.2	

subsamples of the Bologna quasars with $R_{observed} < 0.5$ and $R_{observed} > 0.5$ respectively. Of the quasars that appear compact with the A-array imaging by the VLA, 0909+130, 1211+284 and 1328+307 have steep radio spectra and are thus Compact Steep Spectrum (CSS) sources (cf., this thesis, section 4.3). To reiterate, CSS quasars do not fit in simply into the scheme of Orr & Browne (1982) and are probably a different physical class of object. They have been shown stippled in the distribution.

There is a clear difference in the distributions of apparent optical magnitudes for quasars with low and high values of $R_{observed}$ (which is significant at the 0.01 level as derived by a Kolmogorov-Smirnov two-sample test). While the number of quasars with weak cores ($R_{observed} < 0.5$) continues to increase to the plate limit ($m_p = 21$), the quasars with prominent cores ($R_{observed} > 0.5$) peak before the plate limit. The dependence of apparent optical magnitudes on the relative strength of the nuclear radio component is also evident from the plot of $R_{observed}$ versus m_p seen in Fig. 6.4. These parameters have been plotted for all the quasars in the sample except those for which the core identification (and therefore the $R_{observed}$ value) is uncertain. The two CSS sources have been marked separately. It is clear that there is a significant paucity of optically bright quasars with small values of R.

Indeed, it has been noted earlier that for the Bologna quasars, there is a dependence of the flattening of radio spectral index at high radio frequencies on the ratio of radio-to-optical flux density (Fanti *et al.*, 1975). Since the radio flux density used to calculate this ratio is that measured at 408 MHz where the nuclear component does not contribute significantly, this finding is roughly equivalent to the

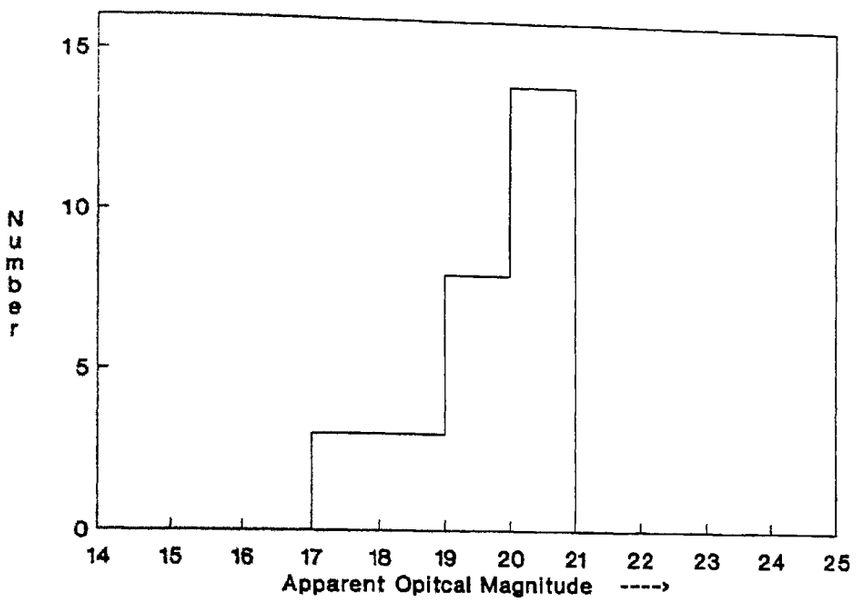

Fig.6.3a Distribution of optical magnitude: B2 quasars with R < 0.5

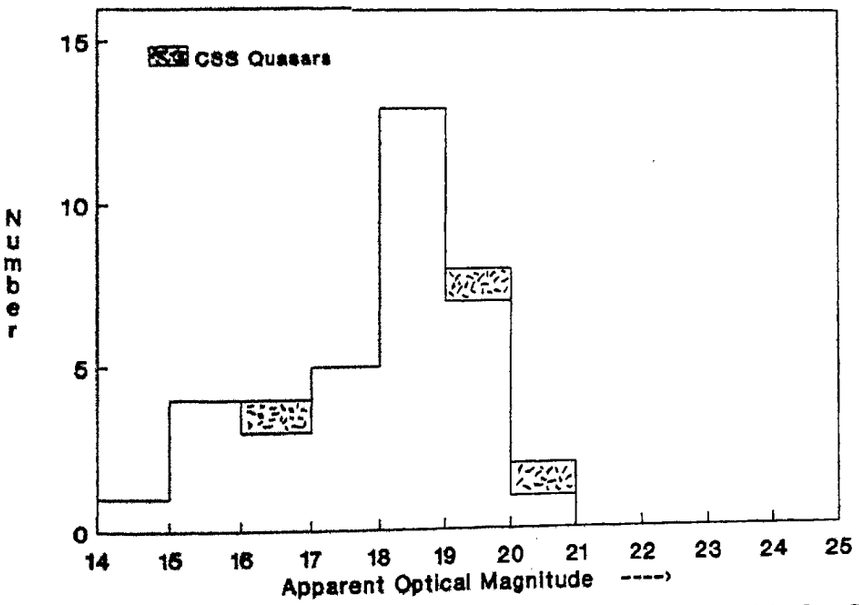

Fig.6.3b Distribution of optical magnitude: B2 quasars with R > 0.5

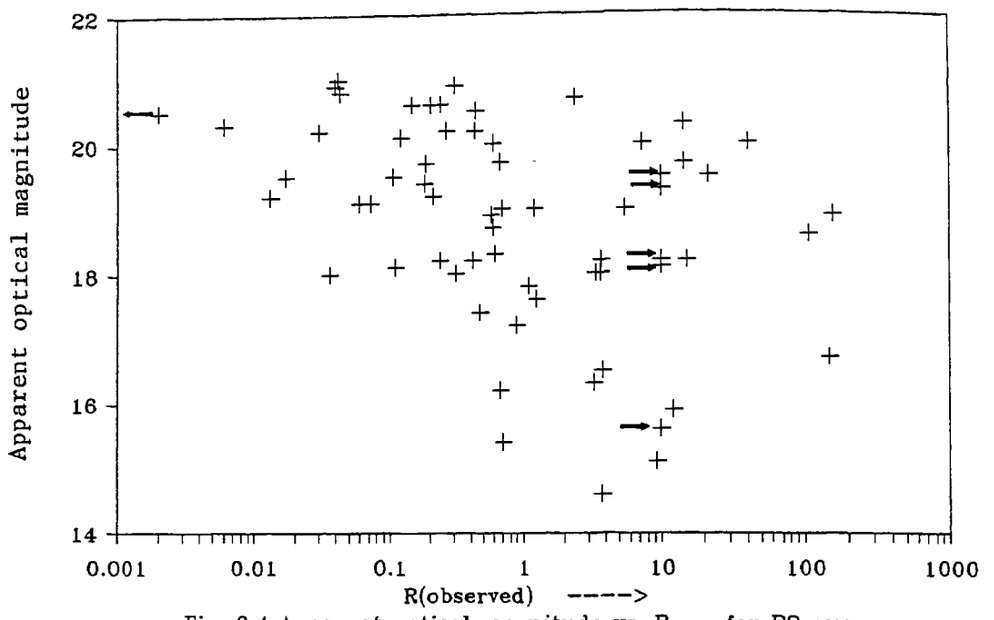

correlation between $R_{observed}$ and m_p described above.

It thus appears that the Bologna sample of quasars may be far from unbiased. A congruence of the distribution of $R_{observed}$ with what is predicted by the model of Orr & Browne (1982) can be expected, if at all, only when the optical identifications for the entire survey are *completed* and the optically fainter quasars thereby identified. The above arguments predict that these optically fainter objects would have relatively low values of $R_{observed}$.

6.3 Search for aspect dependence—other support for the R-m correlation

It turns out that the trend for flat radio spectrum (and therefore core-dominated) quasars to be optically brighter than their lobe-dominated counterparts has been noticed earlier, though the results were not interpreted as a manifestation of the orientation effect. These cases are briefly described below. The more recent

evidence for the same phenomenon from the Molonglo sample is also summarized.

6.3.1 Earlier instances of the same phenomenon

Wills & Lynds (1978) found that quasars with flat radio spectrum were optically brighter than those with steep radio spectrum in their complete samples of quasars selected at 178 MHz, and also for the ones selected at 2.7 GHz (though to lesser level of significance). Condon *et al.* (1981) also pointed out that the Bologna quasars with steep and flat radio spectrum differed in their apparent magnitude distributions. The study of the Parkes sample of quasars selected at 2.7 GHz in the strip of sky of $\pm$ 4° declination by Masson & Wall (1977) is another investigation that showed a similar disparity in apparent magnitude distributions between quasars of flat and steep radio spectrum.

In view of the fact that quasars with flat radio spectrum, in addition to appearing optically brighter, also tend to have compact radio structures, Wills & Lynds (1978) put forth two alternative explanations: (a) that the same physical conditions (within the object or in its environment) that constrict the expansion of the radio source also brighten the optical continuum, or (b) that more compact objects were younger and therefore also optically more luminous. There are several CSS sources now known in whose case it is strongly suspected that a gas-rich interstellar medium constricts the size of the radio source through interactions (cf. section 4.3 and references therein). But in these cases the radio spectrum turns out to be steep and not flat, and it is not clear whether the interaction can occur close enough to the nucleus and thereby produce a brighter optical continuum. In any case, while hypothesis (a) would explain the correlation of R with apparent

misalignments near the nucleus (Chapter 5), it does not explain the correlation of R with large scale misalignments (Kapahi & Saikia, 1982). As for alternative (b), while one might argue that the radio (and optical) nuclear components of younger objects would be more powerful emitters, the conjecture does not explain the the correlation of "nuclear scale" misalignments with R (Chapter 5), much less the correlation of large scale misalignments with R. Neither hypothesis explains the correlation of the apparent superluminal velocity of radio components near the nucleus with R (Browne, 1987).

Condon *et al.* (1981) attributed the similar trend that they found for the Bologna quasars to a correlation between nuclear radio and optical luminosities. The correlation of R with m does not rule out this interpretation. However, it might even be viewed as consistent with orientation effects. For, relativistic beaming of the radio emission results in a higher *observed* radio luminosity for the nucleus, *and*, as has been argued earlier, is *accompanied* by an apparent enhancement of the optical luminosity as well. In any case, this interpretation points to the importance of determining the redshifts for all the B2 quasars. This will not only eliminate the uncertainties in R due to the unknown redshift but also enable testing of the correlation of radio and optical luminosities.

6.3.2 The Molonglo sample of quasars

Motivated by the prediction that unidentified (and therefore optically faint) quasars in complete low frequency samples will turn out to have large R, Kapahi *et al.* (1989) recently determined R values for a sample of radio-faint quasars from the

Molonglo Reference Catalogue of Large et al. (1981). The sample has a radio flux density limit of 0.95 Jy at 408 MHz and optical identifications have been made to a limiting magnitude of ~ 23, with all stellar objects taken to be quasars. Kapahi *et al.* (1989) have shown that the distributions of R for optically brighter ($m_b < 19.5$) and fainter ($m_b \geq 19.5$) objects differ from that for the 3CR quasars in that (a) sources with $R > 10$ appear to be more common, particularly in the optically brighter group, and (b) the peak of the R-distribution for the brighter quasars appears to occur at a larger value of R compared to that for the 3CR sample, while the opposite was true for the fainter quasars.

6.4 Search for optical aspect dependence—host galaxies of quasars

Much progress has been made in the investigation of the local environs of quasars since the early work of Kristian (1973) that detected a "fuzz" around several of them. The advent of charge-coupled device (CCD) detectors, which are of dramatically higher efficacy than the earlier photographic imagery, have hastened this process. It is now well established that the fuzz represents the host galaxy which the quasar inhabits. These hosts are larger and more luminous (massive?) than normal elliptical and spiral galaxies, with peculiar morphologies in several to boot. But of course, these differences from ordinary galaxies are not unexpected, since the presence of a violent energy source at the centre is bound to have its effect on the host. It is also possible that the peculiarities are causal, in that these are galaxies preferentially conducive to ultra–energetic central activity.

It also appears that radio loud quasars sit in giant elliptical hosts (Malkan, 1984; Gehren *et al.*, 1984; Smith *et al.*, 1986), which parallels radio

galaxies being elliptical ones. (But it is not quite so clear if, correspondingly, radio–quiet quasars always occur in spiral hosts.)

6.4.1 Relativistic beaming and the L_{nucl}/L_{gxy} ratio

If (as in the unified scheme) differences among CDQs and LDQs are only due to orientation effects, it is expected that the luminosities of their host galaxies would similar. Hence, if the optical continuum from the active galactic nucleus is dependent on inclination, then the two groups of quasar should differ in their distributions of L_{nucl}/L_{gxy}, which is the ratio of optical emission from the nucleus to that from the host galaxy. This question has been explored in what follows, with an analysis of data from radio quasar images in the optical band available in the literature.

6.4.2 The correlation of L_{nucl}/L_{gxy} with $R_{observed}$

Hutchings *et al.* (1984) have presented photographic optical images (resolution of ~ 1 arcsec) of 78 quasars with redshifts of up to 0.7. Of these, 28 are radio-loud quasars, a set of reasonable size to look for systematic trends. The values of L_{nucl}/L_{gxy} are presented in table 1 of their paper. They decomposed the quasar images into the nuclear and host-galaxy components by subtracting a correctly scaled point-spread-function from the images so as to achieve the best exponential to the profile of the luminosity of the resolved part, averaged over azimuth. The values have been corrected for distance effects of the unresolved luminosity, for the dependence of the ratio on the point-spread-function and the limiting surface

brightness of the image, for K–dimming, and for foreground extinction due to our Galaxy. Three of the quasars appear unresolved in the optical imaging.

For most of these objects, radio flux densities of the nucleus at 5 GHz using the VLA are available in Gower & Hutchings (1985), Perley (1982) and Harris *et al.* (1983). The value of $R_{observed}$ has thereby been derived. Wherever $R_{observed}$ cannot be determined reliably, the high frequency radio spectral index $\alpha_{\sim 5\ \text{to}\ 8\text{GHz}}^{\sim 1\ \text{to}\ 3\text{GHz}}$ has been used to estimate it as done in section 6.2.1.

Of the 28 radio loud quasars, 25 appear resolved (or marginally so) in the R band images and have values/upper limits of L_{nucl}/L_{gxy} tabulated. Of the three that appear unresolved, Gehren *et al.* (1984) have given upper limits for the absolute magnitudes (of the host galaxies) of two (0607–157 and 1203+011), from which approximate upper limits to L_{nucl}/L_{gxy} have been inferred. For 0742+318, an upper limit of ~ 30 has been assumed for the value of L_{nucl}/L_{gxy}. Table 6.2 lists these ratios.

Fig. 6.5 shows the plot of $R_{observed}$ against L_{nucl}/L_{gxy}. A distinct trend for objects with higher $R_{observed}$ to have higher values of L_{nucl}/L_{gxy}. Indeed, the trend is what the unified scheme would predict, because while enhancement of the radio emission from the core component is expected to be accompanied by enhancement of the optical continuum from the nucleus, no such change is expected of the emission from the host galaxy.

Table 6.2 Values of R and L_{nucl}/L_{gxy}

Source	Redshift	R_{obsd}	L_{nucl}/L_{gxy}
0007+106	0.09	2.4	2.6
0241+622	0.04	30	8.4
0607-157	0.32	0.6	> 33.0
0742+318	0.46	2.0	> 30.0
0752+258	0.45	3.9	7.0
0846+100	0.37	0.04	5.5
0851+202	0.31	7.3	> 23.0
0957+227	0.10	0.01	3.2
1011-282	0.25	0.2	13.0
1020-103	0.20	5.5	23.0
1203+011	0.10	10	> 5.9
1254-333	0.19	0.03	1.5
1302-102	0.29	8.8	4.7
1400+162	0.24	0.5	3.7
1425+267	0.37	0.7	1.0
1510-089	0.36	66	11.2
1525+227	0.25	0.4	6.4
1641+399	0.60	258	39.0
1704+608	0.37	0.3	4.0
1725+044	0.29	1.4	2.0
2135-147	0.20	0.1	3.7
2141+175	0.21	1.3	4.6
2201+315	0.30	1.9	3.3
2217+08N	0.62	0.9	0.1
2217+08S	0.22	0.1	0.2
2247+140	0.24	1.4	3.0
2305+187	0.31	0.2	0.2
2318+049	0.63	3.0	5.8

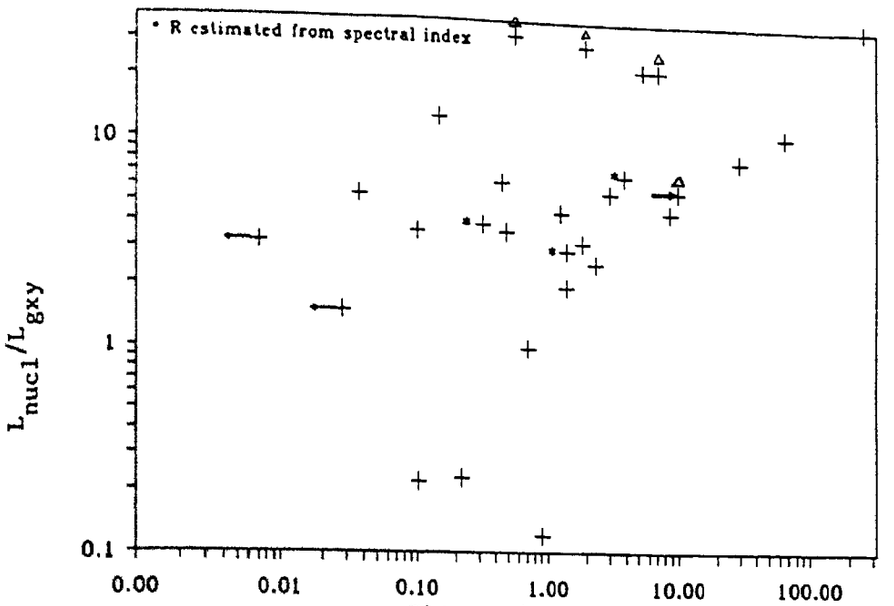

6.4.3 A caveat

It is important to point out here that there is some evidence that the host galaxies of quasars with steep radio spectrum emit O[III] lines of higher equivalent width than do the hosts of quasars with flat radio spectrum. Boroson & Oke (1984) found this on comparing data for three radio-loud quasars of flat radio spectrum with five of steep radio spectrum. Boroson *et al.* (1985) claim an analogous result. Among 10 radio-loud quasars in their list, four out of five with steep radio spectrum have large equivalent widths (i.e., > 23Å) of the O[III] emission line from the host galaxy, while only two out of five of those with flat radio spectrum do so. Stockton & MacKenty (1987) imaged several quasars in the narrow (30 Å) O[III] band, and detected extended O[III] emission from the host galaxy in 10 out of 26 quasars with steep radio spectrum, but only in 1 out of 7 quasars with flat radio spectrum.

The O[III] emission line would be redshifted into the R pass-band for $0.25 \lesssim z \lesssim 0.5$. Therefore, if host galaxies of flat radio spectrum are indeed under-luminous in O[III] emission, then the correlation of L_{nucl}/L_{gxy} with R could be a consequence of the smaller amount of radiation from the host galaxy in CDQs, rather than due to a relatively more luminous nucleus. More importantly, the fact that the host galaxies of quasars with small and large values of $R_{observed}$ may differ in the amounts of line emission that they radiate *would be a severe embarrassment to the unified scheme*, because it means that they are *intrinsically* different kinds of object. It is therefore very important to investigate this result with more systematic observations.

Along these lines, Smith *et al.* (1986) attempted an extensive study of the quasar host galaxies by putting together data from several optical imaging studies and their own. Assuming that data from different observing programmes can be combined if obtained through linear (rather than photographic) detectors (e.g., Gehren *et al.*, 1984) , they have confined their analysis to observations that have used linear detectors (CCD or SIT Vidicon). They obtain a sample of 86 quasars and their host galaxies, including 37 radio-loud quasars. But, in deriving the absolute magnitudes of the host galaxies in the sample, they correct for possible O[III] emission (on the basis of the result of Boroson *et al.* (1985) and using average values from the latter) for the categories of steep radio spectrum, flat radio spectrum, and radio-quiet quasars. While it is not clear that this is the correct procedure to adopt (since the number of objects in the Boroson *et al.* (1985) study is meagre), the corrected values do not show a significant correlation with radio

spectral index.

Since CDQs of apparent radio luminosity comparable to LDQs are intrinsically much less luminous than the latter (cf. section 6.1.2), if one wishes to compare an aspect-independent parameter with a view to confront the unified scheme, then one must chose for the comparison CDQs and LDQs that are *predicted to be intrinsically similar* by the scheme. The observed correlation of O[III] luminosity with radio spectrum may, for example, be simply because more (intrinsically) radio luminous objects are more "O[III] luminous". Further, CSS quasars should be excluded from the comparison, because the unified interpretation does not apply to them. Clearly, the question has to be investigated carefully.

6.4.4 Beaming in optically/x–ray selected quasars—some speculations

Hutchings & Gower (1985) have used the behaviour of the L_{nucl}/L_{gxy} parameter to draw inferences about relativistic beaming in quasars. They have observed 41 of the optically/x–ray selected quasars from the sample of Hutchings *et al.* (1984) at 5 GHz with the VLA A-array. Those that they detect up to a limiting flux density of $\lesssim$ 1 mJy are of markedly higher optical luminosities and L_{nucl}/L_{gxy} values than those that they do not. They conclude that these findings are consistent with the optical and radio nuclear emission being Doppler beamed. They then state that "the luminous, often large, classical [radio-loud quasars] are probably more nearly isotropic emitters".

However, this does not really follow from the correlation of radio flux density with L_{nucl}/L_{gxy} for the non-radio-loud quasars. The correlation may be understood

in the framework of the following unified phenomenology. There are broadly two populations of quasars (e.g., Peacock *et al.*, 1986.): the first consisting of radio-powerful CDQs and LDQs (that reside in elliptical hosts), and the second consisting of radio–quiet quasars (that probably reside in spiral hosts). In the case of the first population, the nuclear emission is relativistically beamed, and the CDQs are the objects oriented close to the line of sight, while LDQs are oriented close to the plane of the sky.

The radio-quiet quasars have their *total* radio emission relativistically beamed. The apparently stronger radio sources are thus close to the line of sight, and the really "radio-silent" ones (e.g., Kellermann *et al.*, 1986) are close to the plane of the sky. In other words, a relativistic beaming model akin to that of Scheuer & Readhead (1979) would apply. Indeed, the numbers of these sources increase with decreasing radio flux density in a manner that is roughly consistent with this model (Kellermann *et al.*, 1986). Thus, the extended radio structures in radio-quiet quasars are probably intrinsically small, and are intrinsically weaker versions of those seen in the radio–loud population. It is plausible that the Lorentz factors in the central components of radio-quiet quasars do not differ very significantly from those in their extensions (which are of the size of only a few kiloparsecs), because they are very close to the central component and have not decelerated significantly. The unified scheme of Orr & Browne (1982) would then not apply, because in this scheme, it is assumed that bulk relativistic motion occurs to a far higher degree in the nucleus than in the extensions. If the (relativistic) speeds are similar in the nuclear and outer components, then the parameter R would no longer be a measure

of the angle of inclination to the line of sight. It is then no surprise that Kellermann *et al.* (1986) do not find a correlation of fraction of the radio core with total radio flux density S, for their sample (of quasars of the second population) with $S < 100$ mJy.

The curvatures observed by Gower & Hutchings (1985) in the extended radio structures, as well as their apparent one–sidedness might well be a consequence of small inclination angles and beaming effects. However, it is probably not meaningful to compare the observed projected linear sizes of optically detected QSOs with those of the radio–powerful quasars within single beaming model, since the difference in sizes is likely to be intrinsic.

6.5 Large-scale bulk relativistic motion and the optical continuum

So far in this chapter, the discussion on bulk relativistic motion has been confined to regions near the nucleus. However, evidence was presented in Chapter 4 in support of the conjecture that the radio emitting effluents continue to move at speeds that are mildly relativistic out to lengths of a few hundred kiloparsecs. This question of large-scale bulk relativistic motion in relation to the behaviour of the optical continuum from the nucleus (which appears to exhibit anisotropic characteristics as discussed in the previous pages) is considered in this section.

6.5.1 Quasars with detected jets–are they optically brighter?

If there is bulk relativistic motion on a large scale in quasars, then large-scale jets that are pointed towards the observer would have their flux density Doppler boosted, and would thereby be more easily detectable than those jets that are

directed closer to the plane of the sky. This question was discussed in relation to other parameters of the radio structure that depend on orientation to the line of sight by Saikia (1984b). It was shown there that radio jets occur more frequently in quasars with relatively larger values of R. This was taken to suggest that the detected jets are generally directed at relatively small angles to the line of sight. Since it appears that the optical continuum is also apparently enhanced when the axis of the radio structure is inclined close to the line of sight (section 6.1), it is natural to ask if large-scale jets are more easily detectable in apparently brighter quasars. This has been done for a sample of well-imaged quasars, and is described in the following subsections.

6.5.2 Description of the sample

To decide if a quasar shows a detectable jet at the sensitivity limits of a given radio image, it is important to have an image of adequate resolution that delineates the elongated jet feature from the nuclear component and the extended lobes. In attempting to compile a sample rigorously, one encounters the expected problem: complete samples of radio quasars, with all the objects imaged with adequate resolution to a uniform sensitivity limit at radio wavelengths, are not available. Therefore, the question has been asked here for the best available eclectic set. A significant number of the radio images of quasars presented in Chapter 3 are adequate for the present purpose. To these have been added data on quasars from the literature for which radio images of the required resolution are available.

The selection criteria that were applied while choosing the sample are as follows. To have the sample homogeneous to the extent of being defined to a

uniform radio flux density limit, the list has been confined to objects with radio flux density at 178MHz > 2Jy. As is customary, narrow elongated structures that are approximately three times longer than they are wide, and pointing to the nucleus at the point closest to it are regarded as jets. The compilation is confined to radio images with at least 10 synthesized beam elements across the elongation of the source so as to have sufficient resolution to delineate a jet structure. Most of the images have been made with the VLA.

The sample has a total of 88 objects; they are listed in Table 6.3, which is arranged as follows. Column 1 lists the name of the quasar. Column 2 indicates whether or not the radio image shows a jet. 'Possibly' in this column indicates that although an elongated structure that is actually three times longer than its width is not manifest, the image suggests that the source is very likely to show a jet at higher angular resolutions. The subsequent columns in the table list the redshift, the apparent V magnitude (as given by Hewitt & Burbidge, 1987), and a code of reference to the radio image. The codes and the corresponding references are listed in Table 6.4.

6.5.3 The distributions of apparent optical magnitudes

The sample has been split into objects that have detected jets and those that have not. The distributions of apparent optical magnitudes for the two categories are shown in Figs 6.6a and b. The distributions show that there is a considerably larger number of optically brighter objects among the quasars with detected large-scale radio jets, than among those which show no jets. This trend is to be expected if, on the one hand, enhancement of the observed optical continuum accompanies bulk

Table 6.3 Detectability of jets and optical magnitudes

Source	Jet detected?	Redshift	Optical Magnitude	Reference
0017+257	possibly	0.284	15.4	HUO
0017+154	YES	2.012	18.2	SSS
0041+119		0.228	19.0	HUO
0109+176	YES	2.157	18.0	Bar
0115+027	YES	0.672	17.5	present
0118+034		0.765	18.1	HUO;SSH
0133+207		0.425	18.1	SSH
0137+012	possibly	0.260	17.1	HUO
0225-014	possibly	2.037	18.2	Bar
0229+341		1.238	19.0	SSH
0312-034		1.072	18.3	SSH
0353+123	possibly	1.616	19.3	Bar
0404+177		1.712	19.2	Bar
0405-123	YES	0.574	14.8	RR
0723+679	YES	0.846	18.0	OP
0726+431		1.072	18.5	HUO
0730+257		2.686	20.0	Bar
0742+318	YES	0.462	16.0	NB
0802+103	YES	1.956	18.4	Bar
0805+046	possibly	2.877	18.2	Bar
0805+578		0.438	19.0	HUO
0812+020	YES	0.402	17.1	Wyck
0835+580		1.534	17.6	SSH
0836+195		1.691	17.6	Bar
0903+169	YES	0.411	18.3	SSH;HUO
0919+218	YES	1.421	18.5	present
0922+149		0.896	18.0	SSH
0926+117		1.754	19.1	Bar
0932+022		0.659	17.4	present;SSH
0957+003	YES	0.907	17.6	HUO;SSH
1004+130	YES	0.241	15.2	F81;MH
1007+417	YES	0.613	16.5	present;OP
1012+232	possibly	0.565	17.5	present
1012+488		0.385	19.0	HUO
1023+067		1.699	18.5	Bar
1040+123	YES	1.029	17.3	present
1100+772	YES	0.311	15.7	SSH;LM
1103-006	possibly	0.426	16.5	HUO
1104+167	YES	0.634	15.7	HUO
1111+408		0.734	18.0	SKN

Table 6.3 (contd.)

Source	Jet detected?	Redshift	Optical Magnitude	Reference
1118+128		0.685	18.0	HUO
1132+303	possibly	0.614	18.2	present
1136-135		0.557	16.1	present
1137+660		0.646	16.3	SSH
1150+497	YES	0.334	16.1	OP
1206+439		1.400	18.4	SKN;LM
1218+339	possibly	1.519	18.6	SBC
1221+186		1.401	18.7	SSH
1222+216	YES	0.435	17.5	present;HUO
1241+166	YES	0.557	19.0	SBC
1244+324	possibly	0.949	17.2	SSH
1248+305		1.061	17.5	SSH
1253-055	YES	0.538	17.8	dPP
1258+404	YES	1.659	19.4	SSS
1305+069		0.602	17.0	SSH
1308+182	YES	1.677	17.5	Bar
1317+520	YES	1.060	17.0	HUO;OP
1323+655		1.618	17.8	Bar
1345+584	YES	2.039	17.5	Bar
1354+195	YES	0.720	16.0	present;RR
1433+177	YES	1.203	18.2	present
1509+158	YES	0.828	18.2	present
1510-089	YES	0.361	16.5	OBC
1540+180	YES	1.662	18.0	Bar
1545+210		0.264	16.7	SSH
1548+114	YES	0.436	17.2	HUO
1602-001		1.625	17.5	Bar
1606+289		1.989	19.0	SSH
1618+177	YES	0.555	16.4	HUO
1620+356		1.473	18.5	HUO
1622+238		0.927	17.5	SSH
1623+173		0.552	19.0	HUO
1628+363	possibly	1.254	17.0	HUO
1704+608		0.371	15.3	SSH
1732+160		1.880	18.4	Bar
1739+184		0.186	16.4	SSH;HUO
1741+279	YES	0.372	17.7	present
1816+475	YES	2.225	18.2	Bar
1819+228		0.628	18.0	HUO
1830+285	possibly	0.594	17.2	HUO

Table 6.3 (contd.)

Source	Jet detected?	Redshift	Optical Magnitude	Reference
1857+566	YES	1.595	17.3	S83;Bar
1928+738	possibly	0.302	16.5	RR
1954+513		1.220	18.5	OBC
2131+175		1.215	19.3	SSH
2150+053		1.979	17.8	Bar
2201+315	YES	0.297	15.5	NB
2248+192	YES	1.806	18.5	Bar
2305+187	YES	0.313	17.5	GH
2325+269		0.875	17.5	present
2325+293		1.015	17.3	SSH
2349+327	YES	0.659	19.9	PW
2354+144		1.810	18.2	Bar

Table 6.4 Radio jets in quasars: list of references

Bar	Barthel (1984)
dPP	de Pater & Perley (1983)
F81	Fomalont (1981)
GH	Gower & Hutchings (1984)
HUO	Hintzen et al. (1983)
LM	Lonsdale & Morrison (1983)
MH	Miley & Hartsuijker (1978)
NB	Neff & Brown (1984)
OBC	O'dea et al. (1988)
OP	Owen & Puschell (1984)
present	Chapter 3, this thesis
PW	Potash & Wardle (1980)
RR	Rusk & Rusk (1986)
S83	Saikia et al. (1983)
SKP	Saikia et al. (1986)
SKN	Schilizzi et al. (1982)
SBC	Stocke et al. (1985)
SSH	Swarup et al. (1984)
SSS	Swarup et al. (1982)
Wyck	Wyckoff et al. (1983)

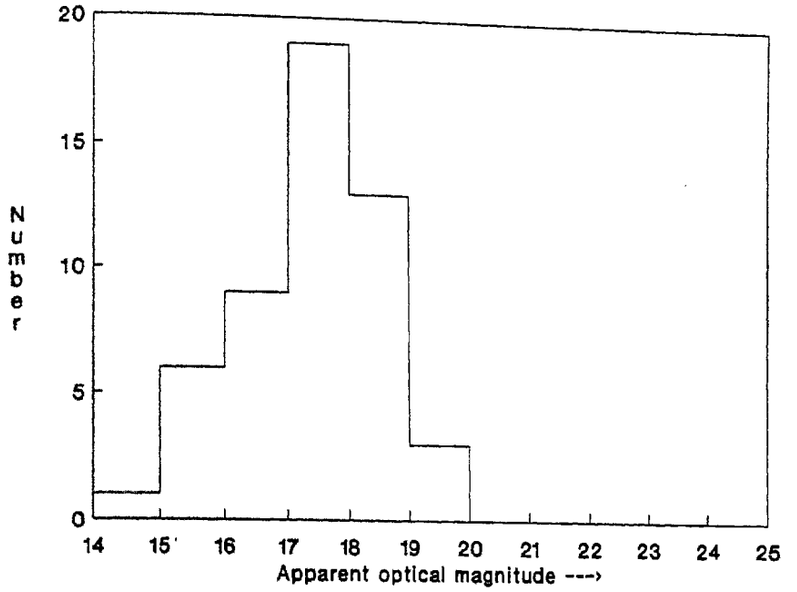

(a) Quasars with jets

Fig.6.6 Distribution of apparent optical magnitude

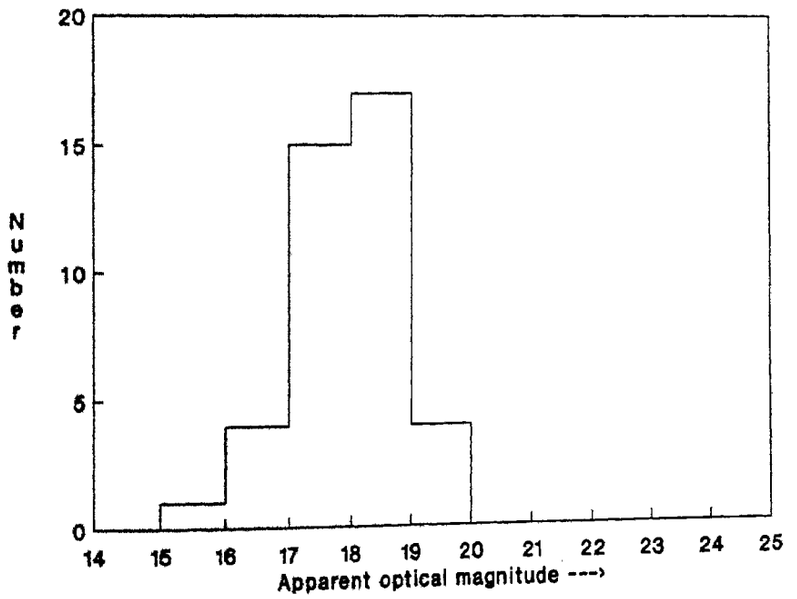

(b). Quasars without detected jets

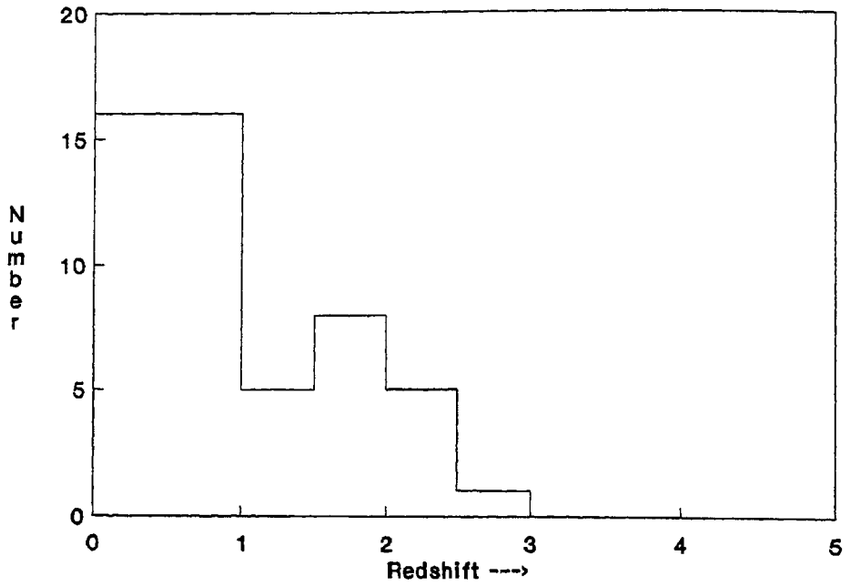

(a) Quasars with jets

Fig.6.7 Distribution of redshift

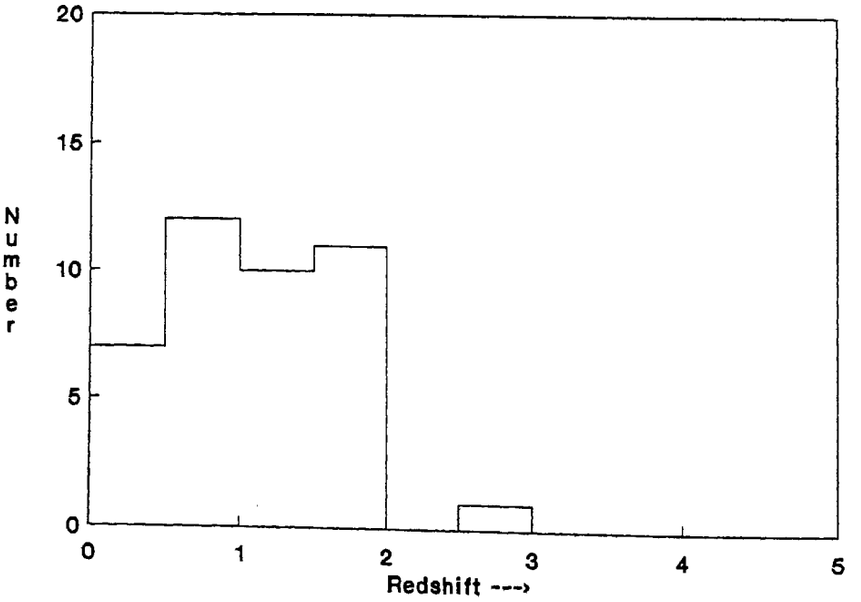

(b) Quasars without jets

relativistic motion in the nucleus, and, on the other hand, relativistic motion on a large scale also occurs. While the trend is not a very strong one, it is interesting that there is any trend at all, given that a good correlation would require alignment of structures ranging from subparsec scales to hundreds of kiloparsecs.

A possible selection effect that might lead to a spurious trend of this sort is related to the fact that surface brightness (at radio wavelengths in this case) diminishes at a very rapid rate with cosmological redshift. If the quasars that do not show the presence of a jet are also those that are at systematically higher redshifts and therefore more distant, they might also appear to have a fainter optical continuum. The redshift distributions for the two categories of quasars with and without jets (Figs. 6.7a and b) show, however, that the quasars with detected jets are not at systematically lower redshifts.

6.6 Causes of optical aspect dependence—relativistic beaming or thin disc?

Both relativistic beaming of the optical continuum (Browne & Wright, 1985) and inclination effects of an optically thick geometrically thin disc (Netzer, 1985) have been suggested as possible causes for the aspect dependence of the optical continuum. In the first case, the relativistically beamed optical and radio emission come from the same physical region, and the effect of an "optical bias" on the distribution of R should be of the same kind as that of a "radio bias" that favours orientations close to the line of sight. Since relativistic beaming effects increase steeply for small orientation angles of the radio axis with the line of sight, the orientation bias due to optical beaming (as in samples at increasingly higher frequencies) is expected to show up at the high–R end (viz., $R \gtrsim 10$) of the R-

distribution (Fig. 2 in Orr & Browne, 1982). Indeed, Fig.6.1 shows an excess of quasars with large values of R. But the distribution also differs from the prediction of Orr & Browne (1982) (which was quantified using the 3CR quasars) at low to intermediate values of R (i.e., $R \lesssim 10$), as mentioned in section 6.1.1. This suggests that the functional dependence of the optical emission on inclination angle may be very different from that of relativistically beamed radio emission.

The shift in the peak of the R-distribution relative to that predicted seems to be consistent with the "thin disc interpretation" for the optical continuum. For such a disc, the most rapid change in optical flux would be expected when the disc (and hence the radio axis) makes fairly large angles with the line of sight (because the apparent optical flux density would vary as the cosine of this angle). The consequent beaming effects at radio wavelengths are therefore expected to influence mainly the low end of the R-distribution. The data described here thus clearly indicate that the optical continuum seems to consist of at least two aspect dependent components: one that is relativistically beamed synchrotron radiation, and the other that is thermal radiation from an optically thick but geometrically thin disc.

Further, the possibility that dust around quasar nuclei may not be distributed isotropically (Netzer, 1987; Thompson *et al.*, 1988) would imply that aspect-dependent obscuration would add to the aspect-dependence of the optical continuum.

It may be added that the result of Hutchings & Gower (1985) (Section 6.4.4) does seem to imply that the radio beaming is accompanied by enhancement of the optical continuum in radio-quiet quasars also. This enhancement could be either due to relativistic beaming *or due to orientation effects of a disc* (as described in section

6.8). The latter is more likely, since given that the radio emission is itself weak, it is improbable that a large amount of jetted synchrotron emission is emitted at optical wavelengths. In fact, violent optical variability, believed to be a sign of relativistically beamed optical emission, is almost unknown radio-quiet quasars.

6.7 Implications of optical aspect dependence

It is generally implicit in investigations of the properties of quasars that the optical continuum from the nucleus is isotropic. Its possible aspect dependence, therefore, has several implications, some of which are discussed below.

6.7.1 Selection effects in low-frequency samples of radio quasars

To reiterate the assertion made in sections 6.1 and 6.2 for the Bologna quasars, *samples of quasars selected at low radio frequencies would necessarily be biased with respect to orientation unless optical identifications for the whole radio survey are complete.* Further, if a thermally emitting, opaque and thin disc present in radio-quiet quasars also (section 6.4.4), then samples selected to be brighter than a certain apparent optical magnitude might also be biased with respect to orientation.

6.7.2 The degree of enhancement of the optical continuum

If the entire difference in the apparent magnitude distributions shown in Fig. 6.3 arises from orientation effects, the figures suggest that the enhancement of the optical continuum can typically be as high as two or three magnitudes for the Bologna quasars, somewhat larger than was suggested by Browne & Wright (1985). But it is possible that they may have underestimated the effect for the following

reason. In comparing the magnitudes of CDQs and LDQs, they have *assumed* (particularly at low flux density levels) that *all* the quasars in the samples selected at 408 MHz (including the Bologna sample) are lobe-dominated. But the examples of the Bologna quasars and those from the samples of Wills & Lynds (1978) show that a substantial fraction from amongst them may turn out to be core-dominated when observed at high radio frequencies. If such (optically bright) objects are removed from the their set of LDQs selected at 408 MHz, a larger difference in the apparent magnitudes of CDQs and LDQs would result.

6.7.3 The luminosity-volume test

The luminosity-volume test (Kafka, 1967; Schmidt, 1968) is a powerful technique to statistically extract cosmological information from samples of objects whose redshifts are known. The test requires that the sample be strictly complete to some limiting flux density. (It does not require, however, that the spread in the intrinsic luminosity be narrow.) The test is applied as follows. For every object, the volume of space out to its redshift is determined in comoving coordinates in some given cosmological model. From its derived luminosity, the maximum redshift which the object could be at and still appear bright enough to be visible above the limiting flux density of the sample is computed, and thereby V_{max}, the volume of space corresponding to this cosmological distance, is calculated. If the cosmology assumed is a good approximation and if the objects in the sample are uniformly distributed in space, then it is expected that half the number of objects would be found with $V < 0.5\ V_{max}$, and the other half with $V > 0.5\ V_{max}$. The mean value of V/V_{max} for the entire sample must be 0.5. As it turns out, the exercise is not

very sensitive to the exact values of H_0 and q_0 used. Thus, if $\langle V/V_{max} \rangle$ exceeds 0.5, that is a demonstration that one is seeing more objects from further out.

The study by Masson & Wall (1977) of the Parkes sample of quasars selected at 2.7 GHz in the strip of sky of ± 4° declination gave a lower value of $\langle V/V_{max} \rangle$ for the quasars with flat radio spectrum than for those with steep radio spectrum (0.52 ± 0.05 as opposed to 0.67 ± 0.05). The result led them to suggest that in the case of radio quasars, cosmological evolution was confined to sources with extended radio structures, while compact objects consisting only of components of high surface brightness have a uniform spatial distribution. Wills & Lynds (1978) also obtained a lower value of $\langle V/V_{max} \rangle$ for flat spectrum objects than for those with steep spectrum, for complete samples of quasars selected at 178 MHz.

But the difference in the value of $\langle V/V_{max} \rangle$ for quasars with flat and steep radio spectrum is entirely consistent with the difference in their respective distributions of apparent optical magnitude. If the latter is just an orientation effect as has been argued in the previous sections, then the mere fact of a lower value of $\langle V/V_{max} \rangle$ is not necessarily evidence that the quasars of flat radio spectrum evolve to a lesser degree than their steep spectrum counterparts. Indeed, in the unified scheme of Orr & Browne (1982), since the quasars with flat and steep spectrum are intrinsically similar objects, one would not in general expect them to have differing evolutionary properties.

However, by the unified scheme, in a given radio flux density limited complete sample, the quasars of flat radio spectrum have a lower intrinsic luminosity than those of steep radio spectrum, because in the former case the apparent luminosity

would be enhanced by Doppler boosting of the core flux density. And therefore, if there is luminosity dependent density evolution, the flat spectrum objects could show lower evolution in comparison. For instance, Peacock *et al.* (1981), using a sample of higher limiting flux density than the samples of Masson & Wall (1977) and Wills & Lynds (1978), have shown that flat radio spectrum quasars do yield a value of V/V_{max} comparable to the corresponding values for steep radio spectrum quasars in the latter samples. More recently, Morisawa & Takahara (1987) have shown that the source counts and redshift distributions of steep and flat spectrum quasars are consistent with the predictions of the unified scheme.

6.7.4 The Hubble diagram for quasars

In this section, the implications of aspect-dependence of the optical continuum for the Hubble diagram of quasars is examined.

For a homogeneous and isotropic expanding universe, assuming a value of 1 for the deceleration parameter q_0, and a value of 50 km s^{-1} Mpc^{-1} for Hubble's constant H_0,

$$\log cz = 0.2\ m_v + B,$$

where

$$B = \frac{-M_v + 5\ \log H_0 - 25}{5},$$

M_v is the absolute magnitude, and the unit distance is 1 Mpc.

Thus, for a given class of extragalactic objects, if it is assumed that the luminosity function is narrow, and that the measured redshift of an object is (almost) wholly of cosmological origin, the Hubble diagram, i.e., a plot of (the

logarithm of) the redshift against the apparent magnitude, is expected to have a slope of 0.2. Since quasars are the most distant objects known, with the largest redshifts, the Hubble diagram of quasars is an important correlation.

The early work of Lang *et al.* (1975) showed that the Hubble plot for all of the then known quasars was compatible, within errors, with the theoretically expected value of 0.2, just as that for the normal and radio galaxies was. Of course, while almost all of the observed brightness of normal and radio galaxies in the visible wavelength region is due to their stellar emission, in quasars, it is due to the non-stellar emission from the active galactic nucleus, with thermal and non-thermal components of currently uncertain relative magnitudes.

Setti & Woltjer (1973) studied the Hubble diagram for *radio* quasars, separating them by their radio spectral index. They found that the quasars with steep spectrum showed a significant Hubble relation, though with much dispersion, and that those with flat spectrum showed an almost pure scatter diagram. The latter result, they concluded, was probably due to the broader luminosity function of the flat spectrum objects. Their result is roughly consistent with the conclusion of Netzer *et al.* (1978), viz., quasars with flat *optical* spectrum show a better Hubble correlation than those with steep *optical* spectrum. (Presumably, quasars with steep *optical* spectrum are those with flat *radio* spectrum and vice versa in the case of the radio-loud quasars (e.g., Wills & Wills, 1986). Notably though, about 50 per cent of the quasars in Netzer *et al.* (1978) were radio-quiet.)

The result of Setti & Woltjer (1973) is clearly relevant to the unified scheme, since in that framework, differences between the two classes of quasar are due to

orientation effects alone. Two questions arise:

(a) Is the result of Setti & Woltjer (1973) borne out by the data that are available for the much larger number of quasars now known?

(b) If so, then can the result be understood as being due to orientation effects alone?

The answer to question (a) is in the affirmative. Fig. 6.8a and b show the Hubble plots for the radio quasars with steep and flat spectrum from the catalogue of Veron-Cetty & Veron (1987). The radio spectral indices listed in the catalogue have been used to classify the radio quasars into steep and flat spectrum categories. The V magnitudes listed in the catalogue have corrected for absorption by our Galaxy, and K-corrected, as follows:

$$m_v^{corrected} = m_v^{catalogue} - K - A_{Galaxy},$$

where, for an optical spectral index α^{opt},

$$K = -2.5\,(1+\alpha^{opt})\,\log(1+z),$$

and

$$A_{Galaxy} = \begin{cases} 0.099\,[csc(|b|)-1] & \text{for } |b|<50^\circ \\ 0 & \text{for } |b|>50^\circ \end{cases}$$

where b is the Galactic latitude (e.g., Lang *et al.*, 1975). The quasars with steep spectrum do show a better Hubble correlation than the ones with flat spectrum, a trend also reflected in the values of the least-squares fit and the absolute magnitude dispersion σ_M (listed in Table 6.5).

Question (b) can now be considered. The larger scatter in the Hubble diagram for quasars is easily understood if the relativistic beaming of the radio emission is accompanied by enhancement of the optical continuum. If a significant fraction of

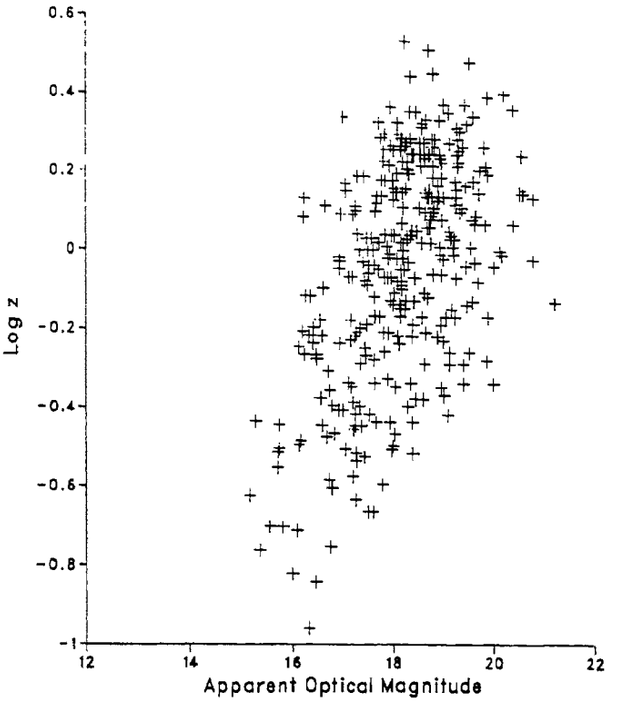

Fig. 6.8a. The Hubble Diagram
Quasars with Steep Radio Spectrum

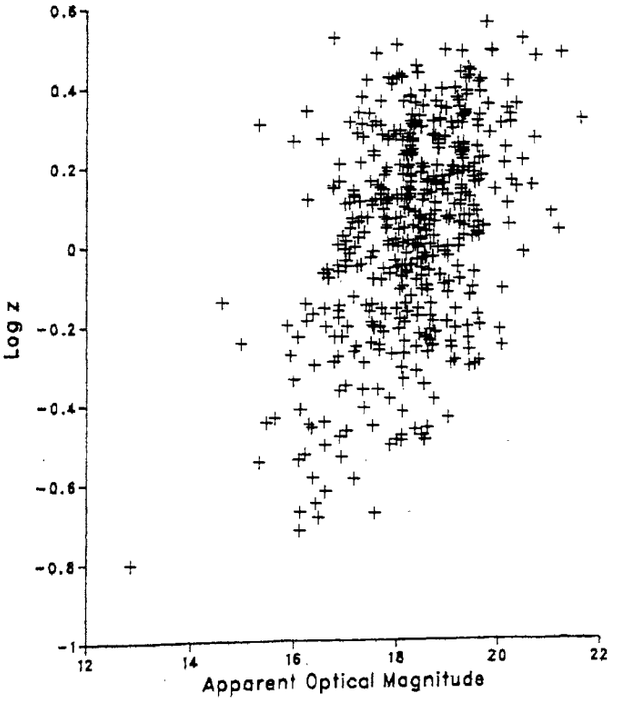

Fig. 6.8b. The Hubble Diagram
Quasars with Flat Radio Spectrum

Table 6.5 Parameters of the Hubble correlation

	Number of Objects	Slope: b	σ_b	Correlation Coeffecient (r)	Magnitude Dispersion (σ_M)
Steep Spectrum Quasars	340	0.14	0.012	0.53	1.72
Flat Spectrum Quasars	498	0.10	0.009	0.44	2.27
"Brightest" Steep Spectrum Quasars		0.23	0.037	0.85	0.85
"Brightest" Flat Spectrum Quasars		0.20	0.034	0.82	1.04

the optical emission is relativistically beamed, the luminosity function would be broadened (e.g., Urry & Shaffer, 1984), and would increase the magnitude dispersion of the Hubble diagram for the flat spectrum objects (besides the variability of the OVV quasars, which are flat radio spectrum objects). *Thus the difference in the two Hubble plots can indeed be qualitatively explained by orientation effects alone.* Further, since the aspect dependence of a thin-disc component of the optical continuum would be strongly manifest at source orientations close to the plane of the sky, it would follow that *the optical luminosity function of the steep radio spectrum sources would be broadened too,* thus contributing to scatter of the Hubble correlation.

For a set of extragalactic objects with a broad luminosity function, the brightest

object at each redshift should show a tighter Hubble correlation (Bahcall & Hills, 1973; McRea, 1972). This is illustrated below. Following the procedure of Bahcall & Hills (1973), the quasars were grouped into redshift bins of 15 objects each, and M_v was calculated according to

$$M_v = m_{corrected} - 5\log z - 43.88 \ .$$

m_v^{bin} for the most luminous quasar in each bin was derived as its apparent magnitude if placed at the average bin redshift, z_{avg}. Thus,

$$m_v^{bin} = M_v^{\min} + 5\log z_{avg} + 43.88 \ .$$

The correlations are indeed better (Figs. 6.8c & 6.8d; Table 6.5).

It should be kept in mind, however, that the Hubble plots presented here are approximate for several reasons:

(a) the catalogue of Veron-Cetty & Veron (1987) is a mere compilation, not "complete" in any sense, and unknown selection effects may therefore be present;

(b) the V magnitudes used are often photographic and therefore inaccurate, and have not been corrected for the emission line luminosities;

(c) the radio spectral index is a two-point value and not necessarily derived from simultaneous measurements;

(d) a universal optical spectral index has been used to derive the K-correction (on an average, the flat radio spectrum sources would have steeper optical spectra and vice versa; therefore the use of a universal value would tend to wash out some of the difference between the two classes);

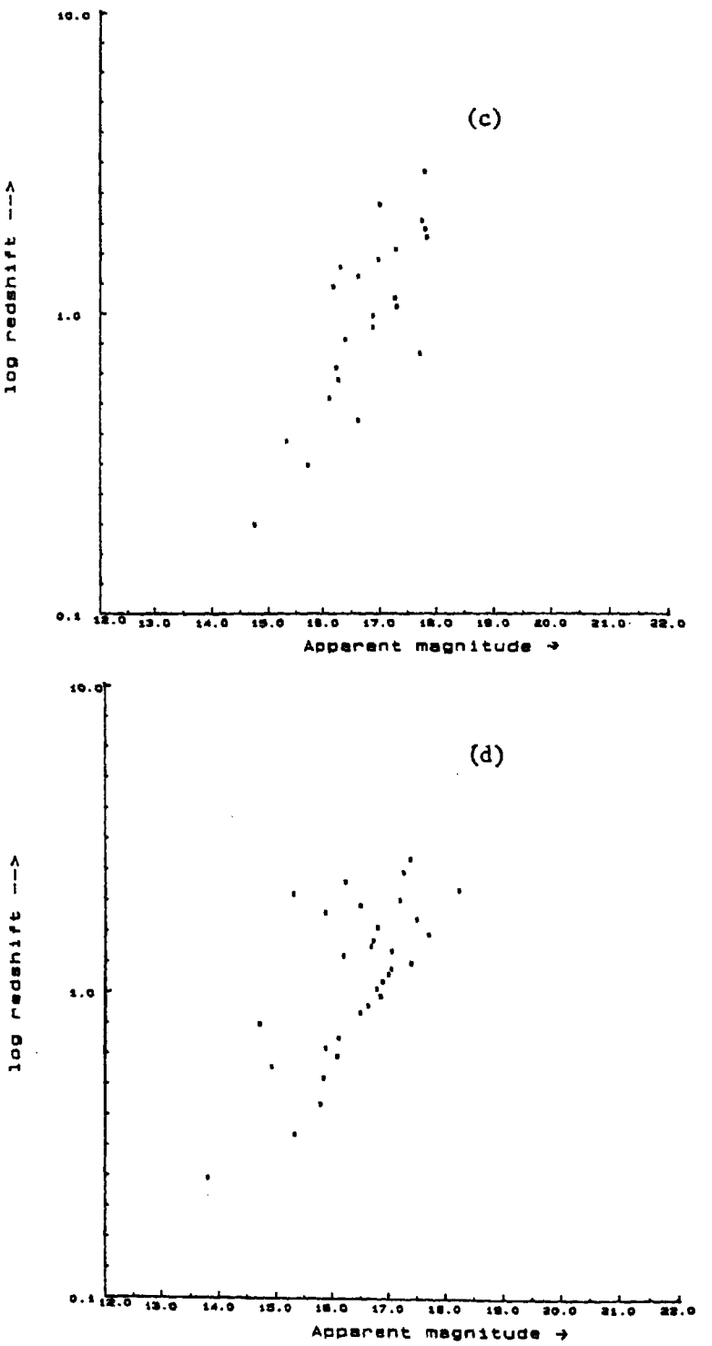

Fig. 6.8c & d. The Hubble diagram for the "brightest" steep and flat spectrum quasars respectively.

(e) the compact steep spectrum (CSS) sources should be considered separately, since they seem to belong to a different physical class, and do not partake in the unified scheme (cf. this thesis, section 4.3);

(f) the plot has not been corrected for the Malmquist bias, nor for the 'volume effect' (Kembhavi & Kulkarni, 1978).

6.7.5 The Baldwin effect

The equivalent width of the CIV emission line has been known to be inversely correlated with the luminosity of the optical continuum ("the Baldwin effect"; see, e.g., Wampler *et al.*, 1984). If a significant fraction of the optical continuum originates from an optically thick, geometrically thin disc, the Baldwin effect may immediately and naturally be explained. Netzer (1985) discusses the arguments in detail.

6.8 Summary

The apparent optical magnitudes of quasars from the Bologna sample show that if R is a statistical measure of the angle of inclination of the quasar to the line of sight, then *their optical continuum is aspect dependent.* The behaviour of the optical luminosity of the quasar nucleus to that of the host galaxy supports this proposition. There is a mild trend for large-scale radio jets to preferentially occur in optically brighter quasars, which is consistent with the suppositions that the jets are relativistically beamed and that the optical continuum is aspect dependent.

Both relativistic beaming and disc orientation effects are likely to play a significant role in causing optical aspect dependence.

Aspect dependence of the optical continuum can introduce a serious selection effect into samples of quasars selected from low-frequency surveys if all the survey objects are not optically identified. It follows that the degree of enhancement of the optical emission that is derived from comparing optical magnitudes of low- and high-frequency samples of radio quasars may be an underestimate.

Differences in the values of $\langle V/V_{max} \rangle$ that obtain for flat and steep radio spectrum quasars are consistent with the corresponding differences in their optical magnitudes. If the optical continuum is aspect dependent, then the different $\langle V/V_{max} \rangle$ values do not imply differing evolutionary properties for the two classes of radio quasars.

Orientation effects due to optical emission from a thin and opaque disc would increase the scatter in the Hubble diagram for quasars with steep radio spectrum, just as relativistic beaming of the optical continuum would increase the scatter in the Hubble diagram for quasars with flat radio spectrum.

While the unified interpretation of Blandford & Königl (1979) clearly cannot incorporate the radio-quiet quasars, a scheme akin to that of Scheuer & Readhead (1979) (wherein the total radio power is relativistically beamed) probably applies to them.

Chapter 7

THE RELATIVISTIC BEAMING HYPOTHESIS—ITS DOMAIN OF VALIDITY

In the introductory chapter, some of the successes of the relativistic beaming hypothesis and the unified interpretation that motivated this thesis were enumerated. Some further successes that were part of the thesis have been described in Chapters 4, 5 and 6. Clearly there is much appeal in the simplicity of the proposition, and it is important to examine its domain of validity. In this chapter, the evidence that has accumulated over the years in favour of the hypothesis, as also the counter-evidence, is summarized. Important disclaimers, possible future confrontations of the assumptions, and some speculations are enumerated.

7.1 Bulk relativistic motion in the nuclear regions of active galaxies

(a) Superluminal motion has been observed in about 23 radio sources (e.g., Zensus & Pearson, 1988), and provides the most direct evidence in support of bulk relativistic motion in the nuclear regions of these quasars. It is now widely accepted that the apparent speeds faster than light are due to bulk relativistic motion at small angles to the line of sight. Note that superluminal motion in the nuclei of quasars accounts for (though is not proven by) the almost universal one-sidedness of the nuclear radio jets detected by VLBI.

(b) From angular sizes of the nuclear radio components (measured using VLBI) and the observed limits to the x-ray flux density, lower limits to the relativistic Doppler

factors can be inferred, which imply bulk relativistic motion in several objects (Cohen, 1985).

(c) The severe problems that arise in the interpretation of the properties of BL Lacertids and Optically Violent Variables (viz., infrared luminosities in excess of the Eddington limit, the large magnetic fields required to prevent the (unobserved) excessive inverse Compton x-rays, etc.) are alleviated if it is assumed that bulk relativistic motion occurs in the nuclei of these objects (Impey, 1987).

(d) The form of the inverse correlation between measured internal proper motion of the superluminally moving components and redshift is consistent with the supposition that relativistic beaming is important in these objects (Cohen *et al.*, 1988).

7.2 Evidence for the unified interpretation

(a) High dynamic range radio imaging has shown that CDQs have outer components of similar nature to those of LDQs (Perley *et al.*, 1980; Browne *et al.*, 1982a).

(b) The prominence of the nuclear radio component of quasars inversely correlates with the projected linear size, and directly with the degree of misalignment of the radio structure away from collinearity (Kapahi & Saikia, 1982).

(c) The unified interpretation correctly predicts the proportions of flat and steep radio spectrum quasars in samples of radio sources selected at high radio frequencies (Orr & Browne, 1982). The Lorentz factors required are consistent with those derived from observed superluminal motion. The scheme also correctly

predicts the form of the source counts of quasars with flat radio spectrum (Orr & Browne, 1982).

(d) If the position angle of the polarization of the radio nuclear component is used to infer the orientation of the nuclear-scale structures, it follows that degree of misalignment between radio structures on the nuclear scale and those on the large scale correlates with R (this thesis, chapter 5).

(e) When looked for, superluminal motion is detected in almost every CDQ, supporting the hypothesis that they are inclined at small angles to the line of sight (e.g., the inventory in Porcas, 1987; Schalinski *et al.*, 1988).

(f) The superluminal speeds that have been detected in sources with extended double structure (e.g., Zensus & Porcas, 1986; Hough, 1986) only serve to emphasize the ubiquity of bulk relativistic motion in quasars. There are already suggestions of a correlation of the measured value of β_{apparent} with R where β is the ratio of the measured velocity to the velocity of light (Browne, 1987).

(g) The redshift distributions and source counts of quasars with steep and flat radio spectrum in high frequency radio surveys are consistent with the unified scheme of Orr & Browne (1982) (Kapahi & Kulkarni, 1986; Morisawa & Takahara, 1987).

(h) For steep and flat spectrum quasars that are intrinsically similar in the scheme of Orr & Browne (1982), the redshift distributions are similar (Kapahi & Kulkarni, private communication), implying that they occur in the same volume, as indeed would be expected in the unified scheme.

7.3 Evidence for relativistic motion in the kiloparsec-scale jets

(a) Both nuclear (VLBI-scale) jets and the larger kiloparsec-scale jets are mostly one-sided in quasars. In every quasar with a large scale jet, a nuclear jet, when looked for, has been found, and it always points towards the base of the large scale jet. This argues for a common cause of asymmetry on both scales. The case for "Doppler favouritism" in nuclear jets is compelling, and thus at least mild bulk relativistic motion must occur on the large scale too (Scheuer, 1987).

(b) The detectability of large scale jets appears to increase with the prominence of the radio nuclear component (Saikia, 1984b; Bridle, 1986).

(c) The kiloparsec-scale (one-sided) jets detected in the quasars from the D2 sample preferentially point towards the outer component with the brighter hot spot, which is consistent with bulk relativistic motion on a large scale and mild relativistic motion in the hot spots (this thesis, chapter 4).

(d) Quasars with relatively large surface brightness ratios for the outermost hot spots tend to have higher values of R, consistent with the contention that they are likely to be oriented closer to the line of sight (this thesis, chapter 4).

(e) High resolution dual-frequency polarimetry of 23 quasars has shown that the "jet side" of the nucleus of radio quasars depolarizes less rapidly with wavelength than the opposite side (Laing, 1988; Garrington *et al.*, 1988). The depolarization is almost certainly due to differential Faraday rotation, and does not correlate with the size or brightness of the components. In the case of the radio galaxy Cygnus A (Dreher *et al.*, 1987), the depolarization has been established as due to Faraday rotation by a foreground screen (as opposed to being internal). Extrapolating this

fact to the case of quasars implies that the "jet side" is seen through less of the foreground screen and is therefore the approaching side, which is consistent with the idea that the jets are relativistically beamed.

7.4 Aspect dependence at other emission wavelengths ?

If the relativistic beaming hypothesis and the unified interpretation are assumed to be valid, then consistency with the data demands that emission at other wavelengths is aspect dependent also. These cases are summarized below.

(a) The Highly optically Polarized Quasars (polarization > 3%) and BL Lacertids show a correlation between the prominence of the radio core component and the r.m.s. scatter in the optical polarization, implying that a significant fraction of the optical continuum is aspect-dependent (Wardle *et al.*, 1984). Further, this correlation would be expected if the emission is synchrotron radiation produced in a relativistic jet. The weak evidence for quasars with a "preferred position angle" of the optical polarization to exhibit relatively prominent extended radio structure is also consistent with this "optical relativistic jet" hypothesis (Wardle *et al.*, 1984; Blandford & Königl, 1979).

(b) Sets of quasars with steep radio spectrum that are chosen to be intrinsically similar (in the unified scheme of Orr & Browne, 1982) to those with flat radio spectrum appear optically fainter than the latter, which requires that the optical continuum be aspect dependent in the same sense as the radio emission is (Browne & Wright, 1985).

(c) The prominence of the radio nuclear component correlates with the apparent optical brightness of the nucleus (this thesis, chapter 6), consistent with the suggestion of Browne & Wright (1985) that the optical continuum may be aspect dependent.

(d) The ratio of the optical luminosity of the nucleus to that of the host galaxy in radio quasars correlates with the prominence of the nuclear radio component (this thesis, chapter 6), again supporting the above.

(e) The Baldwin effect (anti-correlation of equivalent width of the CIV emission line with optical continuum luminosity) may be understood if the optical continuum is assumed to arise from a thin and opaque disc (Netzer, 1985).

(f) The widths of the broad emission lines in quasars inversely correlate with R (Wills & Browne, 1986; Wills & Wills, 1986). This can be understood if the motion of the gas emitting the lines is confined to a plane perpendicular to the radio ejection axis, perhaps in the form of a disc.

(g) The degree of optical polarization of quasars correlates with R, which can be understood if the optical emission is of synchrotron origin and is relativistically beamed (Wills *et al.*, 1988).

(h) The equivalent width of the narrow O[III]5007 emission line and broad MgII line inversely correlates with R. This can be understood if the optical continuum is aspect dependent and the luminosity of the emission line is independent of aspect (Wills & Browne, 1986; Browne & Murphy, 1987).

(i) The rest equivalent width of the CIV absorption doublets observed within $\pm$ 5000 km s^{-1} of the emission line redshift inversely correlates with both the

flatness of the radio spectrum and the optical luminosity (Foltz *et al.*, 1987). The above result suggests that firstly, the absorbing clouds are within the host galaxy of the quasar (as opposed to being associated with the cluster containing the quasar, cf. Foltz *et al.*, 1987) since the anti-correlation is with an intrinsic property of the quasar, viz., R. Secondly, the anti-correlations, if interpreted in the relativistic beaming scenario, suggest that the distribution of the absorbing clouds is not isotropic about the nucleus of the quasar, but lie preferentially along a plane perpendicular to the radio axis.

(j) The curve correlating the x-ray luminosity with nuclear radio luminosity is steeper for CDQs than for LDQs. This is consistent with the suggestion that part of the x-ray emission is aspect-dependent (Browne & Murphy, 1987).

(k) From soft x-ray (2-3.5 keV) spectra of 33 quasars observed on-axis with the IPC of the Einstein satellite, Wilkes & Elvis (1987) have reported a correlation between the flatness of the x-ray spectral index and radio loudness. The attempt to reconcile their results with the earlier HEAO 1(2-10 keV) results led them to conclude that in all quasars is present a x-ray component that obeys a flat power law, and that this component preferentially dominates radio loud quasars above ~0.5keV.

It turns out that for the set of 18 radio quasars from Wilkes & Elvis (1987), the CDQs tend to have systematically flatter soft x-ray spectral indices than the LDQs. (Fig. 7.1 shows the distribution of soft x-ray spectral index, α_E for the radio loud quasars from the sample bifurcated at R = 0.5.) It is thus suggested that there is marginal evidence for the flat x-ray component being aspect-dependent.

7.5 Disclaimers

(a) Radio-quiet quasars are probably a physically different population from the radio-loud ones (Peacock *et al.*, 1986) and tend not to inhabit elliptical galaxies the way the latter do (e.g., Fried, 1986). Thus they clearly cannot be co-opted into the unified interpretation of Blandford & Königl (1979) for radio loud quasars. Further, it is unlikely that this unified interpretation applies to them as an independent class. However, perhaps a unified scheme akin to that of Scheuer & Readhead (1979) is valid, wherein the total radio power (as opposed to primarily the nuclear power) is relativistically beamed, and the objects inclined close to the line of sight are the really "radio silent" quasars (this thesis, Section 6.9.4).

To the extent that the two populations of quasars *do* share some common properties at optical, ultraviolet and infrared wavelengths, it is to be expected that radio-quiet quasars would *appear* similar to CDQs in some respects. Several of the properties of radio-quiet quasars are better studied for the brighter objects, and, given that the optical nuclei of radio-quiet quasars are similar to the radio loud ones, this bias implies a selection effect in favour of more face-on nuclear discs. For instance, radio quiet quasars resemble CDQs both in their Broad Emission Lines (Heckman, 1980; Steiner, 1981), and in Broad Absorption Line properties (e.g., Foltz *et al.*, 1987).

(b) Compact Steep Spectrum quasars are probably seats of intense interaction of the radio jets with the interstellar medium of the host galaxy (van Breugel *et al.*, 1984a; van Breugel *et al.*, 1988). While their radio nuclei are often prominent (this thesis, chapter 4), VLBI mapping has shown that the nuclei exhibit complex

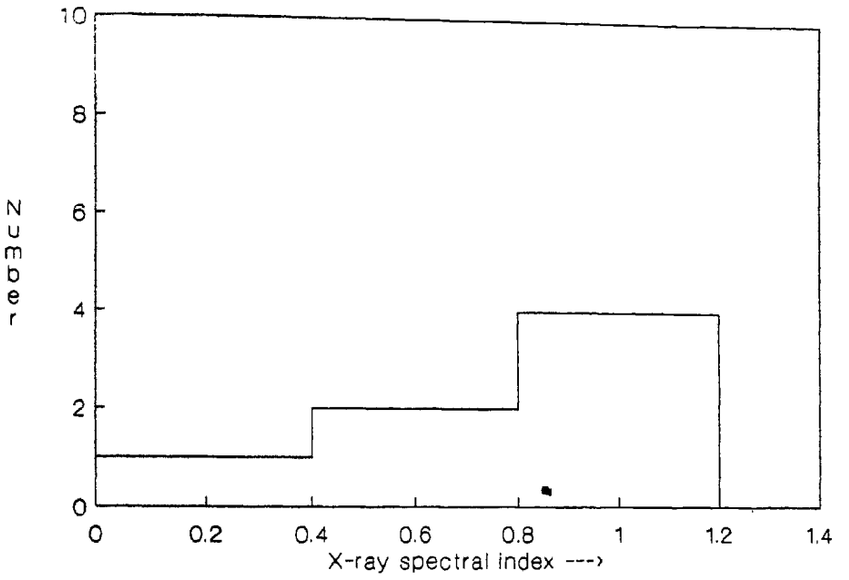

Fig.7.1a Quasars with R < 0.5

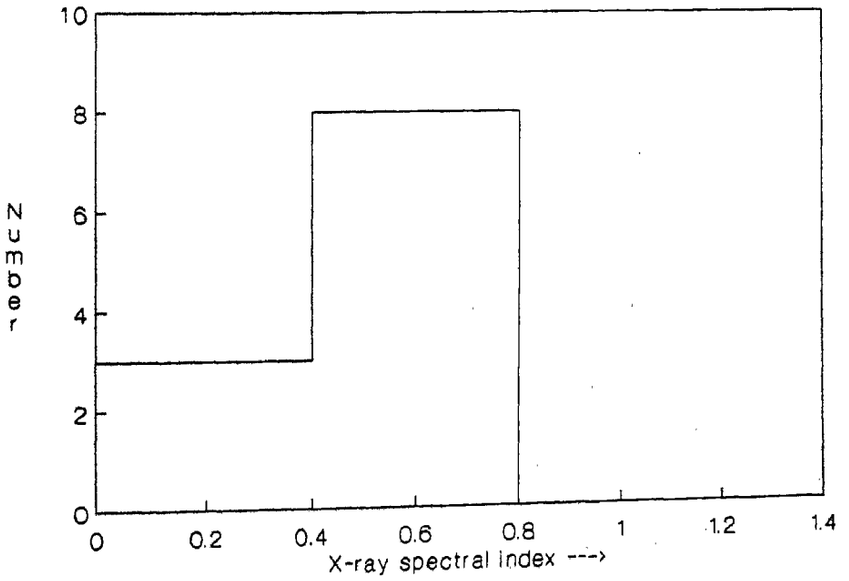

Fig.7.1b Quasars with R > 0.5

structures (Fanti *et al.*, 1988; Nan *et al.*, 1988). Thus while the data do not preclude relativistic motions, the parameter R is clearly not a good measure of the angle of inclination to the line of sight in these objects.

7.6 Disbelief

Several bits of evidence have been cited to argue against relativistic beaming on both small and large scales, and also against the validity of the unified interpretation for radio quasars. They are discussed below.

(a) Heckman (1983) argues that while the unified interpretation requires that CDQs do not differ from LDQs in their emission line properties, they actually do differ in two respects. Firstly, the broad emission lines are wider and more complex in the LDQs. Secondly, the FeII multiplets are weaker in the LDQs. The author further argues that the narrower Broad Emission Lines in CDQs cannot be a mere orientation effect since they are similar to those of the radio-quiet quasars, which are claimed to be viewed from a random direction.

However, in view of the arguments of Section 7.5, it is not at all clear that a bias towards optically brighter radio-quiet quasars for determination of line profiles would not bias the orientation of the radio-quiet sample. Indeed, Wills & Browne (1986) have shown that the data for CDQs and LDQs are consistent with an orientation effect. Further, Wills & Browne suggest that the FeII lines appear weaker in LDQs least partly because the lines blend with each other due to their larger apparent width, leading to an underestimate of their strength. They suggest that in any case the trend may be with line width rather than R, and therefore does

not contradict the unified scheme.

(b) Wardle & Potash (1984) use jet-counterjet ratios derived for the eight largest (angular size) quasars of the 4C sample to argue that Doppler effects alone cannot account for the one-sidedness in these quasars. "The only assumption" they make is that extended quasars in the 4C catalogue are randomly oriented with respect to the line of sight. But it has been argued in Chapter 6 (Section 6.3) that samples of radio sources selected at low frequencies, if not completely identified, could be significantly biased with respect to orientation. Thus the value of 4.1 that Wardle & Potash derive for a maximum possible jet-counterjet asymmetry due to Doppler effects is likely to be an underestimate.

(c) Lonsdale (1986) has argued that the radio structural properties of distant quasars cast "serious shadow" over the relativistic beaming hypothesis. The 23 quasars which do show jets (out of a total of 72 quasars of high redshift and steep radio spectrum), are claimed to not show any of the correlations expected in the relativistic beaming scenario. This is despite the fact that the 23 quasars form a sample of objects "mostly close to the line of sight" (if beaming occurs), and therefore "should be most sensitive to orientation effects".

It should be noted, however, that on a large scale, only mild relativistic beaming is required for the generally observed jet asymmetries to be *statistically* consistent with the relativistic beaming hypothesis. Moreover, ultra-dissipative jets *are* known in quasars (e.g., Saikia, 1984b), and so a sample selected by the presence of large scale jets is not necessarily one with objects mostly close to the line of sight. Further, the sample derives from steep radio spectrum quasars, which

would have relatively weaker nuclear components, and would therefore be relatively closer to the plane of the sky. Indeed, the range of values of R in the sample of Lonsdale (1986) reflects mostly intermediate orientations. Ultra-dissipative jets may well contribute to the correlation of jet prominence with jet curvature. But given the limited range in R in the sample, it *does* correlate with jet curvature, source size and jet prominence in the sense expected from the beaming hypothesis. The exception is in the region of $R < 0.1$, where there are only two objects. Before absence of evidence is taken as evidence of absence, even if only for distant quasars, the correlations need to be examined for a larger range of R. Also, if the jets are ultra-dissipative, they would not be expected to point towards the side with the brighter hot spot, and this needs to be verified.

(d) De Ruiter *et al.* (1986) and Padrielli *et al.* (1988b) use properties of quasars from the "complete" Bologna (B2) sample to argue that the relativistic beaming hypothesis is not sustained. De Ruiter *et al.* (1986) assert that the deviation of the R-distribution of the B2 sample from that for the 3CR sample contradicts unified scheme. But it has been demonstrated in this thesis (Section 6.3) that the B2 sample is biased, and a selection effect accounts for the apparent inconsistency.

Padrielli *et al.* (1988b) show that none of the quasars in the sample with misaligned radio structure are of flat radio spectrum, which again contradicts the relativistic beaming hypothesis wherein flat radio spectrum sources are at small inclinations to the line of sight and therefore small intrinsic misalignments would be preferentially amplified. But in their sample, there are actually a total of 20 objects of flat radio spectrum, of which as many as 10 are unresolved, and are therefore

excluded from the misalignment analysis. It is these objects that are most likely to show non-collinearity, as these authors themselves have demonstrated (misalignment correlates inversely with angular size). Further, among the quasars with steep radio spectrum, at least 9 are likely to turn out to be Compact Steep Spectrum quasars, of which 4 are bent. The unified scheme clearly does not apply to these objects, where there is likely to be a large contribution to the distortions from interaction with the interstellar medium.

7.7 Persisting embarrassments

Even though a cogent argument can be put forth in favour of the relativistic beaming hypothesis and the unified interpretation for radio quasars, there still remain puzzles that cast doubt on the scenario.

(a) Superluminal quasars appear to be too large (e.g., de Bruyn & Schilizzi, 1983; Browne, 1987). If superluminal quasars are inclined at small angles to the line of sight, then their observed sizes are foreshortened by large projection factors, and if deprojected, they appear far larger than their counterparts that are supposedly closer to the plane of the sky.

Quantification of the degree of the problem is tricky, since the deprojection factors in each case are elusive: it is possible that VLBI observes (superluminal motion of) the shocked pattern, which can have a different speed from the underlying (relativistic) flow that causes the nuclear radio flux density to be boosted; intrinsic misalignments of the jets further confuse the issue (Browne, 1987). The latter author argues for a correlation of intrinsic linear size

with Lorentz factor as a resolution of the question. Also, the possibility that some quasars might masquerade as powerful radio galaxies, e.g., Broad Line Radio Galaxies, needs to be looked into, especially given the possibility that aspect dependent obscuration of the central nucleus might be occurring (e.g., Netzer, 1987; Thompson *et al.*, 1988).

(b) The host galaxies of CDQs appear to be different from those of LDQs. The latter appear to be more luminous in the O[III] emission line (Boroson *et al.*, 1985; Stockton & MacKenty, 1987). This observation contradicts the supposition that differences between the two classes are due to orientation effects alone. However, the possibility that the result is merely due to a correlation between luminosity of the O[III] emission and intrinsic (unbeamed) radio power needs to be investigated (this thesis, Section 6.9.2).

7.8 Future confrontations of assumptions, and some speculations

Adopting the view that the relativistic beaming hypothesis and the unified-interpretation-approach promises significant order and progress in the search for a unified phenomenology for active galactic nuclei, some tests of the ideas involved are proposed.

(a) How are the magnetic fields oriented in the nuclear jets of LDQs? In Chapter 5 of this thesis, where the orientation of the core polarization was used to infer the orientation of the nuclear jet, an important assumption was made, *viz.*, that the magnetic field is predominantly *along the nuclear jet.* But if the CDQs *do* intrinsically differ from the LDQs (for instance, if the nuclei of LDQs are

intrinsically less luminous) then it might be expected that the magnetic field structuring would be complex/different. On kiloparsec scales, it is known that for jets emanating from powerful cores, the projected magnetic field is parallel to the jet all along, whereas those from weak cores do have "perpendicular" projected magnetic field configurations. Verification of the premise is therefore an important step. It may be done using VLB Interferometric mapping (that would give the jet orientation) and VLA polarimetric imaging of the central components (for the magnetic field orientation) of LDQs (at a frequency $\geq$ 5 GHz, so as to able to ignore Faraday rotation effects). Currently improved VLBI sensitivities make the mapping of LDQs feasible. Further, constraints need to be placed on the nuclear jet-counter-jet asymmetry, so that the study of the relationship of this asymmetry to the polarization properties of the (unresolved) nuclear jet may be made.

(b) Is the "blue bump" in the spectra of quasars aspect dependent? This bump has been suggested to be thermal emission from an accretion disc (e.g., Edelson & Malkan, 1986). It is important to investigate the extent to which orientation effects due to this disc play a significant role in the observed optical continuum. Determination of the relative prominence of the "blue bump" for a sample of quasars with a range of R values using spectrophotometry would be interesting in this regard. Since the amount of emission observed from a thin opaque disc would be most sensitive to aspect near edge-on inclinations of the disc, in the relativistic beaming framework, these inclinations would correspond to values of $R < 1$.

(c) Is part of the x-ray continuum aspect-dependent? It is important to our interpretation of the x-ray emission from quasars to determine the role of aspect in

their apparent properties. To confirm or refute the suggested dependence of a component of the x-ray continuum on inclination (Section 7.4) x-ray colours of quasars with a range of inclinations need to be determined. The commissioning of telescopes such as the Röntgen satellite and AXAF in the future, make such experiments feasible.

(d) Are the host galaxies of LDQs different from those of CDQs? This question (cf., Section 7.5) needs to be investigated in detail by choosing for the comparison CDQs and LDQs that are *predicted to be intrinsically similar* by the scheme, and by excluding the Compact Steep Spectrum quasars. The possibility that the observed correlation of O[III] luminosity with radio spectrum being simply because more (intrinsically) radio luminous objects are more "O[III] luminous" needs to be tested.

(e) Are there any quasars masquerading as radio galaxies? Quasars with "edge-on" accretion discs may have their optical nuclei further (preferentially) dimmed if there exists surrounding dust that is also confined to a plane parallel to the disc. This possibility needs to be investigated, especially in the light of what was summarized in Section 7.7.

(f) Are the motions of Broad Absorption Line clouds confined to a plane? Given that the radio emission offers a handle on the orientation of the quasar, this needs to be used to explore in detail the possibility that the absorption clouds may perhaps have their motions confined to a plane perpendicular to the radio axis.

CONCLUSIONS

The main conclusions of this thesis are enumerated below.

(1) The parameter R is a reasonably good statistical measure of the angle of inclination to the line of sight in radio quasars, except when they are of the Compact Steep Spectrum kind, where interaction of the radio jet with the interstellar medium is important (Chapter 4).

(2) A sample of quasars of suspected one-sided radio structure was imaged with high angular resolution. The results show that (a) the radio jets almost always point towards the side with the brighter hot spot, consistent with them being at least mildly relativistically beamed, and (b) quasars with relatively larger asymmetry in surface brightness of the outer hot spots have more prominent nuclear radio components, suggesting that they are at preferentially smaller inclinations to the line of sight (Chapter 4).

(3) High angular resolution polarimetry of the nuclear radio components of quasars shows that there appear to be large misalignments between the orientation of the nuclear jets and the overall radio axis for the core-dominated quasars, while lobe dominated quasars show more collinear structures. This is consistent with the unified scheme (Chapter 5).

(4) Several properties of the optical emission from quasars require that if the radio emission is relativistically beamed, then the beaming is accompanied by an enhancement of the optical continuum. The prominence of the nuclear radio component correlates with the apparent optical brightness and the ratio of the

nuclear to host galaxy emission (Chapter 6).

(5) Components moving with bulk relativistic speeds, as well as thermal emission from a thin and opaque disc appear to contribute to the optical continuum. The latter component would enhance the scatter in the Hubble diagram of quasars with steep radio spectrum (Chapter 6).

(6) While the radio-quiet quasars cannot be co-opted into unified scheme, nor can the scheme be applied to them as an independent class, an alternative unified scenario akin to that of Scheuer & Readhead (1979) appears to apply to them (Chapter 6).

(7) Core-dominated quasars appear to have preferentially flatter spectral indices for the soft x-ray emission relative to lobe-dominated quasars, suggesting that part of the x-ray continuum is aspect-dependent (Chapter 7).

(8) The relatively large sizes of "superluminal quasars" and the apparently higher luminosity of the O[III] emission line from the host galaxies of lobe-dominated quasars are persisting embarrassments to the relativistic beaming hypothesis and the unified scheme, and need to be further explored.

(9) In conclusion, several of the observed properties of radio quasars can be understood if relativistic beaming of the radio emission is invoked. Given this hypothesis, observations imply that emission from quasars at other wavelengths may also be aspect-dependent. The appeal of the hypothesis and the unified interpretation is not in consistency or otherwise with rigourous statistics. It lies primarily in its simplicity and simultaneous ability to explain a melange of phenomena using what is essentially one mechanism.

REFERENCES

Abraham, Z., de Medeiros, J. R., and Kaufmann, P., 1984. "22- and 44-GHz continuum observations of extragalactic radio sources," *Astr. J.* **89**, 200-202.

Allington-Smith, J. R., Perryman, M. A. C., Longair, M. S., Gunn, J. E., and Westphal, J. A., 1982. "A complete sample of extragalactic radio sources at 1 Jy at 408 MHz - II. The optical observations," *Mon. Not. R. astr. Soc.* **201**, 331-344.

Altschuler, D. R. and Wardle, J. F. C., 1976. "Observations of the flux density and linear polarization of compact extragalactic radio sources at 3.7- and 11.1-cm wavelength," *Mem. R. astr. Soc.* **82**, 1-67.

Amirkhanyan, V. R., Gorshkov, A. G., Kaputskin, A. A., Konnikova, V. K., Lazutkin, A. N., and others, 1981. "A sky survey at 8.7 and 14.4 GHz: the zone $\delta = 0°–4°$," *Sov. Astr.* **25**, 412-415.

Antonucci, R. R. J., 1984. "Optical spectropolarimetry of radio galaxies," *Astrophys. J.* **278**, 499-520.

Antonucci, R. R. J. and Ulvestad, J. S., 1985. "Extended radio emission and the nature of blazars," *Astrophys. J.* **294**, 158-182.

Antonucci, R. R. J., Hickson, P., Olszewski, E. W., and Miller, J. S., 1986. "Deep radio maps of high-frequency selected BL Lac objects," *Astr. J.* **92**, 1-5.

Artyukh, V. S., Vitkevich, V. V., Dagkesamanskii, R. D., and Kozlukhov, V. N., 1969. "Flux densities and spectral indices for the sources in the 3C and 3CR catalogs at 86-MHz frequency," *Sov. Astr.* **12**, 567-577.

Artyukh, V. S. and Vetukhnovskaya, Y. N., 1981. "A survey of BL Lacertae-type radio sources at 102 MHz," *Sov. Astr.* **25**, 397-402.

Baars, J. W. M., Genzel, R., Pauliny-Toth, I. I. K., and Witzel, A., 1977. "The absolute spectrum of Cas A; an accurate flux density scale and a set of secondary calibrators," *Astronomy and Astrophysics* **61**, 99-106.

Bahcall, J. N. and Hills, R. E., 1973. "The Hubble diagram for the brightest quasars," *Astrophys. J.* **179**, 699-703.

Balick, B. and Heckman, T. M., 1983. "Spectroscopy of the fuzz associated with four quasars," *Astrophys. J.* **265**, L1-L5.

Banhatti, D. G., Ananthakrishnan, S., and Rao, A. P., 1983. "Metre-wavelength fine structure in 30 extragalactic radio sources with sizes of a few arcsec," *Mon. Not. R. astr. Soc.* **205**, 585-591.

Barthel, P. D., Miley, G. K., Schilizzi, R. T., and Preuss, E., 1984. "Compact radio cores in extended quasars," *Astr. Astrophys.* **140**, 399-404.

Barthel, P. D., 1984. "Radio structure in quasars," Ph.D. thesis, University of Leiden.

Barthel, P. D., Miley, G. K., Schilizzi, R. T., and Lonsdale, C. J., 1988. "Observations of the large scale radio structure in high redshift quasars," *Astr. Astrophys. Suppl.* 73, 515-547.

Begelman, M. C., Blandford, R. D., and Rees, M. J., 1984. "Theory of extragalactic radio sources," *Reviews of Modern Physics* **56**, 255-351.

Benford, G., 1977. "Constraints on coherent curvature radiation from quasars," *Mon. Not. R. astr. Soc.* **179**, 595-601.

Bennett, C. L., Lawrence, C. R., and Burke, B. F., 1984. "5 GHz variability and the gain of the NRAO 300 foot telescope," *Astrophys. J. Suppl.* **54**, 211-227.

Bentley, M., Haves, P., Spencer, R. E., and Stannard, D., 1976. "The radio structure of a sample of 101 quasars from the Parkes ± 4° survey," *Mon. Not. R. astr. Soc.* **176**, 275-306.

Binette, L., Carignan, C., Bolton, J. G., and Wright, A. E., 1981. "Positions and flux densities at 5000 MHz for 1133 weak radio sources," *Aust. J. Phys.* **34**, 407-444.

Blandford, R. D. and Rees, M. J., 1974. "A "twin-exhaust" model for double radio sources," *Mon. Not. R. astr. Soc.* **169**, 395-415.

Blandford, R. D., McKee, C. F., and Rees, M. J., 1977. "Super-luminal expansion in extragalactic radio sources," *Nature* **267**, 211-216.

Blandford, R. D. and Konigl, A., 1979. "Relativistic jets as compact radio sources," *Astrophys. J.* **232**, 34-48.

Blandford, R. D., 1984. "Theoretical models of active galactic nuclei," in *VLBI and Compact Radio Sources: IAU Symposium No. 110*, R. Fanti, K. Kellermann, and G. Setti, eds., pp. 215-225, Reidel, Dordrecht, Holland.

Bolton, J. G. and Wall, J. V., 1970. "Quasi-stellar objects in the Parkes 2700 MHz survey: the selected regions and the ±4° declination zone," *Aust. J. Phys.* **23**, 789-815.

Boroson, T. A. and Oke, J. B., 1982. "Detection of the underlying galaxy in the QSO 3C48," *Nature* **296**, 397-399.

Boroson, T. A. and Oke, J. B., 1984. "Spectroscopy of the nebulosity around eight high-luminosity QSOs," *Astrophys. J.* **281**, 535-544.

Boroson, T. A., Persson, S. E., and Oke, J. B., 1985. "More spectroscopy of the fuzz around QSOs: additional evidence for two types of QSO," *Astrophys. J.* **293**, 120-131.

Branson, N. J. B. A., 1967. "A radio survey of the sky north of declination 70 ° at a frequency of 81.5 Mc/s," *Mon. Not. R. astr. Soc.* **135**, 149-174.

Braude, S. Y., Megn, A. V., Rashkovski, S. L., Ryabov, B. P., Sharykin, N. K., and others, 1978. "Decametric survey of discrete sources in the northern sky II. Source catalogue in the range of declinations +10° to +20°," *Astrophysics and Space Science* **54**, 37-128.

Braude, S. Y., Megn, A. V., Sokolov, K. P., Tkachenko, A. P., and Sharykin, N. K., 1979. "Decametric survey of discrete sources in the northern sky V. Source catalogue in the range of declinations 0° to +10°," *Astrophysics and Space Science* **64**, 73-126.

Braude, S. Y., Microshnitchenko, A. P., Sokolov, K. P., and Sharykin, N. K., 1981. "Decametric survey of discrete sources in the northern sky VII. Source catalogue in the range of declinations +10° to +20°," *Astrophysics and Space Science* **74**, 409-451.

Bridle, A. H. and Purton, C. R., 1968. "Observations of radio sources at 10.03 MHz," *Astr. J.* **73**, 717-726.

Bridle, A. H., Davis, M. M., Fomalont, E. B., and Lequex, J., 1972. "Flux densities, positions, and structures for a complete sample of radio sources at 1400 MHz," *Astr. J.* **77**, 405-443.

Bridle, A. H., Fomalont, E. B., and Cornwell, T. J., 1981. "The large- and small-scale structures of 3C293," *Astr. J.* **86**, 1294-1305.

Bridle, A. H., 1986. "Extragalactic jets: trends and correlations," *Can. J. Phys.* **64**, 353-361.

Browne, I. W. A., Orr, M. J. L., Davis, R. J., Foley, A., Muxlow, T. W. B., and Thomasson, P., 1982a. "Jodrell Bank MTRLI observations of nine core-dominated sources at 408 MHz," *Mon. Not. R. astr. Soc.* **198**, 673-688.

Browne, I. W. A., Clark, R. R., Moore, P. K., Muxlow, T. W. B., Wilkinson, P. N., Cohen, M. H., and Porcas, R. W., 1982b. "MERLIN observations of superluminal radio sources," *Nature* **299**, 788-793.

Browne, I. W. A. and Wright, A. E., 1985. "Relativistic beaming and the optical magnitudes of QSOs," *Mon. Not. R. astr. Soc.* **213**, 97-102.

Browne, I. W. A. and Perley, R. A., 1986. "Extended radio emission round core-dominated quasars - constraints on relativistic beaming models," *Mon. Not. R. astr. Soc.* **222**, 149-166.

Browne, I. W. A. and Murphy, D. W., 1987. "Beaming and the x-ray, optical and radio properties of quasars," *Mon. Not. R. astr. Soc.* **226**, 601-627.

Browne, I. W. A., 1987. "Extended structure of superluminal radio sources," in *Superluminal Radio Sources*, J. A. Zensus and T. J. Pearson, eds., pp. 129-147, Cambridge University Press, Cambridge, Massachusetts.

Burbidge, G. R., 1985. "Noncosmological redshifts in galaxies and quasars," in *Extragalactic Energetic Sources: Proceedings of Winter School*, V. K. Kapahi,

ed., pp. 87-104, Indian Academy of Sciences, Bangalore.

Burn, B. J., 1966. "On the polarization of discrete radio sources by Faraday dispersion," *Mon. Not. R. astr. Soc.* 133, 67-83.

Burns, J. O., Feigelson, E. D., and Schreier, E. J., 1983. "The inner radio structure of Centaurus A: clues to the origin of the jet x-ray emission," *Astrophys. J.* 273, 128-153.

Burns, J. O., Basart, J. P., de Young, D. S., and Ghiglia, D. C., 1984. "Radio jets in classical double radio sources with strong cores," *Astrophys. J.* 283, 515-528.

Cawthorne, T. V., Scheuer, P. A. G., Morrison, I., and Muxlow, T. W. B., 1986. "A sample of powerful radio sources for VLBI studies," *Mon. Not. R. astr. Soc.* 219, 883-893.

Clark, B. G., 1980. "An efficient implementation of the algorithm "CLEAN"," *Astr. Astrophys.* 89, 377-378.

Clements, E. D., 1983. "Optical positions of quasars," *Mon. Not. R. astr. Soc.* 203, 861-863.

Cocke, W. J. and Pacholczyk, A. G., 1975. "Coherent curvature radiation and low-frequency variable radio sources," *Astrophys. J.* 195, 279-283.

Cohen, A. M., Porcas, R. W., Browne, I. W. A., Daintree, E. J., and Walsh, D., 1977. "Accurate position measurements and optical identifications for radio sources selected at 966 MHz," *Mem. R. astr. Soc.* 84, 1-44.

Cohen, M. H., 1985. "Inverse Compton x-rays and VLBI radio structure," in *Extragalactic Energetic Sources: Proceedings of Winter School*, V. K. Kapahi, ed., pp. 1-11, Indian Academy Sciences, Bangalore.

Cohen, M. H., Barthel, P. D., Pearson, T. J., and Zensus, J. A., 1988. "Expanding quasars and the expansion of the universe," in *The Impact of VLBI on Astrophysics and Geophysics*, M. J. Reid and J. M. Moran, eds., pp. 23-24, Kluwer, Dordrecht, Holland.

Condon, J. J., Condon, M. A., Jauncey, D. L., Smith, M. G., Turtle, A. J., and Wright, A. E., 1981. "Multifrequency radio observations of optically selected quasars," *Astrophys. J.* 244, 5-11.

Condon, J. J., Condon, M. A., and Hazard, C., 1982. "Complete samples of active extragalactic objects. I. A 1411-MHz VLA survey centered on $\alpha = 12^h04^m$, $\delta = +11°30'$," *Astr. J.* 87, 739-750.

Conway, R. G., Birch, P., Davis, R. J., Jones, L. R., Kerr, A. J., and Stannard, D., 1983. "Multifrequency observations of linear polarization in 94 sources from the 3CR catalogue - I. Observations," *Mon. Not. R. astr. Soc.* 202, 813-823.

Davis, R. J., Stannard, D., and Conway, R. G., 1978. "The alignment of the radio structure and magnetic field in three D2 quasars," *Mon. Not. R. astr. Soc.* 185,

435-440.

Davis, R. J., Stannard, D., and Conway, R. G., 1983. "Interferometric observations of compact components in extragalactic radio sources - II," *Mon. Not. R. astr. Soc.* **205**, 1267-1278.

de Bruyn, A. G., 1985. Presentation made at the IAU General Assembly, New Delhi.

de Bruyn, A. G. and Schilizzi, R. T., 1986. "WSRT observations of core-dominated radio sources," in *Quasars: IAU Symposium No.119*, G. Swarup and V. K. Kapahi, eds., pp. 203-206, D. Reidel, Dordrecht, Holland.

de Bruyn, A. G. and Schilizzi, R. T., 1986. "WSRT observations of core-dominated radio sources," in *Quasars: IAU Symposium No.119*, G. Swarup and V. K. Kapahi, eds., pp. 203-206, D. Reidel, Dordrecht, Holland.

de Pater, I. and Weiler, K. W., 1982. "High-accuracy linear and circular polarization measurements at 21 cm," *Mn* **198**, 747-755.

de Pater, I. and Perley, R. A., 1983. "The radio structure of 3C 279," *Astrophys. J.* **273**, 64-69.

de Ruiter, H. R., Rogora, A., and Padrielli, L., 1986. "B2 quasars and relativistic motion," in *Quasars: IAU Symposium No.119*, G. Swarup and V. K. Kapahi, eds., pp. 197-201, D. Reidel, Dordrecht, Holland.

Dent, W. A., 1965. "Quasi-stellar sources: variation in the radio emission of 3C 273," *Science* **148**, 1458-1459.

Dent, W. A., Kapitzky, J. E., and Kojoian, G., 1974. "15. 5-GHz flux-density measurements of variable radio sources," *Astr. J.* **79**, 1232-1241.

Dixon, R. S. and Kraus, J. D., 1968. "A high-sensitivity 1415-MHz survey between North declinations of 10° and 37°," *Astr. J.* **73**, 381-407.

Douglas, J. N., Bash, F. N., Torrence, G. W., and Wolfe, C., 1980. "The Texas survey: preliminary ±18° strip," Publications in Astronomy No.17, University of Texas.

Downes, A. J. B., Peacock, J. A., Savage, A., and Carrie, D. R., 1986. "The Parkes selected regions: powerful radio galaxies and quasars at high redshifts," *Mon. Not. R. astr. Soc.* **218**, 31-62.

Dreher, J. W., Carilli, C. L., and Perley, R. A., 1987. "The Faraday rotation of Cygnus A: magnetic fields in cluster gas," *Astrophys. J.* **316**, 611-625.

Eckart, A., Witzel, A., Biermann, P., Johnston, K. J., Simon, R., and others, 1986. "Investigation of a complete sample of flat spectrum radio sources from the S5 survey II. Results," *Astr. Astrophys. Suppl.* **67**, 121-146.

Edelson, R. A. and Malkan, M. A., 1986. "Spectral energy distributions of active galactic nuclei between 0.1 and 100 microns," *Astrophys. J.* **308**, 59-77.

Ehman, J. R., Dixon, R. S., and Kraus, J. D., 1970. "The Ohio survey between declinations of 0° and 36° South," *Astr. J.* **75**, 506.

Fanaroff, B. L. and Riley, J. M., 1974. "The morphology of extragalactic radio sources of high and low luminosity," *Mon. Not. R. astr. Soc.* **167**, 31P-35P.

Fanti, C., Fanti, R., Ficarra, A., Formiggini, L., Giovannini, G., and others, 1975. "Westerbork six centimeter observations of a complete sample of quasars from the B2 sample," *Astr. Astrophys. Suppl.* **19**, 143-187.

Fanti, C., Fanti, R., Formiggini, L., Lari, C., and Padrielli, L., 1977. "Radio structures of B2 quasars at 6 cm," *Astr. Astrophys. Suppl.* **28**, 351-362.

Fanti, R., Feretti, L., Giovannini, G., and Padrielli, L., 1979a. "Radio structures of B2 quasars at 1415 MHz," *Astr. Astrophys. Suppl.* **35**, 169-177.

Fanti, R., Feretti, L., Giovannini, G., and Padrielli, L., 1979b. "Radio spectral properties of B2 quasars," *Astr. Astrophys.* **73**, 40-45.

Fanti, C., Fanti, R., Ficarra, A., Mantovani, F., Padrielli, L., and Weiler, K. W., 1981. "Low frequency variable sources 5 year monitoring program at 408 MHz," *Astr. Astrophys. Suppl.* **45**, 61-78.

Fanti, C., Fanti, R., Parma, P., Nan, R., Schilizzi, R. T., and others, 1988. "The radio structure of compact steep spectrum radio sources," in *The Impact of VLBI on Astrophysics and Geophysics*, M. J. Reid and J. M. Moran, eds., pp. 111-114, Kluwer, Dordrecht, Holland.

Feigelson, E. D., Isobe, T., and Kembhavi, A., 1984. "Radio and x-ray emission in radio-selected quasars," *Astr. J.* **89**, 1464-1477.

Feldman, P. A., 1979. "The 1978-79 radio outburst of the bright x-ray-emitting quasar 0241+622," *Bull. Am. Astr. Soc.* **11**, 777.

Feldman, P. A., MacLeod, J. M., and Andrew, B. H., 1981. "Radio outbursts in 3C 345, 3C 454.3 and Q0241+622," IAU Circular No. 3637, Central Bureau of Astronomical Telegrams, Cambridge, Massachusetts.

Feretti, L., Giovannini, G., and Parma, P., 1982. "The quasar B2 1320+29," *Astr. Astrophys.* **115**, 423-427.

Fiedler, R. L., Waltman, E. B., Spencer, J. H., Johnston, K. J., Angerhoffer, P. E., and others, 1987. "Daily observations of compact extragalactic radio sources at 2695 and 8085 MHz, 1979-1985," *Astrophys. J. Suppl.* **65**, 319-384.

Fitch, L. T., Dixon, R. S., and Kraus, J. D., 1969. "A high-sensitivity 1415-MHz survey between declinations of 0° and 20° North," *Astr. J.* **74**, 612-688.

Foltz, C. B., Chaffee, Jr., F. H., Weymann, R. J., and Anderson, S. F., 1987. "QSO absorption systems with $z_{abs} \cong z_{em}$," Preprint Series No.2539, Center for Astrophysics, Cambridge, Massachusetts.

Fomalont, E. B. and Moffet, A. T., 1971. "Positions of 352 small-diameter radio sources," *Astr. J.* **76**, 5-11.

Fomalont, E. B., 1981. "Extended radio sources," in *Origin of Cosmic Rays: IAU Symposium No.94*, G. Setti, G. Spada, and A. W. Wolfendale, eds., pp. 111-125, Reidel, Dordrecht, Holland.

Fried, J. W., 1986. "Host galaxies of quasars," in *Structure and Evolution of Active Galactic Nuclei*, G. Giurcin, F. Mardirossian, and others, eds., pp. 309-315, Reidel, Dordrecht, Holland.

Garrington, S. T., Leahy, J. P., Conway, R. G., and Laing, R. A., 1988. "A systematic asymmetry in the polarization properties of double radio sources with one jet," *Nature* **331**, 147-149.

Gear, W. K., Robson, E. I., Ade, P. A. R., Smith, M. G., and others, 1984. "Millimeter-wave observations of flat spectrum radio sources," *Astr. J.* **280**, 102-106.

Gehren, T., Fried, J., Wehinger, P. A., and Wyckoff, S., 1984. "Host galaxies of quasars and their association with galaxy clusters," *Astrophys. J.* **278**, 11-27.

Geldzahler and Shaffer, 1979. "Very high resolution observations of the nearby quasar 0241+622," *Astr. Astrophys.* **76**, L21-L22.

Gisler, G. R. and Miley, G. K., 1979. "610 MHz observations of the Perseus cluster of galaxies with the Westerbork Synthesis Radio Telescope," *Astr. Astrophys.* **76**, 109-119.

Gopal-Krishna, Singal, A. K., and Krishnamohan, S., 1984. "The exceptionally large flux variability of the quasar 1055+018 at metre wavelengths," *Astr. Astrophys.* **140**, L19-L22.

Gower, A. C. and Hutchings, J. B., 1982. "4C 18.68: a QSO with precessing radio jets," *Astrophys. J.* **253**, L1-L5.

Gower, A. C. and Hutchings, J. D., 1984. "Radio and optical morphology of low-redshift quasars," *Astr. J.* **89**, 1658-1687.

Gregorini, L., Mantovani, F., Eckart, A., Biermann, P., Witzel, A., and Kühr, H., 1984. "The low-frequency spectra of a complete sample of extragalactic radio sources," *Astr. J.* **89**, 323-331.

Högbom, J. A., 1974. "Aperture synthesis with a non-regular distribution of interferometer baselines," *Astr. Astrophys. Suppl.* **15**, 417-426.

Höglund, B., 1967. "Pencil-beam survey of radio sources between declinations +18° and +20° at 750 and 1410 MHz," *Astrophys. J. Suppl.* **15**, 61-96.

Harris, D. E., Dewdney, P. E., Costain, C. H., Butcher, H., and Wills, A. G., 1983. "Discovery of a quasar with a wide angle radio tail in a distant cluster of galaxies," *Astrophys. J.* **270**, 39-47.

Heckman, T. M., 1980. "The broad line region in active nuclei and quasars: correlations with luminosity and radio emission," *Astr. Astrophys.* **88**, 311-316.

Heckman, T. M., 1983. "The emission-line gas in quasars and active nuclei: implications for the nature of core-dominant radio sources," *Astrophys. J.* **271**, L5-L6.

Heeschen, D. S., 1984. "Flickering of extragalactic radio sources," *Astr. J.* **89**, 1111-1123.

Hewitt, A. and Burbidge, G., 1987. "A new optical catalog of QSOs," *Astrophys. J. Suppl.* **63**, 1-246.

Hintzen, P., Ulvestad, J., and Owen, F., 1983. "Are wide-angle radio-tail QSOs members of clusters of galaxies? I: VLA maps at 20 cm of 117 radio quasars," *Astr. J.* **88**, 709-758.

Hintzen, P., 1984. "Wide-angle radio tail QSOs as members of clusters of galaxies. II. Direct optical observations and spectroscopy of QSO fields," *Astrophys. J. Suppl.* **55**, 533-550.

Hooimeyer, J. R., Barthel, P. D., and Schilizzi, R. T., 1987. "Observations of the cores of extended quasars," preprint, Sterrewacht Leiden, Leiden, Holland.

Hough, D. H., 1986. "Parsec-scale structure in the nuclei of double-lobed radio quasars," Ph.D. thesis, California Institute of Technology, Pasadena.

Hough, D. H. and Readhead, A. C. S., 1988. "Relativistic beaming and the nuclei of double-lobed radio quasars," in *The Impact of VLBI on Astrophysics and Geophysics*, M. J. Reid and J. M. Moran, eds., pp. 90-100, Kluwer, Dordrecht, Holland.

Hutchings, J. B., Crampton, D., Campbell, B., Gower, A. C., and Morris, S. C., 1982. "Further morphological studies of QSOs," *Astrophys. J.* **262**, 48-60.

Hutchings, J. B., Crampton, D., and Campbell, B., 1984. "Optical imaging of 78 quasars and host galaxies," *Astrophys. J.* **280**, 41-50.

Hutchings, J. B. and Gower, A. C., 1985. "Evidence for beamed radiation from QSOs," *Astr. J.* **90**, 405-409.

Hutchings, J. B., 1987. "What is the difference between radio galaxies and radio quasar galaxies?" *Astrophys. J.* **320**, 122-134.

Impey, C., 1987. "Infrared, optical, UV, and x-ray properties of superluminal radio sources," in *Superluminal Radio Sources*, J. A. Zensus and T. J. Pearson, eds., pp. 233-250, Cambridge University Press, Cambridge, Massachusetts.

Jenkins, C. J., Pooley, G. G., and Riley, J. M., 1977. "Observations of 104 extragalactic radio sources with the Cambridge 5-km telescope at 5 GHz," *Mem. R. astr. Soc.* **84**, 61-99.

Jennison, R. C. and Das Gupta, M. K., 1953. "Fine structure of the extra-terrestrial radio source Cygnus I," *Nature* **172**, 996-997.

Jones, T. W., Rudnick, L., Aller, H. D., Aller, M. F., Hodge, P. E., and Fiedler, R. L., 1985. "Magnetic field structure in active compact radio sources," *Astr. J.*

290, 627-636.

Joshi, M. N., 1981. "Structure of seven 3C sources at metre wavelengths," *Mon. Not. R. astr. Soc.* **197**, 7-17.

Kühr, H., Nauber, U., Pauliny-Toth, I. I. K., and Witzel, A., 1979. "A catalogue of radio sources," Preprint No. 55, Max-Planck Institut fuer Radioastronomie, Bonn.

Kühr, H., Witzel, A., Pauliny-Toth, I. I. K., and Nauber, U., 1981. "A catalogue of extragalactic radio sources having flux densities greater than 1 Jy at 5 GHz," *Astr. Astrophys. Suppl.* **45**, 367-430.

Kafka, P., 1967. "How to count quasars," *Nature* 213, 346-350.

Kapahi, V. K., 1979. "Westerbork observations of flat spectrum galaxies in the 5 GHz 'S4' survey," *Astr. Astrophys. Suppl.* **74**, L11-L14.

Kapahi, V. K. and Schilizzi, R. T., 1979. "VLBI observations of hot spots in the lobes of distant radio sources," *Nature* 277, 610-615.

Kapahi, V. K., 1981a. "Extragalactic sources with one-sided radio structure," *J. Astrophys. Astron.* **2**, 43-58.

Kapahi, V. K., 1981b. "Westerbork observations of radio sources in the 5 GHz 'S4' survey," *Astr. Astrophys. Suppl.* **43**, 381-393.

Kapahi, V. K. and Saikia, D. J., 1982. "Relativistic beaming in the central components of double radio quasars," *J. Astrophys. Astron.* 3, 465-483.

Kapahi, V. K. and Kulkarni, V. K., 1986. "Redshift distributions of steep and flat-spectrum radio quasars and relativistic beaming," in *Quasars: IAU Symposium No.119*, G. Swarup and V. K. Kapahi, eds., pp. 207-210, D. Reidel, Dordrecht, Holland.

Kapahi, V. K., Subrahmanya, C. R., and D'Silva, S., 1989. "VLA observations of an optically deep sample of Molonglo quasars: aspect dependence of the optical continuum," in *Active Galactic Nuclei: IAU symposium No.134*, D. E. Osterbrock and J. S. Miller, eds., Kluwer, Dordrecht, Holland (to be published).

Katgert-Merkelijn, J., Lari, C., and Padrielli, L., 1980. "Statistical properties of radio sources of intermediate strength," *Astr. Astrophys. Suppl.* **40**, 91-118.

Kellermann, K. I. and Pauliny-Toth, I. I. K., 1969. "The spectra of opaque radio sources," *Astrophys. J.* **155**, L71-L78.

Kellermann, K. J. and Pauliny-Toth, I. I. K., 1981. "Compact radio sources," *Ann. Rev. Astr. Astrophys.* **19**, 373-410.

Kellermann, K., Sramek, R., Shaffer, D., Green, R., and Schmidt, M., 1986. "Radio emission from optically selected quasars," in *Quasars: IAU Symposium No.119*, G. Swarup and V. K. Kapahi, eds., pp. 95-102, D. Reidel, Dordrecht, Holland.

Kembhavi, A. K. and Kulkarni, V. K., 1977. "Absolute magnitudes and Hubble plot for QSOs," *Mon. Not. R. astr. Soc.* **181**, 19P-24P.

Kesteven, M. J. L., Bridle, A. H., and Brandie, G. W., 1976. "Variability of extragalactic sources at 2.7 GHz. I. Results of a 2-yr monitoring program," *Astr. J.* **81**, 919-932.

Kristian, J., 1973. "Quasars as events in the nuclei of galaxies: the evidence from direct photographs," *Astrophys. J.* **179**, L61-L65.

Kronberg, P. P., 1986. "3C 303: a "laboratory" extragalactic jet source," *Can. J. Phys.* **64**, 449-451.

Laing, R. A. and Peacock, J. A., 1980. "The relation between radio luminosity and spectrum for extended extragalactic radio sources," *Mon. Not. R. astr. Soc.* **190**, 903-924.

Laing, R. A., 1981. "Multifrequency observations of 40 powerful extragalactic sources with 5 km telescope," *Mon. Not. R. astr. Soc.* **195**, 261-324.

Laing, R. A., Riley, J. M., and Longair, M. S., 1983. "Bright radio sources at 178 MHz: flux densities, optical identifications and the cosmological evolution of powerful radio galaxies," *Mon. Not. R. astr. Soc.* **204**, 151-187.

Laing, R. A., 1988. "The sidedness of jets and depolarization in powerful extragalactic radio sources," *Nature* **331**, 149-151.

Landau, R., Golisch, B., Jones, T. J., Jones, T. W., Pedelty, J., and others, 1986. "Active extragalactic sources: simultaneous observations from 20 centimeters to 1400 A," *Astrophys. J.* **308**, 78-92.

Lang, K. R., Lord, S. D., Johanson, J. M., and Savage, P. D., 1975. "The composite Hubble diagram," *Astrophys. J.* **202**, 583-590.

Large, M. I., Mills, B. Y., Little, A. G., Crawford, D. F., and Sutton, J. M., 1981. "The Molonglo reference catalogue of radio sources," *Mon. Not. R. astr. Soc.* **194**, 693-704.

Lawrence, C. R., Bennet, C. L., Garcia-Barreto, J. A., Greenfield, P. E., and Burke, B. F., 1983. "5 GHz observations of sources in the ARECIBO 611 MHz survey," *Astrophys. J. Suppl.* **51**, 67-114.

Lind, K. R. and Blandford, R. D., 1985. "Semidynamical models of radio jets: relativistic beaming and source counts," *Astrophys. J.* **295**, 358-367.

Lonsdale, C. J. and Morrison, I., 1983. "Asymmetries in four powerful radio sources," *Mon. Not. R. astr. Soc.* **203**, 833-851.

Lonsdale, C. J., 1986. "Radio jets at higher redshift," *Can. J. Phys.* **64**, 445-448.

Lyne, A. G., 1972. "A study of the lunar occultations of eleven radio sources," *Mon. Not. R. astr. Soc.* **158**, 431-462.

MacDonald, G. H. and Miley, G. K., 1971. "The radio structures of seventy-nine quasi-stellar objects," *Astrophys. J.* **164**, 2327-2247.

Machalski, J., Maslowski, J., Condon, J. J., and Condon, M. A., 1982. "A complete sample of intermediate-strength radio sources selected from the GB/GB2 1400-MHz surveys. II. High-resolution maps and optical identifications of sources with very steep spectra," *Astr. J.* **87**, 1150-1164.

Malkan, M. A., 1984. "The underlying galaxies of quasars. II. Imaging of a radio-loud sample," *Astrophys. J.* **287**, 555-565.

Marscher, A. L. and Broderick, J. J., 1983. "VLBI observations of the quasars CTD20 (0234+285), OJ(0827+243), and 4C19. 44 (1354+195), and the millimeter-x-ray connection," *Astr. J.* **88**, 759-763.

Masson, C. R. and Wall, J. V., 1977. "The cosmological evolution of flat-spectrum quasars," *Mon. Not. R. astr. Soc.* **180**, 193-206.

McCrea, W. H., 1972. "The large-scale variations of quasi-stellar objects," in *External Galaxies and Quasi Stellar Objects: IAU Symposium No.44*, D. S. Evans, ed., pp. 283-284, Reidel, Dordrecht, Holland.

Medd, W. J., Andrew, B. H., Harvey, G. A., and Locke, J. L., 1972. "Observations of extragalactic variable sources at 2.8 and 4.5 cm wavelength," *Mem. R. astr. Soc.* 77, 109-158.

Miley, G. K., 1971. "The radio structure of quasars - a statistical investigation," *Mon. Not. R. astr. Soc.* **152**, 477-490.

Miley, G. K. and Hartsuijker, A. P., 1978. "Radio intensity and polarization distributions of quasars at three frequencies," *Astr. Astrophys. Suppl.* 34, 129-163.

Miley, G., 1980. "The structure of extended extragalactic radio sources," *Ann. Rev. Astr. Astrophys.* **18**, 165-218.

Moffet, A. T., Gubbay, J., Robertson, D. S., and Legg, A. J., 1972. "High-resolution observations of variable radio sources," in *External Galaxies and Quasi Stellar Objects: IAU Symposium No. 44*, D. S. Evans, ed., Reidel, Dordrecht, Holland.

Moffet, A. T., 1975. "Strong nonthermal radio emission from galaxies," in *Stars and Stellar Systems IX: Galaxies and the Universe*, A. Sandage, M. Sandage, and J. Kristian, eds., pp. 211-281, University of Chicago Press, Chicago.

Moore, R. L. and Stockman, H. S., 1984. "A comparison of the properties of highly polarized QSOs versus low-polarization QSOs," *Astrophys. J.* 279, 465-484.

Morabito, D. D., Preston, R. A., Slade, M. A., and Jauncey, D. L., 1982. "Arcsecond positions for milliarcsecond VLBI nuclei of extragalactic radio sources. I. 546 sources," *Astr. J.* **87**, 517-527.

Morabito, D. D., Preston, R. A., Slade, M. A., Jauncey, D. L., and Nicolson, G. D., 1983. "Arcsecond positions for milliarcsecond VLBI nuclei of extragalactic radio sources. II. 207 sources," *Astr. J.* **88**, 1138-1145.

Morisawa, K. and Takahara, F., 1987. "An interpretation of the statistical properties of extragalactic radio sources with a relativistic beaming model," *Mon. Not. R. astr. Soc.* **228**, 745-758.

Nan, R., Schilizzi, R. T., Fanti, C., Fanti, R., van Breugel, W., and Muxlow, T. W., 1988. "The radio structures of the compact steep spectrum sources 3C119, 3C287 and 3C283," in *The Impact of VLBI on Astrophysics and Geophysics*, M. J. Reid and J. M. Moran, eds., pp. 119-120, Kluwer, Dordrecht, Holland.

Neff, S. G. and Brown, R. L., 1984. "Large-scale radio emission in radio quasars: confined radio lobes excited by fast jets," *Astr. J.* **89**, 195-199.

Netzer, H., Yahil, A., and Yaniv, R., 1978. "The Hubble diagram for QSOs," *Mon. Not. R. astr. Soc.* **184**, 21P-25P.

Netzer, H., 1985. "Quasar discs - I. The Baldwin effect," *Mon. Not. R. astr. Soc.* **216**, 63-78.

Netzer, H., 1987. "Quasar discs - II. A composite model for the broad-line region," *Mon. Not. R. astr. Soc.* **225**, 55-72.

O'dea, C. P. and Owen, F. N., 1985a. "VLA observations of 57 sources in clusters of galaxies," *Astr. J.* **90**, 927-953.

O'dea, C. P. and Owen, F. N., 1985b. "The global properties of a representative sample of 51 narrow-angle-tail radio sources in the directions of Abell clusters," *Astr. J.* **90**, 954-972.

O'dea, C. P., Barvainis, R., and Challis, P. M., 1988. "Subarcsecond-resolution radio observations of sixteen core-dominated quasars and active galactic nuclei," *Astr. J.* **96**, 435-454.

Orr, M. J. L. and Browne, I. W. A., 1982. "Relativistic beaming and quasar statistics," *Mon. Not. R. astr. Soc.* **200**, 1067-1080.

Owen, F. N., Porcas, R. W., and Neff, S. J., 1978. "Interferometer observations of quasars from the Jodrell Bank 966-MHz survey," *Astr. J.* **83**, 1009-1020.

Owen, F. N., Spangler, S. R., and Cotton, W. D., 1980. "Simultaneous radio spectra of sources with strong millimeter components," *Astr. J.* **85**, 351-367.

Owen, F. N., White, R. A., Hilldrup, K. C., and Hanisch, R. J., 1982. "A 1400-MHz survey of 1478 Abell clusters of galaxies," *Astr. J.* **87**, 1083-1097.

Owen, F. and Puschell, J. J., 1984. "VLA observations of Jodrell Bank radio quasars," *Astr. J.* **89**, 932-957.

Padrielli, L., Romney, J. D., Bartel, N., Fanti, R., Ficarra, A., and others, 1986. "Two epoch VLBI observations of a sample of low frequency variable sources," *Astr. Astrophys.* **165**, 53-73.

Padrielli, L., Fanti, R., Ficarra, A., Gregorini, L., Mantovani, F., and Spangler, S., 1988a. "The low frequency variability of extragalactic radio sources: a relativistic effect or galactic scintillation," in *The Impact of VLBI on*

Astrophysics and Geophysics, M. J. Reid and J. M. Moran, eds., pp. 297-298, Kluwer, Dordrecht, Holland.

Padrielli, L., Rogora, A., and de Ruiter, H. R., 1988b. "VLA observations of B2 quasars III. Discussion of the radio morphologies," *Astr. Astrophys.* **196**, 49-58.

Peacock, J. A., Perryman, M. A. C., Longair, M. S., Gunn, J. E., and Westphal, J. A., 1981. "Investigation of the optical fields of flat-spectrum radio sources to faint limiting magnitudes," *Mon. Not. R. astr. Soc.* **194**, 601-612.

Peacock, J. A. and Wall, J. V., 1982. "Bright extragalactic radio sources at 2.7 GHz - II. Observations with the Cambridge 5-km telescope," *Mon. Not. R. astr. Soc.* **194**, 843-860.

Peacock, J. A., Miller, L., and Mead, A. R. G., 1986. "The radio emission from optically selected quasars," in *Quasars: IAU Symposium No.119*, G. Swarup and V. K. Kapahi, eds., pp. 103-107, D. Reidel, Dordrecht, Holland.

Pearson, T. J. and Readhead, A. C. S., 1981. "The milli-arcsecond structure of a complete sample of radio sources. I. VLBI maps of seven sources," *Astrophys. J.* **248**, 61-81.

Pearson, T. J. and Readhead, A. C. S., 1984. "Image formation by self-calibration in radio astronomy," *Ann. Rev. Astr. Astrophys.* **22**, 97-130.

Pearson, T. J., Perley, R. A., and Readhead, A. C. S., 1985. "Compact radio sources in the 3C catalog," *Astr. J.* **90**, 738-755.

Perley, R. A. and Johnston, K. J., 1979. "The arcsecond structure of four compact radio sources," *Astr. J.* **84**, 1247-1252.

Perley, R. A., Fomalont, E. B., and Johnston, K. J., 1980. "Compact radio sources with faint components," *Astr. J.* **85**, 649-658.

Perley, R. A., Fomalont, E. B., and Johnston, K. J., 1982. "The extended radio structure of compact extragalactic sources," *Astrophys. J.* **255**, L93-L97.

Perley, R. A., 1982. "The positions, structures, and polarizations of 404 compact radio sources," *Astr. J.* **87**, 859-880.

Perley, R. A., Schwab, F. R., and Bridle, A. H., 1986. *Synthesis Imaging: Course Notes from an NRAO Summer School*, National Radio Astronomy Observatory, Green Bank, WV, U.S.A..

Pica, A. J., Pollock, J. T., Smith, A. G., Leacock, R. J., Edwards, P. L., and Scott, R. L., 1980. "Long-term optical behavior of 114 respect to extragalactic sources," *Astr. J.* **85**, 1442-1461.

Porcas, R., 1987. "Summary of known superluminal sources," in *Superluminal Radio Sources*, J. A. Zensus and T. J. Pearson, eds., pp. 12-25, Cambridge University Press, Cambridge, Massachusetts.

Potash, R. I. and Wardle, J. F. C., 1979. "Radio structures of a complete sample of quasars from the 4C catalog," *Astr. Astrophys.* **84**, 707-717.

Potash, R. I. and Wardle, J. F. C., 1980. "4C 32.69: a quasar with a radio jet," *Astrophys. J.* **239**, 42-49.

Preston, R. A., Morabito, D. D., and Jauncey, D. L., 1983. "A statistical VLBI study of milli-arcsecond cores in extragalactic radio sources," *Astrophys. J.* **269**, 387-399.

Readhead, A. C. S., Cohen, M. H., Pearson, T. J., and Wilkinson, P. N., 1978. "Bent beams and the overall size of extragalactic radio sources," *Nature* **276**, 768-771.

Readhead, A. C. S., Hough, D. H., Ewing, M. S., Walker, R. C., and Romney, J. D., 1983. "Asymmetric structure in the nuclei of NGC 1275 and 3C 345," *Astrophys. J.* **265**, 107-131.

Rees, M. J., 1966. "Appearance of relativistically expanding radio sources," *Nature* **211**, 468-470.

Rees, M. J., 1967. "Studies in radio source structure I. A relativistically expanding model for variable quasi-stellar radio sources," *Mon. Not. R. astr. Soc.* **135**, 345-360.

Rees, M. J., 1971. "New interpretation of extragalactic radio sources," *Nature* **229**, 312-317.

Rickett, B. J., Coles, W. A., and Bourgois, G., 1984. "Slow scintillation in the interstellar medium," *Astr. Astrophys.* **134**, 390-395.

Riley, J. M. and Pooley, G. G., 1975. "Observations of 31 extragalactic radio sources with the Cambridge 5-km telescope at 5 GHz," *Mem. R. astr. Soc.* **80**, 105-137.

Rinsland, C. P., Dixon, R. S., Gearhart, M. R., and Kraus, J. D., 1974. "Ohio survey. VII," *Astr. J.* **79**, 1129-1210.

Roger, R. S., Costain, C. H., and Stewart, D. I., 1986. "Spectral flux densities of radio sources at 22 MHz," *Astr. Astrophys. Suppl.* **65**, 485-496.

Rogora, A., Padrielli, L., and de Ruiter, H. R., 1986. "VLA observations of B2 quasars. I. Extended sources," *Astr. Astrophys. Suppl.* **64**, 557-577.

Rogora, A., Padrielli, L., and de Ruiter, H. R., 1987. "VLA observations of B2 quasars. II. Compact sources," *Astr. Astrophys. Suppl.* **67**, 267-282.

Romanishin, W., Ford, H., Ciardullo, R., and Margon, B., 1984. "Spectrophotometry and image analysis of the nebulosity around the low-redshift quasar 0241+622," *Astrophys. J.* **277**, 487-494.

Romney, J., Padrielli, L., Bartel, N., Weiler, K. W., Ficarra, A., and others, 1984. "The milliarcsecond scale structure of low frequency variable sources," *Astr. Astrophys.* **135**, 289-299.

Rudnick, L. and Adams, M. T., 1979. "4C radio galaxies: structures and optical identifications," *Astr. J.* **84**, 437-469.

Rudnick, L. and Jones, T. W., 1982. "Compact radio sources: the dependence of variability and polarization on spectral shape," *Astr. J.* **255**, 39-47.

Rudnick, L. and Jones, T. W., 1983. "Rotation measures for compact variable radio sources," *Astr. J.* **88**, 518-526.

Rudnick, L. and Edgar, B. K., 1984. "Alternating-side ejection in extragalactic radio sources," *Astrophys. J.* **279**, 74-85.

Rudnick, L., Jones, T. W., Aller, H. D., Aller, M. F., Hodge, P. E., Owen, F. N., Fiedler, R. L., Puschell, J. J., and Bignell, R. C., 1985. "Broad-band polarization observations of active compact radio sources," *Astrophys. J. Suppl.* 57, 693-709.

Rudnick, L., Jones, T. W., and Fiedler, R., 1986. "Weak nuclei of powerful radio sources—spectra and polarizations," *Astr. J.* **91**, 1011-1018.

Rusk, R. and Seaquist, E. R., 1985. "Alignment of radio and optical polarization with VLBI structure," *Astr. J.* **90**, 30-38.

Rusk, R. and Rusk, A. C. M., 1986. "Alignment of milliarcsecond with arcsecond structure in core-dominated radio sources," *Can. J. Phys.* **64**, 440-444.

Saikia, D. J., Shastri, P., Cornwell, T. J., and Banhatti, D. G., 1983. "An interesting radio jet in the high-redshift quasar 1857+566," *Mon. Not. R. astr. Soc.* **203**, 53P-57P.

Saikia, D. J., Swarup, G., and Sinha, R. P., 1984. "Radio observations of the BL Lae object 1400+162," *J. Astrophys. Astr.* **5**, 475-482.

Saikia, D. J., 1984a. "On the separation ratio of the outer radio components in quasars," *Mon. Not. R. astr. Soc.* **209**, 525-531.

Saikia, D. J., 1984b. "Extended radio jets and compact cores in quasars," *Mon. Not. R. astr. Soc.* **208**, 231-238.

Saikia, D. J., Swarup, G., and Kodali, P. D., 1985. "Polarization properties of radio cores in galaxies and quasars," *Mon. Not. R. astr. Soc.* **216**, 385-394.

Saikia, D. J., Kulkarni, V. K., and Porcas, R. W., 1986. "Radio observations of extended sources suspected of having steep-spectrum cores," *Mon. Not. R. astr. Soc.* **218**, 719-728.

Saikia, D. J., Salter, C. J., and Muxlow, T. W. B., 1987a. "A radio study of the compact steep-spectrum quasar 3C2 (0003-003)," *Mon. Not. R. astr. Soc.* **224**, 911-923.

Saikia, D. J., Staveley-Smith, L., Wills, D., and others, 1987b. "A wide-angle radio-tail quasar: B2 1419+315," *Mon. Not. R. astr. Soc.* **229**, 495-503.

Salonen, E., Lehto, H., Urpo, S., Teerikorpi, P., Terasranta, H., Haarala, S., and others, 1983. "Flux density measurements of bright extragalactic sources at

36.8 GHz," *Astr. Astrophys. Suppl.* **51**, 47-62.

Schalinski, C. J., Witzel, A., Kirchbaum, T. P., Hummel, C. A., Biermann, P. L., and others, 1988. "Bulk relativistic motion in a complete sample of flat spectrum radio sources," in *The Impact of VLBI on Astrophysics and Geophysics*, M. J. Reid and J. M. Moran, eds., pp. 71-72, Kluwer, Dordrecht, Holland.

Scheer, D. J. and Kraus, J. D., 1967. "A high-sensitivity survey of the North galactic polar region at 1415-MHz," *Astr. J.* **72**, 536-543.

Scheuer, P. A. G., 1974. "Models of extragalactic radio sources with a continuous energy supply from a central object," *Mon. Not. R. astr. Soc.* **166**, 513-528.

Scheuer, P. A. G. and Readhead, A. C. S., 1979. "Superluminally expanding radio sources and the radio-quiet QSOs," *Nature* 277, 182-185.

Scheuer, P. A. G., 1984. "Explanations of superluminal motion," in *VLBI and Compact Radio Sources: IAU Symposium No. 110*, R. Fanti, K. Kellermann, and G. Setti, eds., pp. 197-205, Reidel, Dordrecht, Holland.

Scheuer, P. A. G., 1987. "Velocities in radio galaxies and quasars," in *Astrophysical Jets and Their Engines*, W. Kundt, ed., pp. 129-136, Reidel, Dordrecht, Holland.

Schilizzi, R. T., Kapahi, V. K., and Neff, S. G., 1982. "VLA observations of hot spots in high luminosity radio sources," *J. Astrophys. Astron.* **3**, 173-187.

Schilizzi, R. T. and de Bruyn, A. G., 1983. "large-scale radio structures of superluminal sources," *Nature* **303**, 26-31.

Schmidt, M., 1968. "Space distribution and luminosity functions of quasi-stellar radio sources," *Astrophys. J.* **151**, 393-409.

Seielstad, G. A., Pearson, T. J., and Readhead, A. C. S., 1983. "10.8 GHz flux density variations among a complete sample of sources from the NRAO-Bonn S4 survey," *Publ. Astr. Soc. Pacific* **95**, 842-872.

Setti, G. and Woltjer, L., 1973. "Hubble diagrams for quasars," *Astrophys. J.* **181**, L61-L63.

Shapirovskaya, N. Y., 1978. "Variability of extragalactic decimeter radio sources," *Soviet Astronomy* **22**, 544-547.

Sholomitski, G. B., 1965. "Fluctuations in the 32.5-cm flux of CTA 102," *Soviet Astronomy* **9**, 516.

Simard-Normandin, M. and Kronberg, P. P., 1980. "Rotation measures and the galactic magnetic field," *Astr. J.* **242**, 74-94.

Simard-Normandin, M., Kronberg, P. P., and Neidhöfer, J., 1980. "Linear polarization measurements of extragalactic radio sources at $\lambda\lambda$ 17.4 and 18.9 cm," *Astr. Astrophys. Suppl.* **40**, 319-321.

Simard-Normandin, M., Kronberg, P. P., and Button, S., 1981a. "The Faraday rotation measures of extragalactic radio sources," *Astrophys. J. Suppl.* **45**, 97-111.

Simard-Normandin, M., Kronberg, P. P., and Neidhofer, J., 1981b. "Linear polarization observations of extragalactic radio sources at $\lambda 2$ cm and at 17-19 cm," *Astr. Astrophys. Suppl.* **43**, 19-22.

Simard-Normandin, M., Kronberg, P. P., and Button, S., 1981c. "Linear polarization of extragalactic radio sources at 3.71 and 11.1 centimeters," *Astrophys. J. Suppl.* **46**, 239-245.

Simard-Normandin, M., Kronberg, P. P., and Button, S., 1982. "Integrated linear polarization of extragalactic radio sources at 10.5 GHz (λ 2.86cm) - II," *Astr. Astrophys. Suppl.* **48**, 137-138.

Singal, A. K., Gopal-Krishna, and Venugopal, V. R., 1979. "Lunar occultation observations of 65 radio sources at 327 MHz: List 7," *Mem. Astr. Soc. India* **1**, 14-24.

Slee, O. B., 1984. "A metre-wave outburst from the QSO 1055+018," *Mon. Not. R. astr. Soc.* **209**, 215-226.

Smith, H. E. and Spinrad, H., 1980. "Spectrophotometry of faint, red 3C QSO candidates," *Astrophys. J.* **236**, 419-429.

Smith, E. P., Heckman, T. M., Bothun, G. D., Romanishin, W., and Balick, B., 1986. "On the nature of QSO host galaxies," *Astrophys. J.* **306**, 64-89.

Spangler, S. R. and Cotton, W. D., 1981. "Broadband radio observations of low-frequency variable sources," *Astr. J.* **86**, 730-746.

Spangler, S. R. and Pogge, J. J., 1984. "VLA observations of the distant radio galaxy 3C 411," *Astr. J.* **89**, 342-349.

Stannard, D. and Neal, D. S., 1977. "A comparative study of the properties of 3CR and 4C quasars," *Mon. Not. R. astr. Soc.* **179**, 719-740.

Steiner, J. E., 1981. "A spectrophotometric classification of low-redshift quasars and active galactic nuclei," *Astrophys. J.* **250**, 460-477.

Stocke, J. T., Burns, J. O., and Christiansen, W. A., 1985. "VLA observations of quasars with "dogleg" radio structure," *Astrophys. J.* **299**, 799-813.

Stockman, H. S., Moore, R. L., and Angel, J. R. P., 1984. "The optical polarization properties of "normal" quasars," *Astrophys. J.* **279**, 485-498.

Stockton, A. and MacKenty, J. W., 1987. "Extended emission-line regions around QSOs," *Astrophys. J.* **316**, 584-596.

Subrahmanya, C. R. and Gopal-Krishna, 1979. "Ooty occultations of 100 radio sources at 327 MHz: List 6," *Mem. Astr. Soc. India* **1**, 1-13.

Subrahmanya, C. R., 1980. "A new method of deconvolution and its application to lunar occultations," *Astr. Astrophys.* **89**, 132-139.

Sutton, J. M., Davies, I. M., Little, A. G., and Murdoch, H. S., 1974. "The Molonglo radio source catalogues 2 and 3," *Aust. J. Phys. Astrophys. Suppl.* **33**, 1-44.

Swarup, G., Sinha, R. P., and Saikia, D. J., 1982. "Extended radio jets in the high-redshift quasars 3C9 and 280.1," *Mon. Not. R. astr. Soc.* **201**, 393-400.

Swarup, G., Sinha, R. P., and Hilldrup, K., 1984. "Hotspots and radio lobes of quasars," *Mon. Not. R. astr. Soc.* **208**, 813-843.

Swarup, G., Saikia, D. J., Beltrametti, N., Sinha, R. P., and Salter, C. J., 1986. "Absorption lines and the radio structure of quasars," *Mon. Not. R. astr. Soc.* **220**, 1-18.

Tabara, H. and Inoue, M., 1980. "A catalogue of linear polarization of radio sources," *Astr. Astrophys. Suppl.* **39**, 379-393.

Thompson, A. R., Clark, B. G., Wade, C. M., and Napier, P. J., 1980. "The Very Large Array," *Astrophys. J. Suppl.* **44**, 151-167.

Thompson, A. R., Moran, J. M., and Swenson, Jr., G. W., 1986. *Interferometry and Synthesis in Radio Astronomy*, J. Wiley, New York.

Thompson, K. L., Wills, B. J., Wills, D., Evans, N. J., Breger, M., and others, 1988. "Polarization and reddening in the QSO IRAS 13349+2438," preprint, Department of Astronomy, University of Texas, Austin, Texas.

Tritton, K. P. and Selmes, R. A., 1971. "Optical monitoring of radio sources - III. Further observations of quasars," *Mon. Not. R. astr. Soc.* **153**, 453-469.

Tzanetakis, A., Spencer, R. E., Masson, C. R., and Baldwin, J. E., 1978. "The radio properties of the nearby quasar 0241+62," *Mon. Not. R. astr. Soc.* **185**, 63P-65P.

Ulvestad, J. S. and Johnston, K. J., 1984. "A search for arcminute-scale radio emission in BL lacertae objects," *Astr. J.* **89**, 189-194.

Urry, C. M. and Shafer, R. A., 1984. "Luminosity enhancement in relativistic jets and altered luminosity functions for beamed objects," *Astrophys. J.* **280**, 569-573.

van Breugel, W., Schilizzi, R. T., Hummel, E., and Kapahi, V. K., 1981. "VLBI observations of a mixed selection of extra-galactic objects," *Astr. Astrophys.* **96**, 310-315.

van Breugel, W., Miley, G., and Heckman, T. M., 1984a. "Studies of kiloparsec-scale, steep-spectrum radio source. I. VLA maps," *Astr. J.* **89**, 5-22.

van Breugel, W., Heckman, T., and Miley, G., 1984b. "Optical line emission associated with the radio galaxy 4C 26.42 in the cluster of galaxies Abell 1795," *Astrophys. J.* **276**, 79-91.

van Breugel, W., Nan, R., Schilizzi, R. T., Fanti, C., and Fanti, R., 1988. "Small steep-spectrum sources: jets colliding with ambient gas," in *The Impact of*

VLBI on Astrophysics and Geophysics, M. J. Reid and J. M. Moran, eds., pp. 115-116, Kluwer, Dordrecht, Holland.

van der Laan, H., 1966. "A model for variable extragalactic radio sources," *Nature* **211**, 1131-1133.

Veron-Cetty, M. P. and Veron, P., 1987. "A Catalogue of Quasars and Active Nuclei," Scientific Report No.5, European Southern Observatory, Munich.

Walsh, D., Wills, B. J., and Wills, D., 1979. "Spectroscopy of QSO candidates from the Jodrell Bank 966 MHz survey," *Mon. Not. R. astr. Soc.* **189**, 667-670.

Wampler, E. J., Gaskell, C. M., and Burke, W. L., 1984. "Spectrophotometry of two complete samples of flat radio spectrum quasars," *Astrophys. J.* **276**, 403-412.

Wardle, J. F. C. and Miley, G. K., 1974. "The radio structure of quasars . II," *Astr. Astrophys.* **30**, 305-315.

Wardle, J. F. C., Bridle, A. H., and Kesteven, M. J. L., 1981. "Variability of extragalactic sources at 2.7 GHz. IV. Evidence for weak extended emission and for rapid variability," *Astr. J.* **86**, 848-853.

Wardle, J. F. C. and Potash, R. I., 1982. "Radio and x-ray observations of large scale jets in quasars," in *Extragalactic Radio Sources: IAU Symposium No.97*, D. S. Heeschen and C. M. Wade, eds., pp. 129-131, Reidel, Dordrecht, Holland.

Wardle, J. F. C. and Potash, R. I., 1984. "Observations of large scale jets in quasars and the sidedness problem," in *Physics of Energy Transport in Extragalactic Radio Sources (Proc. of NRAO Workshop No.9)*, A. H. Bridle and J. Eilek, eds., pp. 30-34, NRAO, Greenbank, WV, U. S. A..

Wardle, J. F. C., Moore, R. L., and Angel, J. R. P., 1984. "The radio morphology of blazars and relationships to optical polarization and to normal radio galaxies," *Astrophys. J.* **279**, 93-111.

Weedman, D. W., 1986. "Evolutionary connection of Seyfert galaxies and quasars," in *Structure and Evolution of Active Galactic Nuclei*, G. Giurcin, F. Mardirossian, and others, eds., pp. 215-229, Reidel, Dordrecht, Holland.

Wehrle, A. E., Morabito, D. D., and Preston, R. A., 1984. "VLBI of 257 extragalactic radio sources in the ecliptic region," *Astr. J.* **89**, 336-341.

Wilkes, B. J. and Elvis, M., 1987. "Quasar energy distributions. I. Soft x-ray spectra of quasars," *Astrophys. J.* **323**, 243-262.

Wilkinson, P. N., Richards, P. J., and Bowden, T. N., 1974. "Observations of radio sources with an interferometer of 24 km baseline - IV. The angular structures at 408 and 610 MHz of 30 quasars with steep radio spectrum," *Mon. Not. R. astr. Soc.* **168**, 515-531.

Wilkinson, P. N., 1982. "Kiloparsec scale structure in high luminosity radio sources observed with MTRLI," in *Extragalactic Radio Sources: IAU Symposium No.97*, D. S. Heeschen and C. M. Wade, eds., pp. 149-156, Reidel, Dordrecht, Holland.

Williams, R. E., Strittmater, P. A., Carswell, R. F., and Craine, E. R., 1975. "Splitting of absorption lines in 3C 191," *Astrophys. J.* **202**, 296-302.

Wills, B. J., Wills, D., and Douglas, J. N., 1973. "Optical identifications of radio sources using accurate radio and optical positions," *Astr. J.* **78**, 521-535.

Wills, B. J., 1976. "Optical identifications of radio sources using accurate radio and optical positions II." *Astr. J.* **81**, 1031-1052.

Wills, D. and Wills, B. J., 1976. "Spectroscopy of 206 QSO candidates and radio galaxies," *Astrophys. J. Suppl.* **31**, 143-162.

Wills, D. and Lynds, R., 1978. "Studies of new complete samples of quasi-stellar radio sources from the 4C and Parkes catalogs," *Astrophys. J. Suppl.* **36**, 17-358.

Wills, D., 1979. "Radio studies of complete samples of QSOs from the 4C and Parkes catalogs," *Astrophys. J. Suppl.* **39**, 291-315.

Wills, B. J. and Wills, D., 1986. "Radio structure and the IR-UV spectra of quasars," in *Quasars: IAU Symposium No.119*, G. Swarup and V. K. Kapahi, eds., pp. 215-216, D. Reidel, Dordrecht, Holland.

Wills, B. J. and Browne, I. W. A., 1986. "Relativistic beaming and quasar emission lines," *Astrophys. J.* **302**, 56-63.

Wills, D., Wills, B. J., Barvainis, R., Antonucci, R. R. J., and Berger, M., 1988. "A survey of high optical polarization in quasars," preprint, Department of Astronomy, University of Texas, Austin, Texas.

Willson, M. A. G., 1972. "Fan-beam surveys of radio sources near declinations +28° and +41°," *Mon. Not. R. astr. Soc.* **156**, 7-49.

Windram, M. D. and Kenderline, S., 1969. "Extension of the radio source luminosity function - I. Observations," *Mon. Not. R. astr. Soc.* **146**, 265-288.

Wright, A. E., Jauncey, D. L., Bolton, J. G., and Savage, A., 1982. "The Parkes 2700 MHz survey: a resurvey of the ±4° declinations zone," *Aust. J. Phys.* **35**, 177-206.

Wrobel, J. M., Pearson, T. J., Cohen, M. H., and Readhead, A. C. S., 1988. "VLA polarimetry of VLBI core-jet sources," in *The Impact of VLBI on Astrophysics and Geophysics*, M. J. Reid and J. M. Moran, eds., pp. 165-166, Kluwer, Dordrecht, Holland.

Wyckoff, S., Wehinger, P. A., and Gehren, T., 1981. "Resolution of quasar images," *Astrophys. J.* **247**, 750-761.

Wyckoff, S., Johnston, K., Ghigo, F., Rudnick, L., Wehinger, P., and Boksenberg, A., 1983. "Optical and radio structure of the quasar PKS 0812+02," *Astrophys. J.* **265**, 43-50.

Wykoff, S., Johnston, K., Ghigo, F., Rudnick, L., and others, 1983. "Optical and radio structure of the quasar PKS 0812+02," *Astrophys. J.* **265**, 43-50.

Zensus, J. A., Porcas, R. W., and Pauliny-Toth, I. I. K., 1984. "VLBI study of 57 spectrum radio sources at 5 GHz," *Astr. Astrophys.* **133**, 27-30.

Zensus, J. A. and Porcas, R. W., 1986. "Search for superluminal motion in the weak cores of extended quasars," in *Quasars: IAU Symposium No.119*, G. Swarup and V. K. Kapahi, eds., pp. 167-168, D. Reidel, Dordrecht, Holland.

Zensus, J. A. and Pearson, T. J., 1988. "Superluminal radio sources," in *The Impact of VLBI on Astrophysics and Geophysics*, M. J. Reid and J. M. Moran, eds., pp. 7-16, Kluwer, Dordrecht, Holland.